DEVELOPMENT OF ^{68}Ga BASED TARGET-SPECIFIC RADIOTRACERS FOR DIAGNOSTIC IMAGING APPLICATIONS

By

Akanksha Jain

CHEM01201304023

Bhabha Atomic Research Centre, Mumbai

A thesis submitted to the

Board of Studies in Chemical Sciences

In partial fulfillment of requirements

for the Degree of

DOCTOR OF PHILOSOPHY

of

HOMI BHABHA NATIONAL INSTITUTE

November, 2017

HOMI BHABHA NATIONAL INSTITUTE

Recommendations of the Viva Voce Committee

As members of the Viva Voce Committee, we certify that we have read the dissertation prepared by **Akanksha Jain** entitled "**Development of ^{68}Ga based target-specific radiotracers for diagnostic imaging applications**" and recommend that it may be accepted as fulfilling the thesis requirement for the award of Degree of Doctor of Philosophy.

Chairman: Prof. S. Chattopadhyay	15/3/18
Ph.D. Guide : Dr. Ashutosh Dash	
Examiner: Dr. Suresh Rayala	15/3/18
Member 1: Dr. Sharmila Banerjee	
Member 2: Dr. S. Kannan	
Member 3: Dr. Sudipta Chakraborty	15/03/18

Final approval and acceptance of this thesis is contingent upon the candidate's submission of the final copies of the thesis to HBNI.

I/We hereby certify that I/We have read this thesis prepared under my direction and recommend that it may be accepted as fulfilling the thesis requirement.

Date: 15/3/18

Place: BARC, MUMBAI

Guide/ Convener

STATEMENT BY THE AUTHOR

This dissertation has been submitted in partial fulfillment of requirements for an advanced degree at Homi Bhabha National Institute (HBNI) and is deposited in the Library to be made available to borrowers under the rules of HBNI.

Brief quotations from this dissertation are allowable without special permission, provided that accurate acknowledgement of the source is made. Requests for permission for extended quotation from or reproduction of this manuscript in whole or in part may be granted by the Competent Authority of HBNI when in his or her judgment the proposed use of the material is in the interests of scholarship. In all other instances, permission must be obtained from the author.

Akanksha Jain

DECLARATION

I hereby declare that the work presented in the thesis has been carried out by me. The work is original and has not been submitted earlier as whole or in part for a degree / diploma at this or any other Institution / University.

Akanksha Jain

LIST OF PUBLICATIONS ARISING FROM THE THESIS

JOURNAL

1. Development of ^{68}Ga labeled fatty acids for their potential use in cardiac metabolic imaging. A. Jindal, A. Mathur, U. Pandey, H. D. Sarma, P. Chaudhari and A. Dash. *Journal of Labeled Compounds and Radiopharmaceuticals*, **2014**, *57*, 463–469.

2. In-house preparation of Macroaggregated albumin (MAA) for Ga-68 labeling and its comparison with Ga-68-MAA prepared using commercial MAA. A. Jain, S. Subramanian, U. Pandey, H.D. Sarma, Ramu Ram, A. Dash. *Journal of Radioanalytical and Nuclear Chemistry*, **2016**, *308* (3), 817-824.

3. Synthesis and evaluation of a Ga-68 labeled folic acid derivative for targeting folate receptors. A. Jain, A. Mathur, U. Pandey, J. Bhatt, A. Mukherjee, H. D. Sarma, R. Ram and A. Dash. *Applied Radiation and Isotopes*, **2016**, *116*, 77-84 .

4. ^{68}Ga labeled fatty acids for cardiac metabolic imaging: Influence of different bifunctional chelators. A. Jain, A. Mathur, U. Pandey, H. D. Sarma, A. Dash. *Bioorganic and Medicinal Chemistry Letters*, **2016**, *26*, 5785-5791.

5. Development of ^{68}Ga labeled human serum albumin for blood pool imaging: A comparison between two ligands. A. Jain, U. Pandey, N. Gamre, H..D. Sarma, A. Dash. *Journal of Radioanalytical and Nuclear Chemistry*, **2017**, *313*, 661-668.

6. ^{68}Ga labeled Erlotinib: A novel PET probe for targeting EGFR over-expressing tumors. A. Jain, M. Kameswaran, U. Pandey, K. Prabhash, H.D. Sarma, A. Dash.
Bioorganic & Medicinal Chemistry Letters, **2017**, *27*, 4552-4557

7. A Systematic Comparative Evaluation of ^{68}Ga-Labeled RGD Peptides Conjugated with Different Chelators. A. Jain, S. Chakraborty, H.D. Sarma, A. Dash.
Nucl Med Mol Imaging, **2017**. https://doi.org/10.1007/s13139-017-0499-0

8. Synthesis and preclinical evaluation of novel ^{68}Ga labeled Erlotinib for targeting EGFR over-expressing tumors. A. Jain, M. Kameswaran, U. Pandey, R. Sharma, H.D. Sarma, A. Dash. *Chemical Biology Letters*, **2018**, *5*, 3-10.

9. Synthesis and preclinical evaluation of ^{68}Ga labeled hexadecanoic acid for PET imaging of heart. A. Jain, U. Pandey, A. Mathur, N. Gamre, H.D. Sarma, A. Dash.
Applied Radiation and Isotopes (*Communicated*)

CONFERENCES

1. Development of ^{68}Ga labeled folic acid derivatives for targeting folate receptor positive tumors. A. Jain, A. Mathur, U. Pandey, A. Mukherjee, R. Ram, J. Bhatt and A. Dash. NUCAR-2015, Mumbai, Pg-500.
2. Evaluation of the effect of chelate on the myocardial uptake characteristics of Ga-68 labeled fatty acids for their potential use in myocardial imaging. A. Jain, U. Pandey, A.

Mathur, H.D. Sarma, A. Dash. Oral Presentation in SNMICON-2016, Pondicherry, Indian Journal of Nuclear Medicine O-25, Pg S23.

3. In-house preparation of Macroaggregated Albumin (MAA) for Ga-68 labelling and its comparison with commercially available MAA. A. Jain, S. Subramanian, U. Pandey, H.D. Sarma, R. Ram, A. Dash. Poster Presentation in SNMICON-2016, Pondicherry, Indian Journal of Nuclear Medicine P-068, Pg S59.
4. Development of ^{68}Ga labeled human serum albumin for blood pool imaging: A comparison between two ligands. A. Jain, U. Pandey, N. Gamre, H.D. Sarma, A. Dash. NUCAR-2017, Bhubaneshwar, Pg 496-497.

Akanksha Jain

Dedicated to my mother

ACKNOWLEDGEMENT

On the completion of my PhD, I would like to express my gratitude to all the people without whom this five year long journey would not have been possible. First and foremost, I would like to express my sincere gratitude to my guide, **Dr. Ashutosh Dash**, Head, Radiopharmaceuticals Division. He has always been a constant source of guidance, encouragement and support during this study. I am grateful to him for introducing me to the exciting field of radiopharmaceuticals and allowing me to explore various aspects of this field.

Further, I would like to express my sincere gratitude towards my immediate superior, **Dr. Usha Pandey**, Head, Therapeutic & Reference Sources Section (T&RSS). Her crucial contributions and insights have always helped me improve the quality of my research. Her ceaseless support and keen interest in my day to day experimental work has kept me on my toes and has been vital in completion of my PhD in time. She has not only been supportive on the professional front but has also been helpful personally whenever needed.

It is my pleasure to thank **Dr. Anupam Mathur**, Radiopharmaceuticals program, Board of Radiation and Isotope Technology. He was the person who initiated me into the field of organic chemistry for development of ^{68}Ga labeled radiotracers, which has formed the major part of my PhD thesis. His guidance in this field has played a vital role in developing my confidence and I believe it would certainly help in my career ahead.

I would also like to thank **Dr. Mythili Kameswaran**, Radiopharmaceutical Evaluation Section, for introducing me to the field of tyrosine kinase inhibitors. Her systematic approach and zeal towards her work, has been inspirational.

I am grateful to **Dr. Suresh Subramanian**, Radiopharmaceutical Evaluation Section, who helped me with the animal studies in the work on ^{68}Ga labeled macroaggregated albumin

(MAA). I learnt a great deal about handling and maintaining animals and performing animal studies from him.

I also thank **Dr. Rubel Chakravarty**, Radiochemical Section, for his guidance on myriad of topics at academic level which have been very helpful to me. He also helped me with access to the BARC in-house $^{68}Ge/^{68}Ga$ generator for certain studies, reported in this thesis.

Further, I thank **Dr. Aruna Korde**, Head, Radiopharmaceutical Evaluation Section, for providing access to the iThemba $^{68}Ge/^{68}Ga$ generator which helped me execute studies requiring high ^{68}Ga activity. It is a great pleasure to thank **Dr. H. D. Sarma**, Head, Laboratory Animal Facility and Radioisotope Laboratory, for helping me carrying out biological evaluations of all the compounds reported in this thesis.

I am also grateful to my doctoral committee Chairman, **Dr. S. Chattopadhyay** (Former Director, Biosciences Group) and the doctoral committee members **Dr. Sharmila Banerjee** (Head, Radiation and Medicine Centre), **Dr. S. Kannan** (Head, Fuel Chemistry Division) and **Dr. Sudipta Chakraborty** (Head, Radiochemical Section, Radiopharmaceutical Division), for their suggestions and constructive criticism during the annual progress reviews and pre-synopsis viva-voce.

I would like to express my sincere gratitude towards my colleagues, **Dr. Mohini Guleria** and **Smt. Kusum Vats** of Radiopharmaceutical Chemistry Section, for their work related discussions which greatly enriched my knowledge on diverse topics. My sincere thanks are due to my colleagues, **Shri. Naresh Gamre** and **Shri Manoj Kumar** of T&RSS and **Kum. Priyalata Shetty** of Radiochemical Section, for their help and support. I thankfully acknowledge the help and technical assistance received from **Shri. M.S. Tikka, Shri. B.J. Jadhav and Shri. G. Gandhale.**

I am deeply and forever indebted to my parents, **Shri. S.K. Jindal** and **Smt. Radha Jindal**, for their love and encouragement throughout my life. Finally I express my deep gratitude towards my husband, **Shri. Priyank Jain**, whose love and persistent confidence in me has always encouraged me to pursue my dreams.

BARC, Mumbai. Akanksha Jain

November, 2017

CONTENTS

Chapter 3: Preparation of ^{68}Ga based receptors-specific radiotracers for targeting tumors

3a. Preparation of ^{68}Ga labeled Erlotinib conjugates towards imaging of EGFR over-expressing tumors

3c. Preparation of ^{68}Ga-labeled folic acid conjugates for imaging of folate receptor over-expressing tumors

SYNOPSIS

Radiopharmaceuticals are radiolabeled drugs or molecules with a definite composition and are routinely used in nuclear medicine for diagnosis or therapy of diseases. Radiopharmaceuticals are classified on the basis of their biological distribution as metal essential radiopharmaceuticals where the biodistribution depends upon the chemical and physical properties of the radiometal complex and receptor-specific wherein the *in vivo* localization is determined by the specific biological interactions such as receptor binding, enzymatic reduction etc. Depending upon their application in nuclear medicine and the nuclear characteristics of the radionuclide used, radiopharmaceuticals can be classified as diagnostic and therapeutic radiopharmaceuticals.[1]

Diagnostic radiopharmaceuticals are molecules radiolabeled preferably with pure gamma emitting or positron emitting isotopes, used to provide information related to the morphological structure of organ or tissue as well as their physiological functions when they localize in the organ. Diagnostic applications in nuclear medicine rely on two imaging modalities: SPECT (Single Photon Emission Computed Tomography) and PET (Positron Emission Tomography). As compared to SPECT, the higher sensitivity and superior resolution of PET makes it more beneficial in the visualization and quantification of the *in vivo* distribution of radiopharmaceuticals.[2] Amongst the various PET based radionuclides such as ^{11}C, ^{18}F, ^{64}Cu, ^{68}Ga etc., ^{68}Ga, is an attractive radionuclide, owing to its on-demand availability as Ga(III) from an $^{68}Ge/^{68}Ga$ generator. This obviates the need for a cyclotron in the vicinity of the radiopharmacy which is required for the other positron emitting radioisotopes (^{11}C, ^{18}F, ^{64}Cu). Further, ^{68}Ga has a well developed coordination chemistry which allows fast and reproducible radiolabeling in the

clinical settings. In addition, its nuclear characteristics ($t_{1/2}$ = 67.71 min; 89% β^+ decay) are suitable for PET imaging.[3-5]

In the present thesis an attempt was made to prepare ^{68}Ga labeled radiotracers for specifically targeting different organs as well as tumors. Towards this purpose, different biological vectors such as fatty acids, Erlotinib, RGD peptides, folic acid and human serum albumin (HSA) protein and HSA macroaggregates were used. The ^{68}Ga labeled agents selectively accumulate in the target organs or tumors on the basis of their chemical/physical properties or their affinity to specific receptors. The thesis consists of four chapters and the contents of each chapter are briefly outlined below.

Chapter 1: Introduction

This chapter explains the basic concepts of radiopharmaceuticals, their categories and their applications in nuclear medicine. Further, the various components of a radiopharmaceutical have been explained such as the target molecule, linker, bifunctional chelator (BFC) and radionuclide. This chapter also elaborates the principal characteristics of the two diagnostic nuclear imaging techniques viz. SPECT and PET and deals with the differences between the two techniques explaining the advantages of PET imaging over SPECT imaging. The radionuclides commonly used for PET imaging and the advantages of ^{68}Ga radionuclide over other PET radionuclides have been described. The Chapter also provides information about the ^{68}Ge/^{68}Ga generators which serve as the exclusive source for ^{68}Ga. Further, the various chelators used for ^{68}Ga complexation have been discussed. This chapter also discusses the targeting molecules used for preparation of the ^{68}Ga labeled agents viz. fatty acids, Erlotinib, RGD peptide, folic acid and HSA and its macro-aggregates. The quality control methods and the biological study protocols which are used for evaluating the radiolabeled molecules are described briefly.

Chapter 2: Preparation of ^{68}Ga labeled fatty acids for cardiac metabolic imaging

Long chain fatty acids serve as the principal energy sources in normal myocardium and are rapidly metabolized by β-oxidation.[6] An alteration of fatty acid oxidation is considered a sensitive marker of ischemia and myocardial damage.[6,7] There are many reports wherein fatty acids with varied chain lengths have been tagged with suitable radionuclides for cardiac metabolic imaging and some of them are mentioned in the Chapter. This Chapter deals with the development of ^{68}Ga labeled fatty acids for heart imaging. In order to investigate the effect of chain length of the fatty acid on the myocardial uptake of the ^{68}Ga labeled fatty acids, three different fatty acid chains were studied viz. 11 carbon chain (11-aminoundecanoic acid) and 12 carbon chain (12-aminododecanoic acid) and 16 carbon chain (16-hexadecanedioic acid) fatty acids. These fatty acids were conjugated with the chelator NOTA (1,4,7-triazacyclononane-N,N',N''-triacetic acid) for ^{68}Ga radiolabeling. The rationale behind choosing 11 and 12 carbon chain length fatty acids was based on previous literature reports on ^{99m}Tc-labeled fatty acids wherein the highest myocardial uptake was exhibited by these smaller chain fatty acids[8,9]. Since the potential of ^{99m}Tc-labeled fatty acids with smaller chain lengths for myocardial imaging is well established, similar parent molecules were chosen for the preparation of ^{68}Ga labeled fatty acids towards PET-based myocardial imaging. The 16 carbon chain fatty acid was chosen to evaluate the potential of ^{68}Ga labeled surrogate of ^{123}I-IPPA for myocardial imaging. Hence, towards the synthesis of ^{68}Ga based fatty acids, two fatty acid conjugates were synthesized by conjugation of *p*-SCN-benzyl-NOTA (*S*-2-(4-isothiocyanatobenzyl)-1,4,7-triazacyclononane-1,4,7-triacetic acid) with the ω-amino group of 11-amino undecanoic acid and 12-amino dodecanoic acid, respectively, under alkaline conditions. The 16 carbon chain fatty acid analogue was synthesized by reaction of ω-COOH group of 16-hexadecanedioic acid with the amine group

of *p*-NH_2-benzyl-NOTA using HATU and DIPEA reagent in DMF under nitrogen atmosphere. The final fatty acid conjugates namely, NOTA-undecanoic acid, NOTA-dodecanoic acid and NOTA-hexadecanoic acid, were characterized by NMR and ESI-MS techniques. The conjugates were then radiolabeled in high yields with $^{68}GaCl_3$ eluted in 0.6 N HCl from a tin oxide based commercial $^{68}Ge/^{68}Ga$ generator and characterized using the ^{nat}Ga-surrogates by HPLC and ESI-MS. Further, the biodistribution studies of the ^{68}Ga-NOTA fatty acid conjugates were performed in Swiss mice. It was observed that the ^{68}Ga labeled 11-carbon chain fatty acid had the highest uptake in the myocardium at 2 min (7.4 ± 2.8% ID/g) followed by 12-carbon chain fatty acid (6.4±2.1%) and16-carbon chain fatty acid (3.6±1.0 %ID/g).

In continuation with the above findings, the influence of bifunctional chelators which are employed to bind ^{68}Ga to the fatty acids on the biodistribution behaviour of the final ^{68}Ga-BFC-fatty acid conjugates in Swiss mice was explored. It is known from literature that in order to have minimum interference in the transport of fatty acid to the heart tissue, the chelator conjugated with the fatty acid should form a neutral metal-complex species with small radiolabel core.[9] Thus, two chelators were chosen which are known to form neutral complexes with ^{68}Ga viz. *p*-SCN-Bn-NODAGA (*S*-2-(4-isothiocyanatobenzyl)-1,4,7-triazacyclononane-1-glutaric acid-4,7-acetic acid) and *p*-SCN-Bn-DTPA (*S*-2-(4-isothiocyanatobenzyl)-diethylenetriaminepentaacetic acid), and these were compared with *p*-SCN-Bn-NOTA chelator which has previously been investigated. The isothiocyanate group of the chelators were conjugated with the ω-amine group of the fatty acid, 11-aminoundecanoic acid to obtain NODAGA-undecanoic acid and DTPA-undecanoic acid, respectively. These two conjugates were characterized by NMR and ESI-MS techniques and then radiolabeled with ^{68}Ga in high yields. The results of their biodistribution studies were compared with that of ^{68}Ga-NOTA-undecanoic acid complex. Initial uptake in the

myocardium for ^{68}Ga-NODAGA-undecanoic acid (3.8±0.6% ID/g) and ^{68}Ga-DTPA-undecanoic acid (1.3±0.5% ID/g) was lower than the previously reported ^{68}Ga-NOTA-fatty acid (7.4±2.8% ID/g) at 2 min p.i. Nevertheless, ^{68}Ga-NODAGA-undecanoic acid exhibited significant myocardial retention at 30 min p.i. (1.2±0.03% ID/g) which was better than the other ^{68}Ga labeled fatty acid conjugates.

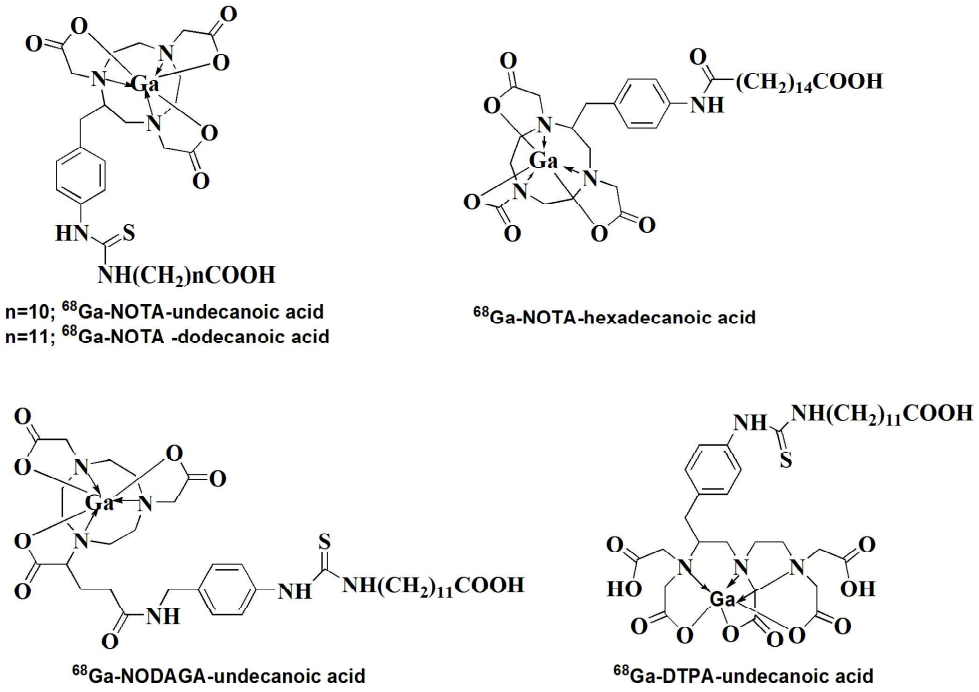

Figure 1: Structures of (a) ^{68}Ga-NOTA-undecanoic acid and ^{68}Ga-NOTA-dodecanoic acid (b) ^{68}Ga-NOTA-hexadecanoic acid (c) ^{68}Ga-NODAGA-undecanoic acid (d) ^{68}Ga-DTPA-undecanoic acid

Chapter 3: Preparation of ^{68}Ga labeled receptor-specific tumor targeting radiotracers

In this Chapter, three different molecular vectors namely Erlotinib, RGD (arginine-glycine-aspartic acid) peptide and folic acid have been discussed for targeting receptor over-expression on specific tumors.

Chapter 3(a) Preparation of ^{68}Ga-labeled Erlotinib complexes for imaging of EGFR over-expressing tumors

Many small molecule tyrosine kinase inhibitors (TKI) have emerged as attractive tools for targeting receptors such as Epidermal Growth Factor Receptors (EGFR), Vascular Endothelial Growth Factor Receptors (VEGFR), Platelet Derived Growth Factor Receptors (PDGFR) etc. which are involved in the growth, proliferation, differentiation and metastasis of tumor cells.[10] One of the earliest and the most potent TKI is the drug Erlotinib (Tarceva®, OSI Pharmaceuticals) which is approved for treatment of EGFR over-expressing cancers, mainly non small cell lung cancer and pancreatic cancer.[11] Development of radiolabeled small molecule TKIs such as Erlotinib can be beneficial for imaging of EGFR over-expressing tumors and thus help in the evaluation of EGFR mutational status before and after treatment to determine the best possible treatment strategy for cancer patients.[12] This Chapter deals with the synthesis and assessment of the potential of novel ^{68}Ga labeled Erlotinib analogues towards PET imaging of EGFR over-expressing tumors. Two novel Erlotinib conjugates were synthesised namely NOTA-Erlotinib and NODAGA-Erlotinib. The synthesis involved reaction of the terminal alkyne group of Erlotinib with the azide group of tert-butyl-3-azidopropylcarbamate using copper(I) catalysed azide-alkyne cycloaddition (CuAAC) 'click' reaction. The BOC protected compound thus obtained was then de-protected. The free amine group of the modified Erlotinib moiety was then reacted with the isothiocyanate group of *p*-SCN-Bn-NOTA and *p*-SCN-Bn-NODAGA to give NOTA-Erlotinib and NODAGA-Erlotinib conjugates respectively. The final conjugates were characterized by NMR and ESI-MS techniques. They were then radiolabeled with ^{68}Ga in high yields (≥95% radiochemical yield) and characterized using ^{nat}Ga-surrogates by HPLC and ESI-MS techniques. The biological efficacy studies of the two conjugates were carried out *in vitro*

using EGFR positive A431 cells. ^{68}Ga-NOTA-erlotinib showed a binding of 9.8±0.4 % with A431 cells which was inhibited by 55.1±0.2 % on addition of 10 µg of unlabeled erlotinib indicating the specificity of the radioconjugate towards EGFRs. In case of ^{68}Ga-NODAGA-erlotinib, 7.8±1.3 % binding was observed. However, low inhibition of 30.7±0.5 % was observed on incubation with excess Erlotinib. Biodistribution studies of ^{68}Ga-NOTA-erlotinib were carried out in NOD/SCID mice bearing EGFR positive tumor. Tumor uptake of ^{68}Ga-NOTA-erlotinib was 1.5±0.1 % ID/g at 30 min p.i. which decreased at 1 h (0.7±0.2 % ID/g) p.i. The ^{68}Ga-NOTA-erlotinib conjugate cleared mainly through hepatobiliary route. Bio distribution studies of ^{68}Ga-NODAGA-erlotinib were carried out in normal Swiss mice. The clearance of ^{68}Ga-NODAGA-erlotinib was majorly via the hepatobiliary pathway as the activity in GI tract increased with time while that in liver decreased with time.

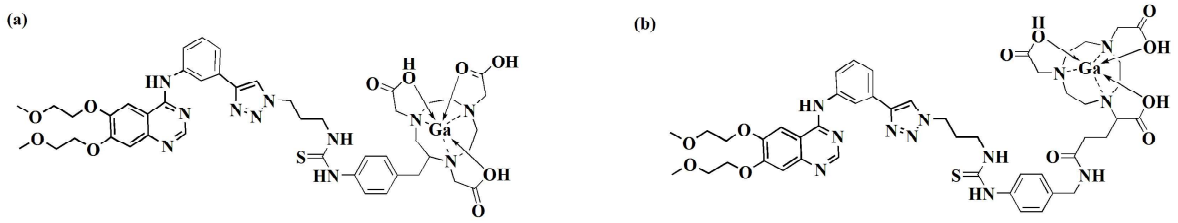

Figure 2: Structures of (a) ^{68}Ga-NOTA-erlotinib and (b) ^{68}Ga-NODAGA-erlotinib

Chapter 3(b) Comparative evaluation of ^{68}Ga-labeled RGD peptides conjugated with different chelators

In the last decade, a variety of RGD peptide based radiotracers have been developed for the imaging of $\alpha_v\beta_3$ integrins which are over-expressed in many cancer cells such as osteosarcomas, neuroblastomas, glioblastomas, melanomas, lung carcinomas and breast cancer.[13] There are numerous reports on the evaluation of ^{68}Ga-labeled RGD peptides in animal models as well as in

human patients wherein the RGD-motif has been conjugated to either DOTA or NOTA/NODAGA chelators.[14] This chapter deals with a detailed systematic evaluation of the role of BFCs on the properties of ^{68}Ga labeled RGD analogues such as the radiochemistry, *in vitro* stability, pharmacokinetics, tumor targeting properties and metabolic stability in melanoma tumor bearing C57BL/6 mice. Comparative evaluation of dimeric cyclic RGD peptide E[c(RGDfK)]$_2$ (E = glutamic acid, R = arginine, G = glycine, D = aspartic acid, f = D-phenylalanine, K = lysine) conjugated with different cyclic and acyclic BFCs namely, *p*-SCN-Bn-NOTA, *p*-SCN-Bn-DOTA [*S*-2-(4- isothiocyanatobenzyl)-1,4,7,10-tetraazacyclododecane-1,4,7,10- tetraacetic acid] and *p*-SCN-Bn-DTPA was performed. The three RGD-conjugates (Fig. 1a-c) were radiolabeled with ^{68}Ga and the radiolabeling conditions were optimized with respect to the peptide amount, reaction temperature and incubation time. The *in vitro* stability of the ^{68}Ga-BFC-RGD conjugates was determined by incubating them in human serum at 37°C up to 2 h as well as in excess EDTA solution for 2 h. The log P values of the three radiotracers in water/octanol system suggested that all the three radiotracers are hydrophilic in nature. The biodistribution studies showed that the clearance of the radiotracers was mainly via the kidneys. In case of ^{68}Ga-DOTA-Bn-(RGD)$_2$, a high tumor uptake was observed but significant accumulation was also observed in non target organs which led to lower tumor/background ratios. Although the uptake in tumor for ^{68}Ga-NOTA-Bn-(RGD)$_2$ was slightly lower as compared to ^{68}Ga-DOTA-Bn-(RGD)$_2$, the low uptake and fast clearance of radioactivity from non target organs like blood, liver, intestine and lungs led to its high tumor/background contrast. In case of ^{68}Ga-DTPA-Bn-(RGD)$_2$, the uptake in melanoma tumor was lower in comparison to the other two radiotracers. On analysis of urine samples of animals injected with ^{68}Ga-DTPA-Bn-(RGD)$_2$, 7-8 % degradation of the radiotracer was observed *in vivo* within 1 h p.i.

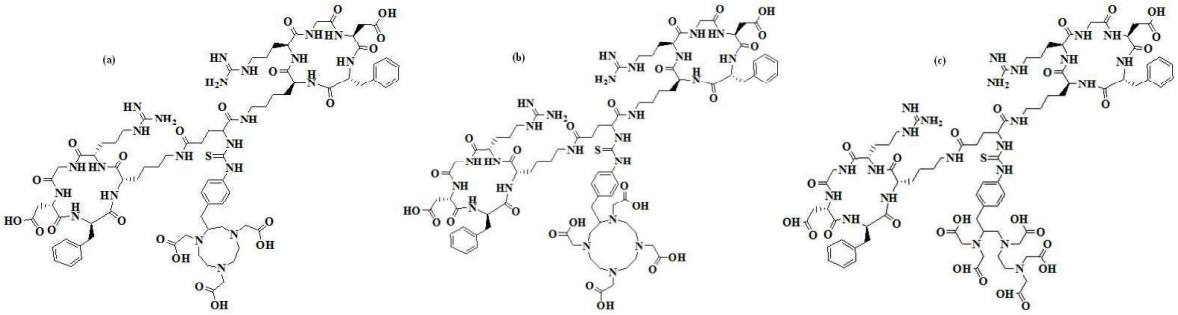

Figure 3: Structures of (a) NOTA-Bn-$(RGD)_2$ (b) DOTA-Bn-$(RGD)_2$ (c) DTPA-Bn-$(RGD)_2$

Chapter 3(c) Preparation of ^{68}Ga-labeled folic acid and its preclinical evaluation

Folate receptors (FR) are over-expressed in many human carcinomas such as breast, cervical, colorectal etc. and have high affinity ($K_d < 10^{-9}$ M) for folic acid.[15] Taking advantage of this mechanism, many radiolabeled folates have been developed in the past for imaging and therapy for selective targeting of FR-positive cancers.[16] This Section of Chapter 3 deals with the synthesis of NOTA conjugated folic acid, its radiolabeling with ^{68}Ga, its *in vitro* cell binding studies in KB cells (which over-express the FR) and preliminary biodistribution studies in normal Swiss mice. In this work, folic acid molecule was synthetically modified to introduce the known BFC, p-NCS-Bn-NOTA in three steps. In the first step, the γ carboxylic acid of folic acid was conjugated with the amine group of Boc propyl diamine linker. The Boc-amine-folic acid compound thus obtained was then de-protected and further conjugated with the isothiocyanate group of *p*-SCN-Bn-NOTA under mild basic conditions. The structure of the final compound, NOTA-folic acid was confirmed by ^{1}H-NMR and ESI-MS. It was then radiolabeled with ^{68}Ga in high yields (≥95% radiochemical yield) and characterized using its ^{nat}Ga-surrogate by HPLC and ESI-MS. ***In vitro*** cell binding studies carried out in FR over-expressing KB cells showed that addition of excess folic acid led to significant decrease in the uptake of ^{68}Ga-NOTA-folic acid which confirmed the specificity of the complex for folate receptors. Biodistribution studies

carried out in normal Swiss mice showed high radioactivity accumulation in the kidney. Further evaluation of the prepared tracer in tumor xenografts is required to quantify the real potential of the synthesized ^{68}Ga-folate conjugate towards FRs.

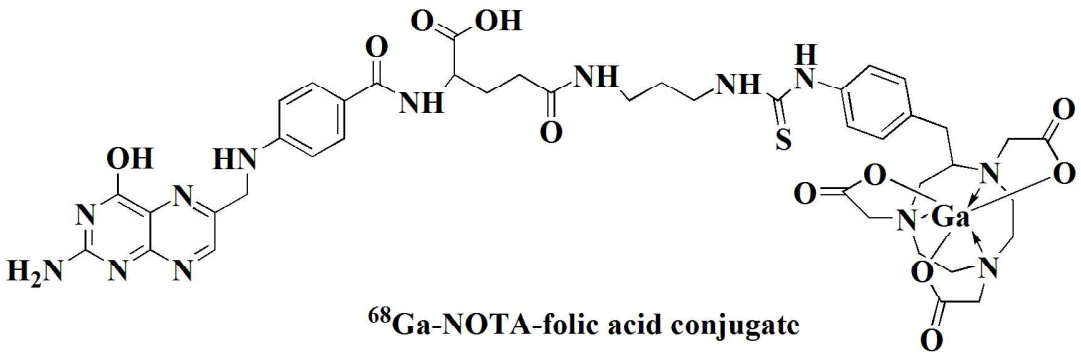

^{68}Ga-NOTA-folic acid conjugate

Figure 4: Structure of ^{68}Ga-NOTA-folic acid

Chapter 4: Development of ^{68}Ga labeled HSA proteins and its aggregates

This Chapter deals with the use of ^{68}Ga labeled human serum albumin (HSA) for blood pool imaging and its macroaggregates for lung imaging

Chapter 4(a) Development of ^{68}Ga labeled HSA for blood pool imaging: A comparison between two ligands

Blood pool imaging quantifies the amount of blood pooling in an organ at different times which can be successfully utilized to identify vascular abnormalities in cardiovascular diseases as well as in the staging of cancers.[17] In the present work, HSA was conjugated with the chelator NOTA-NCS by reacting the amino group of HSA with the isothiocyanato group of NOTA-NCS towards ^{68}Ga labeling. Subsequently, ^{68}Ga labeling of the NOTA-HSA conjugate was carried out and its potential as an agent for blood pool imaging (HSA: Human Serum Albumin) was evaluated in comparison with the reported HSA analogue namely ^{68}Ga-DOTA-HSA. The

influence of chelators on the radiolabeling yields, stability and biodistribution profiles of the respective radiotracers were studied systematically in order to assess their potential utility in blood pool imaging. The time required for completion of ^{68}Ga radiolabeling for NOTA-HSA was about 10 minutes at room temperature while that required for DOTA-HSA was 30 minutes at 37°C. Owing to the short half life of ^{68}Ga, the 30 minute incubation time is fairly long. Both ^{68}Ga-NOTA-HSA and ^{68}Ga-DOTA-HSA had similar biodistribution profiles with ≥ 70% ID/g activity in blood at 2 min p.i. About 50 % of initial activity was retained in blood at 2 h p.i. However, the plasma stability of ^{68}GA-NOTA-HSA was superior to that of ^{68}GA-DOTA-HSA. Results of this study indicate that ^{68}Ga-NOTA-HSA can be further investigated for clinical blood pool imaging applications.

Chapter 4(b): Development of ^{68}Ga labeled Macroaggregated Albumin (MAA) for lung imaging

^{99m}Tc labeled HSA microspheres are routinely used for lung perfusion scanning, a procedure in diagnostic nuclear medicine to assess the presence of emboli or other abnormalities to the pulmonary blood flow. [18,19] This procedure uses albumin microspheres of diameter range 10-100 µm, which are called Macroaggregated Albumin (MAA). This Section of Chapter 4 deals with indigenous development of MAA and its radiolabeling with ^{68}Ga for PET based lung scanning. The synthesis of MAA involves the use of heating to modulate aggregate formation. In order to understand the role of stannous chloride in the formation of MAA, a control experiment was carried out wherein MAA was prepared without the addition of stannous chloride (MAA_0). The synthesised MAA was compared to the commercial MAA for its particle size, radiolabeling and biodistribution properties. The mean particle diameter of MAA_5 (59.9±18.1 µm) was larger than that of MAA_0 (31.9±16.7 µm) and closer to that of the commercial MAA sample (cMAA;

52.9±15.2 μm). This showed that stannous chloride has a strong influence during the particle formation in HSA. Radiolabeling of the synthesized MAA_5 with ^{68}Ga at pH 6 gave good radiolabeling yields (84.5±5.3 %) which were comparable to that of commercial MAA. The *in vivo* biodistribution pattern of ^{68}Ga-MAA_5 was similar to that of ^{68}Ga-cMAA synthesized using the commercially available MAA kit. The uptake of ^{68}Ga-MAA_5 in the lungs at 15 min time point was 82.6±2.1 %ID and that for ^{68}Ga-cMAA was 83.5±2.3 %ID. Cerenkov imaging of ^{68}Ga-MAA_5 showed preferential accumulation of ^{68}Ga-MAA_5 in the lungs at all the time points studied (15 min, 30 min, and 60 min p.i.). Most of the ^{68}Ga activity was localized in the lungs with negligible activity in the liver. Further, six month evaluation of the MAA kit was performed and the biodistribution pattern of the ^{68}Ga labeled kit was similar to that obtained previously.

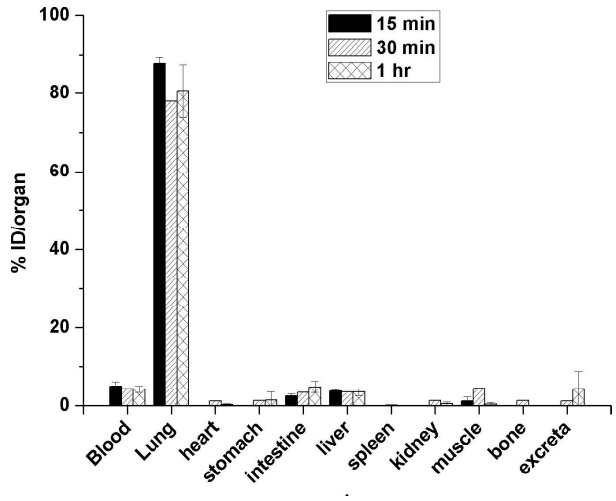

Figure 6: Biodistribution studies of ^{68}Ga-MAA in Swiss mice

References

1. Liu S. The role of coordination chemistry in the development of target-specific radiopharmaceuticals. *Chem Soc Rev.* 2004; 33: 445-461.

2. Ziegle SI. Positron Emission Tomography: Principles, Technology and Recent Developments. *Nucl Phys A*. 2005; 752: 679c-687c.
3. Prata MI, Santos AC, Geraldes CF, de Lima JJ. Structural and in vivo studies of metal chelates of Ga(III) relevant to biomedical imaging. *J Inorg Biochem*. 2000; 79: 359-363.
4. Röesch F, Riss PJ. The Renaissance of the ^{68}Ge/^{68}Ga Radionuclide generator initiates new developments in ^{68}Ga radiopharmaceutical chemistry. *Curr Top Med Chem.* 2010; 10: 1633-1668.
5. Velikyan I. Prospective of ^{68}Ga radiopharmaceutical development. *Theranostics*. 2014; 4: 47-80.
6. Tamaki N, Morita K, Kuge Y, Tsukamoto E. The Role of Fatty Acids in Cardiac Imaging. *J Nucl Med*. 2000; 41: 1525-1534.
7. Corbett JR. Fatty acids for myocardial imaging. *Semin Nucl Med.* 1999; 29: 237–258.
8. Cazzola, E.; Benini, E.; Pasquali, M.; Mirtschink, P.; Walther, M.; Pietzsch, H. J.; Uccelli, L.; Boschi, A.; Bolzati, C.; Duatti, A. Labeling of fatty acid ligands with the strong electrophilic metal fragment $[^{99m}Tc(N)(PNP)]^{2+}$ (PNP=diphosphane ligand). *Bioconjug. Chem*. 2008; 19: 450-460.
9. Walther, M.; Jung, C. M.; Bergmann, R.; Pietzsch, J.; Rode, K.; Fahmy, K.; Mirtschink, P.; Stehr, S.; Heintz, A.; Wunderlich, G.; Kraus, W.; Pietzsch, H. J.; Kropp, J.; Deussen, A.; Spies, H. Synthesis and biological evaluation of a new type of ^{99m}technetium-labeled Fatty Acid for myocardial metabolism imaging. *Bioconjug. Chem*. 2007; 18: 216-230.
10. Zhang J, Yang PL, Gray NS. Targeting cancer with small molecule kinase inhibitors. *Nat Rev Cancer*. 2009; 9: 28–39.

11. Thomasa SM, Grandis JR. Pharmacokinetic and pharmacodynamic properties of EGFR inhibitors under clinical investigation. *Cancer Treat Rev*. 2004;30: 255–268.
12. Hicks JW, VanBrocklin HF, Wilson AA, Houle S, Vasdev N. Radiolabeled small molecule protein kinase inhibitors for imaging with PET or SPECT. *Molecules*. 2010; 15: 8260-8278.
13. Liu S. Radiolabeled multimeric cyclic RGD peptides as integrin alphavbeta3 targeted radiotracers for tumor imaging. *Mol Pharm*. 2006; 3: 472-487.
14. Haubner R, Maschauer S, Prante O. PET radiopharmaceuticals for imaging integrin expression: tracers in clinical studies and recent developments. *Bio Med Res Int.* 2014; 87: 1609.
15. Antony AC. Folate receptors. *Annu Rev Nutr*. 1996; 16: 501-521.
16. Müller C, Schibli R. Folic Acid conjugates for nuclear imaging of folate Receptor-positive cancer. *J Nucl Med*. 2011; 52: 1-4.
17. Alexei A, Bogdanov Jr, Weissleder R, Brady TJ. Long circulating blood pool imaging agents. *Adv Drug Delivery Rev*. 1995; 16: 335–348.
18. Worsley DF, Alavi A. Radionuclide imaging of acute pulmonary embolism. *Semin Nucl Med*. 2003; 33: 259–278.
19. Charidra R, Shamoun J, Braunstein P, DuHov OL. Clinical evaluation of an instant kit for preparation of ^{99m}Tc-MAA for lung scanning. *J Nucl Med*. 1974; 14: 702–705.

LIST OF FIGURES

LIST OF TABLES

CHAPTER 1

INTRODUCTION

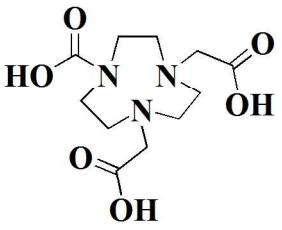

NOTA

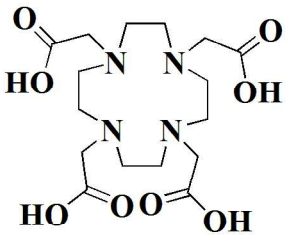

DOTA

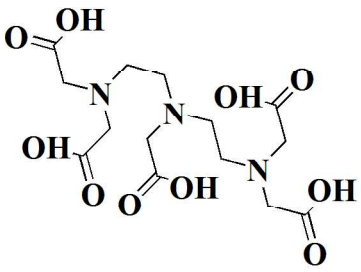

DTPA

Chelators used for radiolabeling with ^{68}Ga

1.1. MOLECULAR IMAGING

Molecular imaging makes visible what would otherwise be invisible and thus helps to reveal the deep hidden truths about the human body. Molecular imaging is a new branch of imaging which enables the visualization, characterization and quantification of biological processes taking place at the cellular and sub-cellular levels in humans and other living systems[1]. It can help in revealing the biology of the disease process and thus help in development of personalize patient care by characterizing specific disease processes in different individuals. It is further useful in drug discovery and development, for example, for studying pharmacokinetics and pharmacodynamics. Molecular imaging differs from the traditional imaging modalities such as X-rays, computed tomography (CT) and ultrasound in that probes known as biomarkers or molecular vectors are used to image particular targets or pathways based on their localization and biological behaviour within the body. While the conventional procedures provide information about the anatomical structure, molecular imaging enables imaging of the *in vivo* functioning of the chemical and biological processes occurring at the cellular level. Unlike the conventional anatomical imaging techniques which can only detect diseases when the structural changes are big enough to be detected, molecular imaging agents have the potential to identify the diseases at much earlier stages. Early detection in turn helps in disease management in a more effective manner. Among the various molecular imaging techniques, '*Nuclear medicine*' that employs '*Radiopharmaceuticals*' is the most popular and promising modality, owing to the simplicity, ease as well as economical aspects involved in its application[1,2].

Molecular imaging in nuclear medicine uses small amounts of radioactive species (radiolabeled molecules, inorganic ions or gases collectively called radiopharmaceuticals) for *in vivo* imaging. Nuclear imaging techniques include Single Photon Emission Computed

Tomography (SPECT), Positron Emission Tomography (PET), autoradiography and a recently developed technique namely Cerenkov radiation imaging.

1.2. RADIOPHARMACEUTICALS

Radiopharmaceuticals are preparations which are of high purity and definite composition containing a radionuclide, that can be used in the diagnosis or monitoring of a disease or physiological functions of the body or for therapy of various diseases[2]. Radiopharmaceuticals can be employed to monitor the functional changes happening *in vivo* and thus form an important part of nuclear medicine. The radiopharmaceuticals can be classified on the basis of their biodistribution characteristics: where the biodistribution depends upon the chemical and physical properties of the radiometal complex[2]. For instance, ^{131}I (Iodine-131) is used routinely for treatment of thyroid cancers. It accumulates in the thyroid since iodine is essential for the biosynthesis of the hormones secreted by the thyroid gland. Another example is ^{99m}Tc labeled macroaggregated albumin (^{99m}Tc-MAA) which by virtue of the particle size of MAA (10-100 μm) gets trapped in the lungs and is used for lung perfusion imaging to assess the presence of emboli and other abnormalities causing obstruction to pulmonary blood flow[3].

Another category of classification of radiopharmaceuticals on the basis of biodistribution is receptor-specific radiopharmaceuticals wherein the *in vivo* localization is determined by their specific biological interactions such as receptor binding, enzymatic reduction etc[2]. This category is best exemplified by peptides or antibodies tagged with radionuclides, which target a specific organ or tissue by virtue of the biological functions of the peptide or antibody. In receptor-specific radiopharmaceutical, a carrier molecule (or biomolecule) which serves as vehicle is tethered to the radionuclide in order to direct the latter to the diseased tissue/cell.

The attachment or the radiolabeling of the biomolecule with the radionuclide of interest can be performed utilising various chemical strategies such as:

Isotope exchange reaction: wherein one or more atoms/molecules of the parent biomolecule are replaced by radioisotopes of the same element. For example: ^{125}I-triiodothryonine (T_3). Since the radiolabeled and the parent molecules are identical except for the isotope effect, they are expected to have same biological and chemical properties.

Introduction of a foreign label: In this type of radiolabeling, a radionuclide is incorporated into a molecule that has a known biological role, primarily by the formation of covalent or coordinate bond. For example,^{177}Lu-DOTMP (1,4,7,10-tetraazacyclododecane-1,4,7,10-tetramethylene phosphonate) is a radiopharmaceutical, in which the ligand DOTMP has affinity for bones. ^{177}Lu incorporates into the cavity of DOTMP by coordinate bonding and ^{177}Lu-DOTMP is used for bone pain palliation therapy.

Labeling with a bifunctional chelator (BFC): In this approach, the biomolecule is conjugated with the BFC which in turn chelates with the radionuclide. Biomolecules are radiolabeled with metallic radionuclides utilising this approach. A typical design of such radiopharmaceuticals consists of: a targeting biomolecule (BM), a pharmokinetic modifying linker (PKM), bifunctional coupling or chelating agent (BFC) and a radionuclide (Figure 1.1). The PKM linker ensures that the biomolecule and the BFC-metal chelate are far apart so as to minimize possible interference of the radiometal on the receptor binding affinity of the biomolecule. The choice of BFC is dictated by the chemical nature and oxidation state of the radionuclide. In addition, the BFC should form a stable complex with the radionuclide in high yields and stability. This approach of radiolabeling a biomolecule using a BFC is the most commonly used approach for designing receptor specific radiopharmaceuticals. This approach combines the ease of direct labelling with the well-defined chemistry of the radiometal and the chelator.

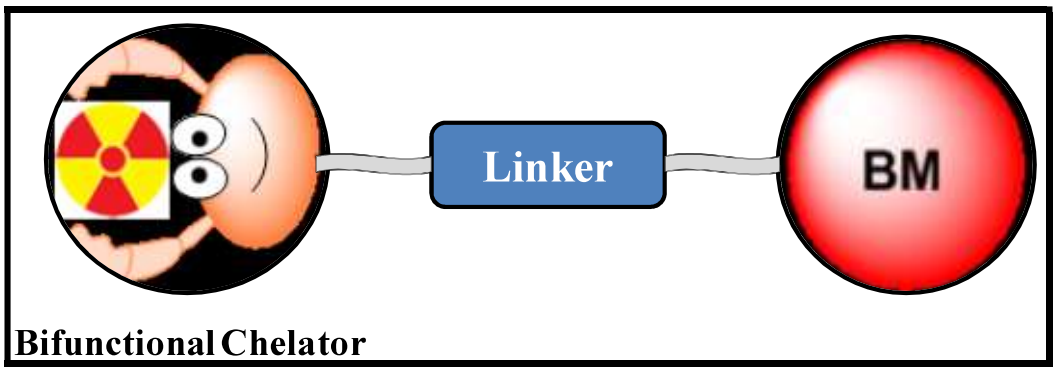

Figure 1.1.Typical design of a radiopharmaceutical using BFC approach

Depending upon the type of radionuclides used, the radiopharmaceuticals are divided into two primary classes: '**diagnostic radiopharmaceuticals**' and '**therapeutic radiopharmaceuticals**'

1.2.1. Diagnostic Radiopharmaceuticals

Diagnostic Radiopharmaceuticals are molecules labeled with gamma emitting isotopes which are employed for single photon emission computed tomography (SPECT) or positron-emission tomography (PET) wherein positron emitting radioisotopes are employed. Diagnostic radiopharmaceuticals are used in very low concentrations, in the range of 10^{-6} M to 10^{-8} M, and hence do not have any pharmacological effect. They are used for imaging of the morphological structure of organs or tissues and physiological functions *in vivo*, through accumulation of radiopharmaceutical. Diagnostic radiopharmaceuticals provide a non-invasive method of assessing the disease or diseased states by SPECT or PET imaging and are also helpful for monitoring the efficacy of a specific therapeutic treatment. SPECT is a nuclear medicine tomographic imaging technique where radiopharmaceuticals containing gamma emitting radionuclides are used for diagnostic purpose. The gamma cameras used for SPECT imaging are fitted with NaI(Tl) detectors which are sensitive to the photons in the range of 80-200 KeV.

PET is another nuclear medicine imaging modality where the imaging agents are radiolabeled with radionuclides that decay by emission of positively charged particles called the positrons (β^+). This imaging technique is based on the coincident detection of two 511 keV gamma rays emitted simultaneously at 180° to each other following the annihilation of the emitted positron with an electron. In PET cameras, the bismuth germanium oxide (BGO) scintillation detectors which are capable of efficiently detecting high energy gamma rays are arranged in a circular array with coincidence circuits designed to specifically detect the 511 keV photons emitted in opposite directions. A few SPECT and PET radioisotopes are listed in Table 1.1 and Table 1.2 respectively.

Table 1.1. List of gamma emitting radionuclides used for SPECT imaging

Radionuclide	**Half-Life**	**E_γ in keV (% Abundance)**
^{99m}Tc	6.02 h	140.5 (89.0)
^{123}I	13.27 h	159.0 (82.8)
^{67}Ga	3.26 d	93.3 (38.3)
^{111}I	2.80 d	245.4 (94.2)
^{201}Tl	72.91 h	167.4 (10.0)

Table 1.2. List of positron emitting radionuclides useful for PET imaging

Radionuclide	Half-Life	E_{max} in MeV (% Abundance)
^{18}F	110 min	0.63 (96.9)
^{11}C	20.4 min	0.96 (99.8)
^{13}N	10.0	1.20 (99.8)
^{15}O	2 min	1.73 (99.9)
^{68}Ga	68 min	1.90 (89.1)
^{64}Cu	12.7 h	0.65 (17.5)

1.2.2. Therapeutic Radiopharmaceuticals

Therapeutic radiopharmaceuticals are radiolabeled molecules which are designed to deliver therapeutic doses of ionizing radiations to specific disease sites (most often cancerous tumors) with high specificity. Radionuclides that decay by particle emission viz. beta emission, alpha emission and Auger electron emission are used in the therapeutic radiopharmaceuticals. For effective therapy, the therapeutic radiopharmaceutical should localize with high specificity at the diseased site in sufficient concentration in order to minimise the radiation damage to normal cells. A list of few alpha and beta emitting radionuclides which are used in the preparation of therapeutic radiopharmaceuticals is presented in Tables 1.3 and 1.4 respectively.

Table 1.3. List of β emitting radionuclides

Radionuclide	Half life (Days)	Max E_β (MeV)	Principal E_γ in KeV (% Abundance)
^{177}Lu	6.7	0.50	11.95 (6.4) 208.36 (11.0)
^{153}Sm	1.9	0.8	103.18 (28.3)
^{131}I	8.0	0.81	364.48 (81.2)
^{186}Re	3.8	1.07	137.16 (8.6)
^{188}Re	0.7	2.11	155.04 (14.9)
^{89}Sr	50.5	1.46	Nil
^{32}P	14.3	1.71	Nil
^{90}Y	2.7	2.27	Nil

Table 1.4. List of α-emitting radionuclides

Radionuclide	Half life (Days)	Max E_α (MeV)	Principal E_γ in KeV (% Abundance)
^{225}Ac	10.00 d	5.93	99.70 (3.5)
^{223}Ra	11.44 d	5.98	269.41 (13.6)
^{213}Bi	45.59 min	5.98	439.70 (27.3)
^{212}Bi	60.55 min	6.21	727.17 (11.08)

1.3. ADVANTAGES OF PET IMAGING

Diagnostic imaging using nuclear medicine relies mainly on two imaging modalities: SPECT and PET. PET radiopharmaceuticals are tagged with radionuclides that decay by emission of positron (β^+). The positron after emission from the parent nucleus, travels a few millimetres through the tissue until it is thermalized by electrostatic interaction with the electrons and the atomic nuclei of the media. The thermalized positron then combines with a free electron in the medium and gets annihilated generating a pair of 511 keV gamma rays which travel in opposite direction. The opposed gamma rays are detected by using a pair of collinearly aligned detectors in coincidence (Figure 1.2). This is called 'coincidence detection' which eliminates the need for physical collimation in PET scanners as the collimation is performed electronically using coincidence detection method.[4] On the other hand, in single-photon imaging, physical collimators are used in order to reject photons that are not within a small angular range (otherwise the angle of incidence will not be known). In physical collimators, the % of emitted photons which are detected (geometric efficiency) is of the order of 0.01% while electronic collimation as in PET improves the efficiency to the order of 1% of the emitted events[4]. This improves the sensitivity of PET by two to three orders of magnitude as compared to SPECT imaging. The increased sensitivity has other associated advantages such as improved image quality due to improvement in signal to noise ratio, possibility of performing shorter scans with multiple field of viewing and also possibility of performing dynamic scanning with improved temporal resolution. Further in PET, there is possibility of quantification of the accumulation of activity in a particular organ as the 511 keV gamma rays are not easily attenuated by the body as compared to the low energy gamma rays detected in SPECT. Thus, higher sensitivity, *in vivo* visualization of physiological processes by dynamic scanning and the quantification of activity by measuring

regional concentration of the radiation source constitute the major advantages of PET imaging over SPECT imaging[5].

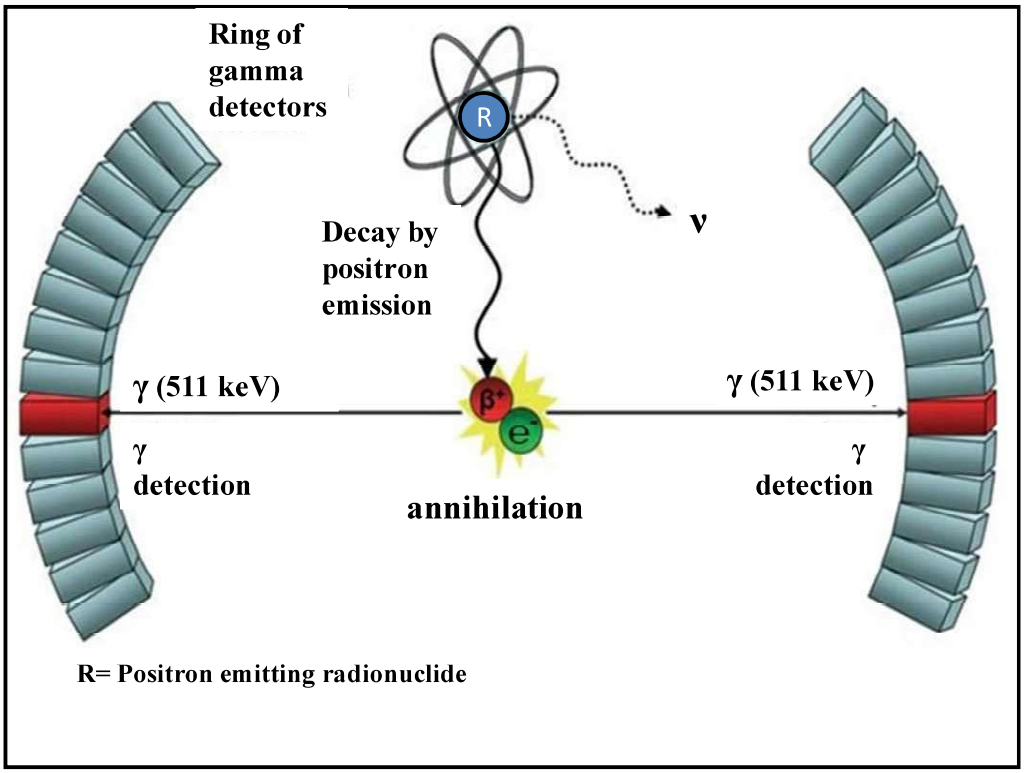

Figure 1.2. Schematic representation of PET principle which shows the positron, after travelling in tissue, annihilates with an electron resulting in two 511 keV γ photons emitted in opposite directions. The 511 keV photons are detected by radiodetectors. *Only photons registered in coincidence are used for image reconstruction.*

A list of positron emitters used for PET imaging is given in Table 1.2. Most of the radionuclides such as ^{11}C, ^{18}F, ^{64}Cu etc. are cyclotron produced which require an onsite cyclotron or shipment from a nearby production site to the place where the investigation is being carried out. The high cost of establishing and maintaining the cyclotron facility increase the final cost of the radiopharmaceuticals. Further, radionuclides such as ^{11}C and ^{18}F are tagged with the biomolecule by covalent bonding due to which the radiolabeling procedures of synthesizing the ^{11}C or ^{18}F based tracers are elaborate with low radiochemical yields. Although automated synthetic modules are available for successful separation of the ^{11}C and ^{18}F based radiotracers in sufficient yields for injection in patients which also serve

protect the working personnel from undue radiation exposure, these modules are exorbitantly priced which has a significant impact on the cost of the final radiopharmaceuticals limiting their widespread use[6].

Amongst the PET radionuclides, ^{68}Ga is available from a ^{68}Ge/^{68}Ga generator which has a long shelf-life, obviating the need of a cyclotron. The radionuclide generators are easily transportable and serve as a convenient source of radionuclide in hospitals/institutions far from the site of cyclotron or reactor facility. Thus, ^{68}Ga is an ideal replacement for other cyclotron-produced PET radionuclides. ^{68}Ga has many other attributes as well which make it a preferred PET radionuclide. The high positron emission fraction (89.14% $E_{\beta+}$(max) =1899 keV; E_{mean}=890 keV) and half-life of 67.71 min of ^{68}Ga provide sufficient levels of radioactivity for high quality images while minimizing the radiation dose to the patient[7]. Besides, the short half-life of ^{68}Ga matches the pharmacokinetics of many peptides and other small molecules resulting in rapid diffusion and localization at the target and fast blood clearance. This ensures that the patient can be discharged from the hospital soon after the diagnostic study. Further, ^{68}Ga is obtained in ionic Ga(III) form from the modern day ^{68}Ge/^{68}Ga generators. In the ionic form, ^{68}Ga(III) can easily complex with ligands in high yields that can satisfy its octahedral coordination sphere with six coordination sites[7]. Owing to the above advantages, research on ^{68}Ga-radiotracers for PET imaging has increased tremendously in the past few years. ^{68}Ga based radiotracers are now routinely used in Europe and other parts of the world for imaging of neuroendocrine tumors and studies linked with somatostatin receptors. A list of ^{68}Ga based radiotracers, in various stages of clinical trials are mentioned in Table 1.5[8].

Table 1.5. List of some ^{68}Ga-radiotracers[8]

Radiotracer	Targeting Organ/ Receptor
^{68}Ga-DOTATOC, ^{68}Ga-DOTANOC, ^{68}Ga-DOTATATE	Somatostatin receptors in neuroendocrine tumors.
^{68}Ga-BPAMD	Bone imaging
^{68}Ga-NOTA-RGD	Tumor Angiogenesis ($\alpha_v\beta_3$integrins)
^{68}Ga-Bombesin analogue (^{68}Ga-BZH$_3$)	Gastrointestinal stromal tumor
^{68}Ga-PSMA	Prostate cancer

This thesis also deals with the development and pre-clinical evaluation of ^{68}Ga based agents for potential diagnostic imaging applications.

1.4. PRODUCTION OF GALLIUM-68

Gallium belongs to group IIIA of the periodic table (Z=31, [Ar]3d^{10} 4s^2 5p^1). 30 different isotopes of gallium are known including two stable, non-radioactive isotopes *viz*. ^{69}Ga and ^{71}Ga with natural abundances of 60.11% and 39.89%, respectively[9]. The widely used radioisotopes in nuclear medicine are ^{67}Ga and ^{68}Ga. ^{67}Ga ($t_{1/2}$=3.3 days) decays by gamma emission and is used for SPECT imaging. ^{68}Ga, as described in Section 1.3, decays by positron emission and is used for PET imaging. It is obtained from a ^{68}Ge/^{68}Ga secular-equilibrium generator system. The relatively long-lived ^{68}Ge ($t_{1/2}$ 270.95 d) decays by electron capture (EC: 100%) to short-lived, ^{68}Ga ($t_{1/2}$ 67.71 min), which subsequently decays to stable ^{68}Zn. The simplified decay scheme of ^{68}Ge is illustrated in Figure 1.3.

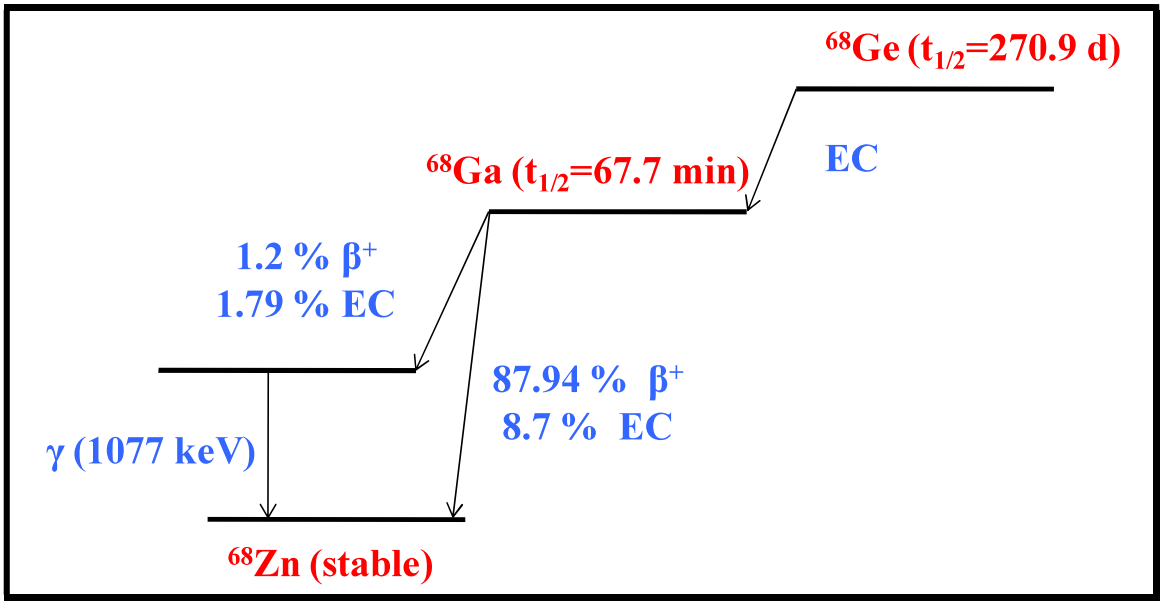

Figure 1.3. Simplified decay scheme of ^{68}Ge *(Energy levels not drawn to scale)*

1.4.1. Production of ^{68}Ge

There are several nuclear reactions used for the production of ^{68}Ge in the cyclotron[10]. In the commercially used process, natural gallium targets are utilized in different forms for the production of ^{68}Ge. The different forms of gallium used are gallium metal encapsulated in niobium container, Ga_2O_3, Ga_4Ni alloy or mixture of gallium metal and Ga_2O_3. The reaction used is $^{nat}Ga(p,xn)^{68}Ge$. A proton beam of 20-30 MeV is used for irradiation. After irradiation, a cooling period of two weeks is given so that the short lived impurities produced such as ^{69}Ge ($t_{1/2}$= 39 h) and ^{67}Ga ($t_{1/2}$=78.3 h) decay with time. The long lived impurities such as ^{88}Y ($t_{1/2}$=106.6 d) and ^{88}Zr ($t_{1/2}$=83.4 d) are removed by chemical extraction of ^{68}Ge wherein ^{68}Ge is extracted into CCl_4 after dissolution of the target in 12 M H_2SO_4. ^{68}Ge is then back extracted into 0.05 N HCl and evaporated to the appropriate volume. No carrier added ^{68}Ge is produced in this manner with 99.9 % or 99.8% radionuclidic purity[10].

1.4.2. ^{68}Ge/^{68}Ga generator

As described above, ^{68}Ge and ^{68}Ga are in secular equilibrium wherein ^{68}Ge (parent) decays to daughter ^{68}Ga which can be periodically removed from the system. In this

$^{68}Ge/^{68}Ga$ system, the time required for maximum growth of daughter activity (^{68}Ga) is 14.1 h. 88-90% growth in ^{68}Ga activity is achieved in 3.4-3.5 h (approximately three half lives of ^{68}Ga). The generator can be eluted in every 3 to 4 h and thus several elutions can be carried out per day which allows for multiple diagnostic imaging procedures each day[11].

The first $^{68}Ge/^{68}Ga$ generator was described by Gleason in 1960 wherein liquid-liquid extraction chemistry was utilized[12]. The liquid liquid extraction did not quantify for a robust route to obtain ^{68}Ga. However, soon after, new improved generator concepts were described utilizing solid phase based column chromatography[13-14]. These generators used alumina column and EDTA (10 mL, 0.005 N) as eluent. As compared to liquid-liquid extraction, no further separation steps were required after elution of the daughter from the column chromatography system. But in these generators, ^{68}Ga was eluted as a Ga-EDTA complex and getting free $^{68}Ga^{3+}$ for preparing the desired radiopharmaceutical from Ga-EDTA was a complex and tedious procedure.

In the 1970s and 1980s, new generators based on column chromatography were developed where inorganic matrices (Me^{IV} O_2-type) were used in the column wherein ^{68}Ge was selectively adsorbed on the solid matrix while ^{68}Ga was selectively desorbed using hydrochloride solutions[15]. In such type of generators, ^{68}Ge, in acidic solution, can be loaded onto the matrix. In acidic solution (pH=1-3), Ge(IV) exists in anionic form $[GeO(OH)_3]^-$, $[GeO_2(OH)_2]^{2-}$, $[[Ge(OH)_4]_8(OH)_3]^{3-}$.[16] These anionic species adsorb by electrostatic attraction on to the positively charged surface of the $Me^{IV}O_2$ matrix surface[17,18]. ^{68}Ga, in cationic form, is then eluted from the generator using mild to strongly acidic solutions. Based on this concept, radiochemists at Obninsk, Russian Federation, in the first years of 21st century, developed a commercial $^{68}Ge/^{68}Ga$ generator with "modified TiO_2" as the column matrix which could be eluted using 0.1 N HCl. Since then many generators based on the

concept of adsorption of ^{68}Ge and desorption of ^{68}Ga were developed with diverse inorganic and organic column matrices and a list of such ^{68}Ge/^{68}Ga generators are given in Table 1.6.

Table 1.6. List of ^{68}Ge/^{68}Ga generator based on ^{68}Ge adsorption and ^{68}Ga desorption[12]

Source	Column Matrix	Eluent
Obninsk Cyclotron Ltd., Russia	TiO_2	0.1 N HCl
iThemba, South Africa	SnO_2	0.6-1 N HCl
Isotope Technologies Garching (ITG), Germany	SiO_2/ Organic matrix	0.05 N HCl
Eckert and Ziegler, USA	TiO_2	0.1 N HCl
BARC generator	Nanoceria-Polyacrylonitrile	0.1 N HCl

With the advent of these commercial ionic generators, research on ^{68}Ga based radiopharmaceuticals has increased by leaps and bounds. The number of publications devoted to ^{68}Ga radiopharmaceuticals in basic and clinical research has increased significantly during the last few years[7,8]. As many new ^{68}Ga radiopharmaceuticals are entering the clinical arena, concerns have been raised on the quality and the characteristics of the ^{68}Ga eluate obtained from the above generator systems such as

a) **High volume and acidic eluate**: Most of the ^{68}Ge/^{68}Ga generators are eluted using large volumes of acidic solutions. The large generator eluate volume would require large amount of ligand and long heating time for radiolabeling resulting in sub-optimal ^{68}Ga incorporation. Further, high concentration of H^+ ions in the eluate protonate the donor atoms of the gallium chelator thereby preventing the metal-ligand complex formation[7].

b) **^{68}Ge breakthrough**: Since the ^{68}Ge/^{68}Ga generators are mostly eluted with HCl solutions, it has been observed that with the passage of time, ^{68}Ge breakthrough takes place due to which the content of ^{68}Ge in the ^{68}Ga eluate increases (10^{-3}% of ^{68}Ga activity is the permissible limit for the ^{68}Ge in the ^{68}Ga eluate[5]). The column material also tends to degrade with time due to multiple elutions using acidic solutions leading to the presence of ions such as Ti and Sn in the eluate which tend to affect the yields of the ^{68}Ga radiopharmaceutical.

c) **Cationic impurities:** Certain cationic impurities such as ^{68}Zn(II) are also present in the ^{68}Ga eluate , generated by decay of ^{68}Ga. In situations wherein the generator is not eluted regularly, the concentration of ^{68}Zn(II) ions increase in the ^{68}Ga eluted subsequently. Fe(III), as a common chemical impurity is also present if highly pure reagents are not used in every step of the process. Both of these cationic impurities can compete with ^{68}Ga(III) for complexation with the chelators.

Thus, in order to use many of the commercial generators for clinical applications, certain post-elution processing methods are employed so also to decrease the concentration of ^{68}Ge as well as the cationic impurities in the ^{68}Ga eluate. The post-elution processing methods are briefly discussed below[7,19].

a) **Fractionation**: As large volumes of ^{68}Ga eluate would lead to low radioactive concentration of ^{68}Ga, fractionation of the eluate is carried out to obtain high radioactive concentration of ^{68}Ga in the eluate which is required for achieving high radiolabeling yields. The fraction of the eluate containing the maximum ^{68}Ga activity is used for further complexation reactions. This elution volume varies for different generators and is typically of the order of 1.5 ± 0.5 mL. Fractionation ensures small eluate volume for radiolabeling and also minimizes the concentration of trace metal impurities in the eluate.

b) **Anion-Exchange based post-processing**: This approach is usually adopted for TiO_2 based $^{68}Ge/^{68}Ga$ generators. The eluate is added to an HCl reservoir so that its overall concentration reaches ~4-5 N. This concentrated solution is then passed through the anion exchange column. In 4 M HCl medium, $[^{68}GaCl_4]^-$ complex is formed which is adsorbed onto the column. On the other hand, Ge(IV) forms the anionic complex at the molarity above 5 and is thus not retained on the resin and passes through. Other impurities like Al, In and Ti cations also pass through without getting adsorbed onto the column. ^{68}Ga is then eluted using small volumes of water, saline or NaOH solution, which tend to strip chloride off the gallium cations. This process concentrates the eluate volume and also reduces the concentration of trace metal impurities in it.

c) **Cation exchange based post-processing**: Here, the generator eluate (0.1-0.6 N HCl) is passed through a small cation exchange resin wherein $^{68}Ga^{3+}$ is adsorbed onto the column while other cations are not adsorbed. Further, a mixture of mineral acid and organic solvent like HCl with acetone or HCl and ethanol are used for desorption of ^{68}Ga from the column. Typically, the cation exchange cartridge is washed by 80% acetone/20% 0.15 N HCl solutions to remove the trace metal impurities. Further, ^{68}Ga is eluted in small amount of 98% acetone/2% 0.05 N HCl[11]. The acetone is removed completely before ^{68}Ga radiolabeling.

These post-elution processing procedures ensure that the ^{68}Ga eluate used has the minimum concentration of trace metallic impurities and also has high radioactive concentration of ^{68}Ga (maximum activity in minimum volume).

1.4.3. $^{68}Ge/^{68}Ga$ generators used in the present thesis

In this thesis, preparation of ^{68}Ga based agents was carried out using two different $^{68}Ge/^{68}Ga$ generators. The details of the generators used are given below.

a) **iThemba ^{68}Ge/^{68}Ga generator**: For some studies a 925 MBq (25 mCi) iThemba generator was used which contains tin oxide as the column material which stably retains the parent ^{68}Ge. Since this generator is eluted using 0.6 N HCl, chances of ^{68}Ge breakthrough are high in its eluate. Post-elution processing was performed using fractionation method. Towards this, initially, the generator column was washed with 0.5 mL of 0.6 N HCl to remove stable ^{68}Zn(II) ions and also other metal ion impurities. Then, the generator was eluted with 2 mL of 0.6 N HCl. The ^{68}Ga activity in each fraction was measured using the dose calibrator. It was observed that ~ 70-80% of the ^{68}Ga activity was obtained in the second fraction which was further used for radiolabeling.

b) **Nanoceria-polyacrylonitrile column based BARC generator**: The second generator used for the preparation of ^{68}Ga based agents described in this thesis was an in-house developed 740 MBq (20 mCi) nanoceria-polyacrylonitrile (nanoceria-PAN) sorbent based ^{68}Ge/^{68}Ga generator. $^{68}GaCl_3$ was eluted from the generator with 2 mL of 0.1 N HCl and directly used for radiolabeling. The levels of ^{68}Ge and trace metal contaminants in the ^{68}Ga eluted from this generator were estimated previously by our group[20]. The levels of ^{68}Ge in the ^{68}Ga eluate was less than 10^{-4} % and the levels of trace metal ions in decayed samples of ^{68}Ga, as analyzed by ICP-AES, were found to be below detectable limits[20-22].

1.5. CHEMISTRY OF GALLIUM

Gallium belongs to group 13 of the periodic table. Its solution chemistry is exclusively represented by its stable oxidation state +III. Its +I oxidation state has no relevance under aqueous conditions. The free hydrated Ga(III) cation is only stable under acidic conditions. It hydrolyses to insoluble $Ga(OH)_3$ in the pH range of 3-7 which further redissolves as $[Ga(OH)_4]^-$ at pH > 7. $Ga(OH)_3$ is amphoteric in nature and dissolves in both

acidic as well as in alkaline medium. During the preparation of ^{68}Ga radiopharmaceuticals, the hydrolysis and formation of insoluble gallium hydroxide can be avoided by using weak stabilizing ligands such as citrate, acetate or oxalate which can stabilize the Ga(III) ion by ligand-exchange reaction[9].

The Ga(III) cation is a Lewis acid due to its high charge density and small ionic radius (0.62 Å) and is known to chelate with highly ionic and non-polarisable hard Lewis bases containing nitrogen and oxygen donor atoms. Thus, ligands with carboxylate, phosphonate, hydroxamate and amine functionalities form thermodynamically stable complexes with Ga(III). However, there are also reports of Ga(III) forming complexes with soft donor atoms such as phenolate and thiol groups as well. Owing to its small cationic radius, Ga(III) usually forms a six co-ordinated distorted octahedron. Although gallium is known to form four and five coordinated complexes as well, these complexes are coordinatively unsaturated and are more prone to ligand exchange hydrolysis[9].

1.6. CHELATORS FOR GALLIUM

The labelling of biomolecules with radiometals such as gallium can be direct (introduction of foreign label) or chelator-mediated. Direct labelling with ^{68}Ga is limited to molecules such as proteins (lactoferrin, transferrin, ferritin) which are designed for iron binding. Since the coordination chemistry and the biological properties of Ga(III) are similar to that of Fe(III) because of their comparable ionic radii (0.65 Å for Fe(III)), charge and also no ligand field stabilization energy (on complexation with weak field ligands), proteins such as lactoferrin, transferrin and ferritin can be directly labeled with ^{68}Ga. Particulate agents such as macroaggregated albumin or carbon nanotubes can also be directly labeled with ^{68}Ga. These agents are mostly used for perfusion imaging or for imaging of biological processes where the uptake of the tracers is governed by factors such as their charge, lipophilicity and size[5].

For chelator-mediated labelling, the chelator should have characteristics such as

a) It should form thermodynamically stable and kinetically inert complexes to avoid trans-metallation or hydrolysis *in vivo*.
b) The chelation of radiometal with the ligand should be rapid and efficient and at a pH wherein the biomolecule does not degrade[9].

When injected into a biological system, there are high chances of transchelation of ^{68}Ga labelled molecules due to the presence of proteins such as transferring, lactoferrin and ferritin in the biological system. Also, there are chances of transmetallation by endogenous metal ions such as Ca(II) and Zn(II). For these reasons, ^{68}Ga complexes must be sufficiently inert for *in vivo* applications since loss or dissociation of the radiometal complex results in undue dose to the non-target organs as well as poor image quality.

Gallium-68 labeling is performed using two classes of chelators namely acyclic or open chain chelators and macrocyclic chelators. Macrocyclic chelators form thermodynamically stable complexes as compared to the acyclic chelators. This is because macrocyclic chelators require minimum physical changes during metal ion coordination, as they possess a pre-organized geometry and have sufficient metal ion binding sites, thereby decreasing the entropic loss experienced upon metal ion coordination[24]. In case of acyclic chelators, they undergo drastic physical changes in orientation as well as geometry in solution in order to arrange the donor atoms to coordinate with the metal ion. Thus, acyclic chelators suffer more significant decrease in entropy as compared to the macrocycles (thermodynamically unfavourable). The thermodynamic driving force for chelation is greater for macrocycles which is called macrocyclic effect.

For *in vivo* applications, kinetic stability, which is the measure of free energy of activation of the reaction, is more important than thermodynamic stability. This is because there are multiple challenging ligands and challenging metal ions *in vivo* whereby there is a

possibility of occurrence of ligand exchange leading to dissociation of metal complex and liberation of free radiometal which can accumulate at undesirable sites. Generally, acyclic complexes are less kinetically inert and more prone to transchelation than the macrocyclic complexes. Macrocyclic complexes have slow rate of dissociation in presence of competing metal ions as well as competing chelators.

At the same time, acyclic chelators, because of their flexible geometry, have fast coordination kinetics and radiolabeling efficiency. Acyclic chelators are able to quantitatively coordinate with the radiometal is less time as compared to their macrocyclic counterparts which often require heating for extended times for complexation with the radiometal. Fast room temperature radiolabeling (as observed for acyclic chelators) is preferred when biomolecules such as heat-sensitive proteins and radioisotopes with short half-life like ^{68}Ga are under consideration.

Few of the acyclic chelators used for the preparation of ^{68}Ga radiopharmaceuticals are ethylenediaminetetraacetic acid (EDTA), diethylene triaminepentaacetic acid (DTPA), *N,N'*-di(2-hydroxybenzyl)ethylenediamine-*N,N'*-diacetic acid (HBED), desferrioxamine (DFO) etc.

The macrocyclic chelators commonly used for ^{68}Ga labelling are 1,4,7-triazacyclononane-1,4,7-triacetic acid (NOTA), 1,4,7,10-tetraazacyclododecane-1,4,7,10-tetraacetic acid (DOTA), 1,4,7-triazacyclononane-1,4,7-tris[methyl(2-carboxyethyl)phosphinic acid] (TRAP), 1,4,7-triazacyclononane-1-[methyl(2-carboxyethyl)phosphinic acid]-4,7-bis[methyl(2-hydroxy- methyl)phosphinic acid] (NOPO), 1,4,7-triazacyclononane,1-glutaric acid-4,7-acetic acid (NODAGA) etc.

The formation constants (log K) of the Ga complexes with these chelators indicating the thermodynamic stability of the metal-chelate complexes are given in Table 1.7.

Table 1.7. Stability constants ($logK_{ML}^{a}$) for complexes of selected chelators with Ga^{3+}

Chelator	log K_{ML}
Transferrin[9]	20.3
EDTA[9]	21.7
DTPA[23]	25.5
DOTA[23]	21.3
NOTA[23]	31.0
TRAP[24]	26.2
HBED[24]	38.5
DFO[24]	28.6

$^{a}K_{ML} = [ML]/[M][L]$

In this thesis for complexation of ^{68}Ga(III), three chelators have been studied namely DTPA, NOTA and DOTA (Figure 1.4). The acyclic chelator DTPA was chosen as it has fast chelation kinetics and is amenable for conjugation of ^{68}Ga with biological vectors prone to degradation. In addition, acyclic and cyclic chelators were chosen so as to have a comparison of the influence of their conjugation on the pharmacokinetics and the *in vivo* stability of the respective radiotracer.

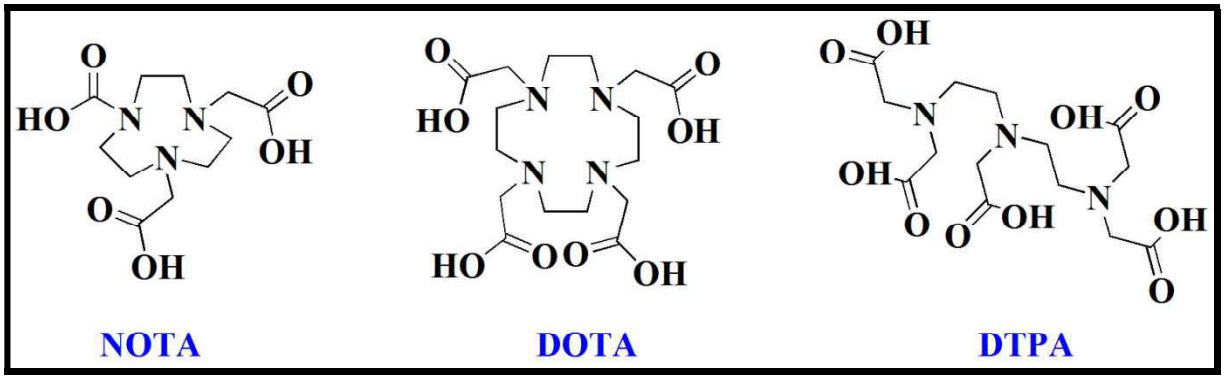

Figure 1.4. Basic structure of the chelators studied in the present thesis

NOTA was chosen as its complex with ^{68}Ga has a high thermodynamic stability constant. NOTA is also known to complex with gallium at ambient temperature. The thermodynamic stability constant of Ga-NOTA is much higher than that of DOTA inspite of both being macrocycles. Further, the reaction time and temperature required for complexation of ^{68}Ga with DOTA (90-100°C heating for 10-15 min) is higher than that with NOTA (ambient temperature radiolabeling within 5-10 min). This is because the 12-membered ring of DOTA is larger than the 9-membered ring of NOTA and thus DOTA needs a higher ring distortion than NOTA to co-ordinate with $^{68}Ga^{3+}$. The cavity size of NOTA and the ionic size of Ga(III) cation are a good match which leads to high stability and selectivity for Ga(III)[25]. Although NOTA is particularly suitable for complexation with ^{68}Ga(III) ion, DOTA was also chosen as it can coordinate with large metallic radionuclides such as ^{213}Bi, $^{86/90}$Y, ^{89}Zr or ^{177}Lu. Thus, use of DOTA as chelator could pave way for imaging or targeted radionuclide therapy applications using the same DOTA-biomolecule (Theranostics).

Since gallium forms six coordinated complexes, its coordination sphere is either N_3O_3 type or the N_4O_2 type with the macrocyclic NOTA and DOTA ligands[26]. The *fac*-N_3O_3type coordination sphere is formed in Ga-NOTA complex with N_{ax}-Ga-O_{ax} bonding. Since three oxygen atoms are involved in complex formation, NOTA forms a neutral complex with Ga(III). Incase of DOTA, *cis*-N_4O_2 type coordination sphere is formed with N_{ax}-Ga-N_{ax}

bonding. At physiological pH, it is observed that one of the free –COOH groups of DOTA deprotonate and it balances the charge of Ga(III) ion forming a neutral Ga-DOTA complex[26]. In case of DTPA, neither single crystal structure analysis nor solution conformational studies have been performed to date to elucidate the coordination geometry of the Ga(DTPA) complex in detail[9].

1.6.1. Bifunctional chelator strategy

Once the chelator has been selected, the chelate has to be functionalized to allow its covalent attachment to the biomolecule. Such functionalized chelators are called 'Bifunctional Chelators (BFC)' as they serve dual purpose: conjugation with biomolecule and complexation with radiometal. In most cases attachment of the chelate-fragment to the biomolecule involves one of its coordinating acetate pendant arms via formation of amide bonds with the primary amine functionality of biomolecules. But this strategy may have an influence on the metal binding. As in case of NOTA, it may change the coordination number of the resulting complex thereby adversely impacting its *in vivo* stability.

Further, for fast and efficient conjugation under mild reaction conditions which would be suitable for maintaining the biological properties of the biomolecule, activated groups such as aromatic isothiocyantes, isocyanates and carboxylic acids as active esters, mixed anhydrides, or azide functionalities etc. are introduced into the chelator backbone[27]. These conjugation groups are electrophiles which require a nucleophilic centre in the biomolecule. Use of ligands containing aromatic isothiocyanates, isocyanates and carboxylic acids aids in carrying out the conjugation reactions under mild aqueous conditions close to physiological pH, short reaction times and minimum purification steps are required to obtain the radiolabeled product.

Two different approaches can be used to introduce the activated group into the chelator:

a) In some cases a pendant arm of the chelator is functionalized such that it consists of both the chelating group and a conjugating functionality. This approach enables coupling with the biomolecule without compromising the stability of the respective metal complex. Such an approach was used with *p*-SCN-Bn-NODAGA (*S*-2-(4-isothiocyanatobenzyl)-1,4,7-triazacyclononane-1-glutaric acid-4,7-acetic acid), which is a derivative of NOTA and has been used for the preparation of ^{68}Ga complexes described in this thesis (Figure 1.5). Here, the functional group is an isothiocyanate group which can readily conjugate with the primary amine group of the biomolecule at mildly alkaline conditions.

b) In another approach, the functional group used to couple with the biomolecule can be introduced in the methylenic backbone of the chelator leaving the carboxylic pendant arms available for coordination with the metal. Four such BFCs were studied in the present thesis namely *p*-SCN-Bn-NOTA (*S*-2-(4-isothiocyanatobenzyl)-1,4,7-triazacyclononane-1,4,7-triacetic acid), *p*-SCN-Bn-DOTA (*S*-2-(4-isothiocyanatobenzyl)-1,4,7,10-tetraazacyclododecane-1,4,7,10-tetraacetic acid), *p*-SCN-Bn-DTPA (*S*-2-(4-isothiocyanatobenzyl)-diethylenetriaminepentaacetic acid) and *p*-NH_2-Bn-NOTA (*S*-2-(4-aminobenzyl)-1,4,7-triazacyclononane-1,4,7-triacetic acid) the chemical structures of which are given in Figure 1.5.

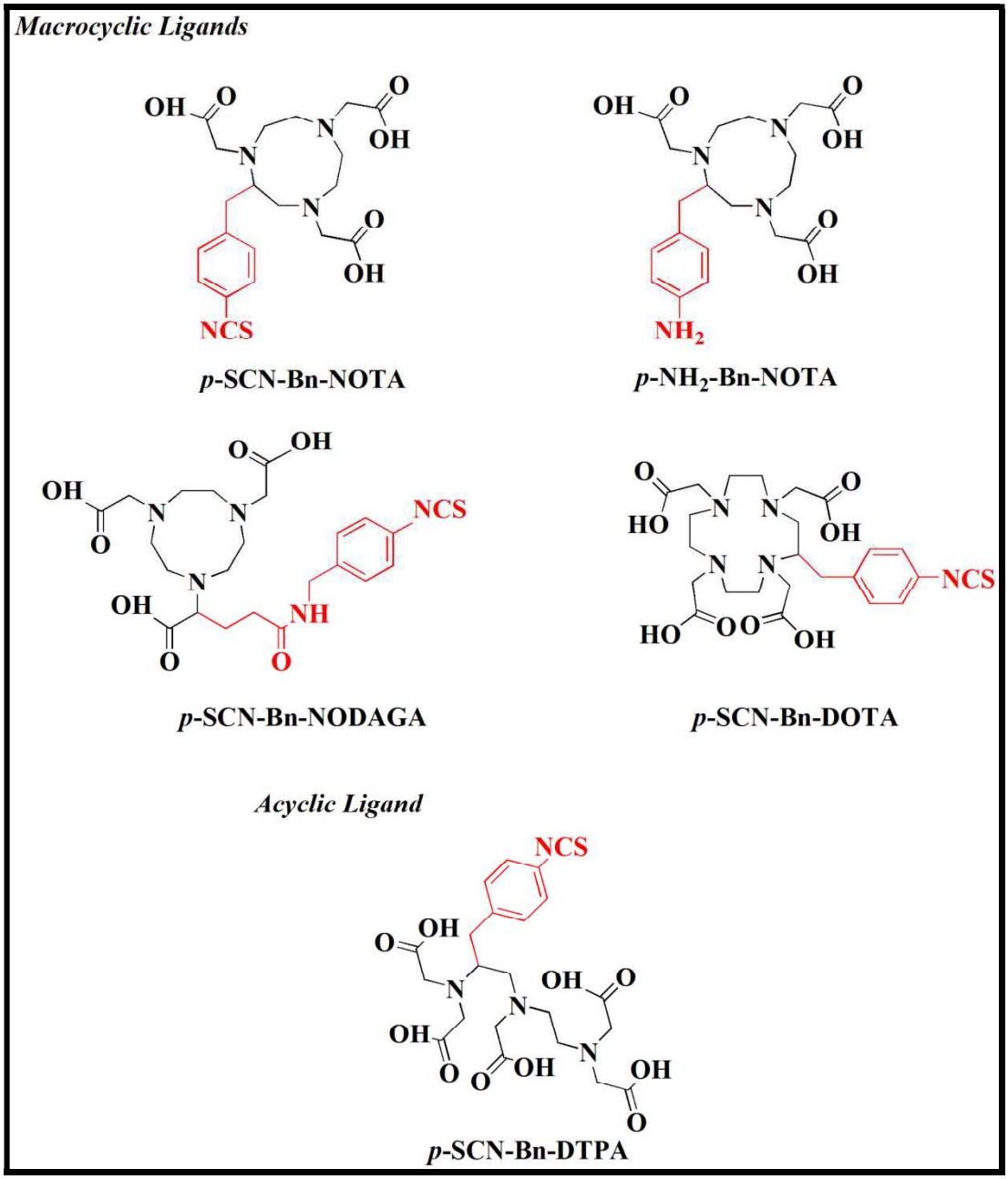

Figure 1.5. Bifunctional chelators studied in the present thesis

1.7. BIOMOLECULES USED IN THE PRESENT STUDY

The biomolecule used in the radiopharmaceutical preparation decides the target directing property and imparts target-specificity to it. It is therefore often termed as the 'biological vector'. While preparing radiopharmaceuticals, it is important to bear in mind that the modifications if any carried out in the structure of biomolecule should be such that they cause minimal damage to its biospecificity or uptake. As discussed before (Section1.2), the

targeting properties of the radiopharmaceuticals are dependent upon the chemical or physical properties of the biomolecule, or upon the biological affinity of the biomolecule. The work carried out and outlined in the thesis describes the use of three different types of carrier molecules viz. fatty acids, receptor-specific biomolecules and human serum albumin macromolecule. Fatty acids are known to target the heart by virtue of their affinity for the heart cells and also due to their lipophilicity. The receptor-specific biomolecules studied in the present thesis are Erlotinib which is a small molecule Epidermal Growth Factor-Tyrosine Kinase Inhibitor (EGFR-TKI), RGD (Arginine-Glycine-Aspartic Acid) peptide having high affinity towards integrin $\alpha_v\beta_3$receptors over-expressed in numerous cancers and folic acid having high affinity for folate receptors over-expressed in many tumor cells. Another carrier molecule studied was human serum albumin (HSA) in two different forms mainly as a long chain protein chelated with the BFC which targets the blood pool *in vivo* by virtue of its molecular weight as well as in the form of macro-aggregates with particle size in the 10-100 μm range, which localise in the lungs by virtue of their size. All these carrier molecules were synthesized or synthetically derivatized to incorporate ^{68}Ga.

1.8. QUALITY CONTROL OF RADIOTRACERS

Quality control of radiotracers is mandatory before they can be administered as *in vivo* injectable preparation. Quality control procedures involve several specific tests and measurements that ensure the purity, potency, product identity, biological safety and efficacy of the radiopharmaceuticals[28]. These procedures include tests for radiochemical purity, radionuclidic purity and chemical purity as well as general tests relevant for pharmaceutical safety. The quality control tests for radiopharmaceuticals are therefore categorized into physiochemical and biological tests.

1.8.1. Physiochemical tests

Various physiochemical tests are performed to check the parameters such as pH, physical appearance etc. and chemical parameters such as radiochemical purity, radionuclidic purity, chemical purity, specific activity and radioactive concentration during the quality control of a radiopharmaceutical. The pH of the radiopharmaceutical is determined using the pH paper. Generally, the pH of the radiopharmaceutical preparation should be between 7 and 8 from the perspective of suitability for *in vivo* administration. The radiopharmaceutical preparation is visually inspected to check for turbidity or suspended particles and is certified with respect to visual clarity.

(a) Chemical Purity

Chemical purity of a radiopharmaceutical refers to the proportion of the radiopharmaceutical that is in the specified chemical form regardless of the presence of radioactivity. Chemical impurities may come in a radiopharmaceutical preparation as some undesired species present in the ligand or radioactivity used for labelling or due to decomposition of the materials before and after radiolabeling. The presence of chemical impurity may affect the radiolabeling thus resulting in undesired labeled molecules or may directly produce adverse biological effects. In the present thesis, purification of ligands used for ^{68}Ga labelling was carried out using column chromatography and semi-preparative HPLC (High Performance Liquid Chromatography). Further, chemical purity evaluation of the ligands was carried out using NMR and ESI-MS analysis.

(b) Radionuclidic purity

Radionuclidic purity of the radiopharmaceutical refers to the percentage of total radioactivity due to the specific radionuclide. Radionuclidic impurities can originate from extraneous nuclear reactions as a result of isotopic impurities present in the target material or due to the fission process occurring in a reactor. The radionuclidic purity is an important

factor as the presence of extraneous radionuclides as impurities increases the radiation dose to the patient as well as impacts the image quality. Thus, accurate determination of the level of radionuclidic impurity is very important and it is mostly assessed by γ-spectrometry using HPGe detector.

(c) Radiochemical purity

Radiochemical purity (RCP) of a radiopharmaceutical is defined as the percent of the total radioactivity present in the desired radiochemical form. Radiochemical impurities in a radiopharmaceutical preparation can come from the chemical impurities present in the target ligand which gets radiolabeled inadvertently or from its decomposition of the radiopharmaceutical on storage due to the action of the solvent, change of temperature and pH, presence of oxidizing or reducing agents and radiolysis. Radiochemical purity is an important factor to be considered in the radiopharmaceutical preparation since it determines the *in vivo* biodistribution of the agent. Radiochemical impurities will have different patterns of biodistribution which may obscure the diagnostic image and increase undue radiation exposure to the patient. Presence of radiochemical impurities in a therapeutic radiopharmaceutical would result in undesired radiation dose to the non-target organs. Radiochemical purity is assessed by a variety of analytical techniques such as liquid chromatography, paper chromatography, thin-layer chromatography and electrophoresis. In the present thesis, some of these techniques viz. paper chromatography and HPLC were used to characterize and determine the extent of radiochemical impurities present in various ^{68}Ga labeled preparations.

The HPLC system used for characterising the radiolabeled preparations was a JASCO PU 2080 Plus dual pump system (JASCO, Japan) equipped with a JASCO 2075 Plus tunable absorption detector and Gina Star radiometric detector system (Raytest, Germany), using a C18 reversed phase HiQSil (5 µm, 4 ×250 mm) column. Radiochemical purity (RCP) of the

^{68}Ga-complexes was determined by peak area measurements in the elution profile using the GINASTAR software (Raytest, Germany).

1.8.2. Biological tests

Biological quality control tests of radiopharmaceuticals are essentially identical with that of non-radioactive, pharmaceutical preparations and these include the determination of sterility, toxicity and apyrogenicity of the radiolabeled preparations.

In order to determine the stability and efficacy of the radiolabeled agents, preliminary bio-evaluation studies are carried out. These involve *in vitro* evaluation of the radiolabeled agents in serum and in cancer cell lines and *in vivo* evaluation of the agents in normal animals and/or animals bearing specific tumors. For example, the analogues of the Erlotinib molecule prepared in the present thesis were evaluated in A431 cells, which over-express epidermal growth factor receptors. Similarly, RGD analogues were evaluated in melanoma bearing C57BL/6 mice.

1.9. THESIS OUTLINE

This thesis describes the preparation of novel ^{68}Ga labeled radiopharmaceuticals for targeting various organs as well as tumors. In this respect biomolecules such as fatty acids, Erlotinib, RGD peptide, folic acid, human serum albumin (HSA) and HSA macro-aggregates were used for preparation of the ^{68}Ga radiopharmaceuticals.

Chapter 2 deals with the synthesis and preclinical evaluation of ^{68}Ga labeled fatty acids for heart imaging. In order to investigate the effect of chain length of the fatty acid on the myocardial uptake of the ^{68}Ga labeled fatty acids, three different fatty acid chains were studied viz. 11 carbon chain (11-aminoundecanoic acid), 12 carbon chain (12-aminododecanoic acid) and 16 carbon chain (16-hexadecanedioic acid) fatty acids. These fatty acids were conjugated with the chelator NOTA for ^{68}Ga radiolabeling. Further in order to study the influence of BFCs on the pharmacokinetics of the ^{68}Ga labeled fatty acids, three

different BFC *viz. p*-SCN-Bn-NOTA, *p*-SCN-Bn-NODAGA and *p*-SCN-Bn-DTPA were conjugated with 11-aminoundecanoic acid, radiolabeled with ^{68}Ga and their myocardial uptake assessed in Swiss mice.

Chapter 3 is divided into three parts and deals with three different molecular vectors namely Erlotinib, RGD (arginine-glycine-aspartic acid) peptide and folic acid for targeting receptor over-expression on specific tumors.

In Chapter 3a, two different analogues of Erlotinib were prepared namely NOTA-Erlotinib and NODAGA-Erlotinib conjugates. They were radiolabeled with ^{68}Ga and their biological efficacy was evaluated in A431 cells.

In Chapter 3b comparative evaluation of dimeric cyclic RGD peptide E[c(RGDfK)]$_2$ conjugated with *p*-SCN-Bn-NOTA, *p*-SCN-Bn-DOTA and *p*-SCN-Bn-DTPA was performed. The role of BFCs on the radiochemistry, *in vitro* stability, pharmacokinetics, tumor targeting properties and metabolic stability of the final radiotracers was evaluated.

In Chapter 3c, NOTA conjugated folic acid was synthesized and the radiolabeled with ^{68}Ga. Further, its *in vitro* cell binding studies in KB cells (which over-express the FR) and preliminary biodistribution studies in normal Swiss mice were carried out.

Chapter 4 is divided into two parts:

In Chapter 4a, HSA molecule was conjugated with *p*-SCN-Bn-NOTA and *p*-SCN-Bn-DOTA and the resulting conjugates were evaluated in Swiss mice for blood pool imaging.

In Chapter 4b, indigenous development of MAA and its radiolabeling with ^{68}Ga for PET based lung scanning was done. Further, Cerenkov imaging of Swiss mice injected with ^{68}Ga-MAA was done. Also, six month evaluation of the indigenously prepared MAA kit was done by radiolabeling it with ^{68}Ga and evaluating its pharmacokinetics in Swiss mice.

CHAPTER 2

SYNTHESIS OF ^{68}GA LABELED FATTY ACIDS FOR CARDIAC METABOLIC IMAGING

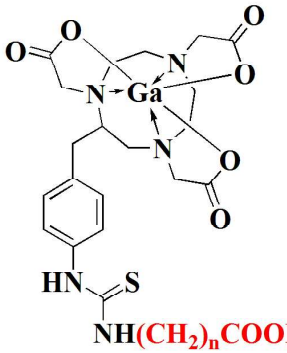

n=10; ^{68}Ga-NOTA-undecanoic acid
n=11; ^{68}Ga-NOTA -dodecanoic acid

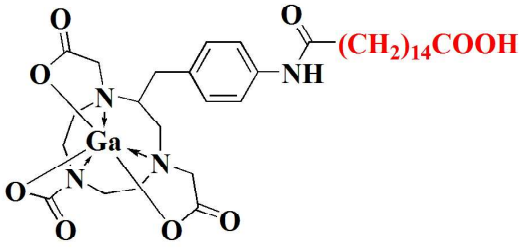

^{68}Ga-NOTA-hexadecanoic acid

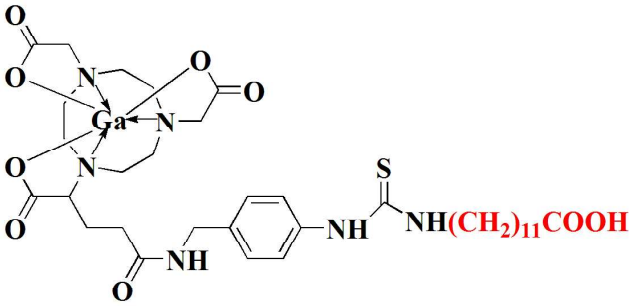

^{68}Ga-NODAGA-undecanoic acid

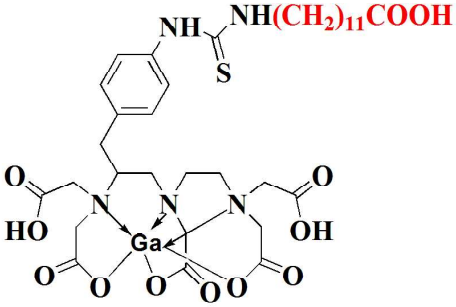

^{68}Ga-DTPA-undecanoic acid

^{68}Ga-fatty acids studied in the present chapter

2.1. INTRODUCTION

Long chain fatty acids are the principle energy sources for normal myocardium and most of the adenosine triphosphate (ATP) produced in aerobic myocardium is derived from fatty acid oxidation[29]. Fatty acids readily pass through the cellular membrane of the myocytes by passive diffusion or via protein carrier mediated pathway. These protein carriers include fatty acid translocase (FAT)/CD36, fatty acid binding protein (FABPpm) and fatty acid transport protein (FATP) where FAT/CD36 plays a major role in the translocation of fatty acids into the cytoplasm of the myocytes. Once inside the cytoplasm, the fatty acids are converted into long-chain fatty acyl CoA esters by fatty acyl CoA synthetase and ATP. The long chain fatty acyl CoA esters can enter the triglyceride pool and be used for synthesis of intracellular lipids or the fatty acid moiety can be transferred to the mitochondria. Carnitine palmitoyl transferase (CPT) 1 enzyme catalyses the conversion of long chain fatty acyl CoA ester to long chain fatty acyl carnitine which is then shuttled into the mitochondria by carnitine translocase. Once inside the mitochondria, fatty acyl carnitine is converted back to fatty acyl CoA ester by CPT 2. The fatty acyl CoA ester is then oxidized by β-oxidation inside the mitochondria. Each cycle of β-oxidation results in shortening of the fatty acyl moiety by two carbons and in the production of acetyl CoA. The acetyl CoA produced enters the tricarbonic acid (TCA) cycle for further oxidation to become water and carbon dioxide[29,30]. The energy produced due to the oxidation of fatty acids is higher than that produced due to the oxidation of glucose. However, activation of free fatty acids for oxidation is an energy driven process[31].

A schematic diagram depicting the metabolism of fatty acids in heart cells is given in Figure 2.1.

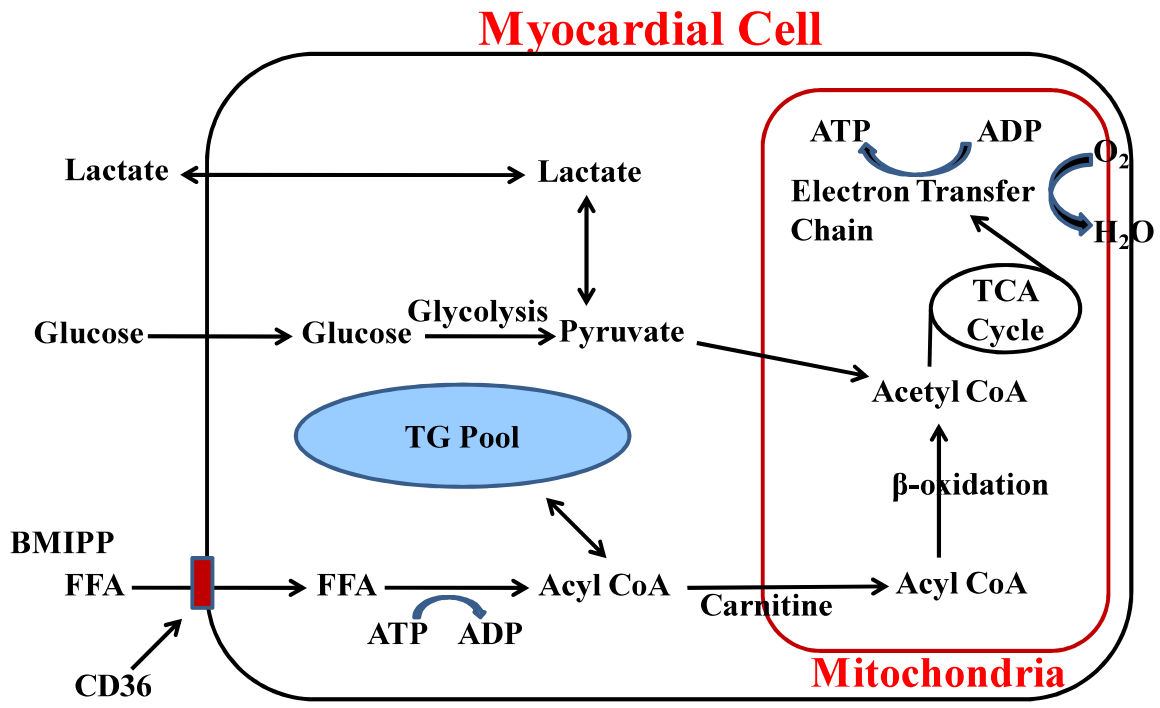

Figure 2.1. Pathway of metabolism of fatty acid in the heart[31] *(FFA: free fatty acid)*

In ischemia, the oxidation of long chain fatty acids is greatly suppressed and this alteration of fatty acid oxidation is considered to be a sensitive marker of ischemia and myocardial damage[32,33]. Although myocardial perfusion imaging is considered as the earliest investigation that can identify ischemia with or without infarction, studies have revealed that metabolic changes precede perfusion abnormalities in the heart during an ischemic or infarction episode. The shift in metabolism in the heart from fatty acids to glucose during a non-lethal ischemic process persists for a long duration of time even after recovery of perfusion[34]. Thus, early identification of such myocardial metabolic shifts would be beneficial in the early detection of ischemia. Radiolabeled fatty acids are potential candidates for diagnosis of such altered myocardial metabolic function resulting from cardiomyopathies of various origins. The development of myocardial metabolic agents has been pursued for decades and both single photon emitting and positron emitting radionuclides have been tagged to fatty acids of varying chain lengths. Amongst them, ^{123}I-IPPA (15-(p-iodophenyl)pentadecanoic acid) and ^{123}I-BMIPP (15-(p-iodophenyl)-3-(R,S)-

methylpentadecanoic acid) are the most widely studied SPECT (Single Photon Emission Computed Tomography) radiotracers which demonstrated rapid accumulation in the heart and are successful in detecting myocardial diseases in the clinic[32,35-36]. ^{123}I-BMIPP is used clinically in many parts of Japan and Europe. Owing to the advantages of PET (as described in Chapter 1) such as the possibility of *in vivo* dynamic imaging and the quantification of uptake of radiotracer in the heart, many PET based radiotracers have also been studied such as ^{11}C-palmitate, ^{18}F-FTP (16-fluoro-4-thiapalmitate) and ^{18}F-FCPHA (trans-9(RS)-fluoro-3,4-(RS,RS)methylene heptadecanoic acid)[37-45]. Presently, the two ^{18}F labeled fatty acid analogues are undergoing clinical trials. The structures of various SPECT and PET based myocardial imaging agents are given in Figure 2.2.

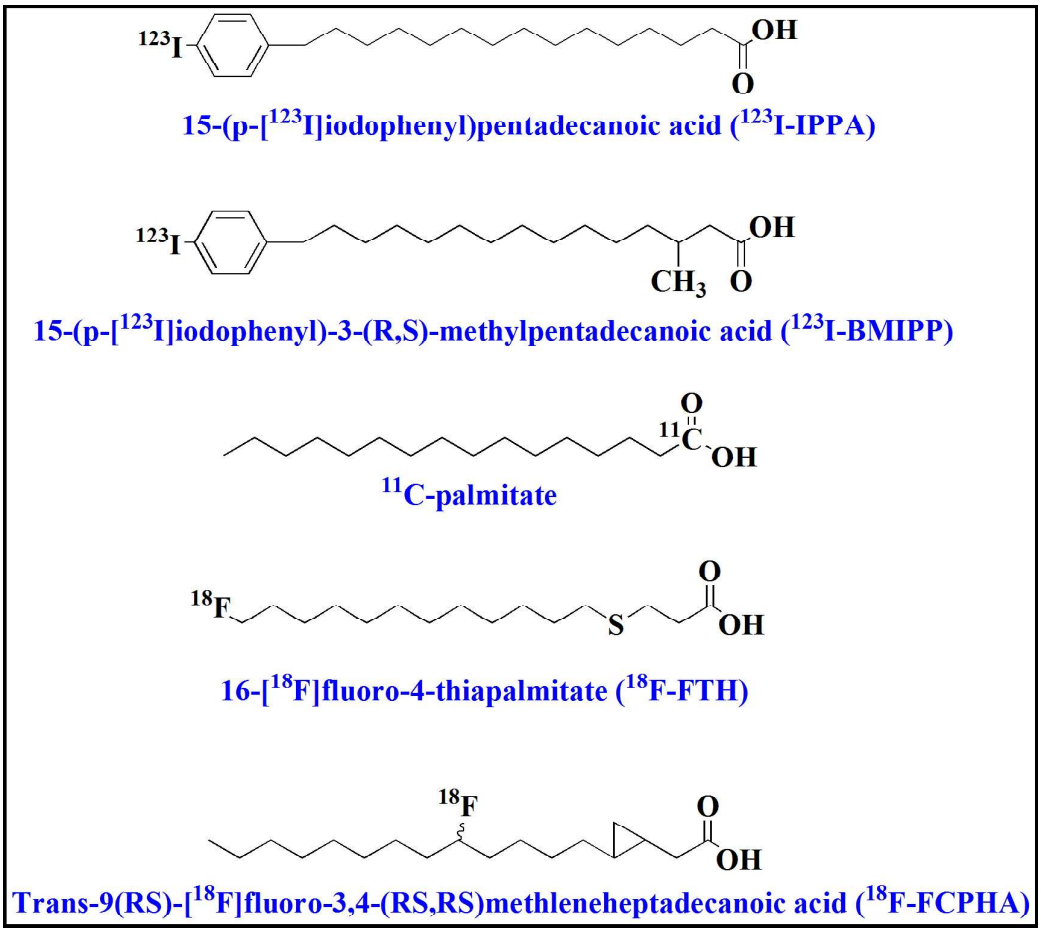

Figure 2.2. Structure of various myocardial metabolic imaging agents

As discussed in chapter 1, the availability of ^{68}Ga ($E_{\beta+}$= (89%); $t_{1/2}$= 67.71 min) through a portable secular equilibrium ^{68}Ge/^{68}Ga generator system and its high yielding labeling chemistry makes it a viable alternative to ^{11}C and ^{18}F based agents Therefore, the development of ^{68}Ga labeled fatty acids for PET based myocardial imaging is highly desirable.

In order to radiolabel fatty acids with ^{68}Ga, the parent fatty acid chain has to be conjugated with a chelator keeping the terminal acid group intact so as to have minimal adverse effect on the biological behaviour of the parent fatty acid molecule. Various factors influence the uptake of fatty acids in the heart such as the chain length wherein 15-21 chain length fatty acids are most effectively extracted by the heart[46]. For myocardial uptake, the radiolabeled core should be neutral with high stability and of small size so as to minimally affect the extraction of radiolabeled fatty acids[47]. In this chapter, ^{68}Ga fatty acid analogues having varying chain lengths were synthesized and the effect of different chain lengths as well as the nature of the ^{68}Ga-metal chelate complexes on the extraction efficiency of the final fatty acid analogues was investigated.

2.2. EFFECT OF CHAIN LENGTH ON THE MYOCARDIAL UPTAKE OF ^{68}Ga-FATTY ACIDS

In order to investigate the effect of chain length on the myocardial extraction of fatty acid analogues, three different fatty acid chain lengths were chosen mainly 11 carbon (11-aminoundecanoic acid), 12 carbon (12-aminododecanoic acid) and 16 carbon (16-hexadecanedioic acid) which were conjugated with the chelator NOTA for radiolabeling with ^{68}Ga. The rationale for using 11 and 12 carbon chains was based on the previous literature reports on ^{99m}Tc-labeled fatty acids wherein these smaller chain fatty acids exhibited high myocardial uptake[48-50]. Since the potential of ^{99m}Tc-labeled fatty acids with smaller chain lengths is well established, similar parent molecules were chosen for the synthesis of ^{68}Ga

labeled fatty acid tracers towards PET based myocardial imaging. Further, a 16 carbon chain fatty acid parent moiety was chosen in an attempt to evaluate the potential of a ^{68}Ga surrogate of myocardial agents like ^{11}C-palmitate. ^{11}C-palmitate has been the most commonly used radiopharmaceutical for assessing the myocardial fatty acid metabolism by PET imaging. Its bi-exponential clearance pattern from the myocardium reflects that of a free fatty acid where a fraction of the molecule enters the intracellular triglyceride pool while the other fraction enters the mitochondria for further oxidation[32,40-42].

The three fatty acid chain lengths were conjugated with the chelator NOTA for radiolabeling with ^{68}Ga. A detailed systematic evaluation of the role of chain length on the *in vitro* stability, lipophilicity and the biodistribution behaviour of the three ^{68}Ga labeled NOTA-fatty acid analogues was carried out. The chelator NOTA was chosen as it is known to complex with ^{68}Ga in high yields at room temperature forming a neutral complex thus adhering to the primary requirements of a radiolabeled fatty acid for myocardial imaging. Further, the thermodynamic stability constant of ^{68}Ga-NOTA complex is very high (log K_{ML} =31.0) as the cavity size of NOTA matches with the ionic size of $^{68}Ga^{3+}$. High complex stability ensures no background activity due to free $^{68}Ga^{3+}$ in the system unlike in case of ^{11}C-palmitate where rapid formation of free ^{11}C *in vivo* prevents the quantification of the uptake of ^{11}C-radiotracer in the heart[32].

2.2.1. MATERIALS AND METHODS

11-aminoundecanoic acid and 12-aminododecanoic acid were obtained from Fluka, Germany. 16-hexadodecanoic acid, O-(7-Azabenzotriazol-1-yl)-N,N,N',N'-tetramethyluronium hexafluorophosphate (HATU) and diisopropylethylamine (DIPEA) were procured from Sigma Aldrich, USA while *p*-SCN-Bn-NOTA and *p*-NH_2-Bn-NOTA were purchased from Macrocyclics, USA. All other reagents used were of analytical grade. HPLC characterization was carried out on a JASCO PU 2080 Plus dual pump HPLC system

(JASCO, Japan) with a JASCO 2075 Plus tunable absorption detector and Gina Star radiometric detector system (Raytest, Germany), using a C18 reversed phase HiQ Sil (5 μm, 4 × 250 mm) column and acetonitrile: water (each containing 0.1% TFA) mixture as the mobile phase. Purification of the synthesized fatty acid derivatives was performed using a JASCO-PU-2086 PLUS Intelligent Prep Pump semi preparative HPLC system (JASCO, Japan) having a Megapak SIL C18-10 column (10 × 250 mm) connected with a JASCO UV-2075 Plus absorption detector. The same solvent system and method was used in both analytical HPLC as well as semi-preparative HPLC. ^{1}H NMR and ^{13}C NMR spectra were recorded on a 300 MHz Varian spectrophotometer. Mass spectra of the samples were recorded on Varian Prostar mass spectrometer using ESI in positive/ negative mode.

2.2.2. EXPERIMENTAL

2.2.2.. Synthesis of NOTA-fatty acid conjugates

(a) Synthesis of NOTA-undecanoic acid and NOTA-dodecanoic acid

In a typical procedure, ω-amino fatty acid (11-aminoundecanoic acid/ 12-aminododecanoic acid**,** 0.08 mmol) was dissolved in 0.1 M NaOH solution (1.6 mL) and stirred until a clear solution was obtained. To the above solution, *p*-SCN-benzyl NOTA (30 mg, 0.053 mmol) was added and the reaction mixture was stirred overnight. The progress of the reaction was monitored by HPLC following the UV profile at 254 nm. The gradient method used was 90% A to 10% A in 28 min at a flow rate of 1 mL/min. Upon completion of the reaction, the pH of the reaction mixture was adjusted to 5-6 using 0.2 M HCl. A white precipitate separated out which was filtered off and re-dissolved in methanol. This crude product in methanol was purified using semi-preparative HPLC with the same solvent system and method as used for analytical HPLC however with a flow rate of 2 mL/min.

NOTA-undecanoic acid:

Yield: 20 mg;

^{1}H NMR (D_2O, δ ppm) 7.05-7.23 ($C_6\underline{H}_4$-, 2H, m); 6.90-7.02 ($C_6\underline{H}_4$-, 2H, m); 3.48-3.62 (-NC$\underline{H}$CH_2N-, 1H, m); 3.20-3.40 (-NC$\underline{H}_2$COOH, 6H, m); 3.10-3.20 (S=CNHC$\underline{H}_2$CH_2-, 2H, m); 2.8-3.04 ($C_6H_4C\underline{H}_2$- and -NC$\underline{H}_2$C$\underline{H}_2$N-, 6H, m); 2.56-2.72 (-NCHC$\underline{H}_2$N-, 2H, m); 2.16-2.38 (-NC$\underline{H}_2$C$\underline{H}_2$N-, 6H, m); 2.10 (-$CH_2C\underline{H}_2$COOH, 2H, t, *J=7.5 Hz*); 1.42-1.60 (-C$\underline{H}_2CH_2$COOH and -C$\underline{H}_2CH_2$NHC=S, 4H, m); 1.22 [$(C\underline{H}_2)_6$, 12H, s].

MS (ESI, +ve mode): Mass (calculated) [$C_{31}H_{45}N_5O_8SNa_4$] 739.26; *m/z* (observed) 738.5.

NOTA-dodecanoic acid:

Yield: 17.5 mg

^{1}H NMR (D_2O, δ ppm) 7.02-7.23 ($C_6\underline{H}_4$-, 2H, m); 6.88-7.01 ($C_6\underline{H}_4$-, 2H, m); 3.48-3.62 (-NC$\underline{H}$CH_2N-, 1H, m); 3.22-3.38 (-NC$\underline{H}_2$COOH, 6H, m); 3.10-3.20 (S=CNHC$\underline{H}_2$CH_2-, 2H, m); 2.78-3.02 ($C_6H_4C\underline{H}_2$- and -NC$\underline{H}_2$C$\underline{H}_2$N-, 6H, m); 2.56-2.74 (-NCHC$\underline{H}_2$N-, 2H, m); 2.16-2.38 (-NC$\underline{H}_2$C$\underline{H}_2$N-, 6H, m); 2.10 (-$CH_2C\underline{H}_2$COOH, 2H, t, *J=7.5 Hz*); 1.42-1.60 (-C$\underline{H}_2CH_2$COOH and -C$\underline{H}_2CH_2$NHC=S, 4H, m); 1.25 [$(C\underline{H}_2)_7$, 14H, s].

MS (ESI, +ve mode): Mass (calculated) [$C_{32}H_{47}N_5O_8SNa_4$] 753.26; *m/z* (observed) 754.5.

(b) Synthesis of NOTA-hexadecanoic acid

16-hexadecanedioic acid (30 mg, 0.1 mmoles) was dissolved in dimethyl formamide (DMF, 1 mL). HATU (40 mg, 0.1 mmoles) and DIPEA (13.4 mg, 0.1mmoles) were added to the reaction mixture and stirred for 10 min under nitrogen atmosphere. Further, *p*-NH_2-Bn-NOTA (54 mg, 0.1 mmoles) was added to it and then left for overnight stirring. The progress of the reaction was monitored using analytical HPLC following the UV peak at 254 nm. The following gradient elution method was adopted for monitoring the progress of the reaction: 0 min 70% A, 15 min 0% A, 20 min 0% A, 25 min 70% A. Purification of the synthesized NOTA-hexadecanoic acid was carried out using semi-preparative HPLC with the same solvent system and method as used for analytical HPLC at a higher flow rate of 2 mL/min.

Yield: 21 mg

^{1}H NMR (500 MHz, DMSO) δ ppm: 7.68 (d, 2H, benzene, *J=7.5 Hz*), 7.25 (d, 2H, benzene, *J=7.5 Hz*), 3.49-3.48 (m, 7H, -NC$\underline{H_2}$COOH and –C_6H_4-CH_2CHN-), 2.93-2.84 (m,12H , NOTA ring -NC$\underline{H_2}$C$\underline{H_2}$N- and -NC$\underline{H_2}$CHN-, C_6H_4-C$\underline{H_2}$CHN-), 2.40 (t, 2H, -C$\underline{H_2}$CONH-), 2.30 (t, 2H, -C$\underline{H_2}$COOH), 1.68 (m, 2H, -C$\underline{H_2}CH_2$CONH-), 1.58-1.57 (m, 2H, -C$\underline{H_2}CH_2$COOH), 1.29 (s, 20 H, -$(CH_2)_{10}$)

MS (ESI, +ve mode): Mass (calculated) [$C_{35}H_{56}N_4O_9$] 676.4; *m/z* (observed) 676.9

2.2.2.2. Radiolabeling with ^{68}Ga

(a) Radiolabeling of NOTA-undecanoic acid and NOTA-dodecanoic acid with ^{68}Ga

$^{68}GaCl_3$ was obtained from a 740 MBq (20 mCi) ^{68}Ge/^{68}Ga nanoceria-PAN generator. $^{68}GaCl_3$ was eluted from the generator with 2 mL of 0.1 M HCl and directly used for radiolabeling.

The radiolabeling procedure followed for NOTA-undecanoic acid and NOTA-dodecanoic acid was similar. Briefly, 200 µL of 0.1 M sodium acetate buffer (pH 6) was added to 100 µL of the NOTA-fatty acid conjugate (1 mg/mL in EtOH). $^{68}GaCl_3$ (0.7 mL, 37-74 MBq) was added to the above solution and the resultant mixture (pH=4) was incubated at room temperature for 10 min. The ^{68}Ga-NOTA-fatty acid conjugates were then characterized by HPLC following their radioactive profile using the solvent system and method as described in Section 2.2.2.1 (a). Stability of the ^{68}Ga-fatty acid conjugates was determined over a period of 4 h at ambient temperature.

(b). Radiolabeling of NOTA-hexadecanoic acid with ^{68}Ga

Gallium-68 was eluted in 0.6 N HCl from a 925 MBq (25 mCi) ^{68}Ge/^{68}Ga radionuclide generator obtained from iThemba Labs (South Africa).

For radiolabeling, NOTA-hexadecanoic acid (100 µL, 1 mM in ethanol) was mixed with 2 M sodium acetate solution (pH=8). $^{68}GaCl_3$ (1 mL, 185 MBq) was added to it and the reaction mixture (pH=4) was incubated for 10 min at room temperature. The radiochemical

yield of ^{68}Ga-NOTA-hexadecanoic acid was determined by radio HPLC using the solvent system and method as described in Section 2.2.2.1(b). The stability of the ^{68}Ga NOTA-hexadecanoic acid conjugate was determined over a period of 4 h at room temperature.

2.2.2.3. Preparation of ^{nat}Ga-NOTA-fatty acid

To the three NOTA-fatty acid conjugates (100 µL, 0.1 M in ethanol), excess gallium nitrate solution (1 mL, 0.1 M) was added. The pH of the reaction mixture was adjusted to 4 with dilute NaOH and it was incubated at 45°C for 30 min. The product was characterized by ESI-MS and HPLC following the UV profile at 254 min using the gradient elution technique as described in Section 2.2.2.

^{nat}Ga-NOTA-undecanoic acid

MS (ESI, +ve mode): Mass (calculated) [$C_{31}H_{46}N_5O_8SGa$] 717.5 g/mol; *m/z* (observed) 718.9 g/mol $[M+H]^+$

^{nat}Ga-NOTA-dodecanoic acid

MS (ESI, +ve mode): Mass (calculated) [$C_{32}H_{48}N_5O_8SGa$] 731.5 g/mol; m/z (observed) 732.4 g/mol $[M+H]^+$

^{nat}Ga-NOTA-hexadeanoic acid

MS (ESI, +ve mode): Mass (calculated) [$C_{35}H_{53}N_4O_9Ga$] 742.3; m/z (observed) 743.4 g/mol $[M+H^+]$

2.2.2.4. Partition coefficient and in vitro stability studies

For determining the partition coefficient (log $P_{o/w}$), ^{68}Ga-NOTA-fatty acid conjugates (100 µL) were mixed with water (0.9 mL) and octanol (1 mL) on a vortex mixer and then centrifuged to effect the complete separation of the aqueous and organic layers. Equal aliquots from both layers were counted in NaI (Tl) detector. Partition coefficient (log $P_{o/w}$) was expressed as the logarithm of the ratio of the counts in n-octanol versus that in the

aqueous layer. Further, the n-octanol layer was repartitioned until consistent partition coefficient was obtained.

In order to determine the stability of the ^{68}Ga-NOTA-fatty acid conjugates in human serum, each conjugate (50 μL) was incubated with human serum (450 μL) at 37 °C for 2 h. Thereafter, the serum proteins were precipitated by addition of acetonitrile (500 μL), the solution was centrifuged and the supernatant was analyzed by HPLC to determine the serum stability.

To determine the stability of the fatty acid conjugates towards transchelation, the ^{68}Ga-NOTA-fatty acids were incubated with 100 fold excess EDTA solution for 2 h at room temperature. Thereafter, their radiochemical purity was determined by HPLC analysis.

2.2.2.5. In vivo evaluation studies

All procedures performed herein were in accordance with the national guidelines pertaining to the conduct of animal experiments. Normal female Swiss mice (20-25 g body weight) were used for the *in vivo* distribution assays of the ^{68}Ga labeled fatty acid conjugates. All the mice used in the study were kept under fasting for 4-5 h prior to the experiment, although water was given ad libitum. The radiolabeled preparation (100 μL) was administered intravenously through the tail vein of each animal. Individual sets of animals (n=4) were utilized for studying the bio-distribution at different time points (2 min, 5 min, 10 min and 30 min). The animals were sacrificed by carbon dioxide asphyxiation immediately at the end of the respective time point and the relevant organs and tissue were excised for measurement of associated activity. The tissues and organs were weighed and the activity associated with each of them was counted in a flat-bed type NaI(Tl) counter with suitable energy window for ^{68}Ga. For the purpose of uniformity, the activity retained in each organ/tissue was expressed as a percent value of the injected dose per gram (% ID/g).

Activity associated with the excreta (urine+feaces) was determined by counting the cage paper which was expressed as percent value of the injected dose (%ID).

2.2.3. RESULTS AND DISCUSSION

2.2.3.1. Synthesis

The scheme followed for the synthesis of NOTA-undecanoic acid and NOTA-dodecanoic acid is shown in Figure 2.3.

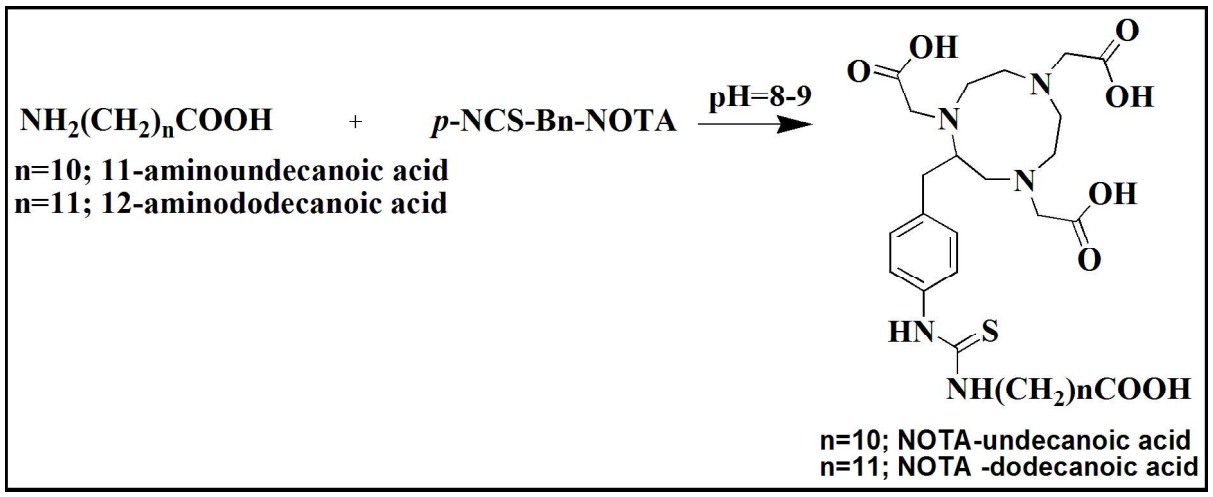

Figure 2.3. Scheme for synthesis of NOTA-undecanoic acid and NOTA-dodecanoic acid

The desired fatty acid conjugates were synthesised in a single step on addition of *p*-SCN-Bn-NOTA to the ω-amino group of long chain fatty acids, under alkaline conditions. The reaction was monitored by HPLC, wherein the decrease in the peak intensity corresponding to *p*-SCN-NOTA indicated the progress of the reaction. The two NOTA-fatty acid conjugates were isolated by semi-preparative HPLC in approximately 60% and 50% yields for the NOTA-undecanoic acid and NOTA-dodecanoic acid, respectively.

The scheme for the synthesis of NOTA-hexadecanoic acid is shown in Figure 2.4. The ω-carboxylic acid group of hexadecanedioic acid was reacted with the amine group of *p*-NH_2-Bn-NOTA using HATU as the coupling agent under nitrogen atmosphere. The progress of the reaction was monitored using HPLC following the UV profile at 254 nm. Two peaks were observed in the HPLC with retention times of 14.5 min and 15.2 min. The two peaks

were separately collected using semi-preparative HPLC and were characterized by ESI-MS. It was observed that the peak at 14.5 min corresponded to the compound formed by conjugation of two NOTA molecules with hexadecanedioic acid. The peak at 15.2 min corresponded to NOTA-hexadecanoic acid. This peak corresponding to the required NOTA-fatty acid conjugate was further characterized by ^{1}H NMR.

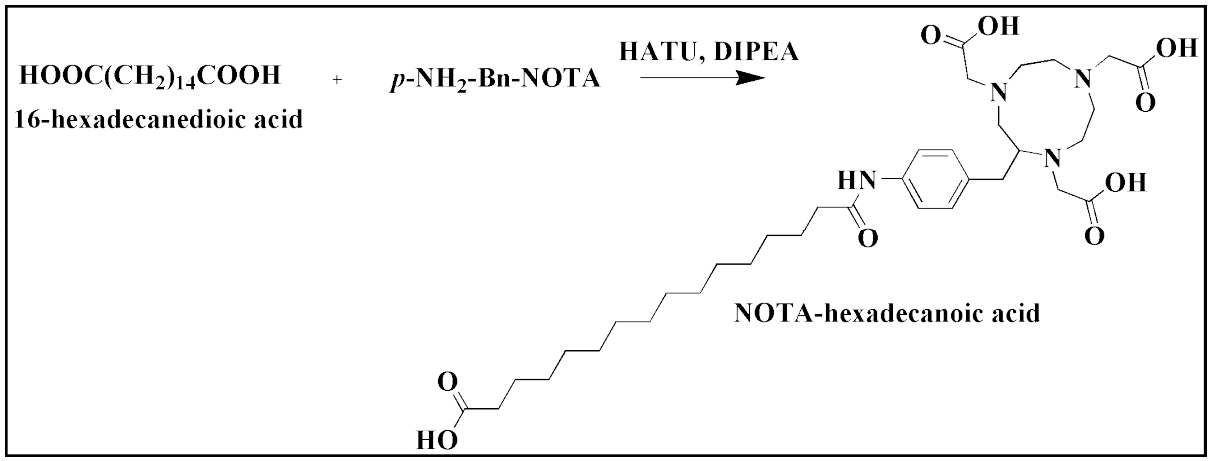

Figure 2.4. Scheme for synthesis of NOTA-hexadecanoic acid

2.2.3.2. Radiolabeling of the fatty acid conjugates with ^{68}Ga

The purified NOTA-fatty acid conjugates were radiolabeled with $^{68}GaCl_3$ and characterized by radioanalytical HPLC. The structures of ^{68}Ga-NOTA-fatty acids are given in Figure 2.5. In HPLC, free ^{68}Ga (III) eluted at around 3.83 min. The HPLC profiles of ^{68}Ga-NOTA-undecanoic acid, ^{68}Ga-NOTA-dodecanoic acid and ^{68}Ga-NOTA-hexadecanoic are given in Figure 2.6a, Figure 2.7a and Figure 2.8a, respectively. The ^{68}Ga-NOTA-undecanoic acid and ^{68}Ga-NOTA-dodecanoic acid conjugates were obtained in 90±2% radiochemical yields while ^{68}Ga-NOTA-hexadecanoic acid was obtained in 95±3% yield. All the three preparations were found to be stable at room temperature and no significant degradation was observed up to a period of 4 h.

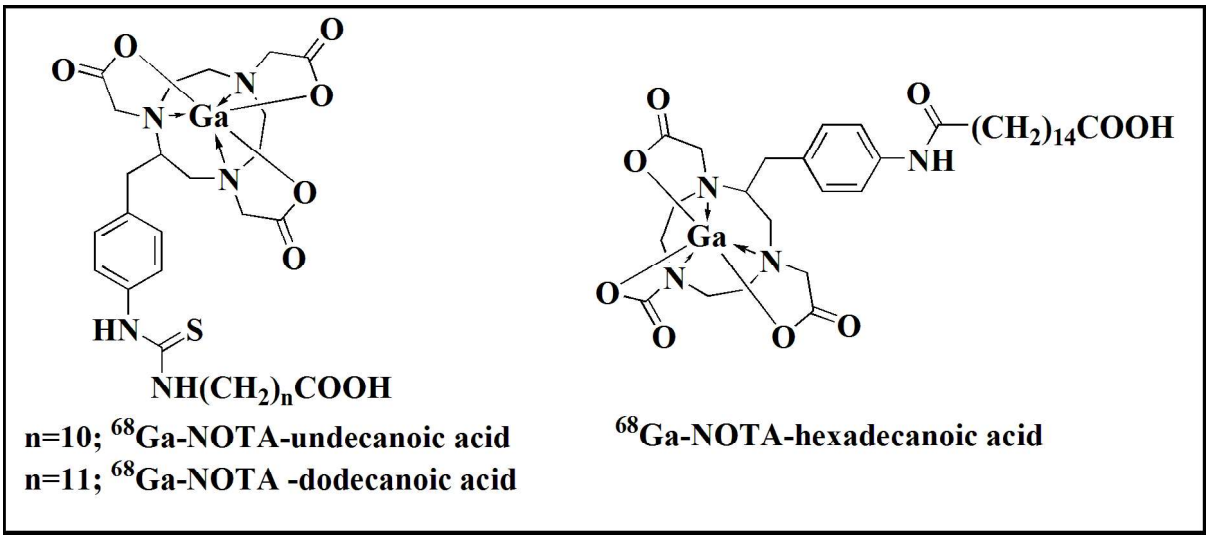

Figure 2.5. Probable structures of ^{68}Ga-NOTA-fatty acids

2.2.3.3. Synthesis of ^{nat}Ga-NOTA-fatty acid conjugates

An attempt was made to synthesize the corresponding inactive NOTA-fatty acid complexes with ^{nat}Ga in order to verify the radiochemical identity of ^{68}Ga-NOTA-fatty acid complexes. The radio-HPLC profile of ^{68}Ga-NOTA-fatty acid complexes compared with the respective UV-profile HPLC of ^{nat}Ga-NOTA-fatty acid are given in Figures 2.6, 2.7 and 2.8. In all the three cases, the proximate retention times of the ^{68}Ga and ^{nat}Ga fatty acid conjugates were indicative of the formation of the desired ^{68}Ga labeled NOTA-fatty acid conjugate. The ESI-MS of ^{nat}Ga-NOTA-fatty acid conjugates further corroborated the successful product synthesis.

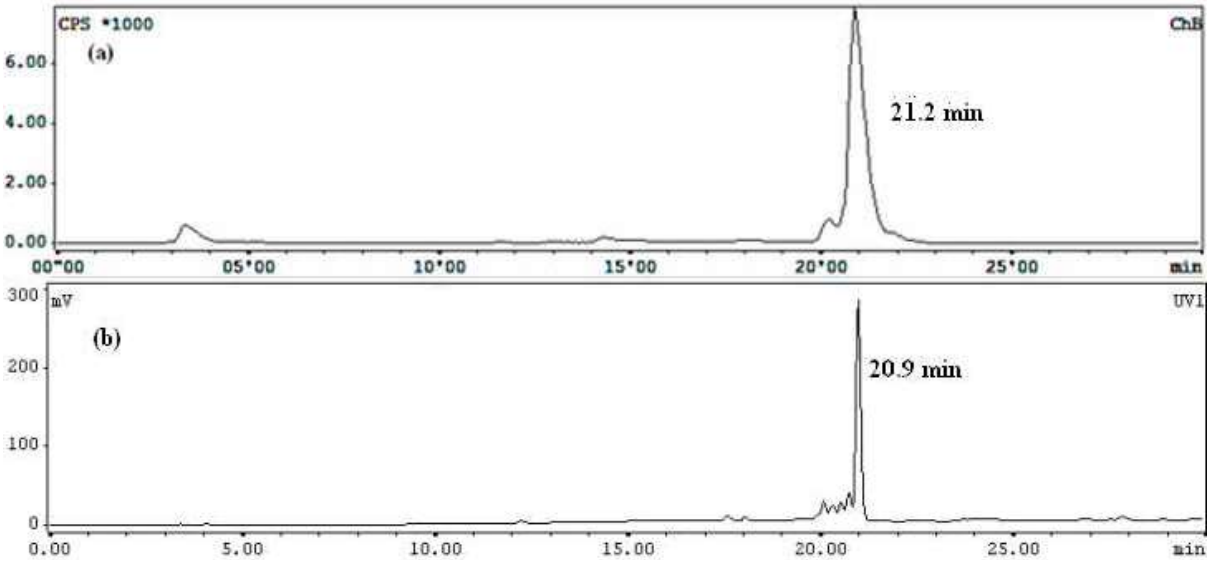

Figure 2.6. HPLC elution profile: (a) ^{68}Ga-NOTA-undecanoic acid and (b) ^{nat}Ga-NOTA-undecanoic acid

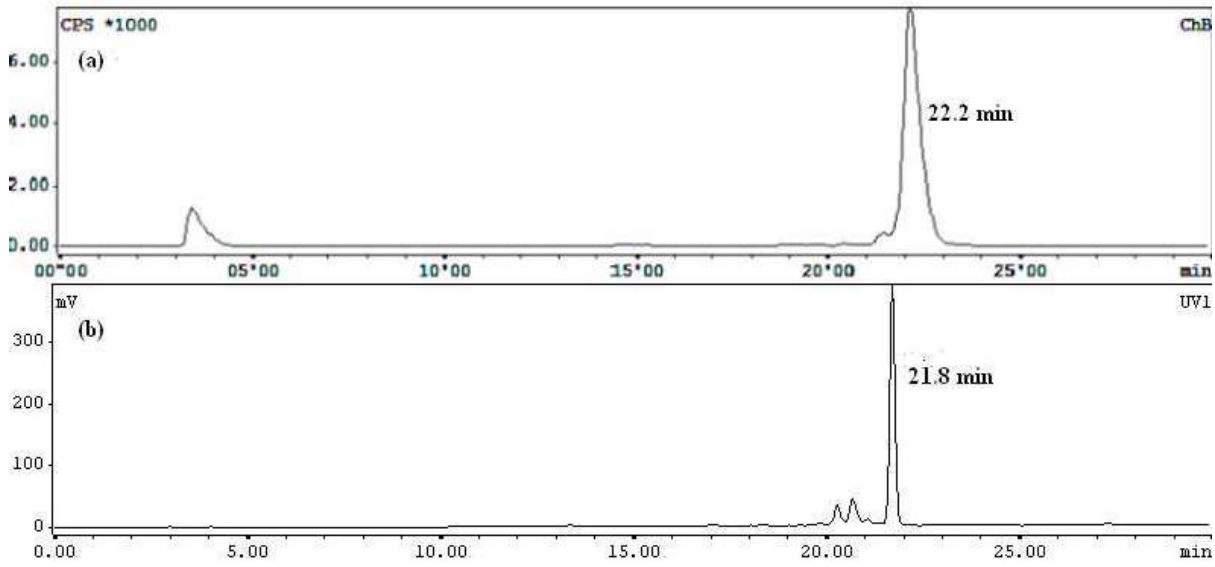

Figure 2.7. HPLC elution profile of (a) ^{68}Ga-NOTA-dodecanoic acid and and (b) ^{nat}Ga-NOTA-dodecanoic acid

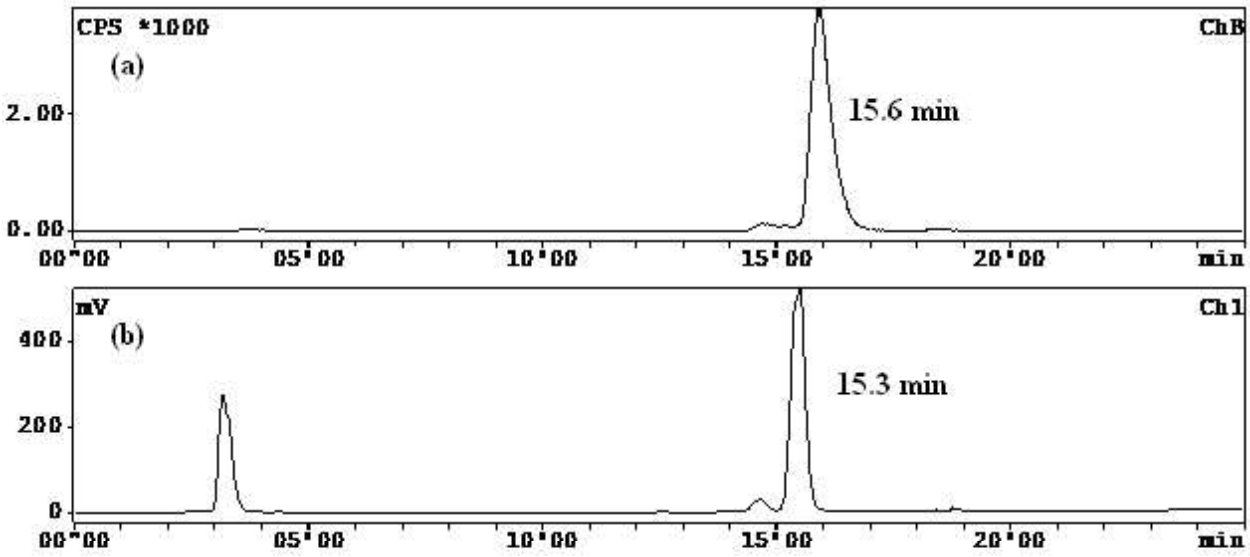

Figure 2.8. HPLC elution profile: (a) ^{68}Ga-NOTA-hexadecanoic acid and (b) ^{nat}Ga-NOTA-hexadecanoic acid

2.2.2.4. Partition coefficient and in vitro stability studies

Fatty acids enter the cardiac myocytes either by passive diffusion or via protein mediated pathway such as FA translocase CD36[29]. Transport of a fatty acid by passive diffusion depends on its lipophilicity which is determined by the log $P_{o/w}$ value. The log $P_{o/w}$ values of the three ^{68}Ga-NOTA-fatty acid conjugates are given in Table 2.1. The log $P_{o/w}$ value of ^{68}Ga-NOTA-hexadecanoic acid was the highest owing to its longer chain length.

Results of the *in vitro* stability values of the three conjugates in human serum and in EDTA solution are given in Table 2.1. All the three conjugates were found to be stable in human serum after incubation for 2 h at 37°C. In addition, the complexes were incubated with 100 fold excess EDTA solution and were found to be stable towards transchelation. The high *in vitro* stability gave the impetus for further bio-evaluation studies in animal models.

Table 2.1. Partition coefficient (log $P_{o/w}$) and in vitro stability of ^{68}Ga-NOTA-fatty acid conjugates

Compound	log $P_{o/w}$	Serum Stability (up to 2 h)	EDTA challenge (up to 2 h)
^{68}Ga-NOTA-undecanoic acid	0.3±0.0	88.0±0.1%	87.0±2.0%
^{68}Ga-NOTA-dodecanoic acid	0.2±0.0	89.0±2.0%	90.0±2.0%
^{68}Ga-NOTA-hexadecanoic acid	1.3±0.2	94.0±0.1%	93.0±3.0%

2.2.3.5. In vivo evaluation studies

The biodistribution studies of the ^{68}Ga-NOTA-fatty acid analogues were carried out in fasting Swiss mice. This was because in the fasting condition, the level of free fatty acids in the plasma and their uptake by the myocardium are high and the glucose oxidation is reduced. On the other hand after a meal, the arterial glucose levels are high due to which glucose oxidation increases and fatty acid use is suppressed[32] .

Results of the biodistribution studies of the three ^{68}Ga-NOTA-fatty acids in Swiss mice are given in Table 2.2. Biodistribution studies in Swiss mice showed reasonable myocardial uptake at 2 min for ^{68}Ga-NOTA-undecanoic acid (7.4±2.8 % ID/g) and ^{68}Ga-NOTA-dodecanoic acid (6.4±2.1 % ID/g). However, the myocardial uptake of ^{68}Ga-NOTA-hexadecanoic acid at 2 min p.i. (3.7±1.3 %ID/g) was significantly lower. The initial uptake of all the three conjugates was not retained in the myocardium and fast washout of the activity from the myocardium was observed. The conjugates cleared rapidly from the non-target organs such as blood, lungs and muscle via the hepatic route. High uptake of the ^{68}Ga-NOTA-fatty acid conjugates in liver indicated clearance of the activity via the hepatic route. ^{68}Ga-NOTA-hexadecanoic acid exhibited highest uptake in the liver amongst the three fatty acid analogues at all the time points possibly because of its high lipophilicity.

Table 2.2. Biodistribution data of ^{68}Ga-NOTA-fatty acid in Swiss mice (n=4)

Organs/Tissues ↓	%Injected Dose/g (I.D./g)± standard deviation (S.D.)			
	2 min	**5 min**	**10 min**	**30 min**
	^{68}Ga-NOTA-undecanoic acid			
Blood	41.2±3.4	17.6±1.3	7.7±3.3	1.4±0.4
Lungs	13.6±7.0	7.7±0.8	3.7±1.7	1.1±0.5
Heart	**7.4±2.8**	**5.2±2.1**	**2.0±1.1**	**0.3±0.0**
Stomach	2.1±1.1	3.1±0.4	3.2±1.5	3.3±1.5
Intestine	3.8±0.2	5.3±1.4	3.6±1.3	9.7±2.7
Liver	38.7±4.2	59.0±2.6	39.3±14.0	26.6±5.4
Spleen	1.5±0.5	2.9±1.3	0.8±1.4	0.7±0.7
Kidney	15.5±3.0	13.3±2.6	8.73±5.7	3.0±1.1
Muscle	14.7±8.3	17.0±7.2	13.0±7.7	3.3±0.2
Bone	0.8±0.2	0.7±0.1	0.5±0.1	0.3±0.0
Excreta(%ID)	0.3±0.1	0.5±0.1	1.9±0.4	2.7±0.1
	^{68}Ga-NOTA-dodecanoic acid			
Blood	34.9±14.5	13.2±3.5	6.9±2.1	2.6±0.2
Lungs	11.4±5.8	3.8±0.4	3.5±0.1	1.9±0.3
Heart	**6.4±2.1**	**2.7±0.8**	**1.4±0.5**	**0.8±0.3**
Stomach	1.8±0.5	1.2±0.1	3.2±1.4	2.2±2.1
Intestine	2.4±0.3	3.1±1.1	8.6±2.3	22.6±0.8
Liver	38.6±4.2	57.5±6.4	59.8±6.8	31.4±8.7
Spleen	2.9±0.9	2.1±0.6	1.0±0.5	1.6±1.2
Kidney	11.6±0.3	12.0±0.4	11.8±5.9	6.0±2.3
Muscle	14.0±4.7	12.4±2.3	7.72±0.9	5.4±0.03
Bone	0.1±0.05	0.2±0.1	0.05±0.0	0.01±0.0
Excreta(%ID)	0.2±0.0	0.5±0.2	0.8±0.1	0.89±0.0
	^{68}Ga-NOTA-hexadecanoic acid			
Blood	41.2±1.2	10.6±6.1	5.9±0.4	3.8±0.8
Lungs	8.3±6.2	5.5±1.5	1.8±0.3	1.6±0.4
Heart	**3.6±1.0**	**1.6±0.3**	**1.0±0.1**	**0.5±0.1**
Stomach	1.6±0.8	2.1±0.2	1.5±1.2	2.0±1.0
Intestine	1.5±0.3	1.0±0.2	0.7±0.1	1.0±0.1
Liver	37.0±7.9	76.8±13.6	78.5±6.3	75.1±10.6
Spleen	2.5±1.4	1.7±0.6	0.7±0.5	5.7±9.4
Kidney	6.2±0.9	2.3±0.3	1.9±0.7	1.1±0.2
Muscle	7.3±2.3	7.4±2.4	6.2±1.7	2.4±2.0
Bone	0.03±1.5	0.05±0.0	0.02±0.0	0.00±0.0
Excreta(%ID)	0.5±0.3	0.7±0.2	0.7±0.3	0.1±0.0

A comparison of the variation of heart/non-target organs ratios with time is given in Figure 2.9.

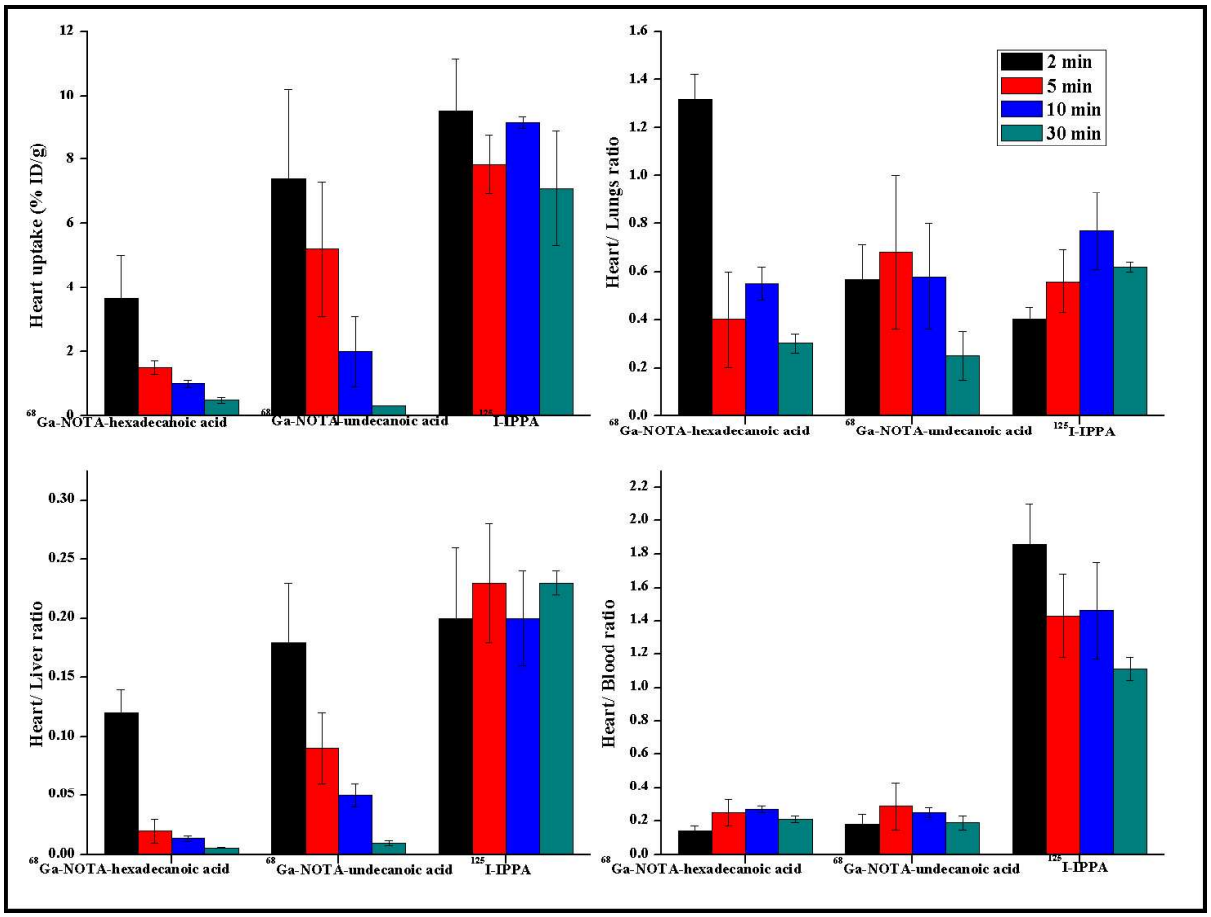

Figure 2.9. Time dependent changes in heart, heart/blood, heart/liver and heart/lung ratios of ^{68}Ga-NOTA-fatty acid conjugates

The extent of clearance of activity from heart along with the heart/blood, heart/lungs and heart/liver ratios of ^{68}Ga-NOTA-undecanoic acid and ^{68}Ga-NOTA-dodecanoic acid were nearly the same. The heart/non target ratios for ^{68}Ga-NOTA-hexadecanoic acid were lower mostly due to its low uptake in the heart. Since the uptake of ^{68}Ga-NOTA-hexadecanoic acid was lower in lungs at 2 min p.i., the heart/lungs ratio was very high at that time point. But it decreased rapidly with time due to rapid clearance of the activity from the heart.

After analyzing the biodistribution profile of the three ^{68}Ga labeled fatty acid analogues, it could be concluded that the uptake of ^{68}Ga-NOTA-undecanoic acid was highest

at 2 min p.i. followed by that of ^{68}Ga-NOTA-dodecanoic acid. Even though their myocardial uptake reduced rapidly with the time, the high initial uptake resulted in improved heart/non-target ratios for ^{68}Ga-NOTA-undecanoic acid and ^{68}Ga-NOTA-dodecanoic acid, especially at 2 min p.i. These might possibly help in obtaining high contrast images at early time points which can be beneficial in differentiating normal/ischemic myocardium and infarct. Early imaging using PET camera can help in allowing *in vivo* tracing of physiological and biochemical functions of the heart.

2.3. INFLUENCE OF BIFUNCTIONAL CHELATOR ON THE HEART UPTAKE OF ^{68}Ga-FATTY ACIDS

In this section of Chapter 2, the influence of chelators namely NOTA, NODAGA and DTPA on the biodistribution of ^{68}Ga-labeled fatty acids for myocardial imaging has been explored. In the previous Section 2.2, it was seen that amongst the three fatty acid chains namely 11 carbon (11-aminoundecanoic acid), 12 carbon (12-aminododecanoic acid) and 16 carbon (16-aminohexadodecanoic acid), 11 carbon parent chain conjugated with *p*-SCN-Bn-NOTA showed the highest uptake in the heart. Therefore, in continuation with the above findings, two new fatty acid conjugates using 11-aminoundecanoic acid as the parent chain were synthesized viz. NODAGA-undecanoic acid and DTPA-undecanoic acid. The conjugates were synthesized, characterized and radiolabeled with ^{68}Ga and further evaluated in normal Swiss mice. The results obtained were compared with the previously reported ^{68}Ga-NOTA-undecanoic acid conjugate. The choice of chelators *viz*. NODAGA and DTPA for the preparation of the new ^{68}Ga labeled fatty acid analogues was based upon literature reports showing that these chelators form structurally neutral and kinetically inert octahedral complexes with $^{68}Ga^{3+}$. Further, from the previous studies it was deduced that a high uptake in the liver reduces the avidity of the ^{68}Ga-fatty acids for myocardial imaging. Thus, it was envisaged that introduction of NODAGA with an extra amide linkage and DTPA with extra

COOH groups (Figure 1.5) might lower the lipophilicity of the final ^{68}Ga-fatty acid conjugate which in turn might reduce their uptake in the liver.

2.3.1. MATERIALS AND METHODS

11-aminoundecanoic acid was obtained from Fluka, Germany. *p*-SCN-Bn-DTPA was purchased from Macrocyclics, USA. *p*-SCN-Bn-NODAGA was purchased from Chematech, France. All other reagents used were of analytical grade. The characterisation techniques used have been discussed in Section 2.2.1. In the HPLC system, water (A) and acetonitrile (B), each containing 0.1% TFA, were used as the mobile phase. The gradient method used was 90% A to 10% A in 28 min at a flow rate of 1 mL/min, The same solvent system and method were used for semi-preparative HPLC at a higher flow rate of 2 mL/min.

2.3.2. EXPERIMENTAL

2.3.2.1. Synthesis of ^{68}Ga-BFC-undecanoic acid conjugates

11-aminoundecanoic acid (30 mg, 0.14 mmol) was dissolved in 0.1 N NaOH solution (1 mL). To this solution, *p*-SCN-Bn-DTPA or *p*-SCN-Bn-NODAGA (0.14 mmol) was added with stirring. The reaction was kept for overnight stirring and the progress of the reaction was monitored using analytical HPLC following the UV profile at 254 nm. Upon completion of reaction, the pH of the reaction mixture was adjusted to 5-6 using 0.2 M HCl. A white precipitate separated out, which was filtered off and re-dissolved in methanol. This crude product in methanol was purified using semi-preparative HPLC. The separated sample was pooled, lyophilized and further characterized by ^{1}H NMR, ^{13}C NMR and ESI-MS.

NODAGA-undecanoic acid conjugate

^{1}H NMR (300 MHz, D_2O) δ ppm: 6.87 (d, *J= 8.5 Hz*, 2H, -$C_6\underline{H}_4$-), 6.74 (d, *J= 8.5 Hz*, 2H, -$C_6\underline{H}_4$-), 4.31(s, 2H, -NHC$\underline{H}_2C_6H_4$-), 3.32 (s, 4H, -NHC$\underline{H}_2$COOH), 3.24-3.16 (m, 3H, -NHC$\underline{H}_2CH_2CH_2$-, COOH(N)C$\underline{H}$CH2-), 2.70-2.61 (m, 12H, -NC$\underline{H}_2C\underline{H}_2$N-), 2.45 (t, *J = 7 Hz,*

2H, -$CH_2CH_2C\underline{H}_2COOH$), 1.9-1.8 (m, 2H, -$CHC\underline{H}_2CH_2CONH$-), 2.04 (t, *J = 7 Hz,* 2H, -$CHCH_2C\underline{H}_2CONH$-), 1.42-1.39 (m, 2H, -$CH_2C\underline{H}_2CH_2COOH$), 1.29-1.27 (m, 2H, -$NHCH_2C\underline{H}_2CH_2$-), 1.2 (s, 12H, -$(C\underline{H}_2)_6$-)

^{13}C NMR (75 MHz, D_2O) δ ppm : 184.102 (NH$\underline{C}$(S)NH), 181.450 (-NCH$\underline{C}$OOH), 180.220 (-$CH_2\underline{C}$ONH-), 175.796, 175.796 (-$CH_2\underline{C}$OOH) , 128.151, 127.862, 125.518, 122.786 (-$\underline{C}_6H_4$), 71.01 (-N$\underline{C}$HCOOH), 61.95 (-N$\underline{C}H_2$COOH), 51.185, 45.97, 42.82 (-NCH_2CH_2N-), 40.698 (-$C_6H_4\underline{C}H_2$-), 37.769 (-$CH_2\underline{C}H_2COOH$), 37.746, 33.603, 31.994, 28.898, 28.853, 28.772, 28.724, 28.686, 26.227, 25.992 (-CH$\underline{C}H_2\underline{C}H_2$CONH-, -$(CH_2)_8$-).

MS (ESI, +ve mode): Mass (calculated) [$C_{34}H_{54}N_6O_9S$] 722.8; m/z (observed)722.9; 744.9 ($M + Na^+$); 766.9 ($M + 2Na^+$)

DTPA-undecanoic acid conjugate

^{1}H NMR (300 MHz, D_2O) δ ppm: 7.36-7.29 (m, 2H, -$C_6\underline{H}_4$-), 7.15- 7.10 (m, 2H, -$C_6\underline{H}_4$-), 3.83-3.74(m, 1H, -NC$\underline{H}CH_2$N-), 3.61-3.52(m, 2H, -C(S)NHC$\underline{H}_2CH_2$-), 3.35-3.34 (m, 10H, -NHC$\underline{H}_2$COOH), 3.01-2.96 (m, 4H, -NC$\underline{H}_2C\underline{H}_2$N-), 2.71 (d, 2H, -NCHC$\underline{H}_2$N-), 2.24-2.18 (m, 2H, -$CH_2C\underline{H}_2$COOH), 1.82-1.78 (m, 2H, -$NHCH_2C\underline{H}_2$-), 1.64-1.56 (m, 2H, -C$\underline{H}_2CH_2$COOH), 1.29 (s, 12H, -$(C\underline{H}_2)_6$-)

^{13}C NMR (75 MHz, D_2O) δ ppm: 181.918 (-NH$\underline{C}$(S)NH-), 178.765 (-$CH_2CH_2\underline{C}$OOH), 169.973 (-$NCH_2\underline{C}$OOH), 136.486, 133.413, 131.128, 126.021 (-$\underline{C}_6H_4$-), 64.586, 62.574, 60.095, 55.120, 54.282, 50.995 (-N$\underline{C}H_2$COOH, -N$\underline{C}H_2\underline{C}H_2$N-, $CH_2\underline{C}$H(N)$\underline{C}H_2$N-), 45.017 (-C(S)NH$\underline{C}H_2CH_2$-), 39.545, 36.059 (-$C_6H_4\underline{C}H_2$CH-, -$CH_2\underline{C}H_2COOH$), 28.562, 26.754, 25.641, 24.326, 23.970 ((-$\underline{C}H_2)_8$-).

MS (ESI, +ve mode): Mass (calculated) [$C_{33}H_{51}N_5O_{12}S$] 741.3; m/z (observed)741.8

2.3.2.2. Radiolabeling of BFC-undecanoic acid conjugates with ^{68}Ga

Gallium-68 was eluted in 0.6 N HCl from a 925 MBq (25 mCi) ^{68}Ge/^{68}Ga radionuclide generator obtained from iThemba Labs (South Africa).

The ^{68}Ga radiolabeling procedure followed for the two BFC-undecanoic acid conjugates was identical. Typically, BFC-undecanoic acid conjugate (100 µL, 1 mM in water) was added to 2 M sodium acetate solution (400 µL, pH~7.5). $^{68}GaCl_3$ (1 mL, 185 MBq) in 0.6 N HCl was added to it and the reaction mixture (final pH ~3.5) was incubated for 15 min at room temperature. The radiochemical yields of the ^{68}Ga-BFC-undecanoic acid conjugates were determined by HPLC. The *in vitro* stability of ^{68}Ga fatty acid conjugates at room temperature was determined over a period of 4 h.

2.3.2.3. Preparation of ^{nat}Ga- BFC-undecanoic acid complexes

The BFC-undecanoic acid conjugate (0.01 mmol) was dissolved in HPLC grade water (500 µL). pH of the solution was adjusted to ~ 4 using 0.1 M HCl. Gallium nitrate solution (2 mM, 20 µL) was added to it and the reaction mixture was incubated at 40°C for 30 min and then left for overnight stirring. The product was separated by semi-preparative HPLC and characterized by ESI-MS and HPLC.

^{nat}Ga-NODAGA-undecanoic acid

MS (ESI, -ve mode): Mass (calculated) [$C_{34}H_{51}N_6O_9SGa$] 788.27; m/z (observed) 786.9 ($M-H^+$).

^{nat}Ga-DTPA-undecanoic acid

MS (ESI, +ve mode): Mass (calculated) [$C_{33}H_{48}N_5O_{12}SGa$] 807.2; m/z (observed) 807.5 (M^+)

2.3.2.4. Partition coefficient and in vitro stability studies

For determining partition coefficient (log $P_{o/w}$), the respective ^{68}Ga-BFC-undecanoic acid conjugate (100 µL, 11.1 MBq) was mixed with water (0.9 mL) and octanol (1 mL) on a vortex mixer and then centrifuged to effect the separation of the two layers. Equal aliquots from both layers were counted in NaI(Tl) well type counter. Partition coefficient (log $P_{o/w}$) was expressed as the logarithm of the ratio of the counts from n-octanol versus that of the

aqueous layer. Further, n-octanol layer was repartitioned until consistent partition coefficient was obtained.

In order to determine the stability of the ^{68}Ga-BFC-undecanoic acid conjugates in human serum, each conjugate (50 µL, 5.6 MBq) was incubated with human serum (450 µL) at 37°C for 2 h. Thereafter, the serum proteins were precipitated by addition of acetonitrile (500 µL), the solution was centrifuged and the supernatant was analyzed by HPLC to determine the stability of the conjugate in serum.

To determine the stability of the ^{68}Ga-BFC-fatty acids towards transchelation, they were incubated with 100 fold excess EDTA solution for 2 h at room temperature. Thereafter, their radiochemical purity was determined by HPLC analysis.

2.3.2.5. In vivo evaluation studies

All procedures performed herein were in accordance with the national guidelines pertaining to the conduct of animal experiments.

(a) Biodistribution Studies

Normal female Swiss mice (20-25 g body weight) were used for the *in vivo* distribution assays of the prepared ^{68}Ga-BFC-undecanoic acids. All the mice used in the study were kept fasting for 4-5 h prior to the experiment, although water was given ad libitum. The radiolabeled preparation (100 µL, 370 KBq/10 µCi) was administered intravenously through tail vein of each animal. Individual sets of animals (n=4) were utilized for studying the biodistribution at different time points (2 min, 5 min, 10 min, 30 min). The animals were sacrificed by carbon dioxide asphyxiation immediately at the end of the respective time point and the relevant organs and tissue were excised for measurement of associated activity. The organs were weighed and the activity associated with each of them was measured in a flat-bed type NaI(Tl) counter with suitable energy window for ^{68}Ga. For the purpose of uniformity, the activity retained in each organ/tissue was expressed as a

percent value of the injected dose per gram (% I.D./g). Activity associated with the excreta (urine+feaces) was determined by counting the cage paper which was expressed as percent value of the injected dose (%I.D.).

(b) Analysis of heart metabolites

Previously reported procedures were followed for carrying out the present study[51-53]. Wistar rats (125 g, n=2) were injected with the respective ^{68}Ga-BFC-undecanoic acid (100 µL, 11.1 MBq/0.3 mCi) via the tail vein. After 15 min of the injection, the animals were sacrificed and their heart tissue excised and flushed with PBS to remove the blood. Further, the heart samples were homogenized in a mixture of $CHCl_3$: MeOH: 0.03 M NaOH (2:1:1) and centrifuged. The organic and aqueous fractions were separated and were counted along with the residual tissue pellets. The aqueous layer was then analysed by HPLC.

2.3.3. RESULTS AND DISCUSSIONS

2.3.3.1. Synthesis

The synthetic scheme for the preparation of the two BFC-fatty acid conjugates is shown in Figure 2.10.

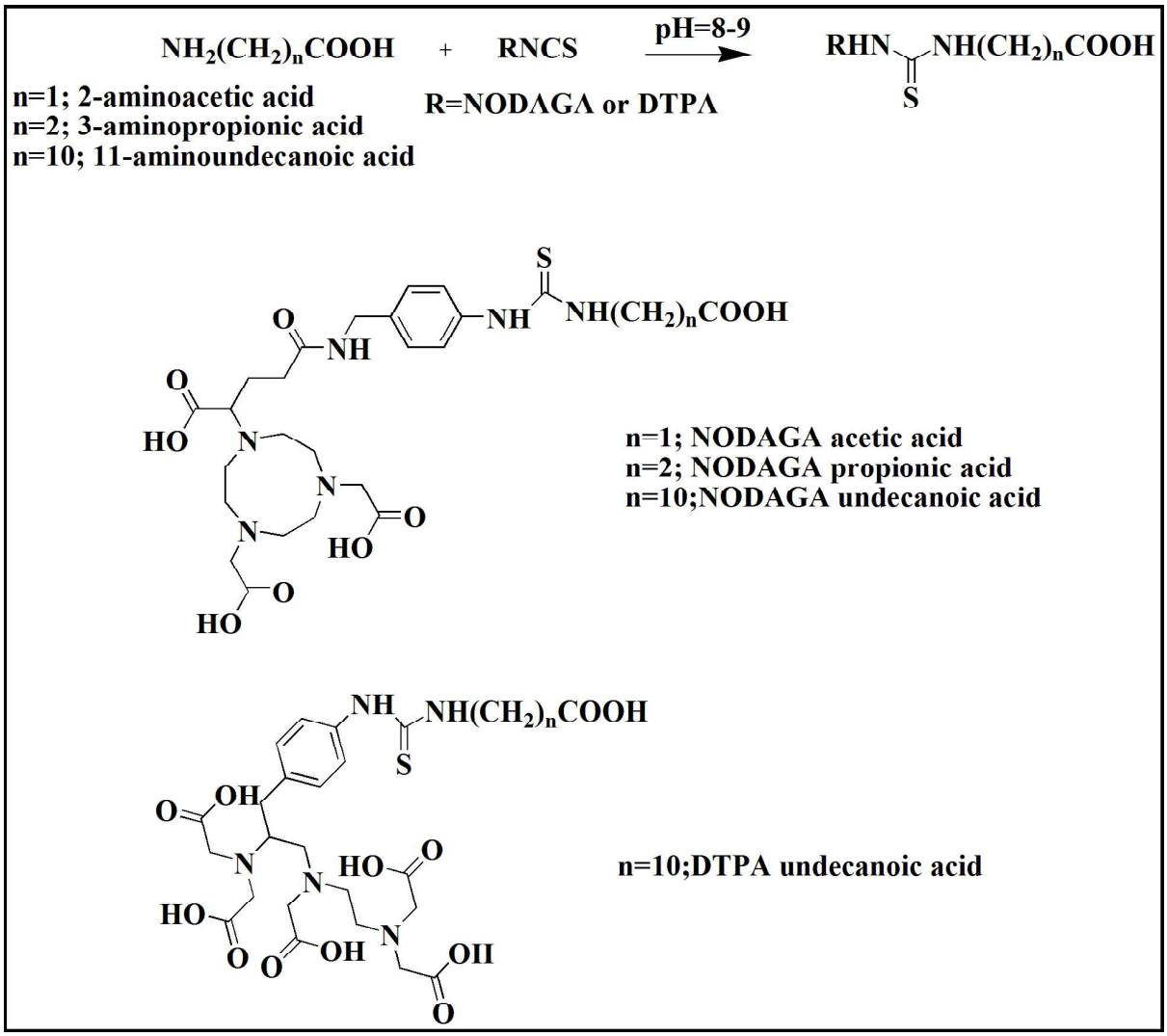

Figure 2.10. Synthetic scheme for preparation of BFC-fatty acid conjugates

The terminal amino group of 11-aminoundecanoic acid was conjugated with the isothiocyanate group of the two BFCs viz. *p*-SCN-Bn-NODAGA and *p*-SCN-Bn-DTPA, respectively. Progress of the reaction was monitored using analytical HPLC over a period of 18 h. Almost quantitative conversion of the BFC was seen for both the synthetic schemes which was indicated by disappearance of the BFC peak at around 18-19 min and appearance of a new peak at around 20-21 min. The conjugates, after HPLC purification, were characterized by ^{1}H NMR, ^{13}C NMR and ESI-MS techniques.

2.3.3.2. Radiolabeling with ^{68}Ga

The purified fatty acid conjugates NODAGA-undecanoic acid and DTPA-undecanoic acid was radiolabeled with ^{68}Ga and characterized using HPLC. The probable structures of ^{68}Ga-NODAGA-undecanoic acid and ^{68}Ga-DTPA-undecanoic acid are given in Figure 2.11 while their HPLC radiochromatograms are given in Figure 2.12 and Figure 2.13, respectively. Both the conjugates were obtained in ≥ 98% yield. Hence, no further purification was carried out before the biological experiments. The ^{68}Ga labeled fatty acid analogues prepared were found to be stable at room temperature and no significant degradation was observed up to a period of 4 h.

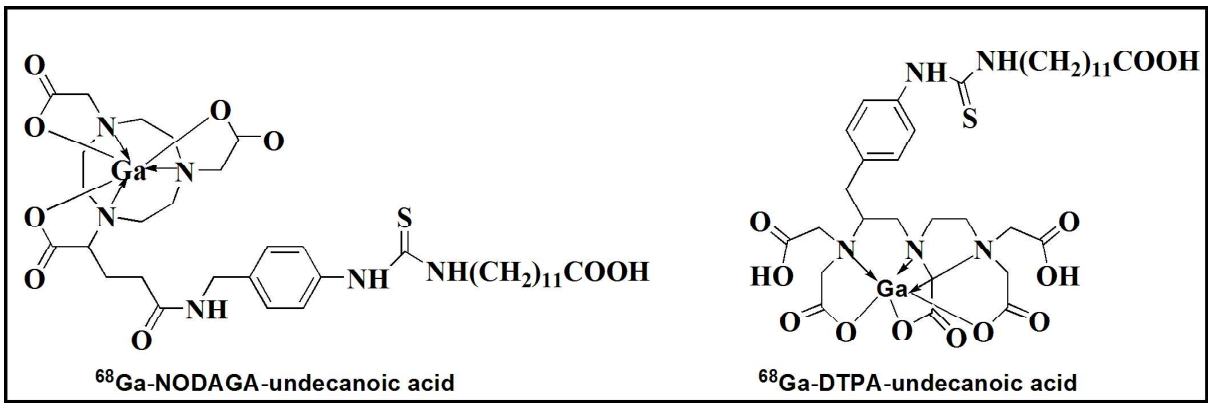

Figure 2.11. Probable structures of ^{68}Ga-BFC-undecanoic acid

2.3.3.3. Preparation of ^{nat}Ga-BFC-undecanoic acid

Since structural characterization of the ^{68}Ga conjugates prepared at tracer concentrations is difficult, the corresponding natural gallium complexes were prepared at macroscopic levels and characterized. The HPLC retention times of the ^{68}Ga fatty acid analogues were found to be analogous to their non-radioactive natural gallium counterparts as shown in Figure 2.12 and Figure 2.13. Further, the characterization of ^{nat}Ga- complexes by ESI-MS corroborated the successful synthesis of the two Ga-fatty acid conjugates.

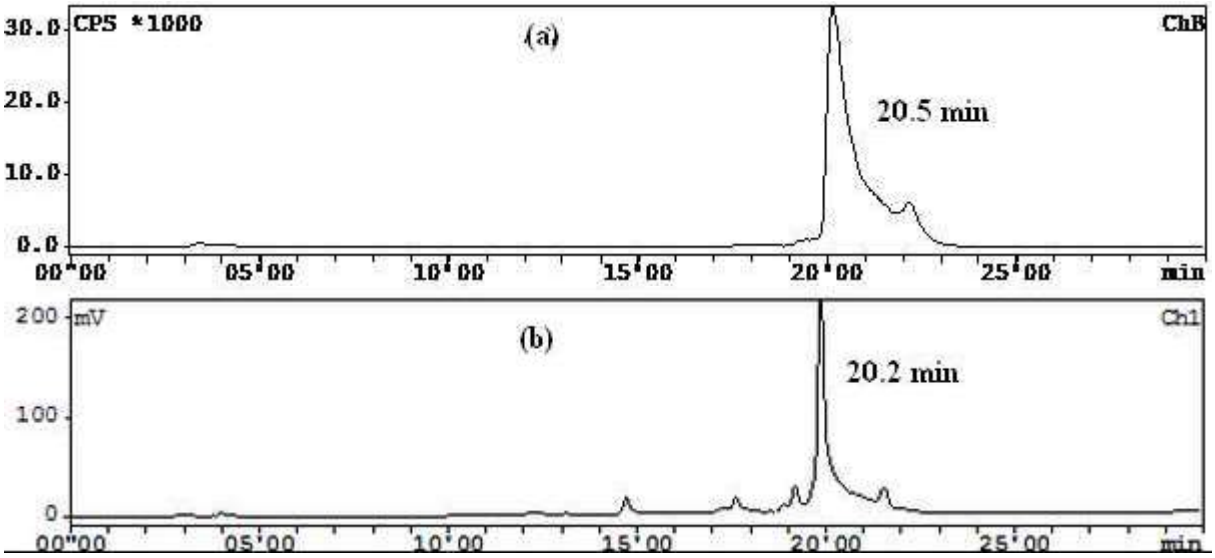

Figure 2.12. HPLC chromatogram of (a) ^{68}Ga-NODAGA-undecanoic acid (b) ^{nat}Ga-NODAGA-undecanoic acid

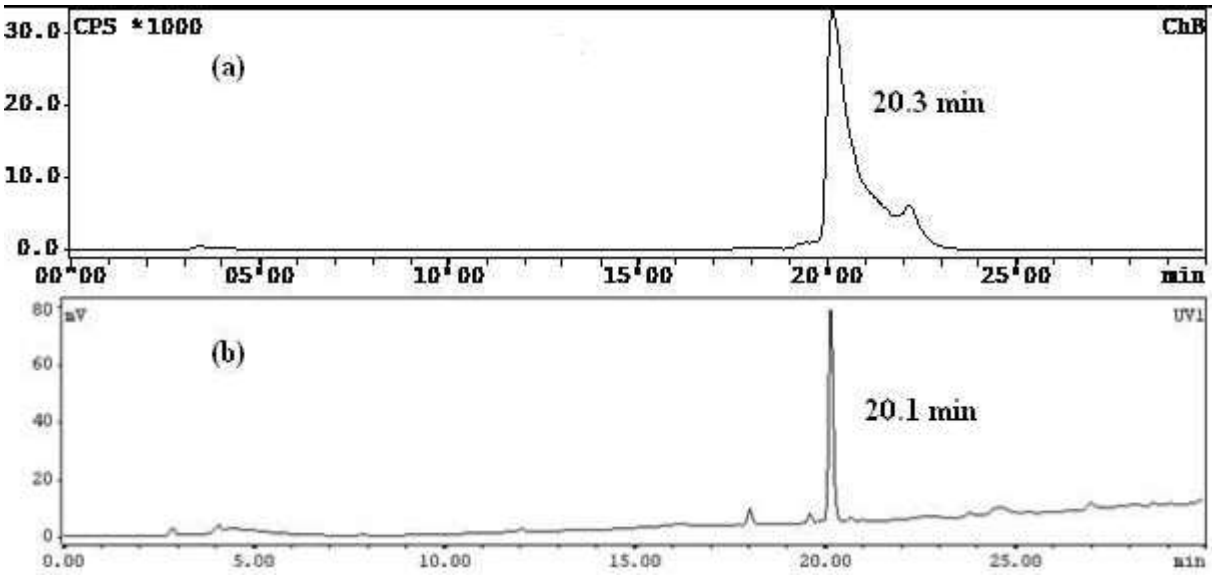

Figure 2.13. HPLC chromatograms of (a) ^{68}Ga-DTPA-undecanoic acid and (b) ^{nat}Ga-DTPA-undecanoic acid complex

2.3.3.4. Partition coefficient and in vitro serum stability studies

The log P values of the two ^{68}Ga-BFC-undecanoic acid analogues in comparison with the previously reported ^{68}Ga-NOTA-undecanoic acid are shown in Table 2.3. The DTPA conjugate was found to be the most hydrophilic among the three preparations. Both the NODAGA and DTPA conjugates were stable in human serum with stability ≥ 95 % (Table

2.3). About 15 % of the radioactivity was associated with the serum proteins. Also, both the complexes were incubated with 100 fold excess EDTA solution and were found to be ≥ 90 % stable towards transchelation.

Table 2.3. Partition coefficient (log $P_{o/w}$) and in vitro stability of ^{68}Ga-NODAGA-undecanoic acid and ^{68}Ga-DTPA-undecanoic acid in comparison with that of ^{68}Ga-NOTA-undecanoic acid

^{68}Ga-BFC-undecanoic acid	**Log $P_{o/w}$**	**Serum Stability (up to 2 h)**	**EDTA challenge (up to 2 h)**
^{68}Ga-NODAGA-undecanoic acid	0.4±0.1	94.0±0.5%	93.0±1.0%
^{68}Ga-DTPA-undecanoic acid	0.2±0.0	92.0±2.0%	90.0±2.0%
^{68}Ga-NOTA-undecanoic acid	0.3±0.0	88.0±0.1%	87.0±2.0%

2.3.3.5. In vivo evaluation studies

(a) Biodistribution studies

Results of the biodistribution studies of the two newly synthesized ^{68}Ga-BFC-undecanoic acid conjugates in normal Swiss mice are given in Table 2.4. Both the new fatty acid conjugates viz. ^{68}Ga-NODAGA-undecanoic acid (3.8±0.6% ID/g) and ^{68}Ga-DTPA-undecanoic acid (1.3±0.5% ID/g) exhibited inferior initial uptake in the myocardium compared to ^{68}Ga-NOTA-undecanoic acid (7.4±2.8% ID/g) at 2 min p.i. However, ^{68}Ga-NODAGA-undecanoic acid exhibited significant retention of activity in the heart (1.2±0.1 % ID/g) even up to 30 min p.i. Retention in the myocardium reflected in the improved heart/background ratios for ^{68}Ga-NODAGA-undecanoic acid with time (Figure 2.14). The uptake of ^{68}Ga-DTPA-undecanoic acid in the myocardium was sub-optimal. All the fatty acid

conjugates cleared rapidly from the blood. However early decline in the liver activity was observed only in the case of ^{68}Ga-DTPA-fatty acid. The latter behaviour could be attributable to the free acid groups present in the final DTPA conjugate (Figure 2.11) which may have contributed to its rapid washout from the liver.

Table 2.4. Biodistribution pattern of ^{68}Ga-NODAGA-undecanoic acid and ^{68}Ga-DTPA-undecanoic acid in Swiss mice (n=4)

Organs/ Tissue ↓	% I.D./g ± S.D.			
	2 min	**5 min**	**10 min**	**30 min**
	^{68}Ga-NODAGA-undecanoic acid			
Blood	19.9±5.1	4.5±0.7	1.4±0.3	1.8±0.1
Lungs	7.2±0.9	2.1±0.5	2.3±0.9	1.4±0.1
Heart	**3.8±0.6**	**1.4±0.3**	**1.2±0.5**	**1.2±0.1**
Stomach	1.5±0.3	8.7±2.5	6.7±0.1	5.7±1.1
Intestine	1.4±0.1	1.1±0.1	5.4±0.2	14.9±0.6
Liver	47.2±8.3	61.9±11.7	58.1±11.0	37.2±2.9
Spleen	1.8±0.5	0.6±0.1	0.5±0.2	0.9±0.3
Kidney	5.4±0.4	3.4±1.0	2.5±1.1	2.7±0.1
Muscle	10.4±2.1	9.6±0.2	7.4±0.7	2.1±0.4
Bone	0.7±0.1	0.6±0.1	0.5±0.1	0.3±0.1
Excreta(%ID)	0.5±0.2	0.5±0.1	1.9±0.5	2.1±0.5
	^{68}Ga-DTPA-undecanoic acid			
Blood	7.3±1.9	4.1±1.4	2.8±0.8	0.5±0.2
Lungs	1.8±1.0	1.5±0.2	1.0±0.1	0.2±0.0
Heart	**1.3±0.5**	**1.1±0.2**	**0.6±0.2**	**0.1±0.0**
Stomach	0.5±0.1	1.8±0.1	19.1±11.6	10.8±0.8
Intestine	1.0±0.3	3.9±0.7	19.0±1.3	31.6±3.1
Liver	34.1±6.1	50.7±12.5	40.2±2.2	15.3±5.9
Spleen	0.8±0.1	2.0±0.2	0.6±0.1	0.3±0.2
Kidney	2.2±0.2	3.9±0.1	2.9±0.7	1.3±0.2
Muscle	3.5±1.6	4.6±0.4	4.3±1.0	0.1±0.0
Bone	0.3±0.1	0.3±0.1	0.3±0.1	0.3±0.1
Excreta(%ID)	0.1±0.1	0.4±0.2	1.2±0.1	1.2±0.1

Figure 2.14 shows the myocardial uptake as well as target/non-target ratios of ^{68}Ga-NODAGA-undecanoic acid and ^{68}Ga-DTPA-undecanoic acid in comparison with the previously reported ^{68}Ga-NOTA-undecanoic acid and ^{125}I-IPPA[54].

Heart/lung ratio (0.8 *vs*. 0.6 at 30 min) of ^{68}Ga-NODAGA-undecanoic acid was found to be superior to the standard agent ^{125}I-IPPA for all the time points under study. The other ^{68}Ga-fatty acid analogues too exhibited improved heart/lung ratios at initial time point in comparison to ^{125}I-IPPA. However, rapid clearance of the activity from the heart led to decreased values with time.

All the three Ga-68 labeled fatty acids were found to be below par in terms of absolute myocardial uptake and retention in comparison to that of ^{125}I-IPPA and their critical organ ratios viz. heart/blood and heart/liver ratios also exhibited analogous behaviour. Only ^{68}Ga-NODAGA-undecanoic acid**,** due to significant myocardial retention, showed an increase in the critical organ ratio values with time.

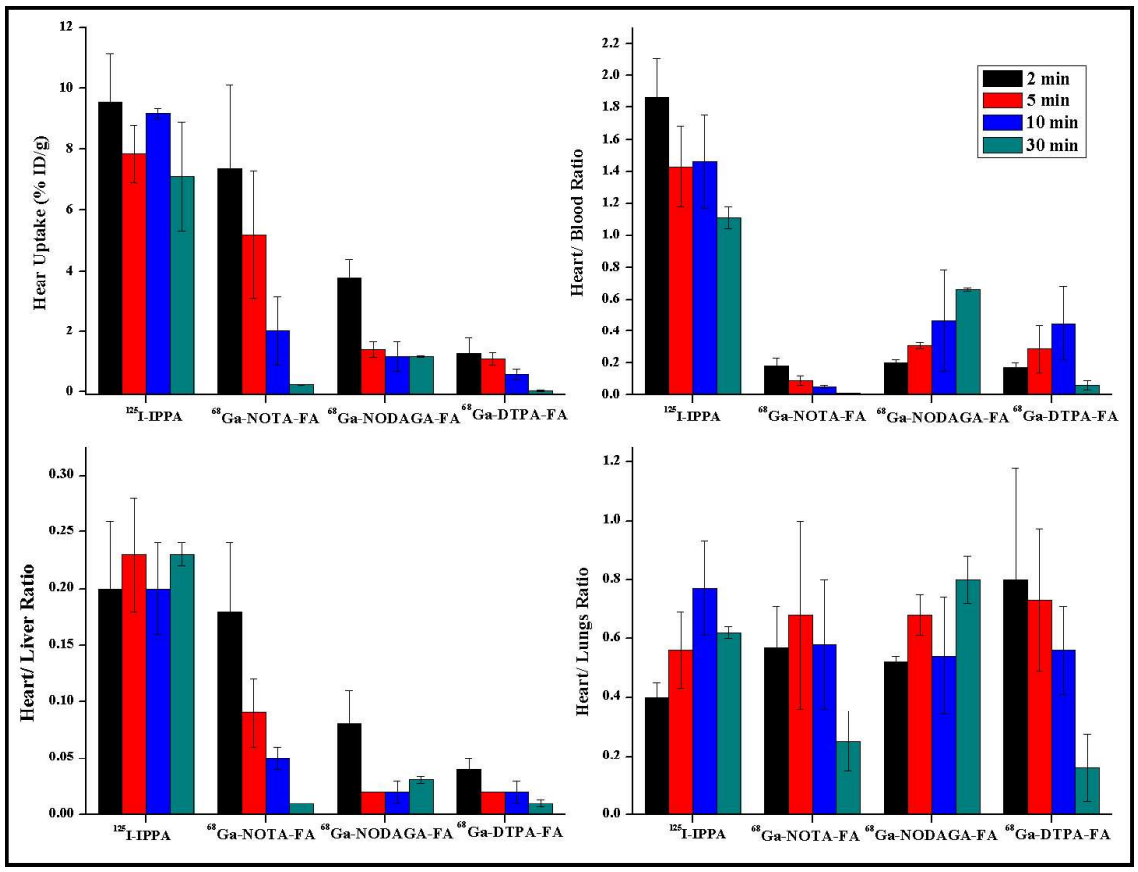

Figure 2.14. Time dependent changes in the heart, heart/blood ratio, heart/liver ratio and heart/ lung ratio of ^{68}Ga-NODAGA-undecanoic acid and ^{68}Ga-DTPA-undecanoic acid conjugates in comparison with ^{68}Ga-NOTA-undecanoic acid and ^{125}I-IPPA[54] in Swiss mice *(FA: fatty acid)*

(b) Analysis of heart metabolites

In order to ascertain whether the synthesized ^{68}Ga labeled fatty acids are true substrates for myocardial energy utilization, heart metabolites were analyzed for all the three ^{68}Ga-BFC-undecanoic acids and their structure was elucidated. The extracts of the homogenized heart samples of rats in different bilayers [$CHCl_3$-CH_3OH-0.01N NaOH] were analyzed where most of the radioactivity partitioned between the aqueous fraction and tissue pellet (Table 2.5). Since the major activity retained with the aqueous samples, it was analyzed by HPLC, where an additional peak corresponding to a polar metabolite was seen along with the parent compound (Figure 2.15). Fatty acids are known to metabolize to shorter chain residues by β-oxidation in the heart which would necessarily elute early from the C-18 column in the gradient elution method used. Thus, the peak observed below 5 min might be a product of the metabolism of the ^{68}Ga-radiolabeled fatty acid in the heart thereby confirming that though the ^{68}Ga-BFC metal chelate conjugate decrease the biological activity of the parent fatty acid moiety yet its biological efficacy is not lost.

Table 2.5. Distribution of radioactivity in the homogenized heart of rat 30 min post injection of ^{68}Ga-BFC-undecanoic acid (n=2)

Compound	Organic	Aqueous	Tissue pellet
^{68}Ga-NODAGA-undecanoic acid	5%	35%	60%
^{68}Ga-DTPA-undecanoic acid	12%	31%	57%
^{68}Ga-NOTA-undecanoic acid	3%	41%	56%

In order to ascertain the structure of the polar metabolites, surrogate molecules were prepared by conjugation of lower chain fatty acids viz. 2-aminoacetic acid and 3-aminopropionic acid with one of the BFC *p*-NCS-Bn-NODAGA (Figure 2.10), radiolabeling them with Ga-68 and analyzing them by HPLC. The retention times of short chain ^{68}Ga-NODAGA-acetic acid (9.0±0.3 min) and ^{68}Ga-NODAGA-propionic acid (12.0±0.5 min) corresponding to acetic acid and propionic acid fatty acids**,** respectively, differed significantly from the peak position of the polar metabolite observed in the HPLC pattern of ^{68}Ga-NODAGA-undecanoic acid heart metabolites. Thus, the structure of the polar metabolites obtained could not be ascertained.

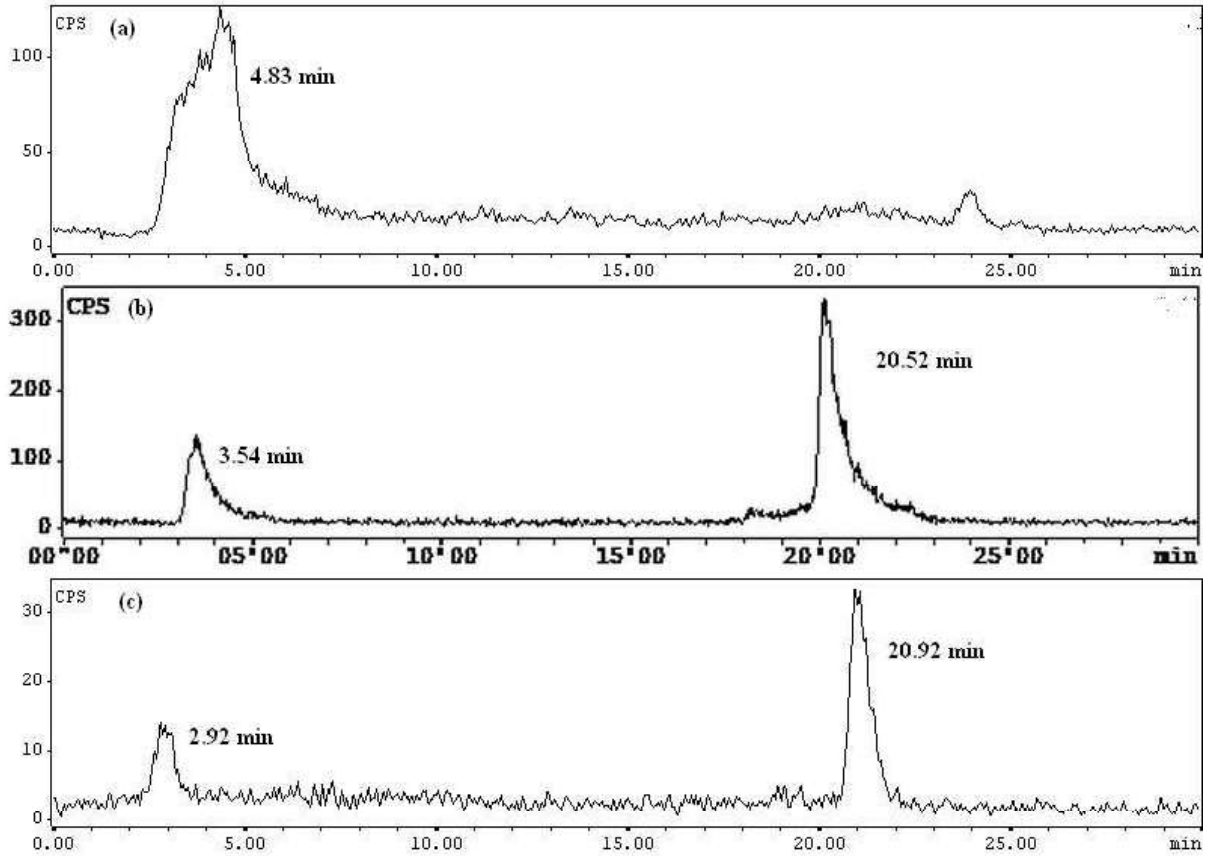

Figure 2.15. Metabolite analysis of heart tissue samples from Wistar rats injected via a tail vein, with (a) ^{68}Ga-NOTA-undecanoic acid (b) ^{68}Ga-NODAGA-undecanoic acid and (c) ^{68}Ga-DTPA-undecanoic acid

In the present section 2.3 of Chapter 2, two new 11 carbon chain fatty acids with NODAGA and DTPA chelates were synthesized and labeled with Ga-68 in high yields and purity. Biodistribution studies in Swiss mice indicated significant retention of ^{68}Ga-NODAGA complex in myocardium. Also, rapid washout of DTPA complex from non-target organs, especially liver, was seen, which is essential for tracers designed for myocardial imaging.

2.4. CONCLUSIONS

The work described in Chapter 2 constitutes the synthesis of ^{68}Ga labeled fatty acid analogues for myocardial imaging. Various ^{68}Ga-BFC-fatty acid analogues were successfully synthesized, characterized and radiolabeled with ^{68}Ga. An attempt was made to study the role of chain length as well as the chelator used on the myocardial extraction efficiency and the pharmacokinetics of the final fatty acid analogues. Amongst the various chain lengths studied, 11-carbon chain length fatty acid (^{68}Ga-NOTA-undecanoic acid) showed the highest uptake in heart followed by the longer chain fatty acids. The myocardial uptake of 16-carbon chain length (^{68}Ga-NOTA-hexadecanoic acid) was the least and its liver uptake was the highest. Amongst the bifunctional chelators studied, while ^{68}Ga-NOTA-undecanoic acid showed the highest uptake in heart, ^{68}Ga-NODAGA-undecanoic acid displayed better heart/ non target organs ratios owing to its retention in the heart. Further, a rapid washout of ^{68}Ga-DTPA-undecanoic acid from non-target organs, especially liver, was seen, which is essential for tracers designed for myocardial imaging. An amalgamation of the structural features of NODAGA and DTPA could be further evaluated for obtaining the desired pharmacokinetics required for cardiac metabolic imaging. Although none of the ^{68}Ga-fatty acid conjugates synthesised had all the characteristics comparable to that of ^{125}I-IPPA, this study opens new avenues for development of ^{68}Ga labeled fatty acids for cardiac metabolic imaging.

CHAPTER 3

PREPARATION OF ^{68}Ga BASED RECEPTOR-SPECIFIC RADIOTRACERS FOR TARGETING TUMORS

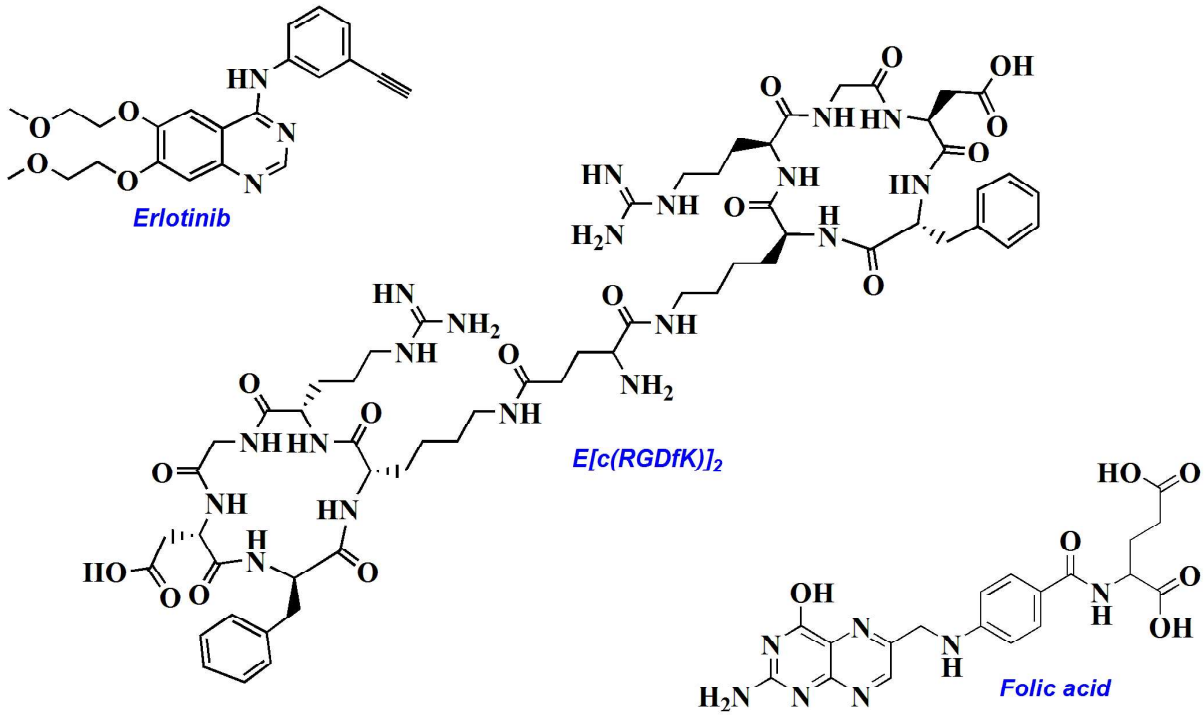

Biomolecules studied in the present chapter

CHAPTER 3a

PREPARATION OF ^{68}Ga-LABELED ERLOTINIB CONJUGATES TOWARDS IMAGING OF EGFR OVER-EXPRESSING TUMORS

3a.1. INTRODUCTION

Erlotinib (Tarceva®) is a small molecule Tyrosine Kinase Inhibitor (TKI) which targets the Epidermal Growth Factor Receptors (EGFR)[55-57]. EGFR belongs to the ErbB family of receptor tyrosine kinases (RTK). It has an extracellular ligand-binding domain, a single hydrophobic trans-membrane domain and a cytoplasmic tyrosine kinase containing domain[58]. These trans-membrane proteins are activated subsequent to binding with the peptide growth factors of the EGF-family of proteins and are known to be involved in the pathogenesis and progression of different types of carcinoma. Over-expression of EGFR has been implicated as a causative factor in the development and progression of cancers such as Non Small Cell Lung Cancer (NSCLC)[56]. In many countries including the USA, Erlotinib is an approved drug for the treatment of NSCLC. Erlotinib was approved by the US FDA in 2004 and by the European Medicinal Evaluation Agency (EMEA) in 2005 for treatment of chemotherapy-resistant advanced NSCLC patients[57,59]. Other cancers which have been targeted using Erlotinib include colon cancer and pancreatic cancer [60-62]. Erlotinib selectively and reversibly inhibits the tyrosine kinase activity of EGFR by competing with ATP (Adenosine Triphosphate) for the ATP binding sites of the TK domain, thus inhibiting the phosphorylation of TK proteins. This further disrupts the signal transduction pathways in the cancer cells[59]. Efficacy of treatment with Erlotinib has been demonstrated in a number of clinical trials performed in patients with NSCLC. However, reports suggest that patients undergoing Erlotinib treatment tend to acquire resistance to the drug in due course owing to the mutation of the target receptors[63-65].

Molecular imaging using radiolabeled TKIs may be instrumental in formulating a personalized treatment strategy for the cancer patients whose treatment can be tailored by suitably modifying the drug dose knowing the expression of particular genes/proteins in the cancer cells before and after the treatment. In this regard, there are many reports on the synthesis of radiolabeled TKI and their bioevaluation towards potential utility in the imaging of cancers over-expressing EGFR including the positron emitting ^{11}C and ^{18}F labeled Erlotinib analogues namely, ^{11}C-Erlotinib and ^{18}F-FEA-Erlotinib (Figure 3a.1)[66-82]. ^{11}C-Erlotinib has been reported to have shown potential in the clinical management of NSCLC patients, possibly as a complimentary tool to biopsy based tumor testing[83].

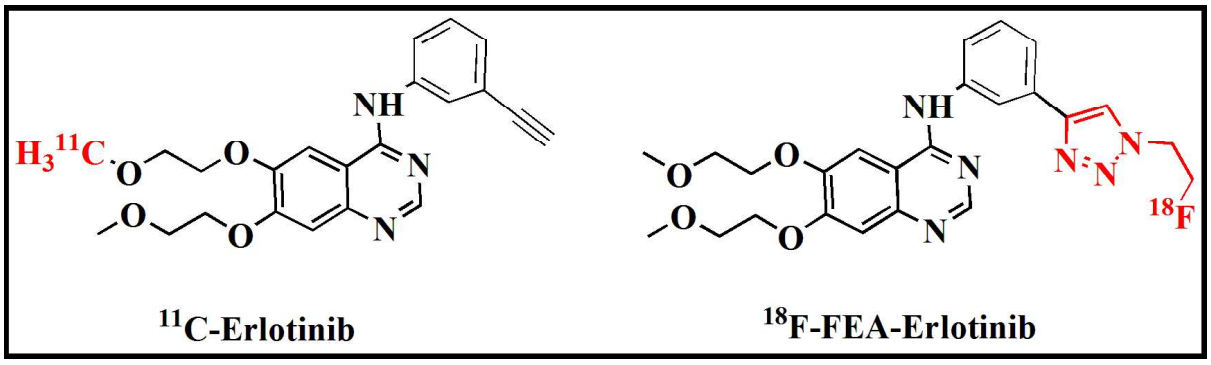

Figure 3a.1. Structures of ^{11}C-Erlotinib[80] and ^{18}F-FEA-Erlotinib[83] *(coloured bonds and atoms highlight the changes in the basic Erlotinib structure)*

However, there are limitations in the widespread availability of ^{11}C and ^{18}F radiotracers owing to their dependence on cyclotron production. The present chapter describes the design, synthesis and biological evaluation of novel ^{68}Ga labeled Erlotinib analogues as alternatives to ^{11}C and ^{18}F based agents. Erlotinib molecule was suitably functionalized at its terminal alkyne position and conjugated with two different bifunctional chelators namely *p*-SCN-Bn-NOTA and *p*-SCN-Bn-NODAGA, for stable binding with ^{68}Ga. The two chelators were chosen so as to make a comparative evaluation of the influence of their differing lipophilicities on the biological characteristics of the parent Erlotinib molecule.

3a.1.1. Click Chemistry: Copper catalyzed azide-alkyne cycloaddition (CuAAC) reaction

The term 'Click Chemistry' was first introduced by Barry Sharpless and refers to the reactions which satisfy a set of conditions[84]. The "Click reactions" are characterized by (a) simple reaction conditions, (b) high to excellent reaction yields (c) generation of harmless by-products that can be easily removed by non-chromatographic methods and (d) stereo-specific products[84,85]. Examples of click reactions are nucleophilic ring opening reactions, cyclo addition reactions, Diels-Alder reaction etc.

The CuAAC reaction has become an icon of click chemistry since its introduction by the Sharpless and Meldal laboratories[86]. This reaction satisfies all the conditions of click chemistry concept such as mild reaction conditions, selectivity and the comparatively straight forward preparation of azide and alkyne building blocks. It is a variant of the Huisgen 1,3-dipolar cycloaddition, in which organic azides and terminal alkynes are reacted to afford only 1,4-regioisomers of 1,2,3-triazoles as sole products (Figure 3a.2) unlike the Huisgen 1,3 dipolar cycloaddition wherein both 1,4 and 1,5-regioisomers of 1,2,3,-triazoles are formed. The click reaction is generally performed in the presence of a Cu(II) salt (eg. Copper sulphate) and a reducing agent (e.g. sodium ascorbate) which produce Cu (I) *in situ*[86]. As the conditions of the reaction are mild, it is well suited for the modification of a wide variety of biomolecules.

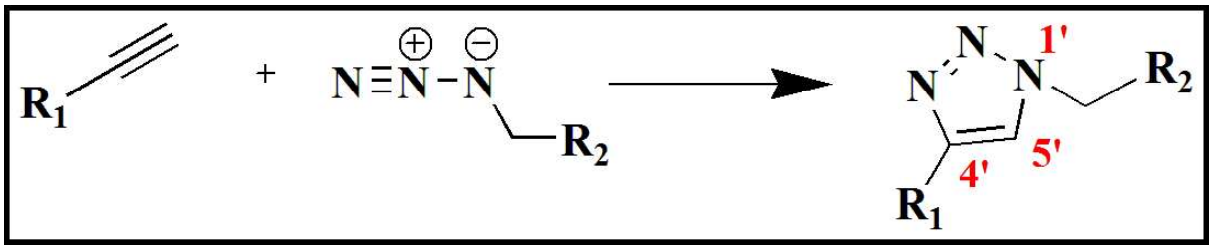

Figure 3a.2. Schematic representation of the synthesis of 1,4- disubstituted 1,2,3-triazole by CuAAC reaction[86]

In this work, the terminal alkyne group of Erlotinib was reacted with azide group of a linker by CuAAC to afford a 1,4-isomer of 1,2,3-triazole.

3a.2. MATERIALS and METHODS

Erlotinib hydrochloride was received as a gift from Tata Memorial Hospital, Mumbai. *p*-SCN-Bn-NOTA was purchased from Macrocyclics, USA while *p*-SCN-Bn-NODAGA was purchased from Chematech, France. *tert*-butyl-3-bromopropylcarbamate and sodium azide were procured from Sigma Aldrich, USA. All other reagents used were of analytical grade. Silica gel plates (Silica Gel 60 F254) were obtained from Merck, India. HPLC was carried out on a JASCO PU 2080 Plus dual pump system (JASCO, Japan) equipped with a JASCO 2075 Plus tunable absorption detector and Gina Star radiometric detector system (Raytest, Germany), using a C18 reversed phase HiQSil (5 μm, 4 ×250 mm) column and water: acetonitrile (0.1% trifluoroacetic acid –TFA) mixture as the mobile phase. Purification of the synthesized BFC-Erlotinib conjugate was performed on a JASCO-PU-2086 PLUS Intelligent Prep Pump semi-preparative HPLC system (JASCO, Japan) having a Megapak SIL C18-10 column (10×250 mm) connected with a JASCO UV-2075 Plus absorption detector. ^{1}H NMR and ^{13}C NMR spectra were recorded on a 500 MHz Varian spectrophotometer. Mass spectra were recorded on a Varian Prostar mass spectrometer using ESI in positive/negative mode. Ga-68 was eluted in 0.6 N HCl from a 925 MBq (25 mCi) ^{68}Ge/^{68}Ga radionuclide generator procured from iThemba Labs (South Africa).

In vitro cell binding studies were carried out with A431 and A549 cell lines obtained from National Centre for Cell Sciences, Pune, India. DMEM (Dulbecco's Modified Eagle's Medium - high glucose), HEPES [4-(2-hydroxyethyl)-1-piperazine ethane sulfonic acid] and sodium bicarbonate were purchased from Sigma, USA while fetal bovine serum (FBS) was procured from GIBCO Laboratories, USA. Tissue culture flasks and multi-well cell culture plates were purchased from BD Falcon™. Cell viability studies were carried out using trypan

blue of Sigma make. Biodistribution studies were carried out in two sets of animals: in Swiss mice procured from Animal House, BARC and NOD/SCID (Severe Combined Immuno Deficiency) mice procured from ACTREC, Navi Mumbai, India. Approval from the Institutional Animal Ethics Committee was obtained for the animal experiments.

3a.3. EXPERIMENTAL

3a.3.1. Synthesis

(a) Synthesis of tert-butyl-3-azidopropylcarbamate (1):

tert-butyl-3-bromopropylcarbamate (100 mg, 0.42 mmoles) and sodium azide (70 mg, 0.84 mmoles) were dissolved in DMF (1 mL). The reaction mixture was refluxed overnight at 75°C with stirring. Subsequently, the solvent was evaporated and the reaction mixture was diluted with chloroform (50 mL) and washed with water (3*50 mL). Organic layer was collected and solvent was evaporated affording the product as pale yellow oil. The product was characterized by IR, ^{1}H NMR, ^{13}C NMR and ESI-MS.

Yield: 70 mg (70%)

IR (ν_{max}, cm^{-1}): 3455*m* (N-H), 3018*s* (C-H), 2099*s* (N_3), 1707*s* (C=O), 1508*s*, 1367*m*, 1216*s*, 1169*s*, 757*m*, 667*m*.

^{1}H NMR (500 MHz, $CDCl_3$) δ ppm: 3.36 (t, 2H, $N_3C\underline{H}_2CH_2$-, *J=6.7 Hz*), 3.23-3.20 (m, 2H, -$CH_2C\underline{H}_2NH$-), 1.78-1.76 (m, 2H, -$CH_2C\underline{H}_2CH_2$-, *J=6.7 Hz*), 1.44 (s, 9H, -$C(CH_3)_3$).

^{13}C NMR (125 MHz, $CDCl_3$) δ ppm: 155.9 (-$\underline{C}(O)OC(CH_3)_3$), 79.4 (-$C(O)O\underline{C}(CH_3)_3$), 49.1 ($N_3\underline{C}H_2CH_2$-), 38.0 (-$\underline{C}H_2CH_2NH$-), 29.6 (-$CH_2\underline{C}H_2CH_2$-), 28.3 (-$(\underline{C}H_3)_3$).

MS (ESI, +ve mode): Mass (calculated) [$C_8H_{16}N_4O_2$] 200.24; m/z (observed)223 ($M+Na^+$);

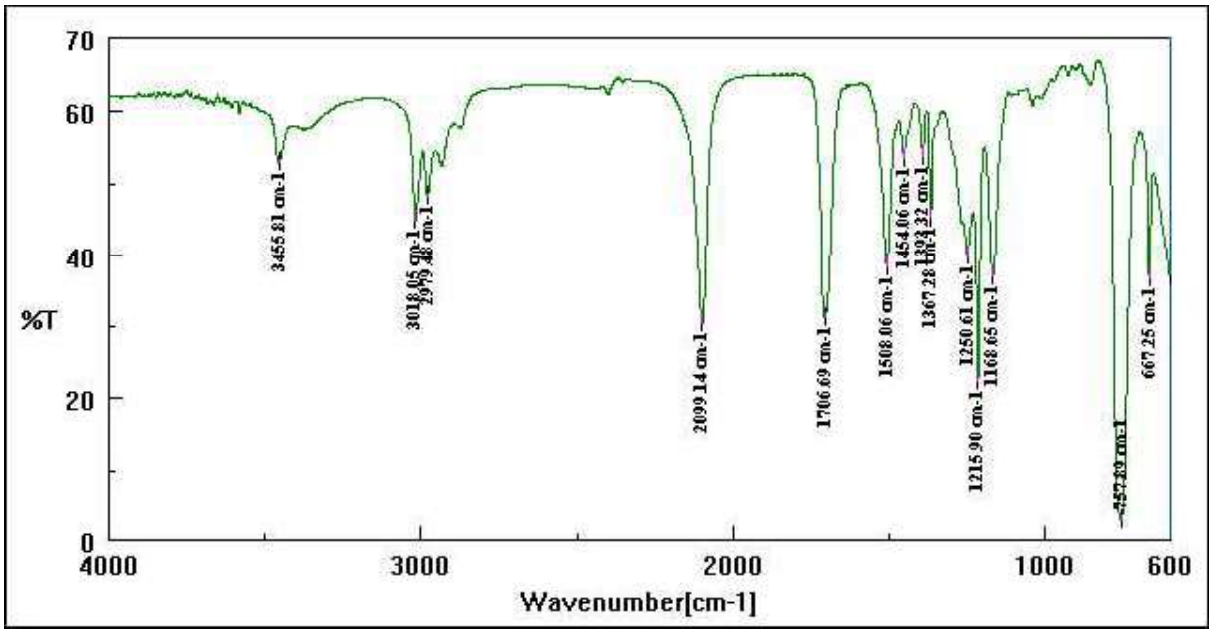

Figure 3a.3. IR spectrum of tert-butyl-3-azidopropylcarbamate (1)

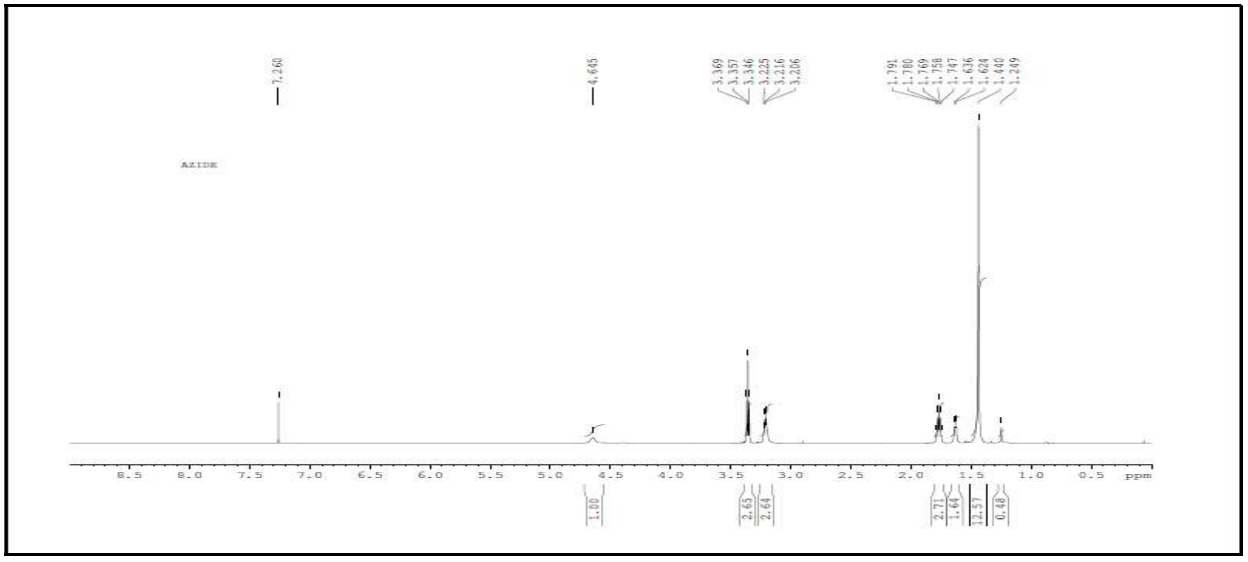

Figure 3a.4. ^{1}H NMR spectrum of tert-butyl-3-azidopropylcarbamate (1)

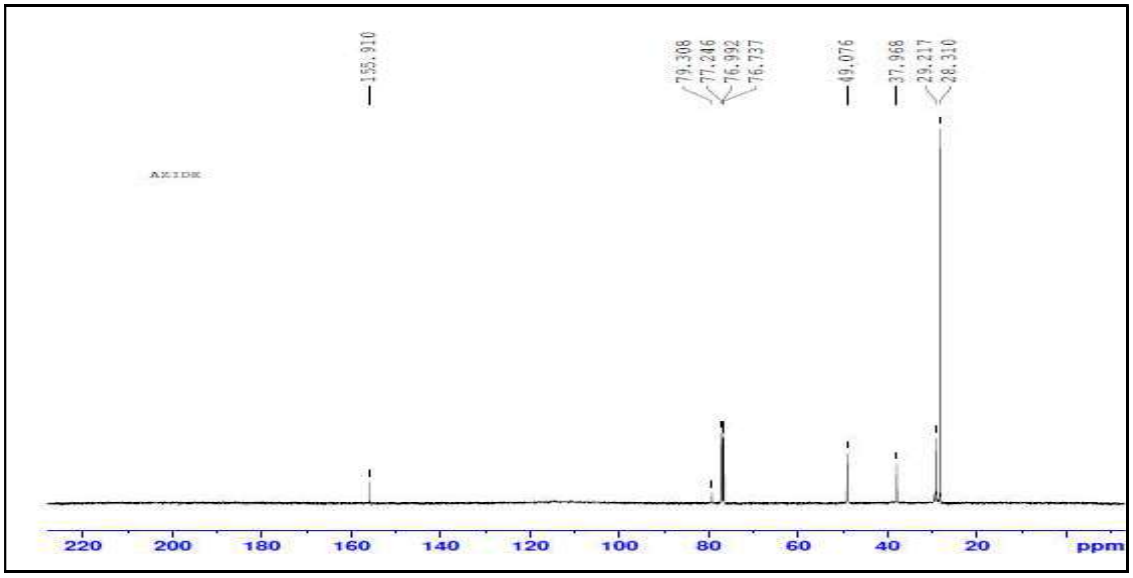

Figure 3a.5. ^{13}C NMR spectrum of tert-butyl-3-azidopropylcarbamate (1)

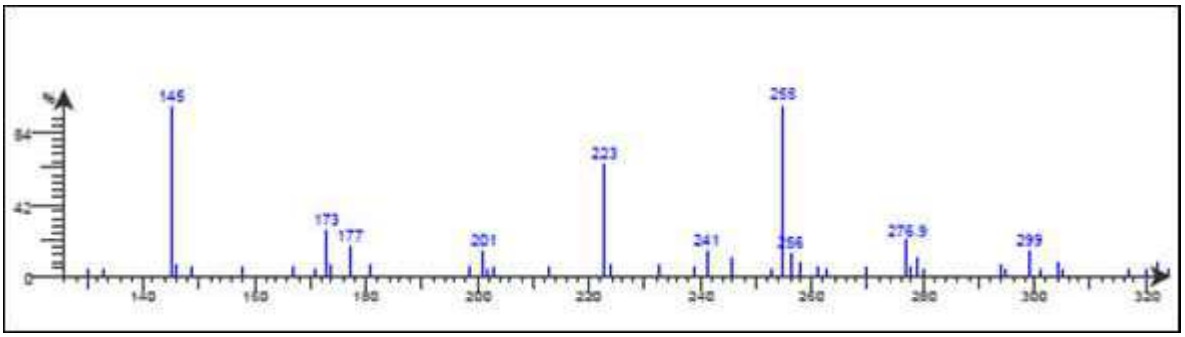

Figure 3a.6. ESI-MS of tert-butyl-3-azidopropylcarbamate (1)

(b) Synthesis of tert-butyl-3-(4-(3-(6,7-bis(2-methoxyethoxy)quinazolin-4-ylamino)phenyl)-1H-1,2,3-triazol-1-yl)propylcarbamate (2)

To a solution of Erlotinib (50 mg, 0.13 mmoles) and compound **1** (25 mg, 0.13 mmoles) in a 1:1 mixture of water and *tert*-BuOH (6 mL), sodium ascorbate (12 mg, 0.06 mmoles) and copper sulphate pentahydrate (3 mg, 0.01 mmoles) were added. The reaction mixture was stirred at 60°C for 4-5 h under nitrogen atmosphere. Progress of the reaction was monitored by TLC (5% MeOH: $CHCl_3$) as well as by analytical HPLC by following the UV profile at 254 nm and using the following gradient elution method: 0 min 90% A, 0-27 min

5% A, 30 min 90% A. After completion of the reaction, solvent was evaporated and the reaction mixture was diluted with chloroform (50 mL) and washed with water (3*50 mL). Organic layer was collected and purified by column chromatography affording a yellow solid: R_f 0.3 (in 5% MeOH in $CHCl_3$). The purified product was characterized by IR, ^1H NMR, ^{13}C NMR and ESI-MS.

Yield: 68 mg (90%)

IR (ν_{max}, cm^{-1}): 3403*m* (N-H), 2928*s* (C-H), 1692*s* (C=O amide), 1623*s*, 1582*s*, 1511*m*, 1449*m*, 1367*s*, 1244*s*, 1166*s*, 1126*s*, 930*s*, 865*s*

^1H NMR (500 MHz, $CDCl_3$) δ ppm: 8.64 (s,1H, *quinazoline*-NC(H)NC-), 8.12 (s, 1H, *triazole*-CH), 7.92-7.90 (m, 3H, *quinazoline*-CC(H)C(N)C-, -CC(H)C(C)C-, *Aryl*-C(H)C(H)C(H)CC(H)-), 7.54 (d, 1H, *Aryl*-C(H)C(H)C(H)CC(H)-), 7.45 (t, 1H, *Aryl*-C(H)C(H)C(H)CC(H)-), 7.37 (s, 1H, *Aryl*-C(H)C(H)C(H)CC(H)-), 4.49-4.46 (t, 4H, $CH_3OCH_2CH_2O$-), 4.32-4.29 (m, 6H, $CH_3OCH_2CH_2O$-, $NCH_2CH_2CH_2NH$-), 3.49 (s, 6H, $CH_3OCH_2CH_2O$-), 3.2-3.19 (m, 2H, $NCH_2CH_2CH_2NH$-), 2.16-2.13 (m, 2H, $NCH_2CH_2CH_2NH$-), 1.28 (s, 9H, -$C(CH_3)_3$)

^{13}C NMR (125 MHz, $CDCl_3$) δ ppm: 156.4 (*quinazoline*–N(H)C(=N)C-), 156.2(-C(O)$OC(CH_3)_3$), 154.3, 153.2, 148.8, 147.4, 146.8 (*quinazoline*-$C_8N_2H_3$-), 139.3 (*triazole quarternary* C-), 131.0, 129.4, 121.5, 121.1, 120.3 (*Aryl* C_6H_4-), 118.7 (*triazole* –CH), 79.6 (-$C(CH_3)_3$), 70.8,70.3, 68.9, 68.18 (-OCH_2CH_2O-), 59.2 (-OCH_3), 47.61 (-$NCH_2CH_2CH_2NH$-), 37.3 (-$NCH_2CH_2CH_2NH$-), 30.6 (-$NCH_2CH_2CH_2NH$-), 28.3 (-$(CH_3)_3$) .

MS (ESI, +ve mode): Mass (calculated) [$C_{30}H_{39}N_7O_6$] 593.3; m/z (observed) 594 ($M+H^+$), 616 ($M+Na^+$)

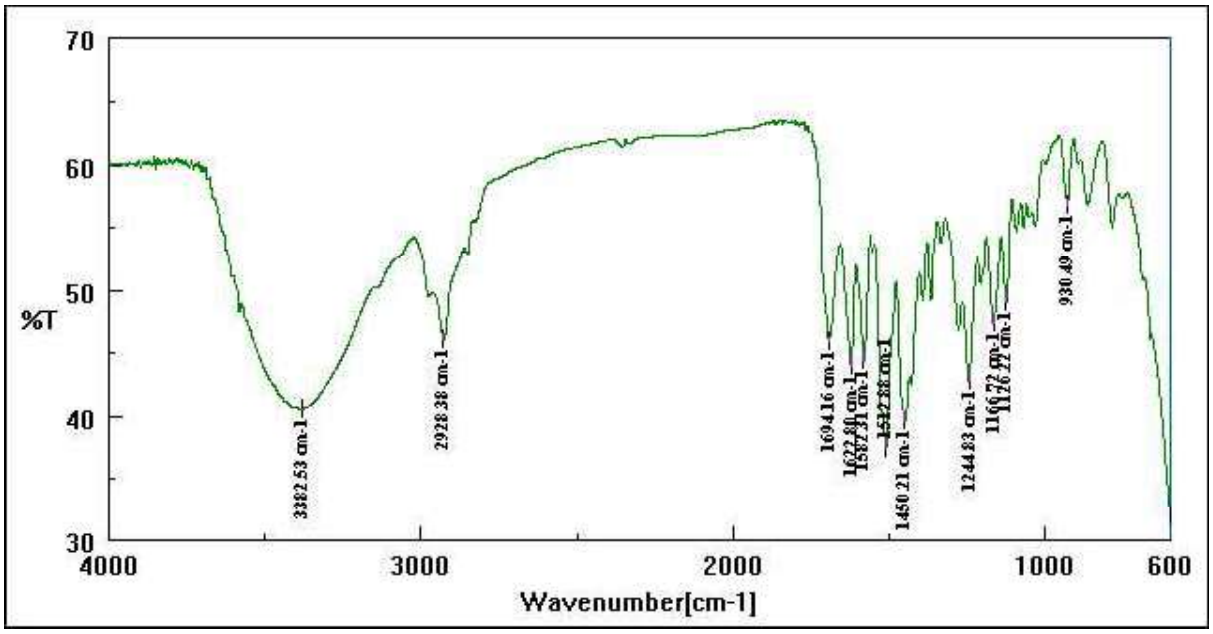

Figure 3a.7. IR spectrum of tert-butyl-3-(4-(3-(6,7-bis(2-methoxyethoxy)quinazolin-4-ylamino)phenyl)-1H-1,2,3-triazol-1-yl)propylcarbamate (2)

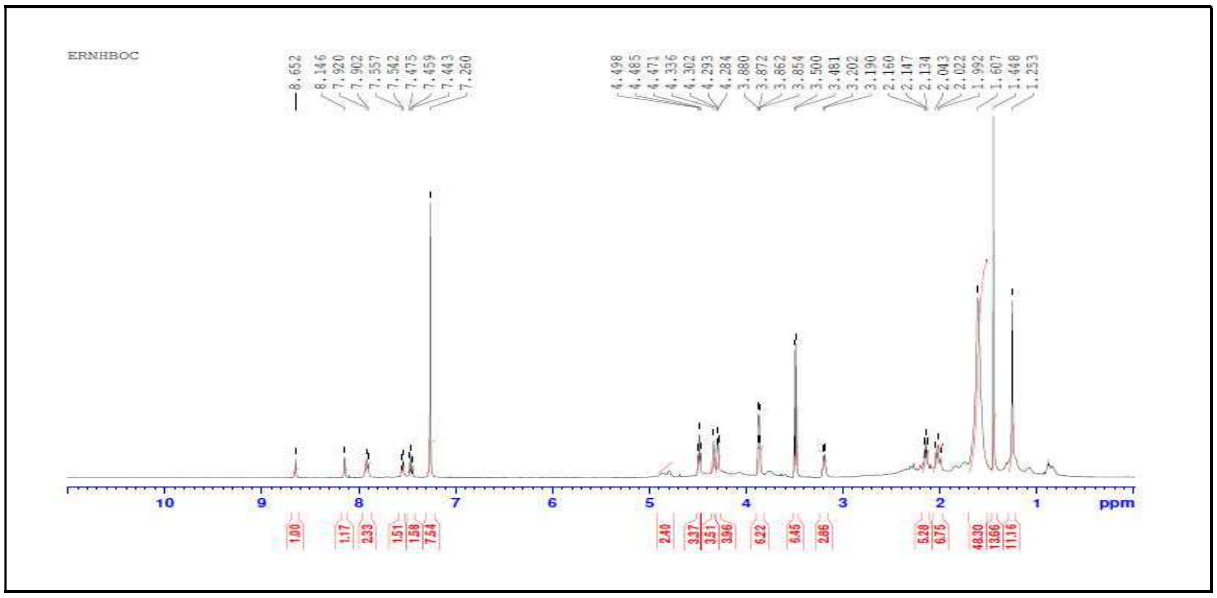

Figure 3a.8. ^{1}H NMR spectrum of tert-butyl-3-(4-(3-(6,7-bis(2-methoxyethoxy)quinazolin-4-ylamino)phenyl)-1H-1,2,3-triazol-1-yl)propylcarbamate (2)

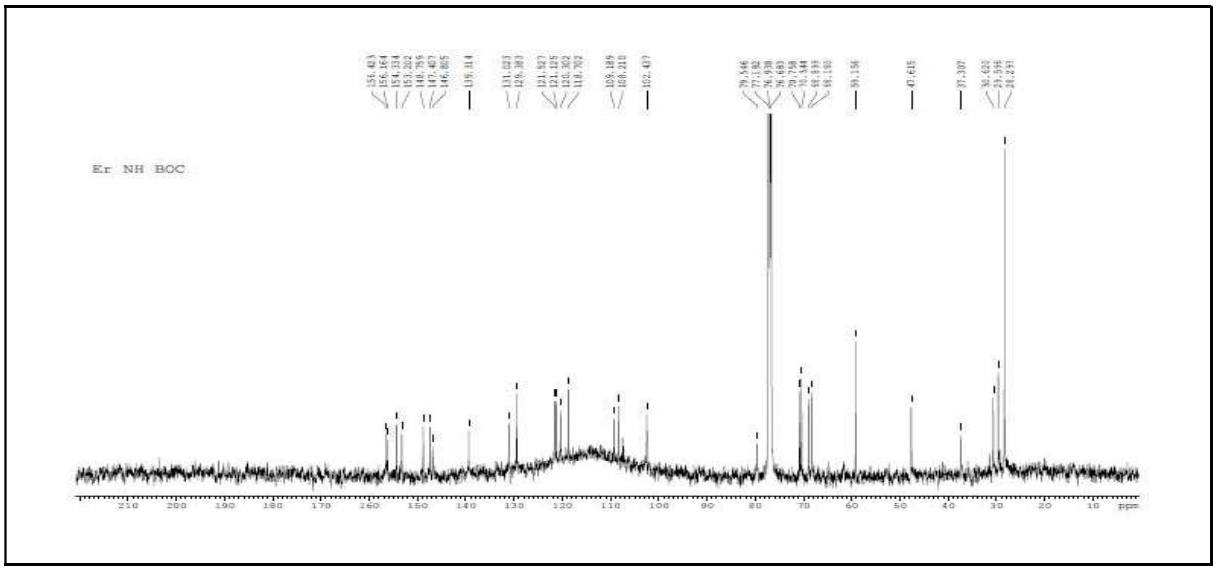

Figure 3a.9. ^{13}C NMR spectrum of tert-butyl-3-(4-(3-(6,7-bis(2-methoxyethoxy)quinazolin-4-ylamino)phenyl)-1H-1,2,3-triazol-1-yl)propylcarbamate (2)

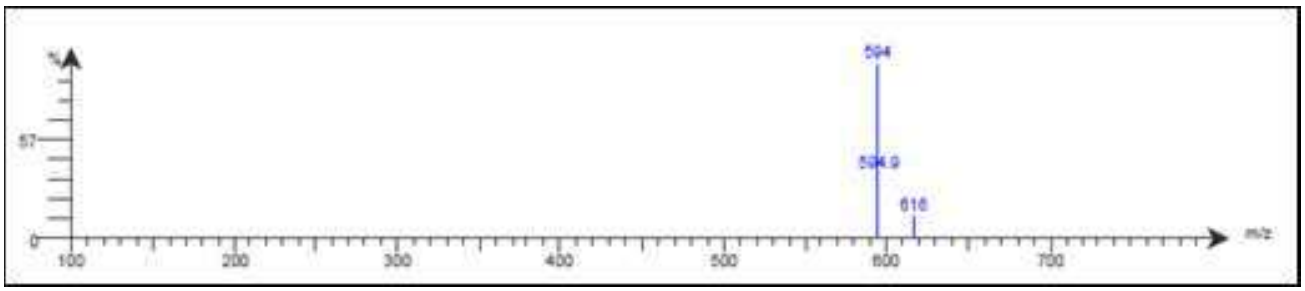

Figure 3a.10. ESI-MS spectrum of tert-butyl-3-(4-(3-(6,7-bis(2-methoxyethoxy)quinazolin-4-ylamino)phenyl)-1H-1,2,3-triazol-1-yl)propylcarbamate (2)

(c) Synthesis of 6,7-bis(2-methoxyethoxy)-N-3-(1-(3-aminopropyl)-1H-1,2,3-triazol-4-yl)phenyl)quinazoline-4-amine (3)

Compound **2** (68 mg, 0.11 mmoles) was dissolved in chloroform (1 mL) to which 4 N HCl (1 mL) was added. The reaction mixture was left for overnight stirring. Progress of the reaction was monitored by analytical HPLC (monitoring the UV peak at 254 nm) with gradient elution method as described in the previous paragraph. On completion of the reaction, solvent was evaporated and the product was washed twice with methanol. The dried

product was characterized by ESI-MS and used directly in the next step without further purification.

Yield: 56 mg (100%).

MS (ESI, +ve mode): Mass (calculated) [$C_{25}H_{31}N_7O_4$] 493.2; m/z (observed) 494.6 ($M+H^+$).

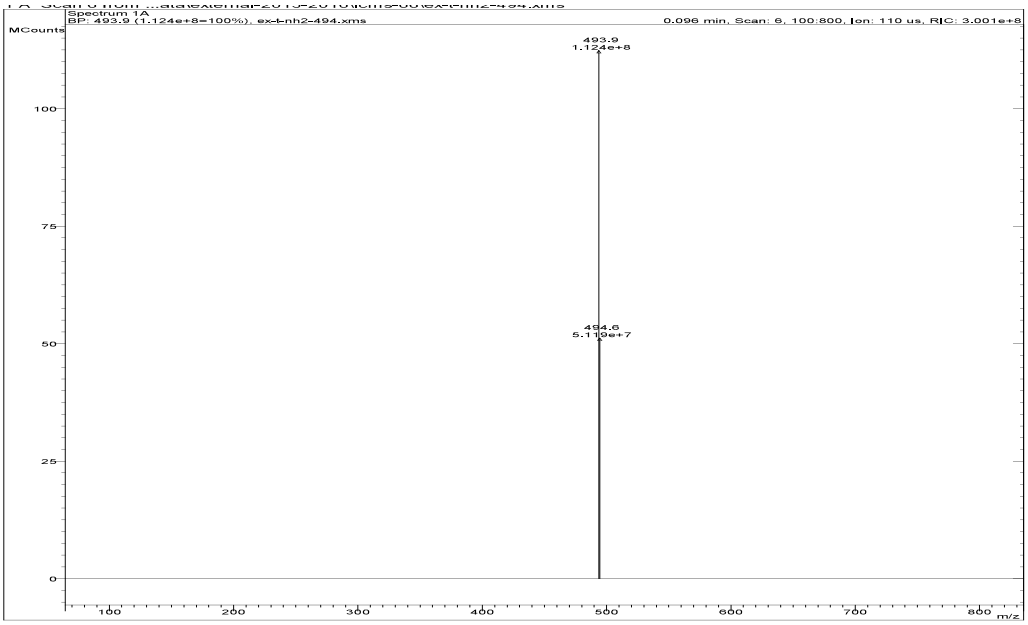

Figure 3a.11. ESI-MS spectrum of 6,7-bis(2-methoxyethoxy)-N-3-(1-(3-aminopropyl)-1H-1,2,3-triazol-4-yl)phenyl)quinazoline-4-amine (3)

(d) ***General procedure for synthesis of BFC-Erlotinib conjugates***

To a solution of compound **3** (10 mg, 0.02 mmoles) and *p*-SCN-Bn-NOTA or *p*-SCN-Bn-NODAGA (0.018 mmoles) in methanol (1 mL), diisopropylethylamine (10 µL, 57 µmoles) was added. The reaction mixture was stirred overnight at room temperature. Progress of the reaction was monitored using analytical HPLC following the UV peak at 254 nm using the gradient elution method described previously. The product was purified using semi-preparative HPLC by using the same method as above at a flow rate of 2 mL/min. The product was characterized by ^{1}H NMR and ESI-MS.

NOTA-Erlotinib (4)

Yield: 16 mg (96%)

^{1}H NMR (500 MHz, MeOH-d_4) δ ppm: 8.71 (s,1H, *quinazoline*-NCHNC-), 8.52(s, 1H, *triazole* CH-), 8.26 (s, 1H, *quinazoline*-CC(H)C(N)C-), 8.11 (s, 1H, *quinazoline*-CC(H)C(C)C-), 7.76 (m, 2H, *Aryl*-C(H)C(H)C(H)CC(H)-,*Aryl*-C(H)C(H)C(H)CC(H)-), 7.55 (m, 1H, *Aryl*-C(H)C(H)C(H)CC(H)-), 7.31 (m, 5H, *Aryl*-C(H)C(H)C(H)CC(H)-, *NOTA Aryl*-C_6H_4-CH_2), 4.42 (m, 4H, $CH_3OCH_2CH_2O$-), 3.91 (m, 6H, $CH_3OCH_2CH_2O$-, $NCH_2CH_2CH_2NH$-), 3.72-3.69 (m, 6H, -OCH_3), 3.5-3.49 (m, 8H, -$NCH_2CH_2CH_2NH$-, *NOTA ring* -NCH_2COOH), 2.7-2.68 (m, 15H, *NOTA ring* -NCH_2CH_2N- and -NCH_2CHN-, *NOTA* $C_6H_4CH_2$-, -$NCH_2CH_2CH_2NH$-)

MS (ESI, +ve mode): Mass (calculated) [$C_{45}H_{57}N_{11}O_{10}S$] 943.4; m/z (observed): 943.4 (M^+), 472.4 (M/2+ H^+)

NODAGA-Erlotinib (5)

Yield: 98% (15 mg)

^{1}H NMR (500 MHz, DMSO) δ ppm: 8.961 (s,1H, *quinazoline*-NCHNC-), 8.84(s, 1H, *triazole* CH-), 8.56 (s, 1H, *quinazoline*-CC(H)C(N)C-), 8.33 (s, 1H, *quinazoline*-CC(H)C(C)C-), 7.88 (d, 2H, *Aryl*-C(H)C(H)C(H)CC(H)-), 7.83 (d, 2H, *Aryl*-C(H)C(H)C(H)CC(H)-), 7.68 (t, 1H, *Aryl*-C(H)C(H)C(H)CC(H)-), 7.57 (s, 1H, *Aryl*-C(H)C(H)C(H)CC(H)-), 7.52 (d, 2H, *J=7 Hz*, *NOTA Aryl*-C6H4-), 7.30 (d, 2H, *J=7 Hz*, *NODAGA Aryl*-C6H4-), 4.62 (t, 4H, $CH_3OCH_2CH_2O$-), 4.52-4.51 (m, 6H, $CH_3OCH_2CH_2O$-, $NCH_2CH_2CH_2NH$-), 4.46 (s, *NODAGA Aryl*-CHNHCO-), 4.34-4.33 (m, 3H, $NCH_2CH_2CH_2NH$, *NODAGA* –NCHCOOH), 3.91 (s, 6H, -OCH_3), 3.62 (s, 4H, *NODAGA* -CH_2COOH), 2.56 (m, 12 H, *NODAGA ring* –NCH_2CH_2N-), 2.29 (t, 2H, *NODAGA* –$NHCOCH_2CH_2C$-), 1.41-1.39 (m, 2H, -$CH_2CH_2CH_2NHCS$), 0.99-0.98 (m, 2H, *NODAGA* –$NHCOCH_2CH_2C$-)

MS (ESI, +ve mode): Mass (calculated) [$C_{48}H_{62}N_{12}O_{11}S$] 1014.4; m/z (observed): 1014.6 (M^+),

3a.3.2. Radiolabeling of BFC-Erlotinib conjugates with ^{68}Ga

Briefly, BFC-Erlotinib (NOTA-Erlotinib/ NODAGA-Erlotinib) conjugate (100 µL, 0.5 mM in ethanol) was mixed with 2 M sodium acetate solution (500 µL, pH ~7.5). $^{68}GaCl_3$ (1 mL, 185 MBq) in 0.6 N HCl was added and the reaction mixture (pH~4) was incubated for 10 min at ambient temperature. Radiochemical yields of ^{68}Ga-BFC-Erlotinib conjugates were determined by HPLC by gradient elution of water (A) and acetonitrile (B) (each containing 0.1% TFA) as mobile phase at 1 mL/min flow rate and using the following gradient elution technique: 0-4 min 95% A, 4-15 min 5% A, 15-20 min 5% A, 20-25 min 95% A. The amount of BFC-Erlotinib conjugate used for ^{68}Ga labeling was optimized so as to obtain ≥ 95% yield.

3a.3.3. Preparation of ^{nat}Ga-BFC-Erlotinib conjugate

To the BFC-Erlotinib conjugate (100 µL, 0.1 M in ethanol), excess gallium nitrate solution (1 mL, 0.1 M) was added and the pH was adjusted to 4 with dilute NaOH. The reaction mixture was incubated at 40°C for 30 min. The product was characterized by ESI-MS and HPLC following the UV profile at 254 min using the gradient elution technique as described for ^{68}Ga-BFC-erlotinib (Section 3a.3.2).

^{nat}Ga-NOTA-Erlotinib

MS (ESI, + ve mode): Mass (calculated) [$C_{45}H_{54}GaN_{11}O_{10}S$] 1009.3; m/z (observed) 1042.7 ($M+MeOH+H^+$)

^{nat}Ga-NODAGA-Elotinib

MS (ESI, +ve mode): Mass (calculated) [$C_{48}H_{62}GaN_{12}O_{11}S$] 1083.4; m/z (observed) 1084.2 ($M+H^+$)

3a.3.4. Partition coefficient (log $P_{o/w}$) and stability studies

For determining log $P_{o/w}$, ^{68}Ga-BFC-Erlotinib conjugate (100 µL, 11.1 MBq) was mixed with water (0.9 mL) and octanol (1 mL) and centrifuged to effect the separation of the two layers. Equal aliquots of both layers were counted in a NaI (Tl) well type counter. log $P_{o/w}$ was expressed as the logarithm of ratio of counts in n-octanol to that in the aqueous layer. The n-octanol layer was further repartitioned until consistent value of partition coefficient was obtained.

In order to assess the extent of trans-chelation in presence of EDTA, 50 µL of ^{68}Ga-BFC-Erlotinib conjugate (6 MBq) was incubated with 10 mM EDTA solution (450 µL) for 2 h. Thereafter, the stability of the complex was determined by HPLC. Likewise, stability in human serum was determined by incubating 50 µL of the radioconjugate (6 MBq) with human serum (450 µL) for 2 h at 37°C. The serum proteins were then precipitated using acetonitrile (500 µL), the solution was centrifuged and the supernatant was analyzed by HPLC to determine the stability in serum.

3a.3.5. Bioevaluation studies

(a) Cell Viability Assay: Trypan Blue Exclusion Assay

A431 cells over-expressing EGFR were grown to confluence in DMEM containing 10% FBS. After harvesting, cells at a density of 5,000 per well were plated in 12 well plates and left overnight at 37ºC in a humidified CO_2 incubator. Three groups of cells in triplicates were taken for this study. The first group was treated with 1 µmol/L of NOTA-Erlotinib, second group with 1 µmol/L of NODAGA-Erlotinib while the last was the untreated group. At intervals of 3, 24, 48 and 72 h post-incubation with NOTA-Erlotinib and NODAGA-Erlotinib, viable cells were counted by trypan blue exclusion assay wherein the adherent and floating cells were collected at each time point, centrifuged and re-suspended in the medium. Cells were then diluted at 1:1 ratio with 0.4 % trypan blue and checked under a light microscope. Viable (unstained) and non-viable (blue-stained) cells were counted and % of

viable cells after treatment with NOTA-Erlotinib or NODAGA-Erlotinib was calculated as [number of viable cells after treatment/total number of cells] × 100.

(b) In vitro cell binding and inhibition assays

To ascertain the specificity of ^{68}Ga-BFC-Erlotinib to EGFR, *in vitro* cell binding studies were carried out in A431 cells. The cell binding studies of ^{68}Ga-NOTA-Erlotinib were also performed in A549 cells. Cells were grown to confluence in DMEM containing 10% FBS. The cells were harvested and ~ 1 x 10^6 cells per well were seeded into 12 well tissue culture plates and incubated overnight at 37ºC in a humidified CO_2 incubator. Subsequently, the cells were incubated with 1 µg of ^{68}Ga-NOTA-Erlotinib or ^{68}Ga-NODAGA-Erlotinib (~ 4 kBq per well) in 0.05 M sodium acetate buffer (pH 7.0) for 1 h at 37°C. Cells were washed twice with 1 mL of 0.05 M sodium acetate buffer (pH 7.0), solubilized with 1 mL of 1 N NaOH and the solution measured for radioactivity associated with the cells. For inhibition studies, same numbers of cells were incubated with the parent Erlotinib and/or the BFC-Erlotinib respectively at various concentrations (viz. 1, 5, 10, 50 and 100 µg) and the same amount of ^{68}Ga-BFC-Erlotinib (1 µg/4 kBq per well) under identical experimental conditions, in order to confirm the specificity of uptake of ^{68}Ga-BFC-Erlotinib to EGFR.

3a.3.6. *In vivo* evaluation studies

(a) Biodistribution studies of ^{68}Ga-BFC-Erlotinib in normal Swiss mice

All procedures performed herein were in accordance with the national laws pertaining to the conduct of animal experiments. Normal male Swiss mice (20-25 g body weight) were used for the *in vivo* distribution assays of the ^{68}Ga-BFC-Erlotinib. The radiolabeled preparation (100 µL, 370 KBq) was administered intravenously through tail vein of each animal. Individual sets of animals (n=4) were utilized for studying the bio-distribution at 1 h time point. The animals were sacrificed by carbon dioxide asphyxiation immediately at the

end of the time point and the relevant organs and tissue were excised for measurement of associated activity. The organs were weighed and the activity associated with each was measured in a flat-bed type NaI(Tl) counter with suitable energy window for ^{68}Ga. For the purpose of uniformity, the activity retained in each organ/tissue was expressed as a percent value of the injected dose per gram (% ID/g).

(b) Biodistribution studies of ^{68}Ga-NOTA-Erlotinib in EGFR^{+} tumor bearing NOD/SCID mice

Biodistribution pattern of ^{68}Ga-NOTA-Erlotinib was also studied in NOD/SCID mice bearing EGFR positive tumor at 30 min and 1 h post injection (p.i.) in groups of four each. For raising the tumors, mice weighing 18-20 g were injected with $3x10^{6}$ A431 cells subcutaneously in the right flank. Palpable tumors (0.5-0.8 g) developed within two weeks of injection. Subsequently, the animals were injected with ^{68}Ga-NOTA-Erlotinib in saline (100 µL, 370 KBq) via the lateral tail vein. A carbon dioxide saturated chamber was used to euthanize the animals. Major organs/tissues and tumor were dissected, weighed and their radioactivity measured using a flat-bed NaI (Tl) gamma counter. Radioactivity associated with the organs was corrected for decay and the percentage of radioactivity dose per gram (% ID/g) was calculated.

(c) Analysis of metabolites

For metabolite analysis, ^{68}Ga-NOTA-Erlotinib (100 µL, 370 KBq) was injected in normal Swiss mice (n=3) intravenously through the lateral tail vein of each animal. Urine samples from the animals were collected 1 h post injection and acetonitrile was added to it to precipitate the proteins. The samples were then centrifuged and the supernatant was analyzed by performing HPLC using the gradient elution method standardized for ^{68}Ga-NOTA-Erlotinib.

3a.4. RESULTS and DISCUSSION

3a.4.1. Synthesis

The scheme for synthesis of BFC-Erlotinib conjugate is given in Figure 3a.12. The terminal alkyne group of Erlotinib was reacted with the azide group of Compound **1** using copper(I) catalysed azide-alkyne cycloaddition (CuAAC) 'click' reaction to give Compound **2**. The rationale behind the modification of the terminal alkyne group of Erlotinib for the conjugation with the chelator originated from some literature reports wherein a similar modification of Erlotinib was carried out[87-89]. In one such report by Zhang et al., Zn(II)-phthalocyanine-Erlotinib conjugates were prepared for photodynamic therapy and the conjugates reportedly exhibited high uptake in HepG2 and A431 tumor cells, both of which over-express EGFR, demonstrating that the synthetic modification of terminal alkyne group did not affect the biological activity of the parent compound. Further, various patents which discuss the derivatization of the alkyne group of Erlotinib have reported high uptake of such conjugates in A431 cells[88,89].

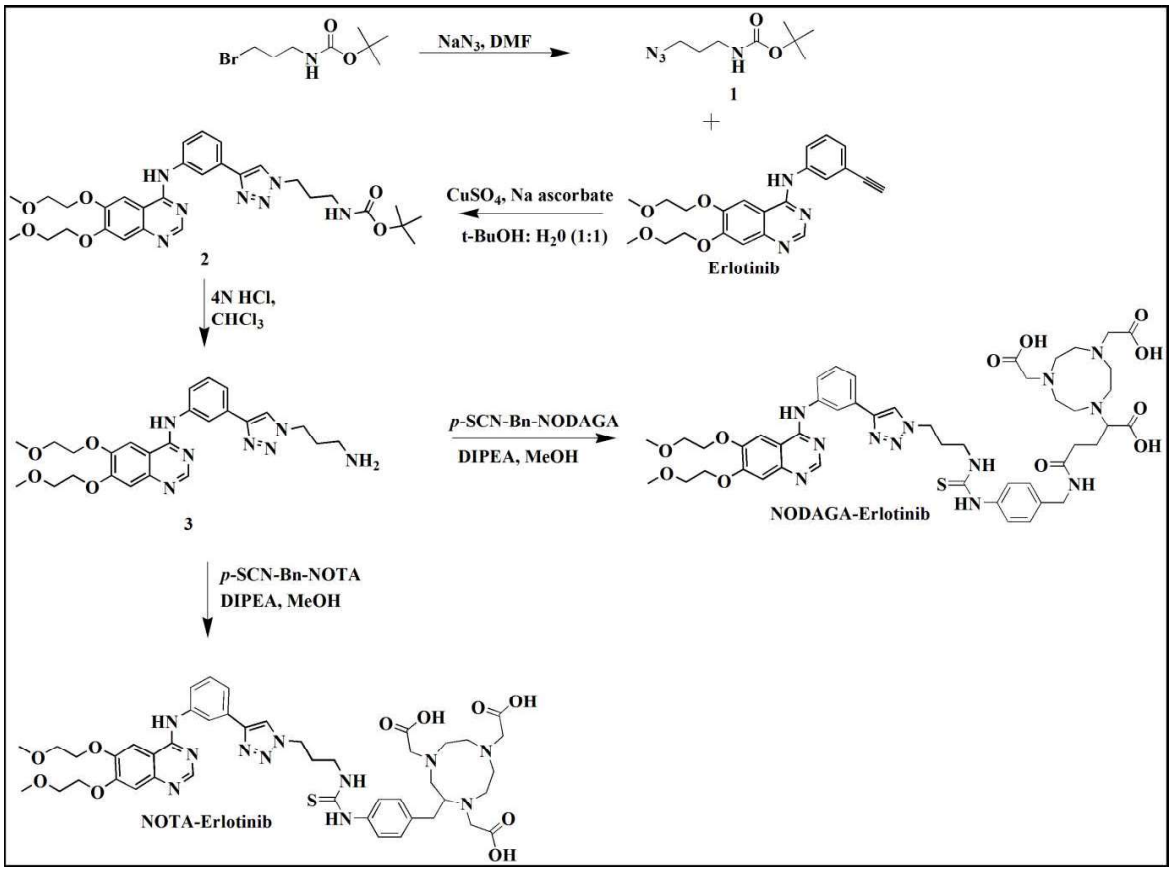

Figure 3a.12. Scheme for synthesis of NOTA-Erlotinib and NODAGA-Erlotinib

The formation of Compound **2** by CuAAC reaction was ascertained using TLC where a new UV active spot was observed at R_f 0.3 along with that of Erlotinib at R_f 0.4 in 5% MeOH/$CHCl_3$ solvent system. In addition, a shift in the parent Erlotinib peak was observed in the analytical HPLC from 19.0±0.1 min to 20.1±0.2 min. Compound **2** was obtained in ~ 90 % yield. A singlet at 8.12 corresponding to the proton of triazole ring in ^{1}H NMR and a peak at 139.5 corresponding to the quaternary carbon of triazole ring in ^{13}C-NMR confirmed the structure of Compound **2**. The ESI-MS data further corroborated its structure. In the next step, the BOC protected amine group of Compound **2** was de-protected in 4 N HCl. A new peak at 15±0.2 min in analytical HPLC along with the ESI-MS data confirmed the de-protection and formation of Compound **3**. In the final step, the amine group of Compound **3** was reacted with the isothiocyanate group of *p*-SCN-Bn-NOTA/ *p*-SCN-Bn-NODAGA under

mild basic conditions. New peaks observed in the analytical HPLC at 18 ± 0.2 min (NOTA-Erlotinib) and 18.4±0.4 min (NODAGA-Erlotinib) was then purified (~95 % purity) by semi-preparative HPLC and their structure confirmed by ^{1}H NMR and ESI-MS.

3a.4.2. Radiolabeling of BFC-Erlotinib with ^{68}Ga

NOTA-Erlotinib/NODAGA-Erlotinib was then radiolabeled with ^{68}Ga following the scheme given in Figure 3a.13. Radiolabeling yield of 95±2 % was obtained for ^{68}Ga-NOTA-Erlotinib as ascertained by HPLC (Figure. 3a.14(a)). It was observed that free $^{68}GaCl_3$ eluted at 4±0.2 min while ^{68}Ga-NOTA-Erlotinib eluted at 17.3±0.1 min (n=3). The optimum amount of NOTA-Erlotinib required for ≥ 95 % radiolabeling yield was determined to be 50-70 µg which resulted in a specific activity of 3.2±0.8 GBq/µmol of ligand for ^{68}Ga-NOTA-Erlotinib(Table 3a.1). No further purification of the ^{68}Ga-NOTA-Erlotinib conjugate was carried out prior to the bioevaluation experiments.

In case of NODAGA-Erlotinib, 100 µg of conjugate was required for achieving radiolabeling yield of 98±1%, as ascertained by HPLC (Figure 3a.15(a)). In the HPLC, ^{68}Ga-NODAGA-erlotinib had a retention time of 17.5 ± 0.2 min (n=3). The specific activity of the final product was 1.6±0.5 GBq/µmol which was lower than that of ^{68}Ga-NOTA-Erlotinib (Table 3a.1).

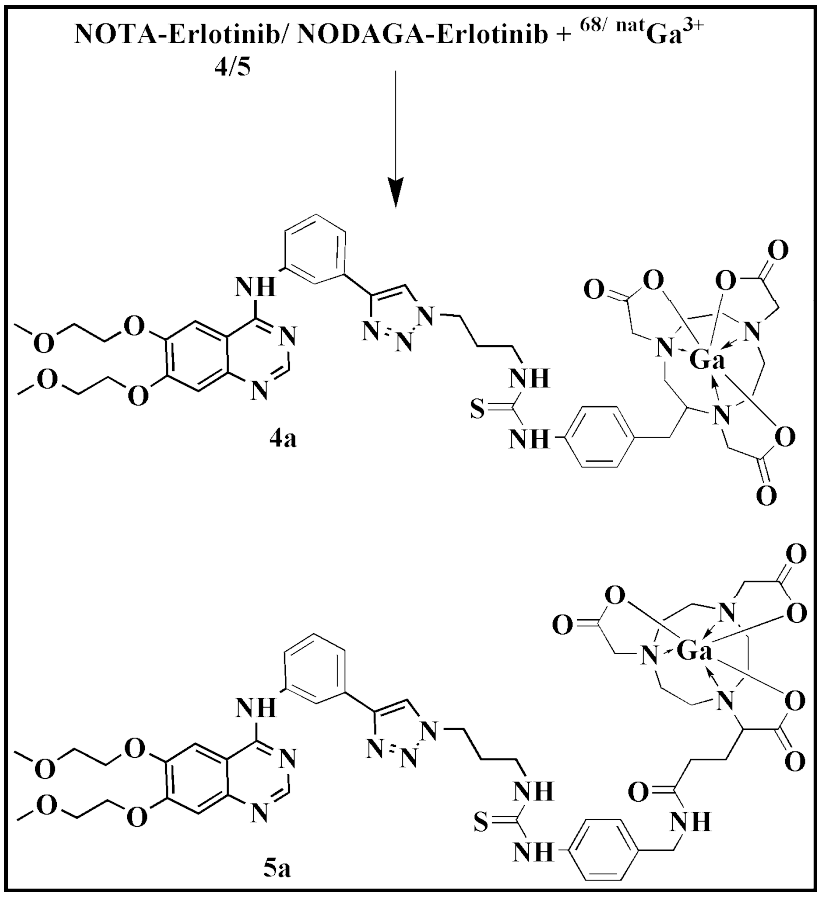

Figure 3a.13. Scheme for radiolabeling of NOTA-Erlotinib/ NODAGA-Erlotinib with $^{68/nat}Ga$

3a.4.3. Characterisation of ^{nat}Ga-BFC-Erlotinib

In order to chemically characterize the ^{68}Ga-BFC-Erlotinib conjugates, their ^{nat}Ga-NOTA-Erlotinib surrogates were synthesized at macroscopic levels. In the HPLC chromatogram of ^{nat}Ga-NOTA-Erlotinib (Figure 3a.14(b)), two peaks were observed at 3.8±0.1 min and 17.05±0.1 min (n=3) respectively. The peak at 3.8 min corresponded to free Ga(III), as excess of gallium nitrate was taken initially to ensure completion of the reaction. The peak at 17.05 min was collected and was evaluated using ESI-MS. Its MS data corresponded to the ^{nat}Ga-NOTA-Erlotinib conjugate further substantiating the successful synthesis of ^{68}Ga-NOTA-Erlotinib conjugate according to Figure 3a.13.

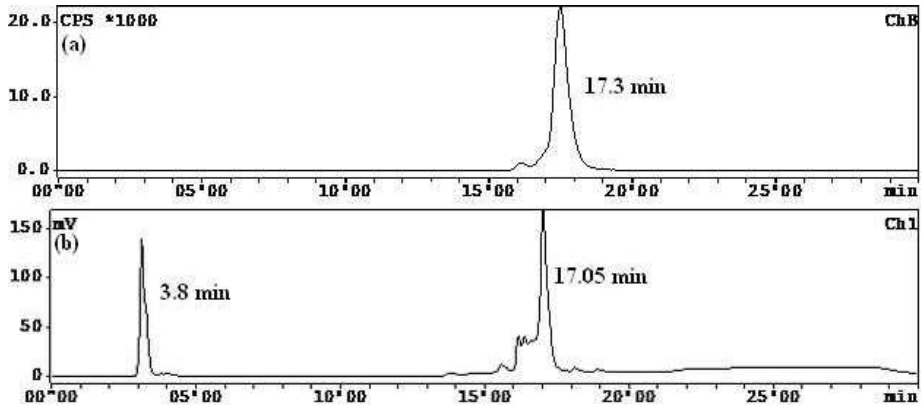

Figure 3a.14. HPLC chromatogram of (a) ^{68}Ga-NOTA-Erlotinib and (b) ^{nat}Ga-NOTA-Erlotinib

Similarly, the proximate retention times of both ^{68}Ga (17.5±0.2 min) and ^{nat}Ga (17.1±0.5 min) NODAGA-Erlotinib conjugates (Figure 3a.15) in the analytical HPLC system suggested that the desired ^{68}Ga-NODAGA-Erlotinib analogue was successfully synthesized and ESI-MS further corroborated the successful synthesis.

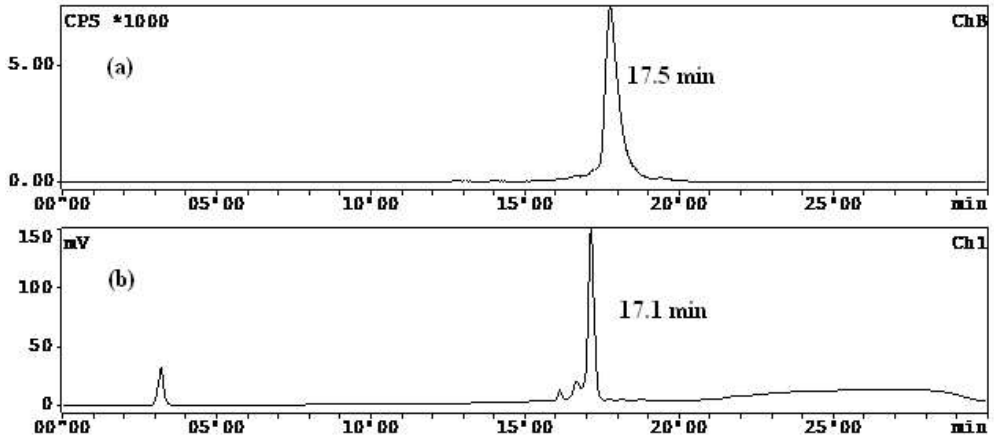

Figure 3a.15. HPLC chromatogram of (a) ^{68}Ga-NODAGA-Erlotinib (b) ^{nat}Ga-NODAGA-Erlotinib

3a.4.3. Partition coefficient and stability studies

The log $P_{o/w}$ value, specific activity and the results of *in vitro* stability studies of ^{68}Ga-BFC-Erlotinib are given in Table 3a.1.

Table 3a.1. Partition coefficient (log $P_{o/w}$), in vitro stability and specific activity of ^{68}Ga-NOTA-Erlotinib in comparison with ^{68}Ga-NODAGA-Erlotinib

Tracer ↓	log $P_{o/w}$	% *In vitro* stability		Specific Activity (GBq/ µmol)
		Serum	EDTA	
^{68}Ga-NOTA-Erlotinib	– (0.6±0.1)	98.0±1	94.0±0.2	3.2±0.8
^{68}Ga-NODAGA-Erlotinib	– (1.21±0.2)	96.0±0.1	97.0±0.5	1.6±0.5

The log $P_{o/w}$ values of both the ^{68}Ga-BFC-Erlotinib analogue suggests that they are hydrophilic in nature with ^{68}Ga-NODAGA-Erlotinib being more hydrophilic in nature. It is known that Erlotinib is a highly lipophilic molecule with poor solubility in aqueous media. Conjugation of Erlotinib with NOTA/ NODAGA with the aim to radiolabel with ^{68}Ga concurrently resulted in decrease in the lipophilicity of the radioconjugates, evident from their log $P_{o/w}$ values and also improved their solubility in aqueous medium.

The *in vitro* stabilities of both ^{68}Ga-NOTA-Erlotinib and ^{68}Ga-NODAGA-Erlotinib in EDTA solution and human serum are given in Table 3a.1. High stability is a primary requirement of a radiopharmaceutical as it ensures no abnormal distribution of activity in the various tissues/organs.

3a.4.5. Bioevaluation studies

(a) Cell Viability Assay: Trypan Blue Exclusion Assay

In order to ascertain the TKI properties of NOTA-Erlotinib/ NODAGA-Erlotinib, cell viability studies were performed in A431 cells and the results are given in Table 3a.2. Cells incubated with 1 µM BFC-Erlotinib conjugates respectively, showed a marked decrease in %

viability when studied up to 72 h post-addition confirming that both the BFC-Erlotinib conjugate retained the TKI properties of the parent Erlotinib molecule. However, only a 39.5 % decrease in viable cells was observed in 72 h in case of ^{68}Ga-NODAGA-Erlotinib, as compared to 87.5% decrease in viable cells observed for ^{68}Ga-NOTA-Erlotinib in 72 h.

Table 3a.2. Cell viability studies of NOTA-Erlotinib and NODAGA-Erlotinib in A431 cells

Time post treatment ⟶	% Cell viability			
	3 h	**24 h**	**48 h**	**72 h**
1 µM NOTA-Erlotinib	40.0±0.2	37.5±0.1	28.5±0.4	12.5±0.3
1 µM NODAGA-Erlotinib	98.0±0.5	88.7±1.3	70.1±1.5	60.5+4.9

(b) In vitro cell uptake and inhibition assays

The specificity of ^{68}Ga-NOTA-Erlotinib to EGFR was determined by *in vitro* cell uptake studies using A431 and A549 cells and the results are given in Figure 3a.16. A431 cells showed an uptake of 9.8±0.4 % with ^{68}Ga-NOTA-Erlotinib. Inhibition up to 55.1±0.2 % was observed using 10 µg of unlabeled Erlotinib indicating the specificity of ^{68}Ga-NOTA-Erlotinib to EGFR. However, ^{68}Ga-NOTA-Erlotinib did not show any uptake with A549 cells indicating the resistance of the cell line to Erlotinib[90].

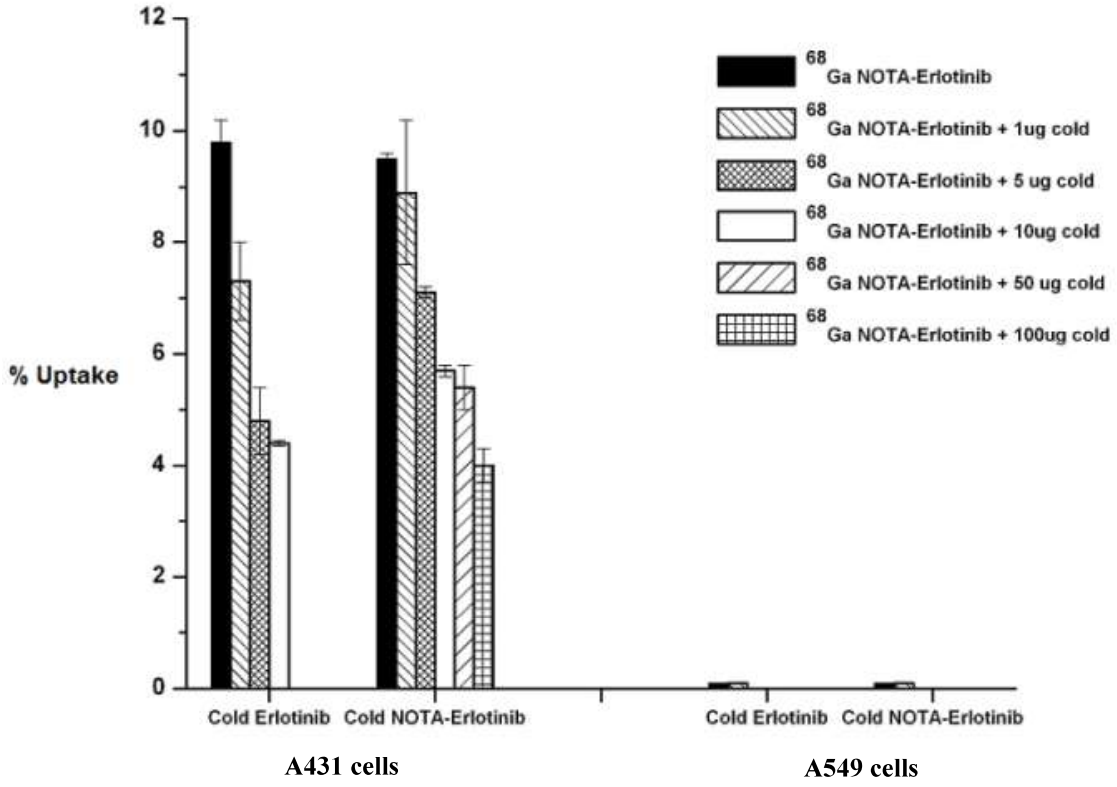

Figure 3a.16. In vitro cell uptake and inhibition studies of ^{68}Ga-NOTA-Erlotinib in A431 and A549 cells

^{68}Ga-NODAGA-Erlotinib exhibited an uptake of 7.8±1.3 % in A431 cells which was significantly lower than the uptake observed for ^{68}Ga-NOTA-Erlotinib in A431 cells. 30.7±0.5 % inhibition in the uptake of ^{68}Ga-NODAGA-Erlotinib was observed on incubation of A431 cells with 10 µg of Erlotinib (Figure 3a.17). Further, an inhibition of up to 20.5±0.3 % was observed when the A431 cells were incubated with 10 µg unlabeled NODAGA-Erlotinib confirming the specificity of NODAGA-Erlotinib to EGFRs.

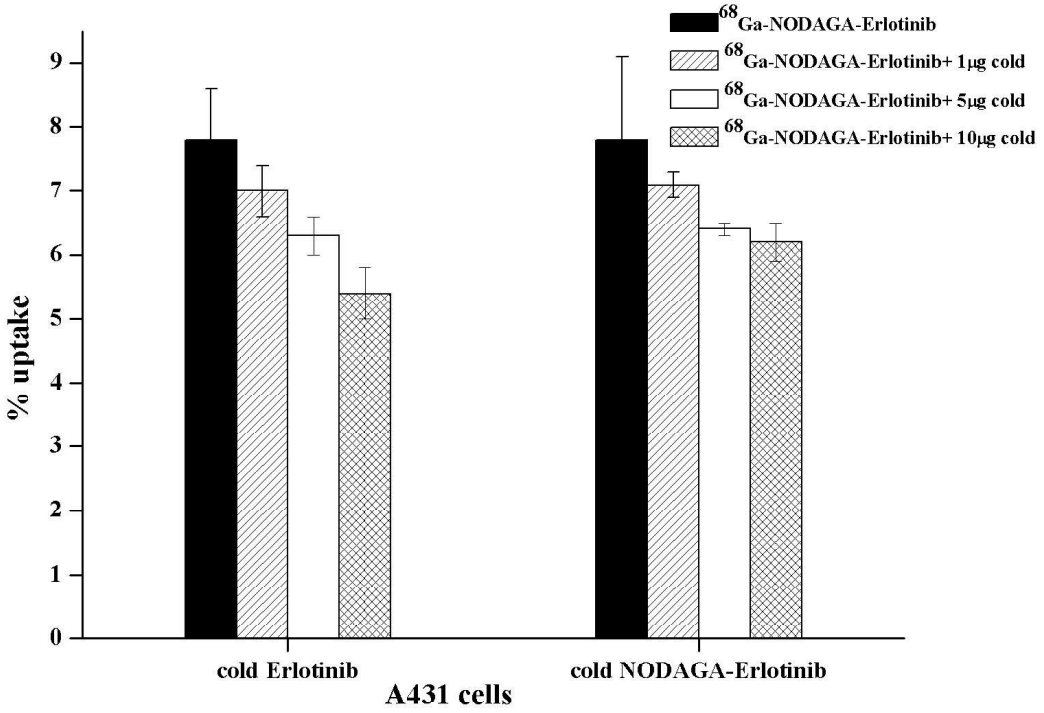

Figure 3a.17. In vitro cell uptake and inhibition results of ^{68}Ga-NODAGA-Erlotinib in A431 cells

For the biological efficacy of a TKI, some level of lipophilicity is required for passage of the tracer through the cell membrane and bind to the ATP binding pocket in the TK domain of EGFRs[91]. It might be possible that due to the increase in hydrophilicity of ^{68}Ga-NODAGA-Erlotinib, there is insufficient cellular penetration and thus a decrease in cellular uptake in A431 cells. However, the % uptake of ^{68}Ga-NODAGA-Erlotinib and ^{68}Ga-NOTA-Erlotinib in A431 cells was higher than the highest uptake at 60 min (5.8±0.6 % of total dose added) reported for ^{18}F-FEA-Erlotinib in EGFR over-expressing cells (HCC827, A431 and HepG2).[82]

3a.4.6. In vivo evaluation studies

(a) Biodistribution studies of ^{68}Ga-BFC-Erlotinib in normal Swiss mice

The biodistribution results of ^{68}Ga-NOTA-Erlotinib in Swiss mice at 1 h in comparison with that of ^{68}Ga-NODAGA-Erlotinib are given in Table 3a.3. As compared to ^{68}Ga-NOTA-Erlotinib, ^{68}Ga-NODAGA-Erlotinib exhibited low uptake at 1 h in organs such

as blood (%I.D./g: 0.5±0.1 *vs* 2.6±1.3), lungs (%I.D./g: 0.6±0.4 *vs* 3.0±1.1), heart (%I.D./g: 0.1±0.1 *vs* 1.0±0.6), spleen (%I.D./g: 0.0±0.0 *vs* 1.1±0.5), kidney (%I.D./g: 0.8±0.4 *vs* 11.0± 4.34) and muscle (%I.D./g: 0.0±0.0 *vs* 0.48±0.18). This shows that an increase in hydrophilicity of ^{68}Ga-NODAGA-Erlotinib in comparison to ^{68}Ga-NOTA-Erlotinib facilitated low uptake in different organs.

Table 3a.3. Biodistribution pattern of ^{68}Ga-BFC-Erlotinib in Swiss mice at 1 h p.i. (n=4)

Organs/ Tissues ↓	**% I.D./g ± S.D.**	
	^{68}Ga-NOTA-Erlotinib	**^{68}Ga-NODAGA-Erlotinib**
Blood	2.6±1.3	0.5±0.1
Lungs	3.0±1.1	0.6±0.4
Heart	1.0±0.7	0.1±0.1
Stomach	0.8±0.3	5.4±3.5
Intestine	12.0±3.8	30.9±6.9
Liver	6.6±2.5	6.3±2.6
Spleen	1.1±0.5	0.0±0.0
Kidney	11.0±4.3	0.8±0.4
Muscle	0.5±0.2	0.0±0.0
Bone	0.06±0.05	0.0±0.0
Excreta (% I.D.)	24.1±12.0	32.3±0.2

However, the uptake of ^{68}Ga-NODAGA-Erlotinib activity in the intestine (%I.D./g: 30.9±6.9 *vs* 12.0±3.8) was significantly higher at 60 min p.i. as compared to that of ^{68}Ga-NOTA-Erlotinib. The high uptake of ^{68}Ga-NODAGA-Erlotinib activity in stomach and intestine indicated fast hepatobiliary clearance of the radiotracer. The excretion of ^{68}Ga-NODAGA-Erlotinib at 60 min (% I.D.: 32.3±0.2 *vs* 24.1±12.0) was also much higher than that of ^{68}Ga-NOTA-Erlotinib.

The uptake of ^{68}Ga-NODAGA-Erlotinib in organs such as liver (^{68}Ga; ^{11}C; ^{18}F (%ID/g):: 6.3±2.6; 14.94 to10.55; 17.1±4.4) and kidney (^{68}Ga; ^{11}C; ^{18}F (% ID/g):: 0.8±0.4; 4.28 to 1.69; 1.6±0.3) was much lower than that reported for ^{11}C-Erlotinib[80] and ^{18}F-FEA-Erlotinib[82], both of which are highly lipophilic in nature. This underscores the effect of hydrophilicity on the clearance of activity from non-target organs.

(b) Biodistribution studies of ^{68}Ga-NOTA-Erlotinib in EGFR^{+} tumor bearing NOD/SCID mice

Since ^{68}Ga-NODAGA-Erlotinib showed low specificity for EGFRs in A431 cells, its *in vivo* studies were not performed in tumor bearing mice as a low retention in tumor tissues was expected. Thus, only the biodistribution pattern of ^{68}Ga-NOTA-Erlotinib was studied in NOD/SCID mice bearing EGFR positive tumor at 30 min and 1 h post injection (p.i.) in groups of four each. Results of the biodistribution studies are given in Table 3a.4. Uptake of ^{68}Ga-NOTA-Erlotinib in the tumor was 1.5±0.1 % ID/g at 30 min p.i. which decreased at 1 h (0.7±0.2 % ID/g) p.i. The tumor/lungs ratios were moderately high at both 30 min and 1 h p.i.. Major excretion of the ^{68}Ga-NOTA-Erlotinib conjugate was via the hepatobiliary pathway as indicated by the high accumulation of activity in the GI tract (12.3±3.9 % ID/g at 30 min; 14.3±3.4 % ID/g at 1 h).

Table 3a.4. Biodistribution pattern of ^{68}Ga-NOTA-Erlotinib in NOD/SCID mice bearing EGFR expressing tumor (n=4)

Organs/ Tissues ↓	**% I.D./g ± S.D.**	
	30 min	**1 h**
Blood	2.4 ± 0.2	1.2 ± 0.2
Lungs	1.5 ± 0.20	0.8 ± 0.1
Heart	0.4 ± 0.2	0.1 ± 0.0
Stomach	4.4 ± 2.2	3.4 ± 2.6
Intestine	12.3 ± 3.9	14.3 ± 3.4
Liver	10.2 ± 0.6	6.0 ± 0.7
Spleen	1.1 ± 0.4	0.1 ± 0.01
Kidney	4.1 ± 0.7	3.3 ± 0.6
Muscle	3.3 ± 1.3	2.4 ± 0.6
Bone	Nil	Nil
Excreta (%I.D.)	23.6 ± 8.0	31.7 ± 10.7
Tumor	**1.5 ± 0.1**	**0.7 ± 0.2**
Tumor/Lungs (Ratio)	1.1 ± 0.2	0.9 ± 0.2

(c) Analysis of Metabolites

In order to ascertain the *in vivo* stability of ^{68}Ga-NOTA-Erlotinib, the urine sample of the Swiss mice injected with the radioconjugate was analysed using HPLC. The radiochromatogram is given in Figure 3a.18 which shows a single peak corresponding to ^{68}Ga-NOTA-Erlotinib at 17.3±0.1 min thereby indicating the stability of ^{68}Ga-NOTA-Erlotinib *in vivo*.

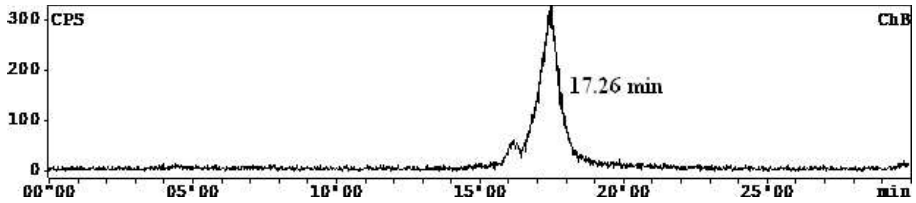

Figure 3a.18. HPLC chromatogram of the urine sample from Swiss mice injected with ^{68}Ga-NOTA-Erlotinib

3a.5. CONCLUSIONS

In this study, novel small molecule EGFR imaging probes namely ^{68}Ga-NOTA-Erlotinib and ^{68}Ga-NODAGA-Erlotinib were designed, synthesized and characterized. The biological evaluation studies of BFC-Erlotinib suggest that the attachment of the chelators to the terminal alkyne group of Erlotinib preserves the TKI property of the parent molecule. The bioevaluation results of ^{68}Ga-NOTA-Erlotinib showed high uptake in A431 cells but a moderate tumor uptake in EGFR positive tumor bearing SCID mice. While in case of ^{68}Ga-NODAGA-Erlotinib, its high hydrophilicity caused low uptake in organs such as lungs, spleen, blood, muscles, kidney and heart. Concurrently, it adversely affected the cellular penetration of the Erlotinib analogue and reduced its specific uptake in EGFR over-expressing A431 cells. The overall properties of the ^{68}Ga radioconjugates are promising. Further studies by altering the linkers attached to the parent Erlotinib molecule might be helpful in modulation of the pharmacokinetics of the resultant ^{68}Ga-Erlotinib conjugates so as

to ensure better cellular penetration and high tumor uptake and along with fast clearance from non-target organs. This work on the development of ^{68}Ga based tracers for imaging TKI is the first such study using ^{68}Ga and is expected to pave the way for in-depth R&D towards development of ^{68}Ga labeled TKI for PET imaging of EGFR over-expressing cancers.

CHAPTER 3b

COMPARATIVE EVALUATION OF ^{68}Ga-LABELED RGD PEPTIDES CONJUGATED WITH DIFFERENT CHELATORS FOR IMAGING OF $\alpha_V\beta_3$ INTEGRINS

3b.1. INTRODUCTION

Angiogenesis, the formation of new blood vessels from pre-existing blood vessels, is an essential requirement for tumor growth and metastasis where integrin $\alpha_v\beta_3$ plays a major role[92-96]. The $\alpha_v\beta_3$ integrins act as a receptor for extracellular matrix proteins with the exposed arginine-glycine-aspartic acid (RGD) tripeptide sequence. They are over-expressed on a large number of activated endothelial cells during angiogenesis in contrast to the resting endothelial cells. $\alpha_v\beta_3$ integrins are also over-expressed in cancers such as osteosarcomas, neuroblastomas, glioblastomas, melanomas, lung carcinomas and breast cancer and help in their growth and metastasis. Thus, imaging of $\alpha_v\beta_3$ integrins is considered as a useful tool in management of cancer[92-96].

In the last decade, a variety of RGD peptide based radiotracers have been developed for imaging $\alpha_v\beta_3$ integrins. In this context, both single photon emitters and positron emitting radionuclides have been explored and tagged with various RGD analogues[97-102]. In recent times, use of positron emitting radionuclides such as ^{18}F, ^{68}Ga, ^{64}Cu etc. in the clinic has been expanding owing to the high resolution, greater sensitivity and possibility of quantification by Positron Emission Tomography (PET). [103,104]. There are numerous reports on the evaluation of ^{68}Ga-labeled RGD peptides in animal models as well as in human patients wherein the RGD-motif has been conjugated to either DOTA or NOTA/NODAGA chelators[105-111]. In this context, a detailed systematic evaluation of the role of BFCs on the radiochemistry, *in vitro*

stability, pharmacokinetics, tumor targeting properties and metabolic stability in suitable animal model would offer important insights towards their effective use.

Thus in this work, a detailed and systemic comparison of the aforementioned properties of ^{68}Ga-complexes of dimeric cyclic RGD peptide E[c(RGDfK)]$_2$ (E = glutamic acid, R = arginine, G = glycine, D = aspartic acid, f = D-phenylalanine, K = lysine) conjugated with different cyclic and acyclic BFCs namely, *p*-SCN-Bn-NOTA, *p*-SCN-Bn-DOTA and *p*-SCN-Bn-DTPA have been discussed. The RGD peptide used was cyclic in nature since cyclic peptides have shown enhanced affinity and selectivity towards $\alpha_v\beta_3$ receptors over the linear ones. Further, a dimeric RGD peptide was used as dimerization increases the local RGD concentration i.e. binding of one RGD motif increases the 'local concentration' of the second RGD motif in the vicinity of integrin $\alpha_v\beta_3$. However, further increase in the multiplicity of the peptide (trimer, tetramer etc) would also significantly increase the uptake of the analogue in kidney, liver, lungs and spleen. Thus, a dimeric cyclic RGD peptide was used in the present study[99,100].

A detailed systematic evaluation of the three RGD analogues namely, NOTA-Bn-E-[c(RGDfK)]$_2$ (NOTA-Bn-(RGD)$_2$), DOTA-Bn-E-[c(RGDfK)]$_2$ (DOTA-Bn-(RGD)$_2$) and DTPA-Bn-E-[c(RGDfK)]$_2$ (DTPA-Bn-(RGD)$_2$), would be helpful in choosing the most appropriate BFC-(RGD)$_2$ peptide conjugates for the development of ^{68}Ga-labeled radiotracers for routine PET imaging of tumor angiogenesis in clinical settings.

3b.2. MATERIALS and METHODS

The RGD peptide conjugates namely NOTA-Bn-(RGD)$_2$, DOTA-Bn-(RGD)$_2$ and DTPA-Bn-(RGD)$_2$ (Figure 3b.1 (a-c)) were custom synthesized by ABX Advance Biomedical Compounds, Radeber, Germany. Suprapure hydrochloric acid (99.999% pure) was procured from Sigma-Alrich, India. MilliQ water (resistivity > 18.2 MΩ) was used in all the wet chemistry studies. All other chemicals used were of analytical grade and were

procured from Sigma-Aldrich, India. Gallium-68 was eluted in 0.6 M HCl from a 925 MBq (25 mCi) $^{68}Ge/^{68}Ga$ radionuclide generator obtained from iThemba Labs, South Africa.

High performance liquid chromatography (HPLC) analyses were carried out on a JASCO PU 2080 Plus dual pump HPLC system (JASCO, Japan) coupled with a JASCO 2075 Plus tunable absorption detector and Gina Star radioactivity detector system (Raytest, Germany). C18 reversed phase HiQ Sil (5 μm, 4 × 250 mm) column was used as the stationary phase, while mixture of acetonitrile and water (both containing 0.1% TFA) was used as the mobile phase. A well-type NaI(Tl) detector (Mucha, Raytest, Germany) was used for radioactivity measurements during all other radiochemical studies. Radioactivity measurements during animal biodistribution studies were carried out using a flat-type NaI(Tl) counter (Harshaw, UK).

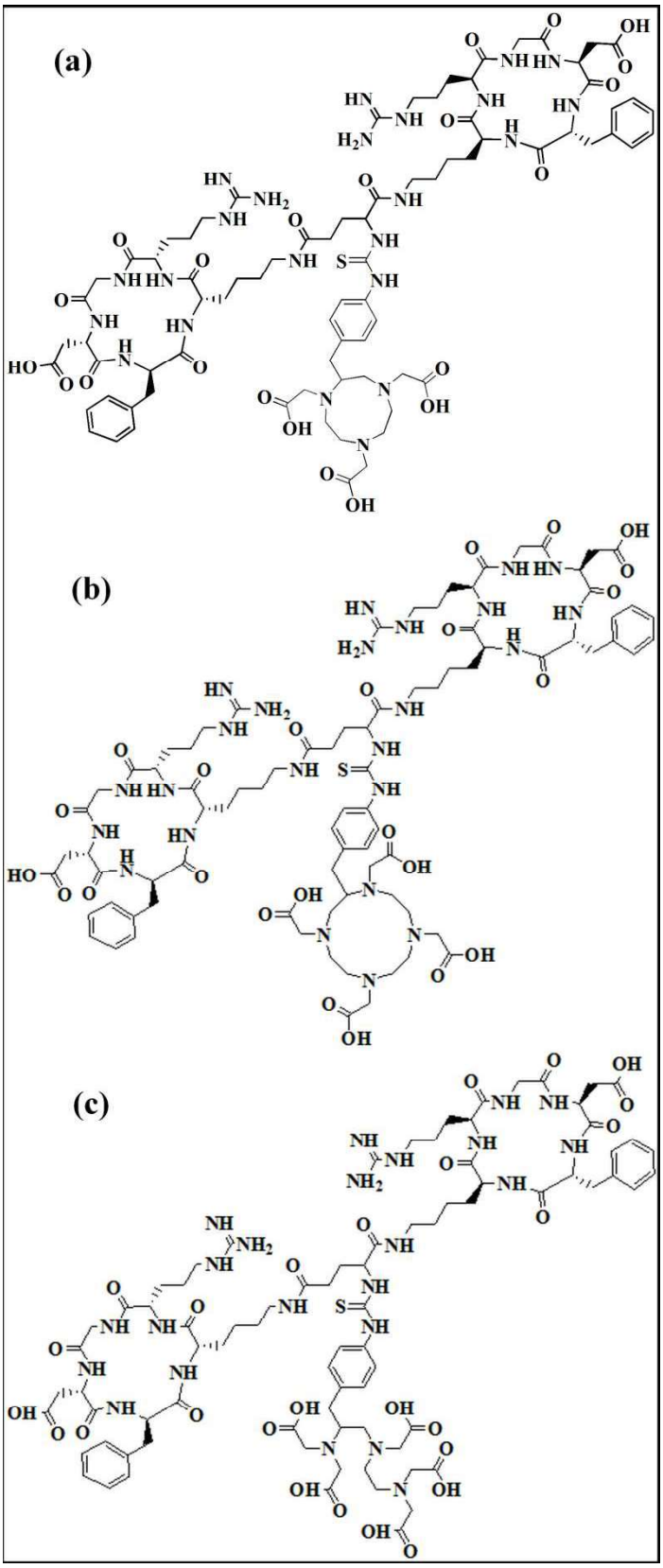

Figure 3b.1. The chemical structures of (a) NOTA-Bn-(RGD)$_2$ (b) DOTA-Bn-(RGD)$_2$ and (c) DTPA-Bn-(RGD)$_2$

3b.3. EXPERIMENTAL

3b.3.1. Radiolabeling of BFC-$(RGD)_2$ conjugates with ^{68}Ga

The ^{68}Ga radiolabeling procedure followed for the three BFC-$(RGD)_2$ conjugates was identical. Typically, the respective BFC-$(RGD)_2$ conjugate (1 µg/µL) in MilliQ water was mixed with 2 M sodium acetate solution (450 µL, pH~7.5). Further, $^{68}GaCl_3$ (1 mL, 185 MBq/5 mCi) in 0.6 N HCl was added to it and the reaction mixture was then incubated at ambient temperature (25°C) or in a water bath at 90°C. The final reaction volume was ~ 1.5 mL and the final pH was ~ 3.5. The experimental parameters were optimized by varying the amount of BFC-$(RGD)_2$ as well as the incubation time and temperature in order to maximize the radiochemical yield. All subsequent reactions were carried out in the optimized conditions for the respective ^{68}Ga-BFC-$(RGD)_2$ conjugate.

3b.3.2. Determination of radiochemical yield and purity

The radiochemical yield of ^{68}Ga-BFC-$(RGD)_2$ was determined by paper chromatography as well as by high performance liquid chromatography (HPLC) techniques.

(a) Paper chromatography

Paper chromatography was performed using Whatman No. 1 chromatography paper. 5 µL (600 KBq/ 17 µCi) of test solution was applied at 1.5 cm from the lower end of the strip and it was developed in 10 mM sodium citrate solution (pH=5). The strips were then dried and cut into segments of 1 cm each and the activity associated with each segment was measured in NaI (Tl) well type counter.

(b) HPLC technique

HPLC was carried out following gradient elution technique using a dual pump HPLC system and C18 reversed phase HiQ Sil (5 µm, 4 × 250 mm) column. Water [A] and acetonitrile [B] with 0.1% trifluoroacetic acid were used as the mobile phase and the

following gradient elution method was used for separation: 0-4 min 95% A, 4-15 min 95% A to 5% A, 15-20 min 5% A, 20-25 min 5 % A to 95% A, 25-30 min 95% A. All the solvents were of HPLC grade, degassed and filtered prior to use. The flow rate was maintained at 1mL/min. About 10 μL (~1.20 MBq/30 μCi) of the test solution was injected into the HPLC. The elution was monitored both by UV and by radioactivity signal.

3b.3.3. Determination of partition coefficient (log $P_{o/w}$) of ^{68}Ga-BFC-(RGD)$_2$ radiotracers

For determining log $P_{o/w}$, an aliquot of the ^{68}Ga-BFC-(RGD)$_2$ complex (100 μL, 12.3 MBq/300 μCi) was mixed with water (0.9 mL) and octanol (1 mL) on a vortex mixer and then centrifuged to effect the separation of the aqueous and organic layers. Equal aliquots from both layers were counted in a well-type NaI(Tl) counter. Partition coefficient *(*log $P_{o/w}$) was expressed as the logarithm of the ratio of the counts from n-octanol versus that of the aqueous layer. Further, n-octanol layer was repartitioned until consistent partition coefficient was obtained.

3b.3.4. In vitro stability of ^{68}Ga-BFC-(RGD)$_2$ radiotracers

(a) Stability in EDTA solution

In order to ascertain the stability of the ^{68}Ga-BFC-(RGD)$_2$ on EDTA challenge, aliquot of each conjugate (50 μL, 6.2 MBq/0.16 mCi) was incubated with 5 mM EDTA solution (450 μL) for different time intervals. Aliquots were withdrawn at intervals of 30 min, 60 min, 90 min and 120 min and analyzed by HPLC to assess the stability of the complex.

(b) Stability in human serum

The *in vitro* stability of ^{68}Ga-BFC-(RGD)$_2$ radiotracers in human serum was determined by incubating each RGD conjugate (50 μL, 5.6 MBq/0.15 mCi) with human serum (450 μL) at 37°C for different time intervals. Aliquots were withdrawn at intervals of 30 min, 60 min, 90 min and 120 min, ethanol was added to precipitate the serum proteins, centrifuged and the supernatant was analyzed by paper chromatography using 10 mM sodium

citrate solution (pH = 5) to determine the stability of the complex. In 10 mM sodium citrate solution, ^{68}Ga labeled RGD conjugate (R_f = 0.0) remained at the point of spotting while free $^{68}Ga^{3+}$ moved with the solvent front (R_f = 0.9-1.0).

3b.3.5. In vivo evaluation of ^{68}Ga-BFC-(RGD)$_2$ radiotracers

All *in vivo* procedures performed herein were in strict compliance with the approved protocols of Institutional Animal Ethics Committee of Bhabha Atomic Research Centre, India.

(a) Biodistribution studies in animal model

Biological efficacy of the ^{68}Ga-BFC-(RGD)$_2$ radiotracers was evaluated in female C57BL/6 mice (age: 6-8 week, weight: 20-25 g weight) bearing melanoma tumors. Melanoma B16-F10 cell line (ATCC-CRL-6475TM) used for growing the tumors, was purchased from National Centre for Cell Science (India), Pune. The tumors were induced by injecting ~ 1 × 10^6 melanoma cells, suspended in 200 µL of PBS, subcutaneously into the right thigh of each C57BL/6 mice weighing 20–25 g. The animal were reared and kept in the laboratory animal facility of our Institute under standard management practice for about 2 weeks. The animal experiments were performed when palpable tumors were observed and a tumor mass of 0.2-0.4 g was attained. The radiolabeled preparation (100 µL, 370 KBq/10 µCi) was administered intravenously through tail vein of each animal. Individual sets of animals (n=4) were utilized for studying the biodistribution at different time points (30 min, 60 min). The animals were sacrificed by carbon dioxide asphyxiation immediately at the end of the respective time point and the relevant organs and tissue were excised for measurement of associated activity. The organs were weighed and the activity associated with each of them was measured in a flat-bed type NaI(Tl) counter with suitable energy window for ^{68}Ga. For the purpose of uniformity, the activity retained in each organ/tissue was expressed as a percent value of the injected dose per gram (% I.D. /g). Activity associated with the excreta

(urine+feaces) was determined by counting the cage paper which was expressed as percent value of the injected dose (%I.D.).

(b) Assay of Metabolic stability

Metabolic stability of the radiotracers was analyzed by the following method. ^{68}Ga-BFC-$(RGD)_2$ radiotracers (100 µL, 370 KBq/10 µCi) were injected in normal Swiss mice (n=2) intravenously through lateral tail vein of each animal. The urine samples of the animals were collected 1 h post injection. Acetonitrile was added to the urine samples to precipitate the proteins. The samples were then centrifuged and the supernatants were analyzed using HPLC.

3b.4. RESULTS and DISCUSSIONS

3b.4.1. Radiolabeling of BFC-$(RGD)_2$ conjugates with ^{68}Ga

The radiolabeling yields of the three ^{68}Ga-BFC-$(RGD)_2$ tracers namely, ^{68}Ga-NOTA-Bn-$(RGD)_2$, ^{68}Ga-DOTA-Bn-$(RGD)_2$ and ^{68}Ga-DTPA-Bn-$(RGD)_2$ were determined by paper chromatography and HPLC technique. In paper chromatography, it was observed that free ^{68}Ga migrated to the solvent front (R_f = 0.9-1) while ^{68}Ga labeled RGD analogue remained at the point of spotting (R_f=0.0). A typical paper chromatography pattern is depicted in Figure 3b.2. The radio-HPLC profiles are given in Figure 3b.3. It was observed that ^{68}Ga-NOTA-Bn-$(RGD)_2$, ^{68}Ga-DOTA-Bn-$(RGD)_2$ and ^{68}Ga-DTPA-Bn-$(RGD)_2$ exhibited retention times of 15.3 min, 15.6 min and 16.1 min, respectively, while free $^{68}GaCl_3$ eluted before 4 min.

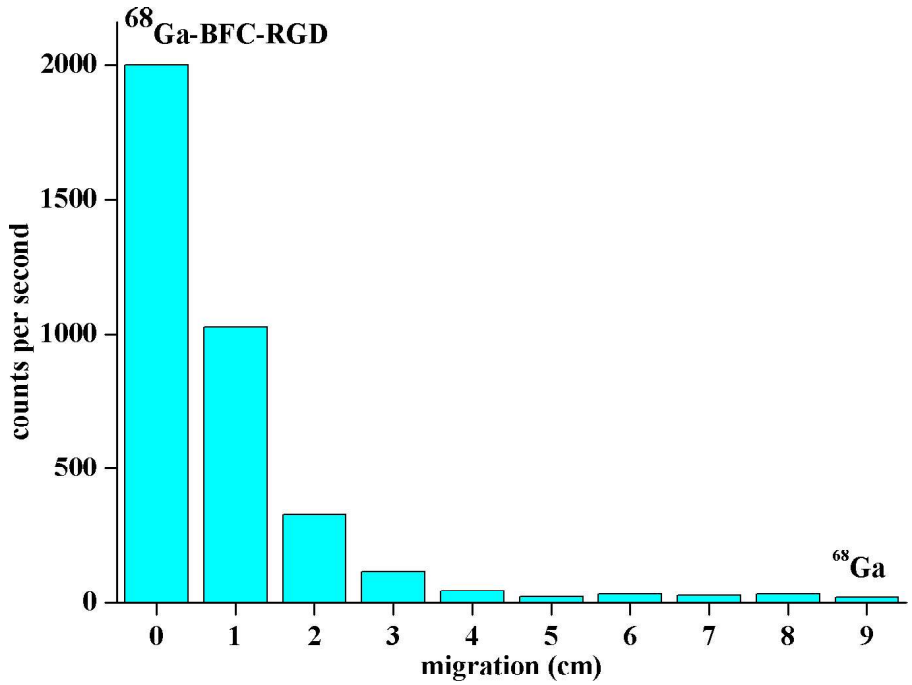

Figure 3b.2. Typical PC pattern of ^{68}Ga-BFC-(RGD)$_2$ in 0.01 N sodium citrate solution (pH=5)

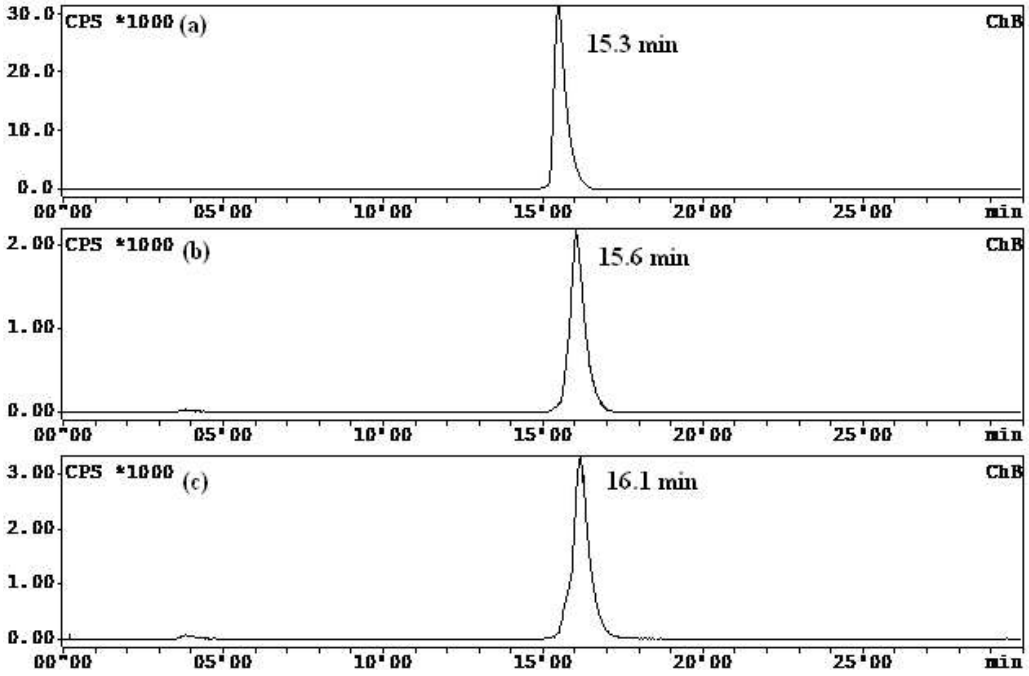

Figure 3b.3. HPLC profiles depicting the radiolabeling yields of (a) ^{68}Ga-NOTA-Bn-(RGD)$_2$ (b) ^{68}Ga-DOTA-Bn-(RGD)$_2$ and (c) ^{68}Ga-DTPA-Bn-(RGD)$_2$

With an aim of preparing ^{68}Ga-BFC-(RGD)$_2$ conjugates with maximum yield, the radiolabeling experiments were carried out by varying different reaction parameters such as ligand concentration, incubation temperature and reaction time. Figure 3b.4 a and b illustrate the effect of ligand concentration on the radiolabeling yield of ^{68}Ga-BFC-(RGD)$_2$ radiotracers at ambient temperature (25°C) and at 90°C, respectively, when the reaction mixtures were incubated for 10 min. It was observed that only 10 µg of NOTA-Bn-(RGD)$_2$ was sufficient for ≥ 98% radiolabeling yield at ambient temperature. In case of DTPA-Bn-(RGD)$_2$, radiolabeling yield ≥ 98% could be achieved using 10 µg of peptide conjugate when the reaction mixture was heated at 90°C for 10 min. On the other hand, in order to achieve ≥ 95% yield with DOTA-Bn-(RGD)$_2$, 50 µg of peptide conjugate was required and the reaction mixture needed to be heated at 90°C for 10 min.

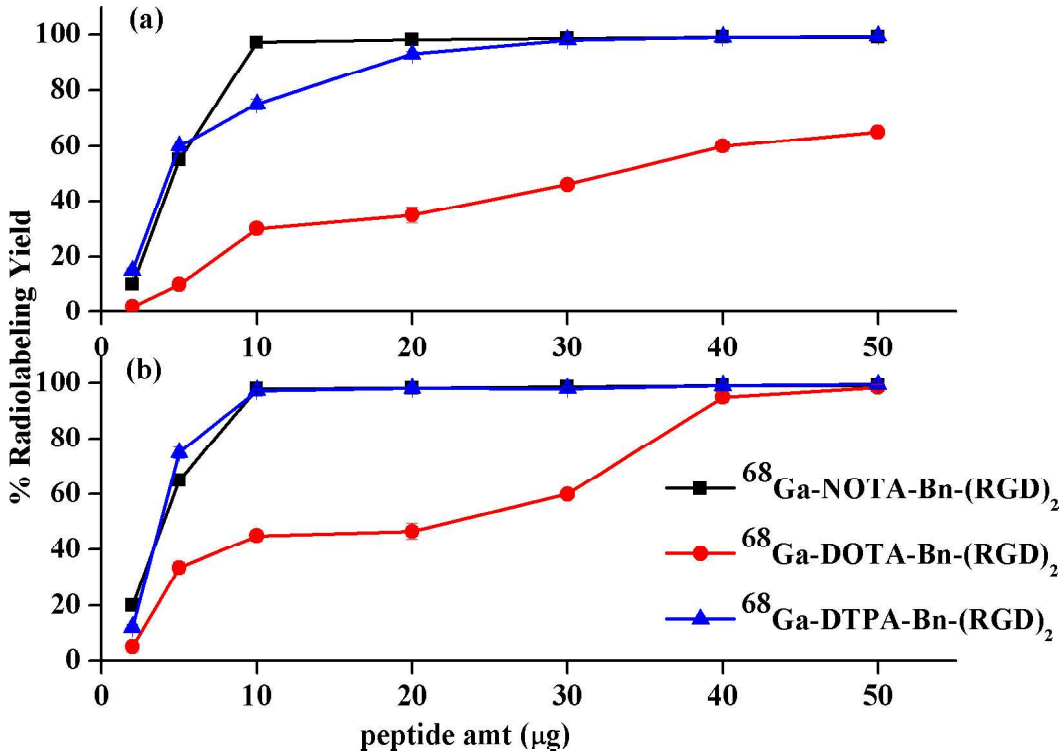

Figure 3b.4. Effect of ligand amount on the radiolabeling yield of ^{68}Ga-BFC-(RGD)$_2$ at (a) 25°C and (b) 90°C

In order to have a comparative assessment of the kinetics of formation of ^{68}Ga-RGD conjugates, the radiochemical yields were determined at different time intervals on incubation of reaction mixtures at ambient temperature as well as at elevated temperature. The results are illustrated in Table 3b.1. It is evident from the Table that when the reaction mixture of ^{68}Ga-NOTA-Bn-$(RGD)_2$ was incubated at ambient temperature, ≥95% yield could be obtained within 5 min of incubation. However, in case of ^{68}Ga-DTPA-Bn-$(RGD)_2$ and ^{68}Ga-DOTA-Bn-$(RGD)_2$, a maximum yield of 80-85% could be achieved when the reaction mixtures were incubated for at least 20 min at ambient temperature. When the reaction mixtures were incubated at 90°C, the kinetics of ^{68}Ga complexation with DTPA-Bn-$(RGD)_2$ and DOTA-Bn-$(RGD)_2$ improved significantly.

The optimization experiments are very important to facilitate development of kits which can further be translated to clinical settings for routine preparation of ^{68}Ga based radiotracers for imaging. Since the half-life of ^{68}Ga is short ($t_{1/2}$=68.1 min), a fast radiolabeling protocol resulting in high radiolabeling yields obviating the need for post-labeling purification would be desirable as it would ensure a minimum loss of the imaging agent to decay. Also, a final product with high specific activity would be advantageous towards receptor based imaging since an excess cold peptide might compete for the receptor binding sites, effectively reducing target uptake. It was observed that NOTA-conjugated RGD derivative could be radiolabeled with ^{68}Ga at ambient temperature with high radiolabeling yield (≥ 98%) and high specific activity (~ 20.3 GBq/μmol). The DTPA-conjugated analogue could also be synthesized at high specific activity (~ 22.6 GBq/μmol) but at a higher temperature. On the other hand, DOTA-conjugated peptide could be radiolabeled in adequately high yield only at elevated temperature as well as with higher peptide amount, so that the specific activity of ^{68}Ga-DOTA-conjugated peptide was significantly lower (~ 4.6 GBq/μmol). Thus amongst the BFC-$(RGD)_2$ peptide conjugates

studied, the radiolabeling conditions of NOTA-Bn-$(RGD)_2$ are most suitable for kit preparation in clinical settings. The optimized protocols for the syntheses of ^{68}Ga-BFC-$(RGD)_2$ conjugates along with their maximum specific activity achieved are given in Table 3b.2.

Table 3b.1. Effect of incubation time and temperature on the radiolabeling yields (%) of ^{68}Ga-BFC-$(RGD)_2$ conjugates

^{68}Ga-BFC-$(RGD)_2$	Radiolabeling yield (%)							
	Ambient Temperature (25 °C)				Elevated Temperature (90 °C)			
	2 min	5 min	10 min	20 min	2 min	5 min	10 min	20 min
^{68}Ga-NOTA-Bn-$(RGD)_2$	20±4	96±2	99±1	99±1	66±2	98±1	98±2	99±1
^{68}Ga-DOTA-Bn-$(RGD)_2$	0±0	25±2	60±4	72±3	5±4	69±1	94±2	97±2
^{68}Ga-DTPA-Bn-$(RGD)_2$	30±5	50±2	70±2	85±4	50±2	84±2	96±4	98±1

Table 3b.2. Optimized protocols for ^{68}Ga radiolabeling of BFC-$(RGD)_2$ conjugates

Radiotracer	Amount/ Volume of reagent			Incubation temperature and time	Specific Activity (GBq/ µmol)	log $P_{o/w}$
	$^{68}GaCl_3$ (in 0.6 N HCl)	Peptide µg (nmol)	Sodium acetate (2 N)			
^{68}Ga-NOTA-Bn-$(RGD)_2$	1 mL	10 (5.6)	400 µL	25 °C, 5 min	20.3	-(0.3±0.05)
^{68}Ga-DOTA-Bn-$(RGD)_2$	1 mL	50 (26.7)	400 µL	90 °C,10 min	4.6	-(0.39±0.04)
^{68}Ga-DTPA-Bn-$(RGD)_2$	1 mL	10 (5.3)	400 µL	90 °C, 10 min	22.3	-(0.58±0.02)

3b.4.2. log $P_{o/w}$ of ^{68}Ga-BFC-(RGD)$_2$

The log $P_{o/w}$ values for ^{68}Ga-NOTA-Bn-(RGD)$_2$, ^{68}Ga-DOTA-Bn-(RGD)$_2$ and ^{68}Ga-DTPA-Bn-(RGD)$_2$ were determined to be -0.3 ± 0.05, -0.39 ± 0.04 and -0.58 ± 0.02, respectively. It can be inferred from these results that ^{68}Ga-DTPA-(RGD)$_2$ is the most hydrophilic amongst the three radiotracers. The log $P_{o/w}$ values of the radiotracers are given in Table 3b.2.

3b.4.3. In vitro stability studies

The radiochemical purities of ^{68}Ga-BFC-(RGD)$_2$ radiotracers when incubated in EDTA solution and human serum are given in Figure 3b.5. a and b, respectively. No significant transchelation was observed when the three tracers were incubated in excess EDTA solution and their radiochemical purities were ≥ 90% up to 120 min. The radiochemical purities of ^{68}Ga-NOTA-Bn-(RGD)$_2$ and ^{68}Ga-DOTA-Bn-(RGD)$_2$ were found to be ≥ 95% up to 120 min in human serum. However, in case of ^{68}Ga-DTPA-Bn-(RGD)$_2$, a gradual decrease in its radiochemical purity with time was observed. This might be because of the higher kinetic lability of the ^{68}Ga-chelate with acyclic chelator DTPA compared to those with macrocyclic chelators DOTA and NOTA (as discussed in Chapter 1, Section 1.6).

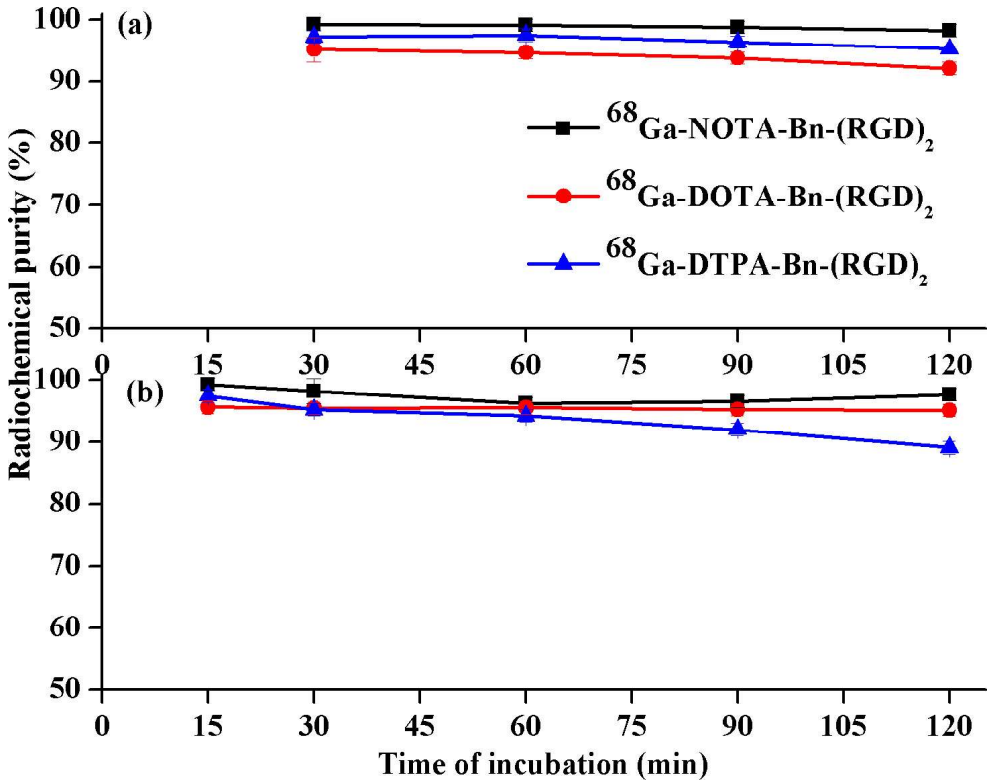

Figure 3b.5. In vitro stability of ^{68}Ga-BFC-(RGD)$_2$ in (a) EDTA solution and in (b) human serum

3b.4.4. *In vivo* evaluation ^{68}Ga-BFC-(RGD)$_2$ radiotracers

The results of biodistribution studies of the three ^{68}Ga-BFC-(RGD)$_2$ analogues in C57BL/6 mice bearing melanoma tumors are given in Table 3b.3. Amongst the three radiotracers, ^{68}Ga-DOTA-Bn-(RGD)$_2$ exhibited the highest tumor uptake of 5.08±0.05% ID/g at 30 min p.i., which decreased to 3.08±1.10 %ID/g at 1 h p.i. The melanoma tumor uptake of ^{68}Ga-NOTA-Bn-(RGD)$_2$ was also high at 30 min p.i. (4.50±0.18% ID/g), however it also decreased at 1 h p.i. (2.78±0.38 %ID/g). On the other hand, the highest tumor uptake observed in case of ^{68}Ga-DTPA-Bn-(RGD)$_2$ was considerably lower compared to the other two radiotracers (3.51±0.69 %ID/g at 30 min p.i), which nearly retained up to 1 h p.i. (3.36±0.49 %ID/g). All the three radiotracers exhibited predominantly urinary excretion owing to their hydrophilic nature. A comparison of the tumor/ background ratios of the three radiotracers is illustrated in Figure 3b.6. Although the uptake in tumor for ^{68}Ga-NOTA-Bn-

$(RGD)_2$ was slightly lower as compared to ^{68}Ga-DOTA-Bn-$(RGD)_2$, the low uptake and fast clearance of radioactivity from non target organs like blood, liver, intestine and lungs led to its high tumor/background contrast. This is a very desirable characteristic for a PET-radiotracer tumor imaging.

Table 3b.3 Biodistribution data of ^{68}Ga-BFC-$(RGD)_2$ radiotracers in C57BL/6 mice bearing melanoma tumor (n=4)

Organs/ Tissues ↓	% I.D./g ± S.D.					
	^{68}Ga-NOTA-Bn-$(RGD)_2$		**^{68}Ga-DOTA-Bn-$(RGD)_2$**		**^{68}Ga-DTPA-Bn-$(RGD)_2$**	
	30 min	**1 h**	**30 min**	**1 h**	**30 min**	**1 h**
Blood	2.80±0.35	1.88±1.01	3.87±1.07	1.14±0.06	2.77±0.41	2.57±0.21
Lungs	3.19±0.8	1.46±0.45	4.5±0.92	2.31±0.28	2.92±0.14	2.24±0.42
Heart	0.88±0.3	0.62±0.03	1.48±0.21	0.8±0.16	0.75±0.18	0.66±0.35
Stomach	2.17±0.55	1.29±.01	3.00±0.61	2.34±0.27	3.13±0.9	2.03±0.5
Intestine	2.11±0.49	2.08±0.54	2.88±0.65	2.38±0.53	3.38±0.77	2.48±0.55
Liver	2.27±0.69	1.66±.04	4.47±1.02	3.59±0.18	2.88±0.65	2.53±0.08
Spleen	2.25±0.86	1.96±0.27	2.95±0.5	2.58±0.37	2.17±0.25	1.94±0.35
Kidney	7.94±1.91	5.43±0.24	9.2±0.06	4.71±0.17	6.32±0.39	4.41±0.55
Bone	0.01±0.01	.01±.00	0.00±0.00	0.00±0.00	0.00±0.00	0.00±0.00
Urine (% I.D.)	29.48±2.41	56.76±9.23	30.20±2.6	50.36±1.2	35.00±0.6	60.90±2. 60
Tumor	**4.50±0.18**	**2.78±0.38**	**5.08±0.05**	**3.08±1.10**	**3.51±0.69**	**3.36±0.49**

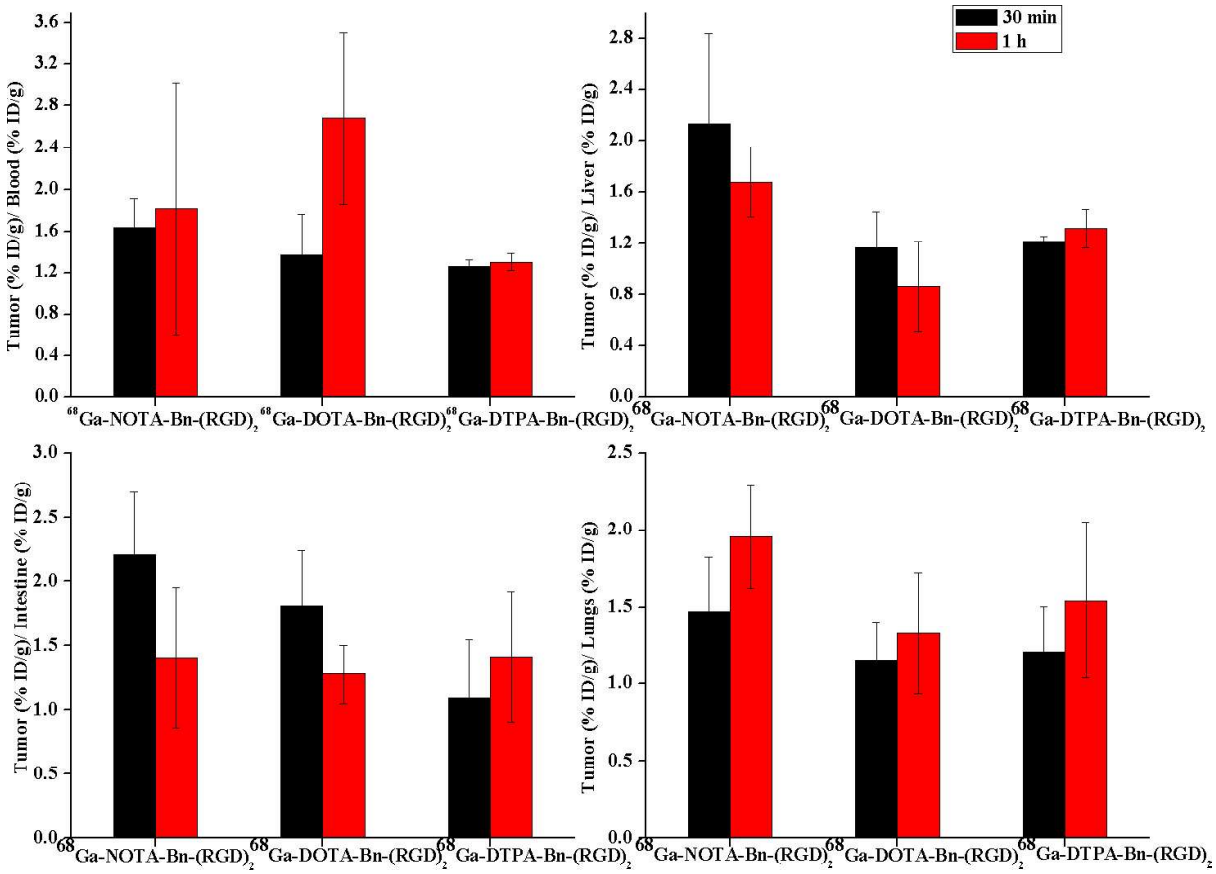

Figure 3b.6. Tumor/ background ratios of C57BL/6 mice bearing melanoma tumor, injected with ^{68}Ga-BFC-(RGD)$_2$ (n=4)

In order to ascertain the *in vivo* stability of ^{68}Ga-BFC-(RGD)$_2$ radiotracers, the urine samples of Swiss mice injected with the respective radiotracers were analyzed by HPLC 1 h p.i.. The radiochromatograms of the urine samples of the three tracers are given in Figure 3b.7. From the figure it is evident that both ^{68}Ga-NOTA-Bn-(RGD)$_2$ and ^{68}Ga-DOTA-Bn-(RGD)$_2$ were stable *in vivo* as only one peak corresponding to the tracers at 15.3 min and 15.6 min respectively, were observed. However, in case of ^{68}Ga-DTPA-Bn-(RGD)$_2$, a small metabolite peak below 5 min (8 %) was observed along with radiotracer peak at 16.07 min (92 %). This shows a decrease in stability of ^{68}Ga-DTPA-Bn-(RGD)$_2$ *in vivo*. The low *in vitro* and *in vivo* stability of ^{68}Ga-DTPA-Bn-(RGD)$_2$ can be attributed to the acyclic nature of DTPA ligand which forms kinetically labile complexes with ^{68}Ga.

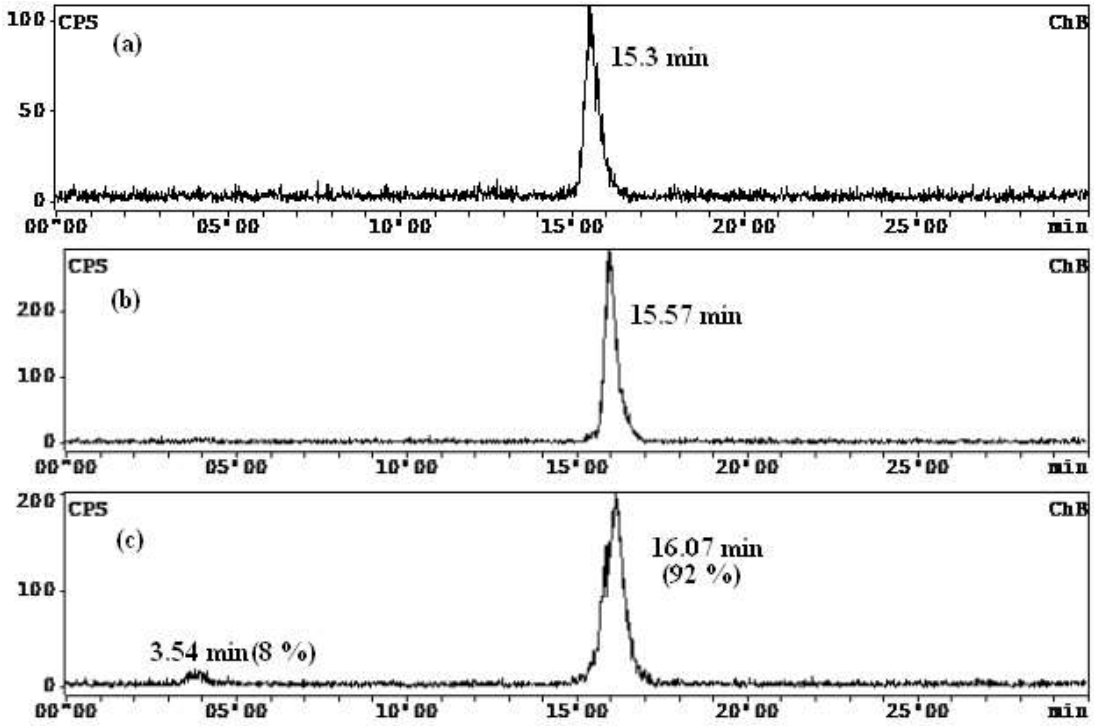

Figure 3b.7. Urine analysis of Swiss mice injected with (a) ^{68}Ga-NOTA-(RGD)$_2$ (b) ^{68}Ga-DOTA-(RGD)$_2$ and (c) ^{68}Ga-DTPA-(RGD)$_2$(n=2)

3b.5. CONCLUSIONS

In summary, a comparative evaluation of three ^{68}Ga-labeled RGD conjugates namely, NOTA-Bn-(RGD)$_2$, DOTA-Bn-(RGD)$_2$ and DTPA-Bn-(RGD)$_2$ was carried out. It was found that ^{68}Ga-NOTA-Bn-(RGD)$_2$ could be efficiently radiolabeled with ^{68}Ga at ambient temperature with high radiochemical purity, specific activity and *in vitro* and *in vivo* stability. Its preliminary biodistribution studies carried in C57BL/6 mice indicated high tumor/background ratio along with clearance of the activity via the renal pathway. ^{68}Ga-DTPA-Bn-(RGD)$_2$ could be also radiolabeled with high purity and high specific activity. However, its *in vitro* and *in vivo* stabilities were low. In case of ^{68}Ga-DOTA-Bn-(RGD)$_2$, although the tumor uptake of the radiotracer was high its tumor/background ratio was comparatively low due to high accumulation of activity in non-target organs. These studies indicate that ^{68}Ga-NOTA-Bn-(RGD)$_2$ would be the most suitable choice for further

investigations toward the development of ^{68}Ga based radiotracers for imaging tumor angiogenesis in clinical settings.

CHAPTER 3c

PREPARATION OF ^{68}Ga LABELED FOLIC ACID CONJUGATES FOR IMAGING OF FOLATE RECEPTOR OVER-EXPRESSING TUMORS

3c.1. INTRODUCTION

Folic acid is a water soluble Vitamin B, vital for several bodily functions including the synthesis of DNA and RNA, cell division and the synthesis and growth of red blood cells[112]. Since folates are hydrophilic in nature, they are transported inside the cells by several active transport/receptor mediated internalization mechanisms[112]. Amongst these, the folate receptor (FR) mediated transport has been widely pursued for pharmaceutical applications, since these receptors have limited expression in healthy tissues but are over-expressed in human carcinomas such as that of the breast, cervix, colorectum, ovary and endometrium[113]. The FRs bind folic acid and its conjugates with high affinity ($K_d < 10^{-9}$ M)[112] and internalize through endocytosis[114]. Radiolabeled folates for imaging (SPECT/PET) and therapy for selective targeting of FR-positive cancers have been developed in the past taking advantage of this mechanism[115-129]. Amongst the radiolabeled folates evaluated two SPECT based folate conjugates viz. ^{111}In labeled DTPA-folate and ^{99m}Tc labeled EC20 have been clinically evaluated in patients with ovarian cancer and various solid tumors[130-135]. Owing to the inherent ability of PET to acquire images with higher resolution and greater sensitivity as compared to SPECT, attempts to radiolabel folic acid with diverse PET radioisotopes (^{18}F, ^{68}Ga, ^{64}Cu, ^{11}C, ^{124}I etc.)[136-138] for imaging FRs with high precision have been made. Amongst the PET radioisotopes, ^{68}Ga [$t_{1/2}$= 67.71 min, E_{β^+} = 1899 KeV (89%)] has garnered significant attention in recent times due to its ease of availability through a ^{68}Ge/^{68}Ga generator and its well defined coordination chemistry.

Several attempts were made in the past to design ^{68}Ga labeled folate analogues which could target FRs with high specificity *in vivo* along with less non-target uptake. In this context, a variety of pharmacokinetic modifiers, linkers and bifunctional chelators (BFCs) such as deferoxamine[139-141], DOTA[142-143] and NOTA[144-145] have been used to obtain the desired *in vivo* distribution and excretion kinetics of ^{68}Ga labeled folates. Amongst the different ^{68}Ga labeled folate conjugates, ^{68}Ga-NOTA-folate conjugates *viz.* ^{68}Ga-NODAGA-folate conjugate (NODAGA: 1,4,7-triazacyclononane-1-glutaric acid-4,7-acetic acid)[144] and ^{68}Ga-NOTA-folate conjugate[145] exhibited high tumor uptake and better *in vivo* pharmacokinetics in comparison to the previously reported ^{68}Ga-DOTA-folic acid conjugates in animal models[142,143]. Considering the superiority of NOTA over the other BFCs for ^{68}Ga labeling, the present work explores a new approach of linking the parent folic acid to NOTA wherein a three carbon hydrophobic chain linker was used for linking *p*-SCN-Bn-NOTA to folic acid. The rationale for the linker approach was based on recent literature reports[119,146] which stated that use of long chain linkers between the folic acid moiety and the chelator resulted in improved tumor targeting as well as fast clearance from non-target organs. Thus, the present paper describes the synthesis and characterization of a NOTA-Bn-(3-aminopropyl) folic acid conjugate, radiolabeling of the conjugate with ^{68}Ga obtained from the in-house developed nanoceria-PAN sorbent based ^{68}Ge/^{68}Ga generator, *in vitro* cell binding studies in KB cells (which express the FR) and preliminary biodistribution studies in normal Swiss mice.

3c.2. MATERIALS AND METHODS

Folic acid was obtained from Fluka, Germany. 1-Ethyl-3-(3-dimethylaminopropyl) carbodiimide (EDC), N-Boc-1,3-propanediamine and gallium nitrate were purchased from Aldrich, USA. *p*-SCN-Bn-NOTA was purchased from Macrocyclics, USA. All other reagents used were of analytical grade. Cocktail W purchased from Spectrochem Pvt. Ltd., Mumbai,

India was used as the liquid scintillation cocktail for counting the ^{3}H activity during the *in vitro* cell binding studies.

Silica gel plates (Silica Gel 60 F254) were obtained from Merck, India. HPLC characterization was carried out on a JASCO PU 2080 Plus dual pump HPLC system (JASCO, Japan) equipped with a C18 reversed phase HiQ Sil (5 μm, 4 × 250 mm) column serially connected to an integrated UV detector (JASCO 2075 Plus) and a Gina Star radiometric detector (M/s Raytest GmbH, Straubenhardt, Germany). Purification of the synthesized folic acid derivatives was performed using a JASCO-PU-2086 PLUS Intelligent Prep Pump semi preparative HPLC system (JASCO, Japan) having a Megapak SIL C18-10 column (10 × 250 mm) and connected with a JASCO UV-2075 Plus absorption detector. ^{1}H NMR spectra were recorded on a 300 MHz Varian VXR 300S spectrophotometer (Varian, USA). Mass spectra of the samples were recorded on a Varian Prostar mass spectrometer (Varian, USA) using the ESI in positive and negative modes. ^{3}H activity counting during the *in vitro* cell binding experiments was carried out using a liquid scintillation counter purchased from Hidex, Finland.

3c.3. EXPERIMENTAL

3c.3.1. Synthesis of NOTA-Bn-(3-aminopropyl) folic acid conjugate

(a) Synthesis of tert-butyl N-(3-aminopropyl)carbamate folic acid (1)

The synthesis of *tert*-butyl N-(3-aminopropyl) carbamate folic acid conjugate was carried out as per the reported procedure[147]. Briefly, N-Boc-1,3- propanediamine (181 mg, 1.03 mmol) was added to a solution of folic acid (500 mg, 1.13 mmol) and dissolved in minimum amount of DMSO. The above reaction mixture was stirred, to which EDC (218.5 mg, 1.13 mmol) was added and the reaction continued overnight at room temperature. Progress of the reaction was monitored by analytical HPLC using 0.01 M phosphate buffer

(pH 6) (Solvent A) and MeOH (Solvent B) as the mobile phase, 1 mL/ min flow rate and following gradient elution: 0 min 100% A, 15 min 40% A, 25 min 40% A . Upon completion of the reaction, the reaction mixture was gradually poured into a vigorously stirred solution of dry Et_2O (300 mL) cooled to 0°C. The yellow precipitate obtained was collected by filtration, washed with Et_2O after isolation to remove trace amounts of DMSO and dried under high vacuum to yield the product in desired purity. The product was characterized using ^{1}H NMR and ESI-MS techniques.

Yield: 60 % (373 mg).

^{1}H NMR (DMSO, δ ppm): 1.34 (s, 9H, -C(C***H***$_3$)$_3$), 1.88-1.92 (m, 4H,- NHCH$_2$C***H***$_2$CH$_2$NH, -NHCHC***H***$_2$CH$_2$CO-), 2.00-2.21 (m, 2H,- NHCHCH$_2$C***H***$_2$CO-), 2.45-2.55 (m, 2H,- NHCH$_2$CH$_2$C***H***$_2$NH-), 3.06-3.10 (m, 2H, -NHC***H***$_2$CH$_2$CH$_2$NH-), 4.33 (s, 2H, -NHC***H***$_2$C-), 4.48 (m, 1H, -NHC***H***CH$_2$CH$_2$CO-), 6.55 (d, *J=8.1 Hz*, 2H, -CHC***H***CC***H***CH-), 7.59 (d, *J=8.1 Hz*, 2H, -C***H***CHCCHC***H***-), 8.66 (s, 1H, -NCC***H***N-).

MS (ESI, negative mode): Mass (calc.) $[C_{27}H_{35}N_9O_7\text{-}H]^-$ 596.56; m/z (observed) 596.5

(b) Synthesis of (3-aminopropyl) folic acid (2)

Compound **1** (373 mg, 0.62 mmoles) was treated with 1 mL of 0.4 N HCl and the reaction mixture was stirred at room temperature for 4 h. Upon completion of the reaction, HCl was removed under vacuum. The precipitate was washed twice with MeOH and dried under vacuum. It was used for conjugation with NOTA without further purification and characterization.

Yield: 99 % (307 mg)

(c) Synthesis of NOTA-Bn-(3-aminopropyl) folic acid conjugate (3)

Compound **2** (307 mg, 0.62 mmol) was added to 0.1 M $NaHCO_3$ solution (pH 8) and stirred until it dissolves completely. To the above solution, *p*-SCN-Bn-NOTA (278 mg, 0.62 mmol) was added and the reaction mixture was stirred overnight. Progress of the reaction was

monitored by HPLC following the UV profile at 254 nm. This crude product was then purified by carrying out semi-preparative HPLC on a C18 reverse phase column to remove unreacted NOTA. 0.01 M Phosphate buffer (pH 6) (Solvent A) and methanol (Solvent B) were used as the mobile phase and the gradient elution technique was used as described previously. Flow rate was maintained at 1 mL/min. The peak corresponding to pure NOTA-folic acid conjugate was collected, pooled and lyophilized to get the desired product which was characterized using ^{1}H NMR and ESI-MS.

^{1}H NMR (D_2O, δ ppm): 1.83-1.87 (m, 4H,- $NHCH_2C\boldsymbol{H}_2CH_2NH$, $-NHCHC\boldsymbol{H}_2CH_2CO-$), 2-2.21 (m, 2H,$-NHCHCH_2C\boldsymbol{H}_2CO-$), 2.61-2.50 (m, 12H, $-NC\boldsymbol{H}_2CH_2N-$, $NC\boldsymbol{H}_2C\boldsymbol{H}_2N-$, $NC\boldsymbol{H}_2CHN-$, $-CC\boldsymbol{H}_2CHN-$), 3.30-3.08 (m, 11H, $-NC\boldsymbol{H}_2COOH-$, $-NC\boldsymbol{H}_2COOH-$, $-NC\boldsymbol{H}_2COOH-$, $-CCH_2C\boldsymbol{H}N-$ $-NHCH_2CH_2C\boldsymbol{H}_2NH-$), 4.2 (s, 2H, $-NHC\boldsymbol{H}_2C-$), 4.48 (m, 1H, $-NHC\boldsymbol{H}CH_2CH_2CO-$), 6.40 (d, 2H, *J=7.5 Hz*, $-C\boldsymbol{H}CHCCHCHC-$,), 6.58 (d, 2H, *J=8.1 Hz*, $-CC\boldsymbol{H}CHCCHCHC-$), 6.75 (d, 2H, J=7.5 Hz, $-CHC\boldsymbol{H}CCHCHC-$), 7.59 (d, 2H, *J=8.1 Hz,* $-CHC\boldsymbol{H}CCHCH-$), 8.5 (s, 1H, $-NCC\boldsymbol{H}N-$)

MS (ESI, positive mode): Mass (calc.) $[C_{42}H_{53}N_{13}O_{11}S+H]^{+}$ 949.02; m/z (observed) 949.1.

3c.3.2. Radiolabeling of NOTA-folic acid with ^{68}Ga

For radiolabeling, 0.1 mL of the NOTA-folic acid conjugate (20 µg) was mixed with 0.3 mL of 0.5 M sodium acetate solution to which $^{68}GaCl_3$ (111-148 MBq, pH=1) eluted from the ^{68}Ge/^{68}Ga nanoceria-PAN generator was directly added. The pH of the solution was adjusted to ~ 3.5. The reaction mixture was incubated at 37°C for 10 min. The radiochemical yield of ^{68}Ga-NOTA-folic acid conjugate was determined by HPLC using a C-18 reversed phase column using H_2O (0.1% TFA) as solvent A and acetonitrile (0.1% TFA) as solvent B under gradient elution (0 min 95% A, 4 min 95% A, 15 min 5% A, 20 min 5% A, 25 min 95% A) at a flow rate of 1 mL/min. For HPLC characterization, the test solution (25 µL) was injected into the column and elution was monitored by following the radioactivity profile.

3c.3.3. Preparation of ^{nat}Ga NOTA- folic acid conjugate

The NOTA-folic acid conjugate (1 mM) was dissolved in water and the pH of the solution was adjusted to pH 4 using dil. HCl. To this solution, 2 mM solution of gallium nitrate was added and the reaction mixture was incubated at 37°C for 30 minutes and then left overnight at room temperature with stirring. The product was separated by semi preparative HPLC **(**same method used as that for ^{68}Ga-NOTA-folic acid**)** and characterized by HPLC following its UV profile at 254 nm as well as by ESI-MS.

MS (ESI, positive mode): Mass (calc.) [$C_{42}H_{50}GaN_{13}O_{11}S$] 1013.3; m/z (observed) 1013.5, 1031.0 ($M+NH_4^+$), 1036.1 ($M+Na^+$).

3c.3.4. Partition coefficient (log $P_{o/w}$) and in vitro serum stability

For determination of log $P_{o/w}$, 0.1 mL of ^{68}Ga-NOTA-folic acid conjugate was mixed with 0.9 mL of water and 1 mL of n-octanol on a vortex mixer and centrifuged for effecting complete separation of the water and octanol layers. Equal aliquots from both the layers were then counted on a NaI (Tl) counter. Partition coefficient (log $P_{o/w}$) was expressed as the logarithm of the ratio of the counts in the n-octanol phase to that of the water phase. Further, n-octanol layer was repartitioned until consistent partition coefficient value was obtained.

For assessment of serum stability, ^{68}Ga-NOTA-folic acid conjugate (50 µL) was incubated with human serum (450 µL) at 37°C for 1 h. Thereafter, the serum proteins were precipitated by addition of acetonitrile (500 µL), the solution was centrifuged and the supernatant was analyzed by HPLC to determine the stability of the conjugate in serum.

3c.3.5. In vitro cell uptake studies

In vitro cell uptake studies were carried out in KB cells (human nasopharyngeal carcinoma cell line) that over-express folate receptors. Both the synthesized NOTA-folic acid conjugate **3** as well as the final ^{68}Ga-NOTA-folic acid conjugate were evaluated for their affinity towards FRs. The uptake of the cold conjugate **3** was evaluated by estimating

inhibition it causes in the uptake of ^{3}H-Folic acid in FR positive cells. The results obtained were compared with that obtained with cold folic acid. Towards this, KB cells were cultured in Rosewell Park Memorial Institute (RPMI) medium supplemented with 10 % FCS in humidified atmosphere under 5 % CO_2 at 37°C. Trypsin-EDTA solution was used for sub-culturing and isolation of cells from confluent cultures. 20 h prior to the experiment, 1×10^{5} cells/well were seeded in 6 well plates in RPMI medium without folic acid and incubated at 37°C to form a confluent monolayer overnight. The experiment was carried out in triplicates for each concentration. Cell monolayers were rinsed with ice cold PBS (pH 7.4). Ice cold folate deficient medium without FCS (475 µL) was added to each well. For inhibition studies, four different concentrations of cold folic acid and NOTA-folic acid conjugate (0.001, 0.01, 0.1, 0.5 µM), respectively were added separately to the cells in well plates (500 µL) and incubated at 4°C for 40 min. ^{3}H-Folic acid (25 µL, 0.8 µM/7.4 KBq) was added to each well and plates were incubated at 4°C for 2 h. After incubation, cells were washed twice with ice cold PBS and the cell monolayer was dissolved in DMSO. Liquid scintillation cocktail (3 mL) was added after transferring the cells to vials and ^{3}H activity associated with the cells was estimated by liquid scintillation counting.

After ascertaining the specificity of the synthesized NOTA-folic acid conjugate **3** to the FR in KB cells, % uptake of ^{68}Ga-NOTA-folic acid conjugate per million cells was determined in KB cells. For this purpose, ^{68}Ga-NOTA-folic acid conjugate was added to 10^{6} KB cells at various concentrations (0.15 µM, 0.75 µM and 1.5 µM) respectively and incubated for 1 h at 4°C. In order to ascertain the specificity towards FR, another set of cells were pre-incubated with 100 fold excess of cold folic acid for an hour at 4°C. After incubation, cells were washed twice with ice cold PBS and cell monolayers were dissolved in 1 N NaOH. Activity associated with the cells was counted in a NaI (Tl) counter.

3c.3.6. Biodistribution studies

All procedures performed herein were in accordance with the national laws pertaining to the conduct of animal experiments. Normal female Swiss mice (20-25 g body weight) were used for studying the biodistribution of the synthesized ^{68}Ga-NOTA-folic acid conjugate. The radiolabeled preparation (100 µL, 370 KBq) was administered intravenously through the lateral tail vein of each animal. Individual sets of animals (n=4) were utilized for studying the biodistribution at two different time points (30 min and 1 h). Another set of animals (n=4; 30 min and 1 h) were intravenously injected with cold folic acid (100 µg/100 µL in phosphate buffered saline) half an hour prior to the injection of ^{68}Ga-NOTA-folic acid-conjugate. The animals were sacrificed at the end of the respective time points by carbon dioxide asphyxiation and the relevant tissues and organs were excised for measurement of associated activity. The organs were weighed, rinsed and the activity associated with each was counted in a flat-bed NaI (Tl) counter with suitable energy window for ^{68}Ga. For the purpose of uniformity, the activity retained in each organ/tissue was expressed as a percent of the injected dose per gram (%ID/g).

3c.4. RESULTS and DISCUSSION

3c.4.1. Synthesis of NOTA-Bn-(3-aminopropyl) folic acid conjugate

The scheme followed for the synthesis of NOTA-Bn-(3-aminopropyl) folic acid conjugate **3** is given in Figure 3c.1. The folic acid molecule was synthetically modified in three steps to introduce the BFC, *p*-NCS-Bn-NOTA. The first step involved the synthetic modification of the γ carboxylic acid of folic acid to introduce a Boc propyl amine linker**.** The formation of conjugate **1** was ascertained by analytical HPLC (UV chromatogram), wherein a shift in the parent folic acid peak was observed from 11.4 min to 15.1 min. The structure of the conjugate at 15.1 min was confirmed by ^{1}H-NMR. Conjugate **1** was then Boc de-protected to generate folate derivative **2** with a free amino group**.** Finally, the target molecule **3** was obtained through an isothiourea forming addition reaction between the free

amino group of **2** and the p-SCN group of NOTA under mild basic conditions. Again, the formation of compound **3** was confirmed by HPLC and the peak observed at 11.3 min was purified using semi-preparative HPLC to yield the target ligand with ~ 90 % purity.

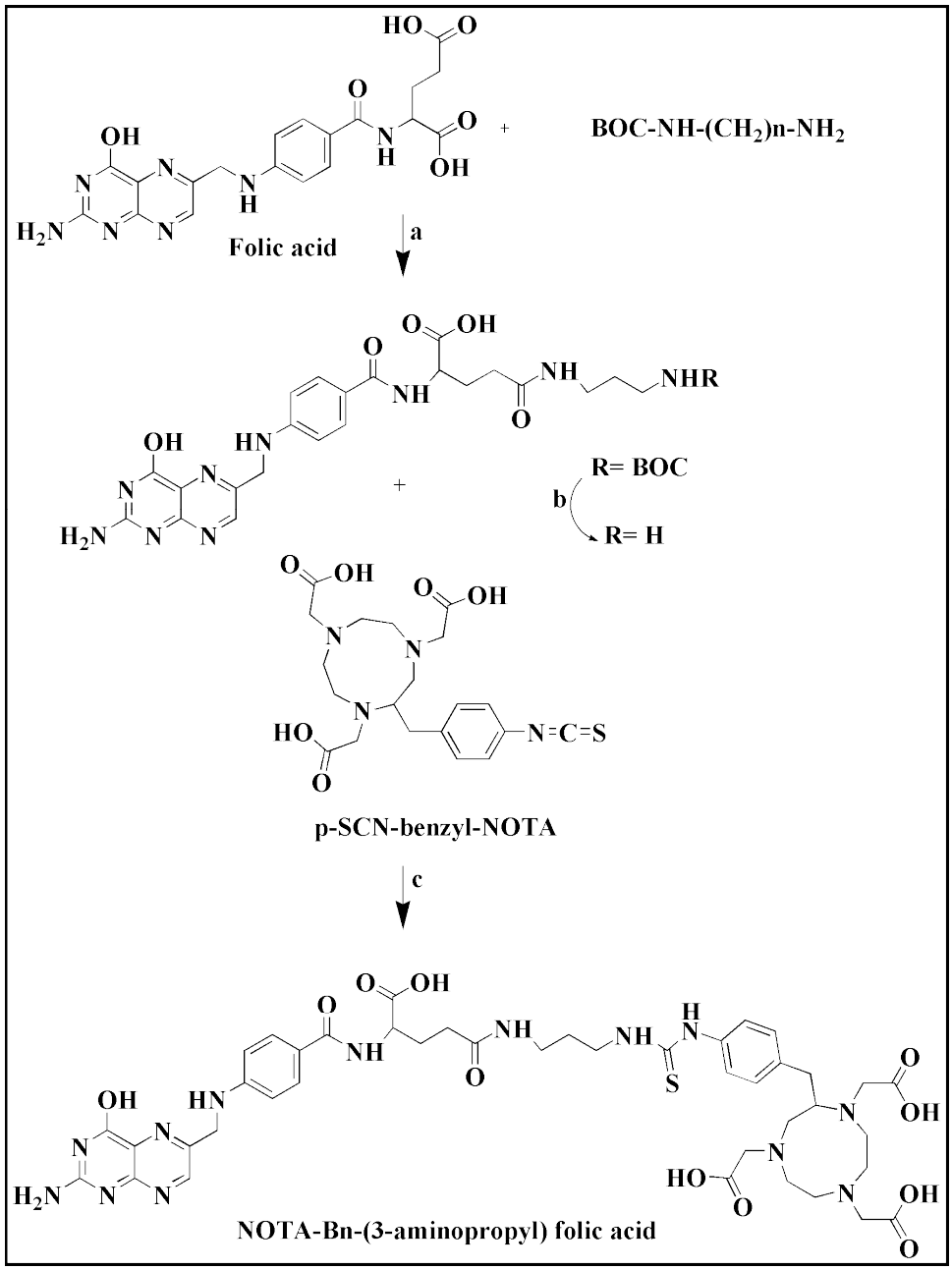

Figure 3c.1. Synthetic scheme for preparation of NOTA-Bn-(3-aminopropyl) folic acid conjugate (3) (a) EDAC, DMSO (b) TFA (c) 0.1 M $NaHCO_3$ (pH=8)

3c.4.2. Radiolabeling of NOTA-folic acid with ^{68}Ga

The scheme for the radiolabeling of compound **3** with ^{68}Ga is shown in Figure 3c.2. The ^{68}Ga-NOTA-folic acid conjugate was obtained in a single step wherein the addition of $^{68}GaCl_3$ to the NOTA-folic acid conjugate yielded the final radioconjugate. HPLC characterization showed that ^{68}Ga-NOTA-folic acid eluted out at 15.4 min (Figure 3c.3). The radiochemical yield of ^{68}Ga-NOTA-folic acid conjugate was 95±3 % as ascertained by HPLC. Structural characterization of the ^{68}Ga-NOTA-folic acid was carried out by preparation of the ^{nat}Ga-NOTA-folic acid. The retention time of ^{nat}Ga-NOTA-folic acid in analytical HPLC was 15.2 min (Figure 3c.3) which was quite close to that of ^{68}Ga-NOTA-folic acid. Further, results of the ESI-MS analysis of ^{nat}Ga-NOTA-folic acid corroborated the successful synthesis of the corresponding ^{68}Ga-NOTA-folic acid as per the radiolabeling scheme.

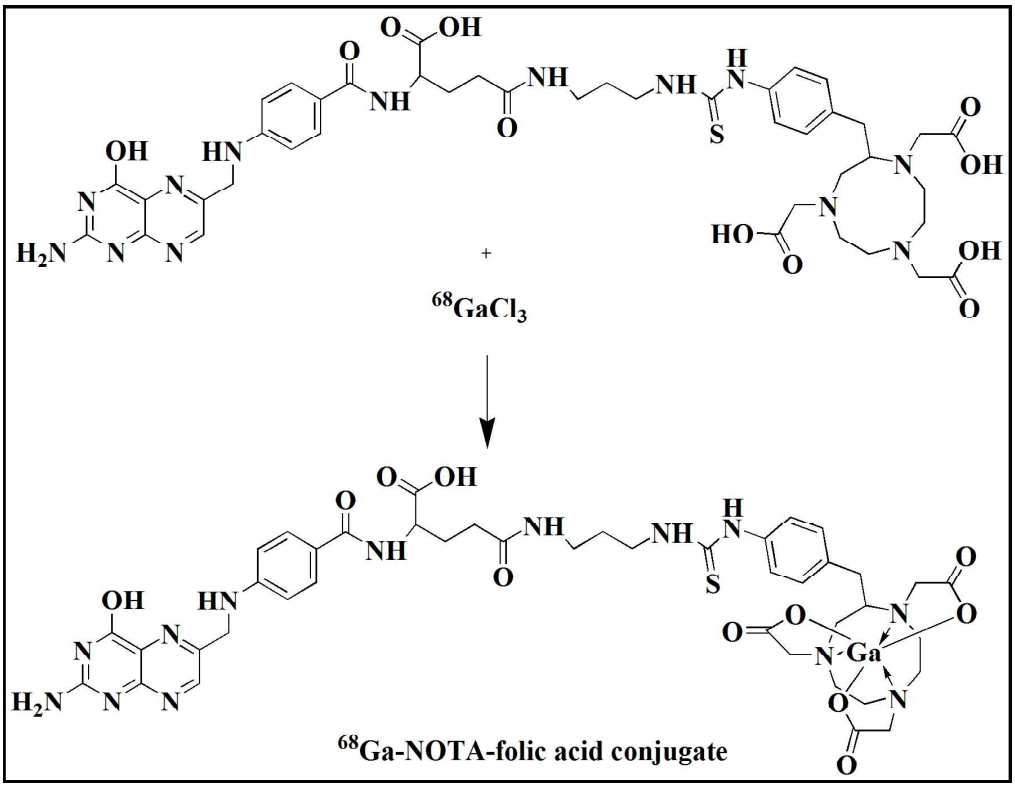

Figure 3c.2. Scheme for the synthesis of ^{68}Ga-NOTA-Bn-(3-aminopropyl) folic acid conjugate

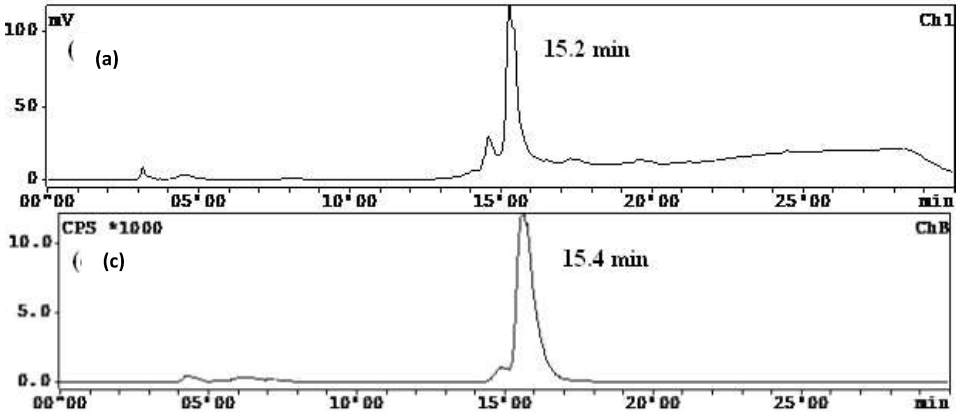

Figure 3c.3. HPLC profile of (a) ^{68}Ga-NOTA-Bn-(3-aminopropyl) folic acid conjugate (b) ^{nat}Ga-NOTA-Bn-(3-aminopropyl) folic acid conjugate

3c.4.3. Partition coefficient (log $P_{o/w}$) and in vitro serum stability

log $P_{o/w}$ value of ^{68}Ga-NOTA-folic acid conjugate was determined to be -2.2±0.3, which revealed the hydrophilic nature of the complex. The radiolabeled folic acid conjugate exhibited good stability in human serum wherein < 5 % degradation of the parent conjugate was observed up to 1 h incubation at 37°C.

3c.3.4. In vitro cell binding studies

In vitro cell binding experiments were carried out in KB cells in order to ascertain the affinity of the synthetically modified NOTA-folic acid conjugate **3** and ^{68}Ga-NOTA-folic acid conjugate for FR targeting. Figure 3c.4 shows the results of the cell binding experiments carried out with the NOTA-folic acid conjugate **3** in comparison with parent folic acid at different concentrations (0, 0.001, 0.01, 0.1 and 0.5 μM). ^{3}H-folic acid showed a net positive uptake (31.5±0.1 %) in KB cells. 90-95 % decrease in the uptake of ^{3}H-folic acid was observed on addition of cold folic acid at 0.5 μM. A similar decrease in binding of ^{3}H-folic acid to the order of ~80 % could be achieved with compound **3** at the highest concentration (0.5 μM), thereby confirming the specificity of the synthesized NOTA-folic acid conjugate for FRs. These results indicate that the modification carried out in the primary structure of the

folic acid moiety to incorporate *p*-SCN-Bn-NOTA does affect the conjugate's affinity for FR receptors to some extent, however, the specificity to FR is not completely lost.

Figure 3c.5 illustrates the results of the *in vitro* cell binding studies of ^{68}Ga-NOTA-folic acid conjugate in KB cells. Three different dilutions of the ^{68}Ga labeled folic acid conjugate containing different amounts of the cold folic acid-NOTA conjugate **3** were evaluated to assess the cell uptake. Maximum cell uptake of 1.7±0.4 % per million KB cells was observed for ^{68}Ga complex carrying minimum amount of free ligand (0.15 μM). Complete blocking of the cell uptake was effected by addition of 100 fold excess (200 nM) of folic acid. The inhibition results indicate significant reduction ($p < 0.05$) in uptake of the ^{68}Ga-NOTA-folic acid conjugate indicating its specificity for the FR receptors.

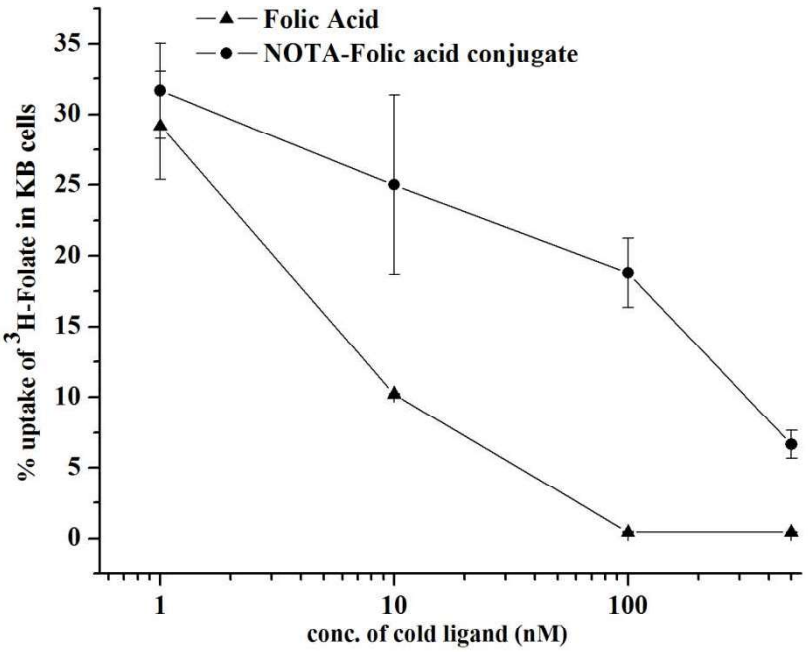

Figure 3c.4. In vitro cell uptake studies showing inhibition in uptake of ^{3}H-folate using cold folic acid and cold NOTA-Bn-(3-aminopropyl) folic acid conjugate in KB cells

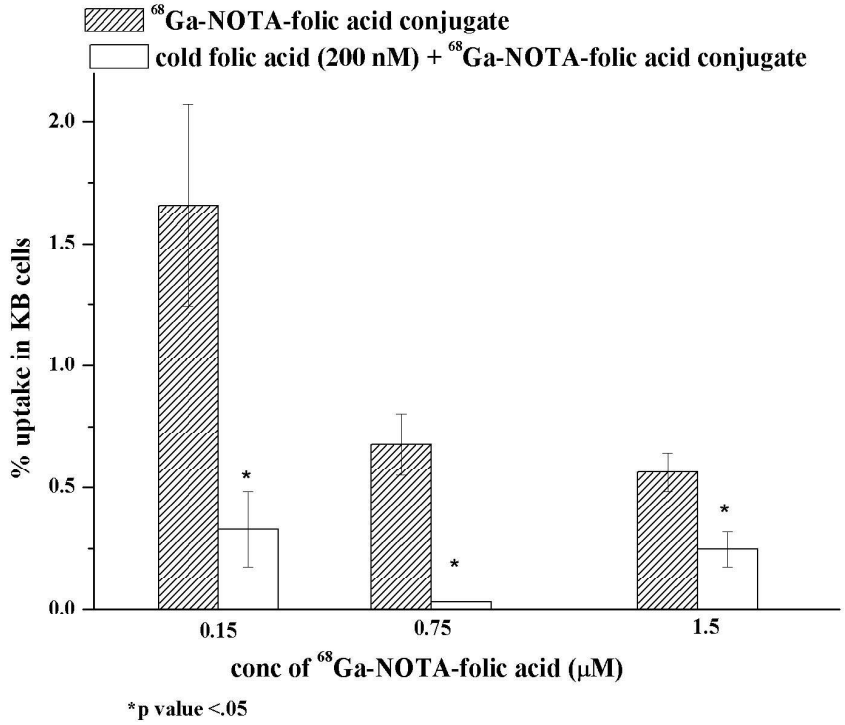

Figure 3c.5. In vitro cell binding studies showing inhibition in uptake of ^{68}Ga-NOTA-Bn-(3-aminopropyl) folic acid conjugate in presence of cold folic acid

3c.4.5. Biodistribution studies

FRs are found to be over-expressed in various types of cancers[114]. Nevertheless, normal organs also express FRs on their cell surface to a limited extent. Kidney is one such organ that has the highest density of FRs[114]. Since no tumor xenograft studies could be carried out using the synthesised ^{68}Ga-NOTA-folic acid conjugate, preliminary *in vivo* evaluation of the complex was carried out in normal Swiss mice with kidney as the organ of interest. The biodistribution data of ^{68}Ga-NOTA-folic acid conjugate at 30 min and 1 h p.i. in normal Swiss mice is depicted in Table 3c.1. Uptake in the kidney was found to be significant (15.8±3.9 %ID/g) at 30 min p.i. The renal uptake and retention may be due to FR or due to the process of excretion or a combination of both the factors. The ^{68}Ga labeled folate was found to clear rapidly from the blood, liver and other non-target organs, which may be due to the high hydrophilic nature of the complex. A small percentage of the

conjugate was found to clear via the hepatobiliary pathway as evident from the activity accumulation in the liver and intestines. However, the retention in these non-target organs may not significantly interfere with the imaging of tumors located in the abdominal region.

Table 3c.1. Biodistribution pattern of ^{68}Ga-NOTA-folic acid conjugate in Swiss mice (n = 4)

Organ/ Tissues ↓	% I.D./g ± S.D.	
	30 min	**1 h**
Blood	1.3±0.3	1.1±0.3
Lungs	1.1±0.5	1.0±0.4
Heart	0.4±0.2	0.6±0.6
Stomach	1.3±0.4	0.8±0.8
Intestine	6.8±1.6	5.7±0.2
Liver	3.4±0.8	2.0±0.6
Spleen	0.4±0.3	1.0±0.8
Kidney	15.9±3.9	15.0±4.1
Muscle	2.6±1.0	4.0±1.2
Tibia	0.3±0.1	2.0±1.2
Excreta (% I.D.) (urine + faeces)	22.6±6.4	19.0±8.2

3c.5. CONCLUSIONS

A new NOTA-folic acid conjugate was synthesized and radiolabeled with ^{68}Ga in high radiochemical yield and purity. *In vitro* studies carried out in KB cell line indicated significant retention of specificity of both the synthesized conjugate and the ^{68}Ga-NOTA-folic acid complex towards FRs. Further, biodistribution studies of the ^{68}Ga-NOTA-folic acid conjugate carried out in normal mice indicated significant association of the tracer with kidneys. Rapid clearance of the tracer from other non-target organs mainly via the renal pathway favors imaging tumors located in the abdominal region. However, further evaluation of the prepared tracer in tumor xenografts is required to quantify the real potential of the synthesized ^{68}Ga-folate complex towards FRs.

CHAPTER 4

DEVELOPMENT OF ^{68}Ga LABELED HUMAN SERUM ALBUMIN (HSA) PROTEIN AND HSA MACROAGGREGATES

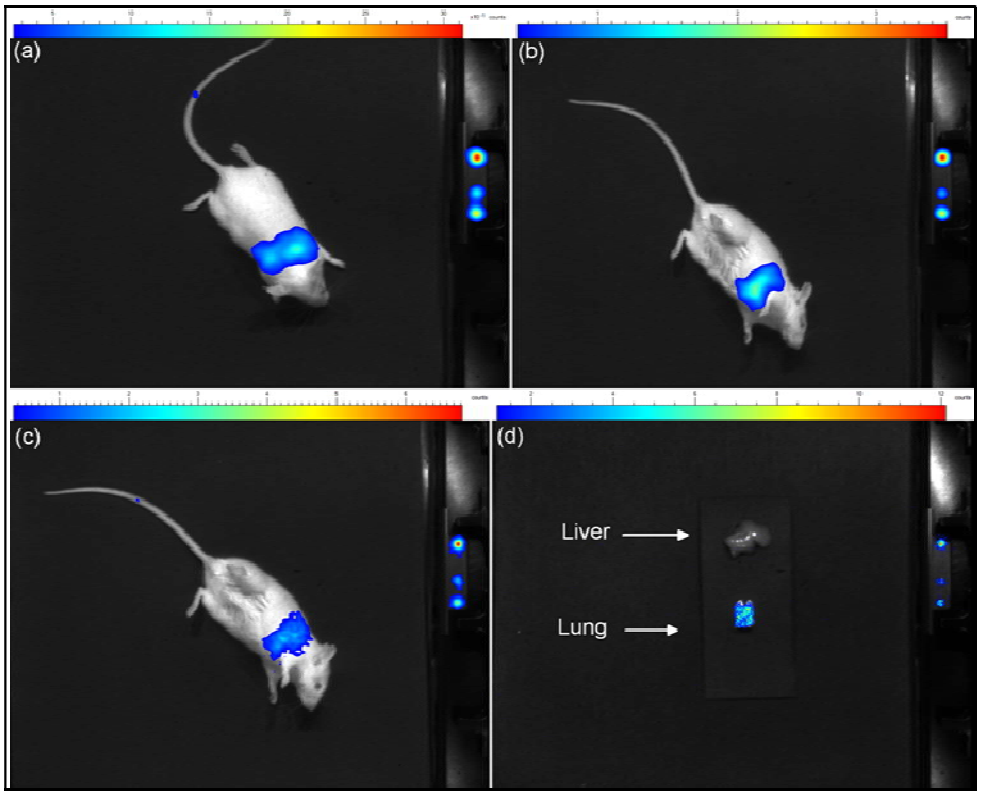

Cerenkov Images of Swiss mice injected with ^{68}Ga labeled Macroaggregated albumin

CHAPTER 4a

DEVELOPMENT OF ^{68}Ga LABELED HUMAN SERUM ALBUMIN FOR BLOOD POOL IMAGING: A COMPARISON BETWEEN TWO LIGANDS

4a.1. INTRODUCTION

Blood pool imaging helps to quantify the blood flow and vascular permeability and analyze the cellular and molecular abnormalities in blood vessel walls (such as defective endothelial barrier) [1]. It helps to characterize the vessel leakiness by determining the size, number, distribution and cellular basis of the endothelial defects, how increased endothelial permeability affects drug delivery to tumor cells and whether vessel leakiness changes after treatment. This information can help to better design the drug delivery systems and to understand the effect of angiogenesis inhibitors on the access of cancer therapeutics to tumor cells. Further, blood pool imaging can also help to identify vascular abnormalities in cardiovascular diseases as well as in the staging of cancers[148-153]. ^{99m}Tc labeled red blood cells (RBC) and human serum albumin are amongst the radiopharmaceuticals employed for measurement of regional blood volume by means of SPECT imaging[150,153]. Despite the numerous advantages of PET over SPECT, the numbers of blood pool agents based on positron emitting radioisotopes are very few. One such example is RBC labeled with [^{15}O]CO [154]. However, due to the short half life of ^{15}O (2.05 min), it can only be used in institutions having access to cyclotrons in their vicinity.

Majority of the research on radiolabeled blood pool imaging agents is based on red blood cells (RBC) or albumin both of which are abundant plasma proteins. However, in the present study HSA was used rather than RBC as HSA is readily available in pure form for research and clinical use and possess no known toxicological effects both of which are the

desired characteristics of a blood pool imaging agent[155]. Use of HSA also obviates the need of drawing blood which is required for *in vitro* labeling of RBCs which exposes the staff to potential infectious material. Further, *in vivo* labeling of RBCs suffers from poor labeling efficiencies rendering radiolabeled RBCs unattractive for the purpose[153].

In the recent years, there have been several pre-clinical reports on human serum albumin (HSA) radiolabeled with positron emitting radioisotopes such as ^{18}F, ^{64}Cu and ^{68}Ga for blood pool imaging[156-161]. Towards application in blood pool imaging, HSA has been radiolabeled with ^{68}Ga/^{67}Ga through diverse bifunctional chelators (BFC) which have been subjected to bioevaluation studies[156,157,162,163]. Amongst the ^{68}Ga based albumin tracers, ^{68}Ga-HSA-DOTA has been reported to be a promising tracer for quantification of regional blood volume[156]. However, the chelator DOTA (1,4,7,10-tetraazacyclo-dodecane-1,4,7,10-tetraacetic acid) has slow complexation kinetics under mild reaction conditions which is a drawback for radiolabeling owing to the short half life ($t_{1/2}$= 67.71 min) of ^{68}Ga. As discussed in Chapter 1, ^{68}Ga readily complexes with the BFC NOTA (1,4,7-triazacyclononane-1,4,7-triacetic acid) at ambient temperature as compared to DOTA. Thus, in this chapter, a detailed comparison of ^{68}Ga labeled HSA conjugated to the BFCs namely *p*-SCN-Bn-NOTA and *p*-SCN-Bn-DOTA towards application in blood pool imaging has been described. The influence of chelators on the radiolabeling yields, stability and biodistribution profiles of the respective radiotracers was studied systematically in order to assess their potential utility in blood pool imaging.

4a.2. MATERIALS AND METHODS

Human serum albumin (lyophilized; > 97 % pure) and anhydrous sodium acetate (≥ 99.999 % pure, metal basis) were obtained from Sigma-Aldrich, USA. All other chemicals used were of analytical grade. HPLC grade water was used for preparing all the reagent solutions. PD-10 Sephadex G-25 columns were procured from M/s. GE Healthcare, USA.

Whatman No.1 chromatography paper (Whatman, UK) was used for paper chromatography. Lyophilizations were carried out on an Alpha 1-2 LD Plus lyophilizer (Martin-Christ, Germany). Thin layer chromatography (TLC) plates (Silica Gel 60 F254) were obtained from Merck, India. Size exclusion HPLC (SE-HPLC) analyses were performed on a system (M/s. JASCO, Japan) equipped with a TSK gel column (G3000 SWXL) having a SWXL Guard column and connected with UV/VIS (JASCO) and NaI(Tl) detectors (Raytest GmBH, Germany). 0.05 M phosphate buffer containing 0.05 % sodium azide (pH 6.8) was used as the mobile phase in the SE-HPLC system at a flow rate of 0.6 mL/minute. The radiochromatograms were analyzed using GINA STAR software Version 5.01 (Raytest GmBH, Germany). UV absorbance measurements were carried out on a Chemito Spectroscan UV2600 spectrophotometer (Thermo Scientific, India) using a 1 cm sample cell. A well-type NaI(Tl) detector (Electronic Corporation of India (Ltd.), India) was used to count radioactive samples for determining the radiolabeling yield and *in vitro* stability. Organ activity measurements during *in viv*o studies were performed on a flat-bed NaI(Tl) radioactivity detector (Harshaw, UK). Gallium-68 for the work was obtained from a 925 MBq $^{68}Ge/^{68}Ga$ generator purchased from iThemba Labs, South Africa.

4a.3. EXPERIMENTAL

4a.3.1. Synthesis of NOTA-HSA/DOTA-HSA (1/2)

The two HSA conjugates NOTA-HSA (1) and DOTA-HSA (2) were prepared following the similar synthetic scheme (Figure 4a.1). Human serum albumin (20 mg, 1 eq.) was conjugated with the respective bifunctional chelator (*p*-SCN-Bn-NOTA/*p*-SCN-Bn-DOTA, 2.0 eq.) in $NaHCO_3$ (0.1 M) solution (pH=9). The reaction mixture was stirred for 2 h followed by incubation overnight at 4°C. Progress of the reaction was monitored with TLC

using a 90:10 mixture of methanol and ammonia. Subsequently, the NOTA-HSA/DOTA-HSA conjugates were purified using PD-10 column.

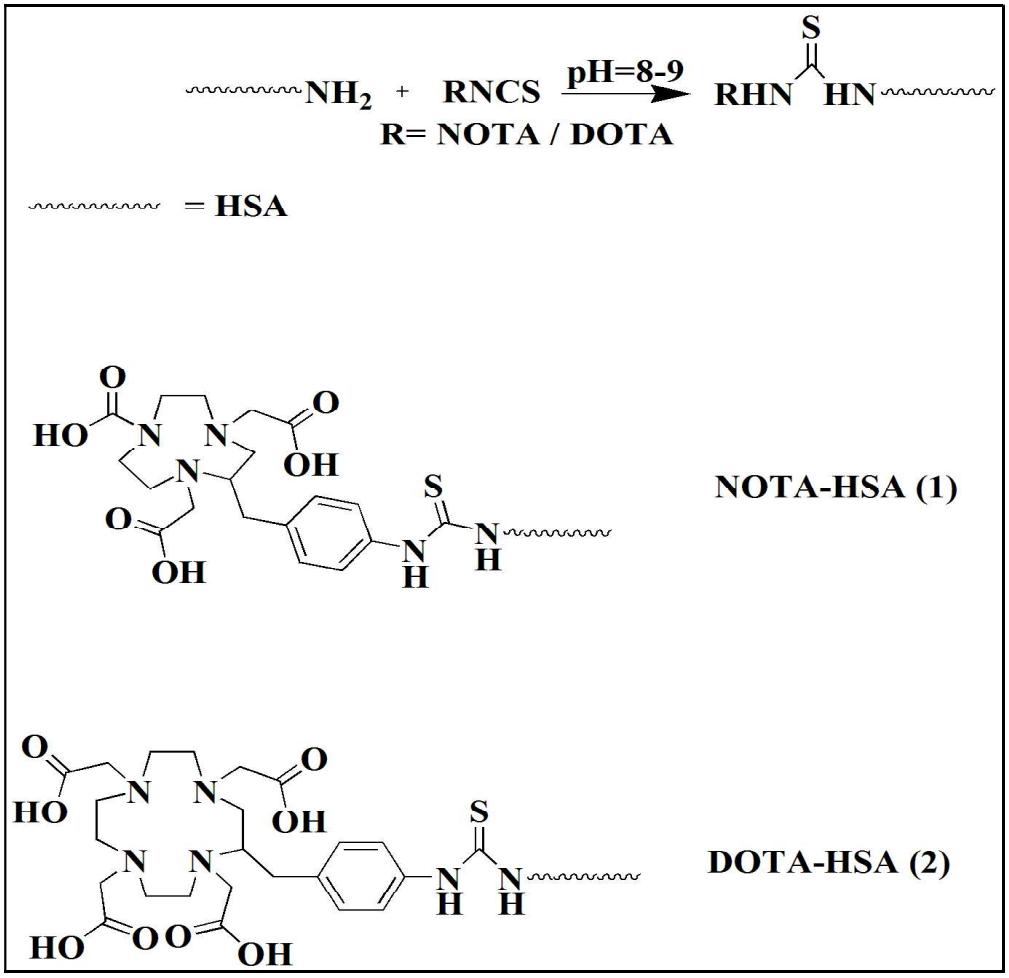

Figure 4a.1. Synthetic scheme for preparation of NOTA-HSA and DOTA-HSA (1/2)

PD-10 column purification was carried out as depicted in Figure 4a.2. Prior to purification, the column was equilibrated with 20 mL of 0.05 M sodium acetate solution. Subsequently, the BFC-HSA reaction mixture was loaded onto the PD-10 column which was then eluted with 0.05 M sodium acetate. Ten fractions of 1 mL each were collected. The UV absorbance of the collected samples was determined at 280 nm. The fractions containing BFC-HSA conjugates were pooled, aliquoted and then lyophilized.

Brady et al had reported on a spectroscopic assay using Cu-(II)-Arsenazo (III) complex to determine the number of bifunctional chelators such as DOTA and DTPA conjugated to biomolecules such as monoclonal antibodies[164]. In this assay, the extent of transchelation of Cu(II) from the Cu(II)-Arsenazo(III) complex to NOTA-HSA was quantified. The same method was employed for determination of the number of NOTA/DOTA molecules conjugated to each HSA molecule. Towards this aim, a stock solution containing 25 μM of Cu (II) and 50 μM of Arsenazo (III) in ammonium acetate solution (0.15 M, pH 7.0) was prepared. Serial dilutions of this reagent were made whose absorbance was measured at 652 nm. A standard curve was constructed and the molar extinction coefficient (ε) was calculated. Subsequently, 25 μL out of the 1 mL Cu reagent was replaced with an equal amount of appropriately diluted NOTA-HSA conjugate and the absorbance was measured at 652 nm at regular intervals up to 30 minutes until the readings stabilized. The extent of decrease in absorbance at 652 nm, dilution factor and the molar extinction coefficient (ε) were used to determine the number of NOTA molecules per molecule of HSA. Previously, the concentration of HSA in the NOTA-HSA conjugate was independently determined by Lowry's method[165]. The number of DOTA molecules conjugated per molecule of HSA was also determined by the same procedure.

4a.3.2. Radiolabeling of HSA-NOTA/HSA-DOTA (1/2) with ^{68}Ga

$^{68}GaCl_3$ was obtained from the $^{68}Ge/^{68}Ga$ generator on elution with 5 mL of 0.6 N HCl. For radiolabeling, the conjugates **1/2** were dissolved in 0.5 mL of 2 M sodium acetate to which 1 mL of $^{68}GaCl_3$ (111-185 MBq) eluted in 0.6 N HCl was added. The final pH of the reaction mixture was maintained at 5. The ^{68}Ga-NOTA-HSA (**1a**) reaction mixture was incubated for 10 minutes at ambient temperature while the reaction mixture of ^{68}Ga-DOTA-HSA (**2a**) solution was incubated at 37°C for 30 minutes. Radiolabeling yield of the ^{68}Ga labeled HSA conjugates was determined using SE-HPLC as well as by paper chromatography

(in 10 mM sodium citrate solution at pH 5 as mobile phase). For HPLC characterization, an aliquot of the reaction mixture was injected into the SE-HPLC gel column by isocratic elution of 0.05 M phosphate buffer, pH 6.8 at 0.6 mL per min. Both the UV absorbance and radioactivity profile were monitored using a UV/VIS detector and a flow-through NaI(Tl) detector respectively.

For separation of ^{68}Ga labeled HSA from free ^{68}Ga(III), PD-10 column purification was carried out as given in Figure 4a.2. Prior to purification, the column was equilibrated with 20 mL of 0.05 M sodium acetate solution. Subsequently, the ^{68}Ga-BFC-HSA reaction mixture was loaded onto the PD-10 column which was then eluted with 0.05 M sodium acetate. Ten fractions of 1 mL each were collected. Activity associated with each fraction was counted using a NaI(Tl) well type counter. It was observed that maximum activity corresponding to ^{68}Ga-BFC-HSA eluted in the 4th and 5th fractions while free ^{68}Ga eluted from 8th fraction onwards. The activity corresponding to ^{68}Ga-BFC-HSA in the 4th and 5th fractions were pooled for further studies as these fractions contain the ^{68}Ga labeled HSA. The purified ^{68}Ga-NOTA-HSA and ^{68}Ga-DOTA-HSA conjugates were characterized by SE-HPLC using the same method which was used for characterizing the reaction mixture.

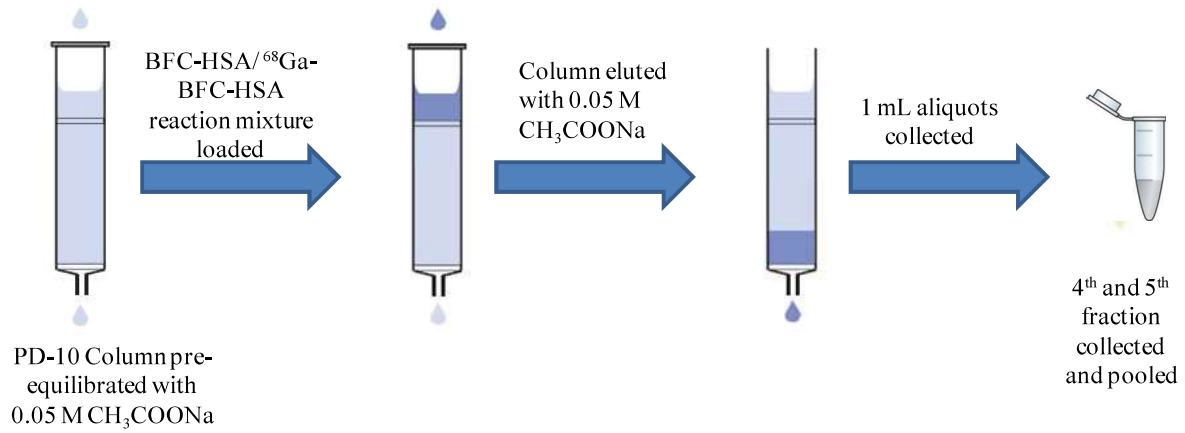

Figure 4a.2. Scheme for purification of BFC-HSA or ^{68}Ga-BFC-HSA reaction mixtures using PD-10 column

4a.3.2. In vitro stability of 1a/2a

In vitro stability of the ^{68}Ga labeled albumin conjugates was assessed in 10 mM EDTA solution as well as in human serum. Towards evaluation of stability in presence of EDTA, 0.1 mL of the ^{68}Ga-BFC-HSA solution was incubated with 0.9 mL of 10 mM EDTA solution at ambient temperature and the stability of the complex was determined by paper chromatography (10 mM sodium citrate solution at pH 5 as mobile phase) for up to 2 h post incubation.

In order to assess the serum stability of the preparation, 0.1 mL of the ^{68}Ga-BFC-HSA solution was incubated with 0.9 mL of human serum at 37°C for up to 2 h which was monitored by the standardized paper chromatography method described above for EDTA stability.

4a.3.3. In vivo evaluation studies

(a) Biodistribution Studies

All the experimental procedures involving animals were performed in accordance with the national guidelines pertaining to the conduct of animal experiments. Normal female Swiss mice (20-25 g body weight) were used for the *in vivo* distribution assays of the prepared BFC-HSA conjugates (**1a**/**2a**). The radiolabeled preparation (100 µL, 370 KBq) was administered intravenously through the tail vein of each animal. Individual sets of animals (n=4) were utilized for studying the bio-distribution at various time points (2 min, 10 min, 30 min, 1 h, 2 h). The animals were sacrificed by carbon dioxide asphyxiation immediately at the end of the respective time point and the relevant organs and tissue were excised for measurement of associated activity. The organs were weighed and the activity associated with each organ was measured in a flat-bed type NaI(Tl) counter with the suitable energy window set-up for ^{68}Ga. For the purpose of uniformity, the activity retained in each organ/tissue was expressed as a percent value of the injected dose per gram (%ID/g). Activity

associated with the excreta (urine+feaces) was determined by counting the cage paper which was expressed as percent value of the injected dose (%ID).

(b) Analysis of metabolites

For metabolite analysis, sixty minutes after the injection of ^{68}Ga-BFC-HSA into the tail vein of Swiss mice, a blood sample from the aorta was drawn into the heparinized vial. After centrifugation of the heparinized blood, plasma was obtained. The plasma sample was analyzed by the standardized paper chromatography method.

4a.4. RESULTS and DISCUSSIONS

4a.4.1. Synthesis of NOTA-HSA/DOTA-HSA (1/2)

The synthesis scheme for preparation of the BFC conjugated HSA 1/2 is given in Figure 4a.1. Typically, the terminal amine group of HSA was reacted with the isothiocyanate group of the respective BFC, *p*-NCS-Bn-NOTA and *p*-NCS-Bn-DOTA, forming an isothiourea bond. The progress of the reaction was monitored using TLC with 90:10 methanol: ammonia solvent mixture. It was observed that in this solvent system, free BFC moved with the solvent front (R_f = 0.9) while the BFC-HSA conjugates remained at the point of spotting (R_f = 0.0). After completion of the reaction, the conjugates were purified using PD-10 column. Measurement of the UV absorbance (at 280 nm) of the fractions eluted from the PD-10 column confirmed the elution of the BFC-HSA conjugates in the 4th and 5th fractions while any free BFC eluted in the 8th fraction onwards. Fractions 4 and 5 were therefore pooled, aliquoted equally and then lyophilized.

One molecule of BFC was found to be conjugated with each HSA molecule using 1:2 molar ratios of HSA and BFCs, as determined by the spectroscopy assay carried out with Cu(II)-Arsenazo(III) complex. Higher BFC to HSA ratios were not used for conjugation as it has been reported previously that a higher degree of functionalization of HSA with the BFC

may lead to alterations in the physiochemical properties of HSA molecule with chances of greater accumulation of the injected albumin in liver [157, 166].

4a.4.2. ^{68}Ga radiolabeling of NOTA-HSA/ DOTA-HSA (1/2)

The radiolabeling yields of ^{68}Ga-NOTA-HSA (**1a**) and ^{68}Ga-DOTA-HSA (**2a**) conjugates were determined by paper chromatography using 10 mM sodium citrate solution (pH=5) as well as by HPLC technique. In the paper chromatography system, it was observed that free ^{68}Ga(III) migrated to the solvent front (R_f=0.9-1) while the ^{68}Ga labeled HSA remained at the point of spotting (R_f=0.0). The radiolabeling yield of **1a** was 85±3% while that of **2a** was 70±4%. The specific activity of **1a** was 5.3 GBq/µmol while that of **2a** was 4.3 GBq/µmol. The two ^{68}Ga labeled albumin conjugates were purified using PD-10 column for further studies. The HPLC profiles (radioactive and UV) of the purified samples of **1a** and **2a** are given in Figure 4a.3 and Fig4a.4, respectively. In the HPLC system, **1a** and **2a** exhibited retention times of 14.8 min and 14.4 min respectively which matched with their respective UV profiles (measured at 280 nm). This confirms the stable binding of ^{68}Ga to HSA. In the standardized SE-HPLC system, ^{68}Ga-NOTA had a retention time of 20.2 minutes, very well separated from that of ^{68}Ga-NOTA-HSA (14.8 min). Similarly, ^{68}Ga-DOTA had an R_t of 19.6 min which is distinctly different from that of ^{68}Ga-DOTA-HSA (R_t = 14.4 min). The small hump before the main albumin peak in Figures 4a.3 and Figure 4a.4 is due to the presence of albumin aggregates. The radiochemical purities of both **1a** and **2a** were determined to be ≥ 99 % based on the HPLC data.

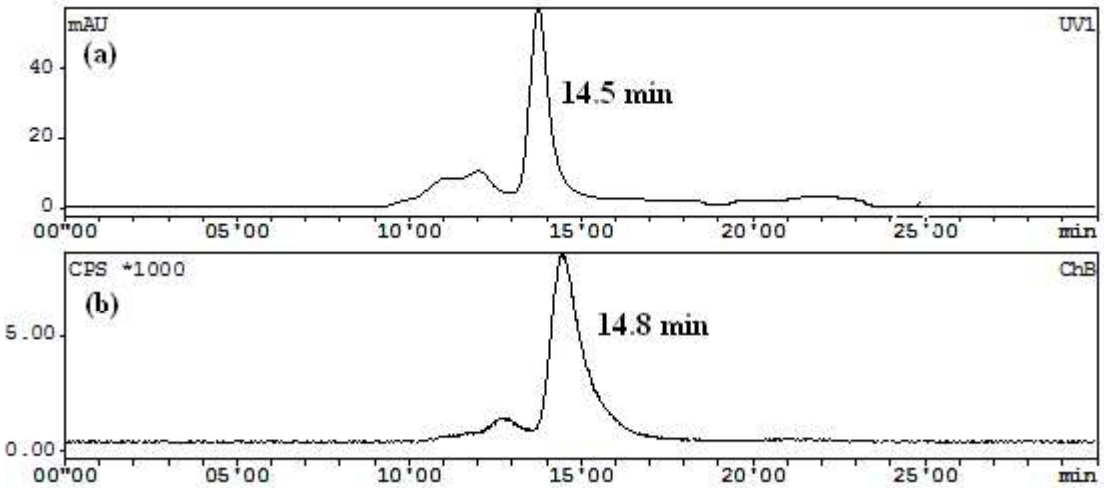

Figure 4a.3. SE-HPLC profile of ^{68}Ga-NOTA-HSA (1a) (a) UV profile at 280 nm (b) radioactive profile

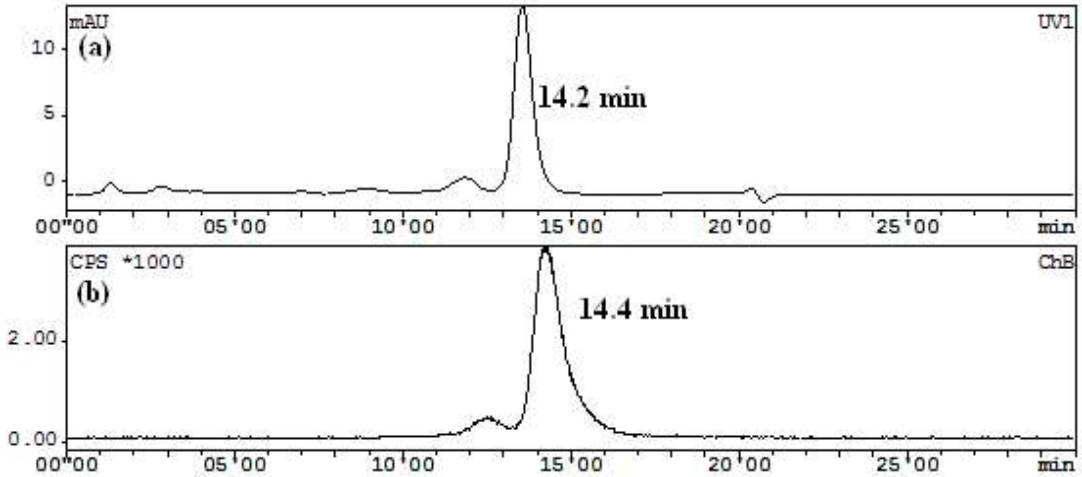

Figure 4a.4. SE-HPLC profile of ^{68}Ga-DOTA-HSA (1a) (a) UV profile at 280 nm (b) radioactive profile

The time required for completion of radiolabeling for NOTA-HSA was about 10 minutes at ambient temperature while that required for DOTA-HSA was 30 minutes at 37°C. Owing to the short half life of ^{68}Ga, the 30 minute incubation time is fairly long. It is desirable that ^{68}Ga tracers intended for widespread clinical use should have a quick and reproducible synthesis scheme.

4a.4.3. In vitro stability of 1a/2a

The results of the *in vitro* stability studies of 1a/2a are given in Table 4a.1. No significant transchelation was observed when 1a/2a were incubated in excess EDTA solution and their radiochemical purities were ≥ 90 % up to 2 h (period of study). Further, both the radiolabeled conjugates exhibited excellent stability in human serum.

Table 4a.1. In vitro stability of complexes (1a/2a)

Radioconjugate	EDTA solution (10 mM)	Human serum
^{68}Ga-NOTA-HSA	96±0.5 %	94±1.0 %
^{68}Ga-DOTA-HSA	92±1.0 %	90±2.0 %

4a.4.4. In vivo evaluation studies

(a) Biodistribution studies

Results of the biodistribution studies of **1a**/**2a** are given in Figure 4a.5. Both the conjugates showed almost similar retention in blood at all the time points studied. In **1a**, the highest retention was observed in blood (73.2±2.9 %ID/g) at 2 min p.i followed by that in lungs, heart, liver and kidney. At 10 min p.i., a further increase in blood activity (76.5±1.2 %ID/g) was observed which then decreased gradually with time. A 27 % decrease in the blood activity from the initial time point (2 min p.i.) was observed at 1 h p.i. (53.7±3.8 %ID/g) while 37 % decrease in activity (from 2 min p.i.) was observed at 2 h p.i. Simultaneously, a decrease in activity was observed with the passage of time in organs such as the lungs, heart and kidney. On the other hand, a slight increase in activity was observed in liver as well as in intestine showing that the conjugate predominantly cleared from the system

by hepatobiliary pathway, as expected. Similarly in **2a**, the high retention of activity in blood at 2 min p.i. (75.4±9.8 %ID/g) decreased by 26 % up to 1 h p.i. and further decreased by 38 % up to 2 h p.i. Also, a high retention of activity was observed in lungs, heart and kidney which decreased with time. However, the activity in the liver gradually increased showing the hepatobiliary clearance of the conjugate.

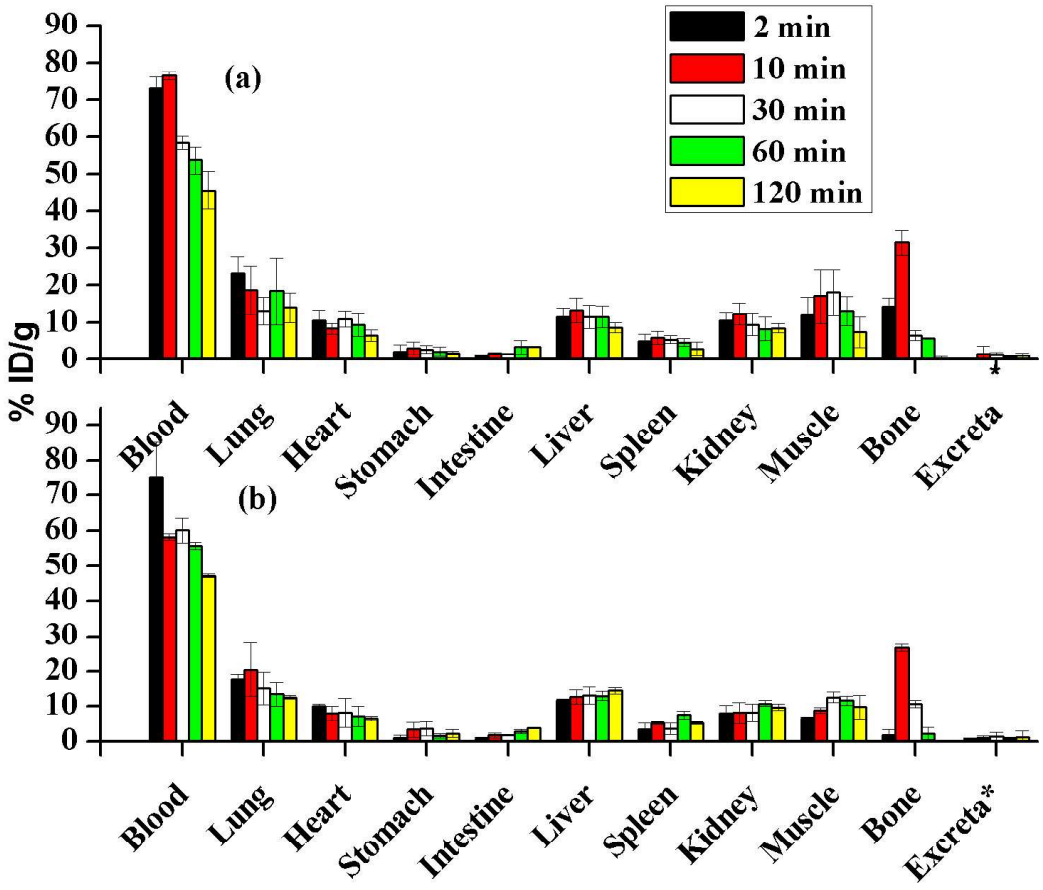

Figure 4a.5. Biodistribution profile of (a) ^{68}Ga-NOTA-HSA (1a) and (b) ^{68}Ga-DOTA-HSA (2a) in Swiss mice

The conjugates showed similar retention in blood and it was observed that even after 2 h, close to 50% of the initial activity (%ID/g) was still remaining in the blood in both **1a** and **2a**. A high retention in the blood is an important characteristic of an ideal blood pool imaging agent as it eliminates the need for re-injection of the radiolabeled product during

data acquisition. Also it helps in the detection of slow processes like leakage from tumor vessels, endovascular leaks, gastrointestinal bleeding or for delayed steady-state imaging[161].

The tissue to blood ratio of **1a**/**2a** at the various time points is given in Figure 4a.6. The tissue to blood ratio was < 0.2-0.3 at all time points except the liver/blood ratio where it increased to > 0.3 with time. In **2a**, a similar retention in blood and liver was observed as in the case of **1a**. However, in **2a** slightly higher activity was also observed in bone. The bone/blood ratio increased to 0.46 at 10 min time p.i. which then decreased with time. Since the uptake of the two tracers in the other organs with respect to that in blood was low, the two radiotracers can be used to determine the individual organ blood volumes as the agents are present primarily in the blood of that organ.

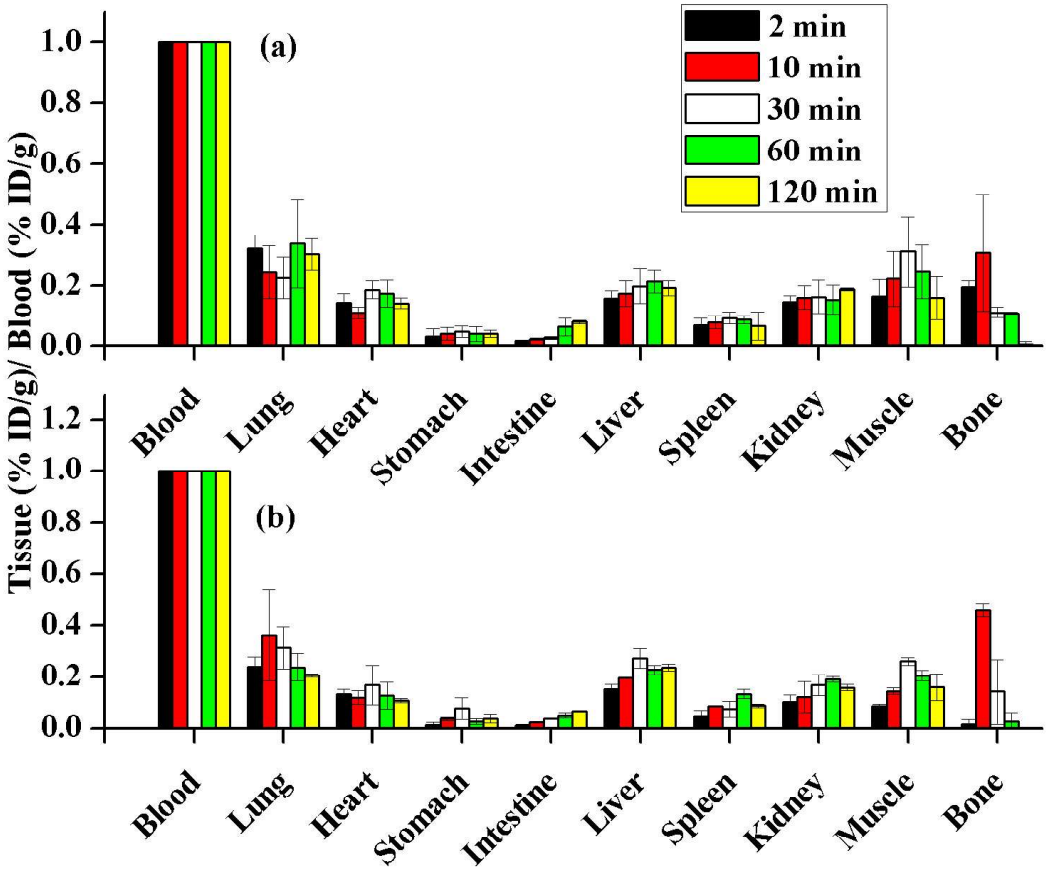

Figure 4a.6. Blood (% ID/g): Tissue (% ID/g) ratios of (a) ^{68}Ga-NOTA-HSA (1a) and (b) ^{68}Ga-DOTA-HSA (2a)

(b) Analysis of Metabolites

The plasma samples of animals injected with **1a** and **2a** (biodistribution at 1 h p.i.) were analyzed by paper chromatography using 10 mM sodium citrate solution as mobile phase (pH 5) and it was observed that conjugate 1a was 96±1 % stable in plasma after 1 h post intravenous injection while 2a was only 88±3 % stable. This decrease in stability of ^{68}Ga-DOTA-HSA may lead to unwanted accumulation of activity in non target organs.

4a.5. CONCLUSIONS

Towards utility in blood pool imaging, ^{68}Ga-NOTA-HSA conjugate was synthesized and compared for its radiolabeling and biodistribution characteristics to ^{68}Ga-DOTA-HSA conjugate. NOTA-HSA conjugate could be efficiently labeled with ^{68}Ga under milder conditions and in short time as compared to the DOTA-HSA conjugate. Biodistribution profiles of both conjugates were similar in Swiss mice except that an increase in bone activity was observed in ^{68}Ga-DOTA-HSA. Stability in plasma was more for ^{68}Ga-NOTA-HSA. Based on these results, it could be concluded that ^{68}Ga-NOTA-HSA can be further investigated for clinical blood pool imaging applications.

CHAPTER 4b.

DEVELOPMENT OF ^{68}GA LABELED MACROAGGREGATED ALBUMIN (MAA) FOR LUNG IMAGING

4b.1. INTRODUCTION

^{99m}Tc labeled HSA microspheres are routinely used for lung perfusion scanning, a procedure in diagnostic nuclear medicine to assess the presence of emboli or other abnormalities to the pulmonary blood flow[167]. This procedure uses microspheres of diameter range 10-100 μm, which are called Macroaggregated Albumin (MAA). Conventionally, MAA is radiolabeled with ^{99m}Tc, obtained as $^{99m}TcO_4^-$ from a ^{99}Mo/^{99m}Tc generator. On account of their size, intravenously administered ^{99m}Tc-MAA particles are trapped in the lung capillary bed during the first pass of circulation and are thus employed to study perfusion in the lung tissue.

^{99m}Tc-MAA used in lung perfusion is imaged by Single Photon Emission Computed Tomography (SPECT)[168,169]. Owing to the advantages of PET over SPECT, my endeavour was to tag the positron-emitting radionuclide ^{68}Ga to MAA for obtaining the desired perfusion information through PET imaging. In recent times there has been a significant increase in the number of PET imaging facilities in India and other countries[170], which makes a PET-based lung perfusion tracer an increasingly relevant alternative to the existing ^{99m}Tc radiopharmaceutical. Among the various PET radionuclides, ^{68}Ga [$t_{1/2}$=67.7 min, $E_{\beta+}$(max)=1.92 MeV (89%)], is a favourable alternative to ^{99m}Tc to radiolabel MAA. Additionally, the shorter half-life of ^{68}Ga is better suited to the mechanics of perfusion imaging, allowing for requirement of less activity for a quality image, thereby resulting in low non-specific dose to the patient. In the literature, there are already several reports on ^{68}Ga labeling of commercially available MAA kits[171-176]. In recent times, there has been a sharp increase in the price of MAA kits for lung perfusion in the US, which has led to a decrease in

the availability of V/Q lung scans in the hospitals. As in India, the kits are currently imported, this is likely to be an issue as well, especially considering the large number of economically disadvantaged patients. In this context, an attempt was made to prepare an indigenous, inexpensive kit of MAA synthesized from ground up for labeling with ^{68}Ga to use as a lung perfusion radiopharmaceutical. Since radiolabeling with ^{68}Ga does not require stannous chloride in contrast to ^{99m}Tc, the role of stannous chloride on the formation of MAA and the ^{68}Ga labeling yield/stability of the MAA thus synthesized was also studied. A comparison was also made with the ^{68}Ga-MAA prepared using commercially available MAA kits (conventionally used to make ^{99m}Tc-MAA). In addition to biodistribution studies, in order to explore the potential utility of ^{68}Ga-MAA for optical imaging of lungs, Cerenkov imaging of ^{68}Ga labeled MAA was also carried out in Swiss mice.

4b.1.1. Cerenkov Imaging

Cerenkov Luminescence (CL) is a phenomenon which was first described by Russian Scientist Pavel Alekseyevich Cherenkovin 1934[177]. He observed blue light from a bottle of water when it was subjected to radioactive decay. Later it was revealed that charged particles emitted from radionuclides, when travelling faster than the speed of light in that particular medium transfer their kinetic energy through interactions with the surrounding dipoles in the medium (mostly water in biological tissues). The randomly oriented dipoles in the medium align themselves with the charged particle and relax by releasing the transferred energy in the form of light in the ultraviolet and blue end of the visible region. Depending upon the refractive index of the medium, charged particles with certain threshold energy only are able to produce CL. For example β particles with kinetic energy ≥ 263 keV can produce CL in water and the E_{min} reduces to ≥ 219 keV in tissue (using an approximate refractive index of 1.4)[177].

The Cerenkov light can be used for direct optical imaging using a Charged Coupled Device (CCD)[178]. This is called Cerenkov Luminescence imaging (CLI) which pairs the production of visible light from radiotracers with the widely used small animal imaging equipment optimized for preclinical imaging. Many medical isotopes such as ^{15}O, ^{13}N, ^{68}Ga, ^{89}Zr, ^{64}Cu, ^{225}Ac, ^{90}Y, ^{124}I and ^{74}As have been evaluated for CLI applications both in *in vitro* and *in vivo* systems. Unlike PET and SPECT imaging, CLI can be used for imaging of both β^- and β^+ emitters. It is considered as "Cheap man's PET" as its instrumentation is cheaper and also faster. Further, CLI is known to have higher ability to resolve smaller structures than PET or SPECT imaging systems. However, the major disadvantage of CLI is its lack of sensitivity as most of the Cerenkov photons travelling through the tissues are strongly absorbed by the haemoglobin which absorbs in the blue-green visible region. Further the photons also get scattered on travelling through areas of different refractive indices[177,178].

In this work, Cerenkov imaging of Swiss mice injected with ^{68}Ga-MAA was carried out. The main aim was to determine the extent of localisation of theparticles in the lungs and if there is any leakage from the target organ.

4b.2. MATERIALS AND METHODS

Human serum albumin (lyophilized), stannous chloride, sodium acetate, disodium hydrogen phosphate and sodium dihydrogen phosphate were obtained from Sigma-Aldrich, USA. Commercial MAA vials (Jubilant DraxImage Inc., Canada) for comparison with the indigenously synthesised MAA were obtained as a gift from Dr. V. Rangarajan, Head, Nuclear Medicine and Bioimaging Division, Tata Memorial Hospital, Mumbai, India. All other chemicals used were of analytical grade. HPLC grade water was used for preparing all solutions, after purging with nitrogen gas (Inox Chemicals, India). Whatman No.1 chromatography paper (Whatman, UK) was used for carrying out paper chromatography. Alpha 1-2 LD Plus freeze-drier (Martin-Christ, Germany) was used for lyophilization. A

well-type NaI(Tl) detector (ECIL, India) was used to count radioactive samples for determining the radiolabeling yield and *in vitro* stability. Organ activity measurements during *in vivo* studies were performed on a flat-bed NaI(Tl) radioactivity detector (Harshaw, UK). Cerenkov Luminescence Imaging was performed with a Photon Imager (Biospace lab, France).

4b.3. EXPERIMENTAL

4b.3.1. Preparation of MAA

MAA was prepared using the reported procedure[179,180]. In brief, 20 mg of HSA was dissolved in saline to get a 20 % solution. An aqueous solution of stannous chloride (5 mg/mL) was prepared and added dropwise with stirring to the HSA solution under inert atmosphere. The reaction mixture was then stirred for 10 min. Sodium acetate salt was added with mixing to raise the pH of the reaction mixture to 5. The reaction mixture was further diluted with phosphate buffer (0.1 mol/L, pH 5.1) to get a 2 % solution of HSA. Tween-80 was added to this reaction mixture, which was then heated at 75°C for 10 min in a water bath with stirring. The reaction mixture was subsequently cooled to room temperature, followed by a second round of heating at 80°C for 5 min. After cooling to room temperature, 500 µL each of the solution containing 1 mg of MAA and 250 µg of stannous chloride was dispersed into vials (with 5 % glucose as cryoprotectant) and lyophilized. This batch of MAA was named MAA_5.

In order to study the effect of stannous chloride on the formation and ^{68}Ga radiolabeling of MAA, another batch of MAA was prepared in which no stannous chloride was added (named hereafter as MAA_0).

4b.3.2. Particle Size distribution

The lyophilized vials (MAA_0, MAA_5) and commercial MAA (cMAA) were reconstituted with saline. Towards the determination of particle size, a small amount of the MAA suspension was pipetted onto a clean glass slide, which was then overlaid with a cover slip and viewed using a light microscope at 100X final magnification. In case of elongated particles, the longer axis was considered as the particle diameter. A minimum of 100 particles per suspension were measured for obtaining the mean diameter.

4b.3.3. Radiolabeling of the synthesized MAA with ^{68}Ga

The MAA particles synthesized with and without the addition of stannous chloride during the synthesis process (MAA_5 and MAA_0 respectively) were radiolabeled with ^{68}Ga (74-148 MBq) eluted from the nanoceria-PAN sorbent based in-house $^{68}Ge/^{68}Ga$ generator (Chapter 1, Section 1.4.3). Prior to ^{68}Ga labeling, the MAA particles were reconstituted in 1 mL of saline and centrifuged at 3000 rpm for 5 min. This washing procedure was repeated twice and the supernatant containing free stannous chloride, Tween-80, acetate and phosphate salts was discarded. The ^{68}Ga radiolabeling was optimized with respect to the pH and temperature of the reaction. For optimization of pH, the radiolabeling reactions were carried out using 2 mg of MAA particles at two different pH conditions (pH 4 and 6) at different temperatures (25°C, 50°C and 75°C) for 15 minutes. In brief, 1 mL of $^{68}GaCl_3$ (~ 74-148 MBq) in 0.1 N HCl from the in-house $^{68}Ge/^{68}Ga$ generator was added to 2 mg of MAA particles which were suspended in 0.4 mL of 0.5 mol/L sodium acetate solution. The desired pH was maintained by addition of HCl (0.1 mol/L) to the reaction mixture. After optimizing the pH of the reaction, the reaction mixture was incubated at various temperatures (25°C, 50°C and 75°C) for 15 min. At the end of the incubation period, radiolabeling yield was determined by centrifugation, wherein the reaction mixture was centrifuged at 3000 rpm for 10 min, leading to settling down of the MAA particles. The relative proportion of ^{68}Ga activity associated with the MAA particles and the supernatant, as determined by NaI(Tl)

detector, gave a quantitative measure of the radiolabeling yield. The ^{68}Ga labeled MAA particles were washed twice with 2 mL of saline each to completely remove free ^{68}Ga, subsequent to which radiochemical purity was determined by carrying out paper chromatography on Whatman No.1 strips using sodium citrate (0.1 mol/L, pH 5) as the mobile phase in which free ^{68}Ga(III) moved to the solvent front (R_f=0.9-1.0) while ^{68}Ga-MAA remained at the point of spotting (R_f=0.0). Radiolabeling of commercial MAA kit (cMAA) was also carried out with ^{68}Ga, using the procedure optimized for ^{68}Ga labeling of in-house prepared MAA.

4b.3.4. In vitro stability studies

In order to determine the *in vitro* stability of ^{68}Ga-MAA$_5$ and ^{68}Ga-MAA$_0$ prepared using MAA synthesized in-house, the respective radiolabeled preparation was centrifuged and the supernatant was removed. The particles were washed twice with saline to remove any free ^{68}Ga and then re-suspended in 1 mL saline. 100 µL of the respective ^{68}Ga-MAA product was incubated with 0.9 mL of Wistar rat serum at 37°C. Aliquots were removed after 45 min and the stability of ^{68}Ga-MAA$_5$ and ^{68}Ga-MAA$_0$ was determined by comparing the relative proportion of ^{68}Ga activity associated with the supernatant and the particles after centrifugation at 3000 rpm.

4b.3.5. In vivo studies of ^{68}Ga-MAA$_5$

(a) Biodistribution studies of ^{68}Ga-MAA$_5$ in comparison with that of ^{68}Ga-cMAA

In vivo studies of ^{68}Ga-MAA$_5$ were carried out in normal Swiss mice by intravenous injection. For comparison, biodistribution studies of ^{68}Ga-MAA prepared using the commercial kits (^{68}Ga-cMAA) were also carried out by adopting the same procedure. All procedures performed herein were in accordance with the national laws pertaining to the conduct of animal experiments. Normal female Swiss mice (20-25 g) (n=4) were used for *the in vivo* distribution assays of the in-house prepared ^{68}Ga-MAA$_5$ particles and the product

prepared using the commercial kits (^{68}Ga-cMAA). The radiolabeled preparation (100 µL per animal, ~370 KBq) was administered intravenously in each mouse. After 15 min post-injection, the animals were sacrificed by exposure to carbon dioxide atmosphere. Blood was collected by cardiac puncture and relevant organs and tissues were excised for measurement of associated activity. The organs were weighed and rinsed, and the radioactivity associated with each was measured in a flat bed type Na(I) counter with suitable energy window for ^{68}Ga. The activity retained in each organ/tissue was expressed as a percentage of the total injected dose per organ (%ID/organ).

(b) Cerenkov Imaging

For Cerenkov imaging, normal Swiss mice were injected intravenously with 100 µl of ^{68}Ga-MAA$_5$ (18.5 MBq). Animals were anaesthetized by intraperitoneal injection of ketamine and zylaxine. Anaesthetized animals were placed in the dark imaging chamber of the Photon Imager for imaging under intensified CCD Camera. Reconstruction of the luminescent signals from the mice was done by M3 Vision Analysis Software in-built with the Imager.

(c) Biodistribution studies of six month old MAA$_5$ kit radiolabeled with ^{68}Ga

In order to assess the long term stability of MAA$_5$ lyophilized kit, its six month old kit (stored at 2-4 °C) was radiolabeled with ^{68}Ga using the procedure described in Section 4b.3.3. (pH=6). Further, the biodistribution of the radiolabeled particles was determined in Swiss mice (n=4) at time points 15 min, 30 min and 1 h using the procedure as described in Section 4b.3.5 (a).

4b.4. RESULTS AND DISCUSSIONS

4b.4.1. Particle size distribution and morphology of synthesized MAA

The lyophilized kits of MAA easily dispersed during reconstitution in saline. Figure 4b.1(a) shows the average particle size of MAA$_0$, MAA$_5$ and cMAA and Figure 4b.1(b)

shows the particle size distribution of MAA_0, MAA_5 and cMAA in the 10-100 μm range. In case of MAA_0 which was synthesized without addition of stannous chloride during the synthetic process, 40 % of the particles were below 20 μm size with an average particle size of 31.9±16.7 μm. MAA_5 (synthesized using stannous chloride during the reaction) samples had a particle size distribution similar to that of cMAA with a mean particle size of 59.9±18.1 μm and 52.9±15.2 μm respectively. No particles above 100 μm and below 10 μm size were observed both in MAA_0 and MAA_5.

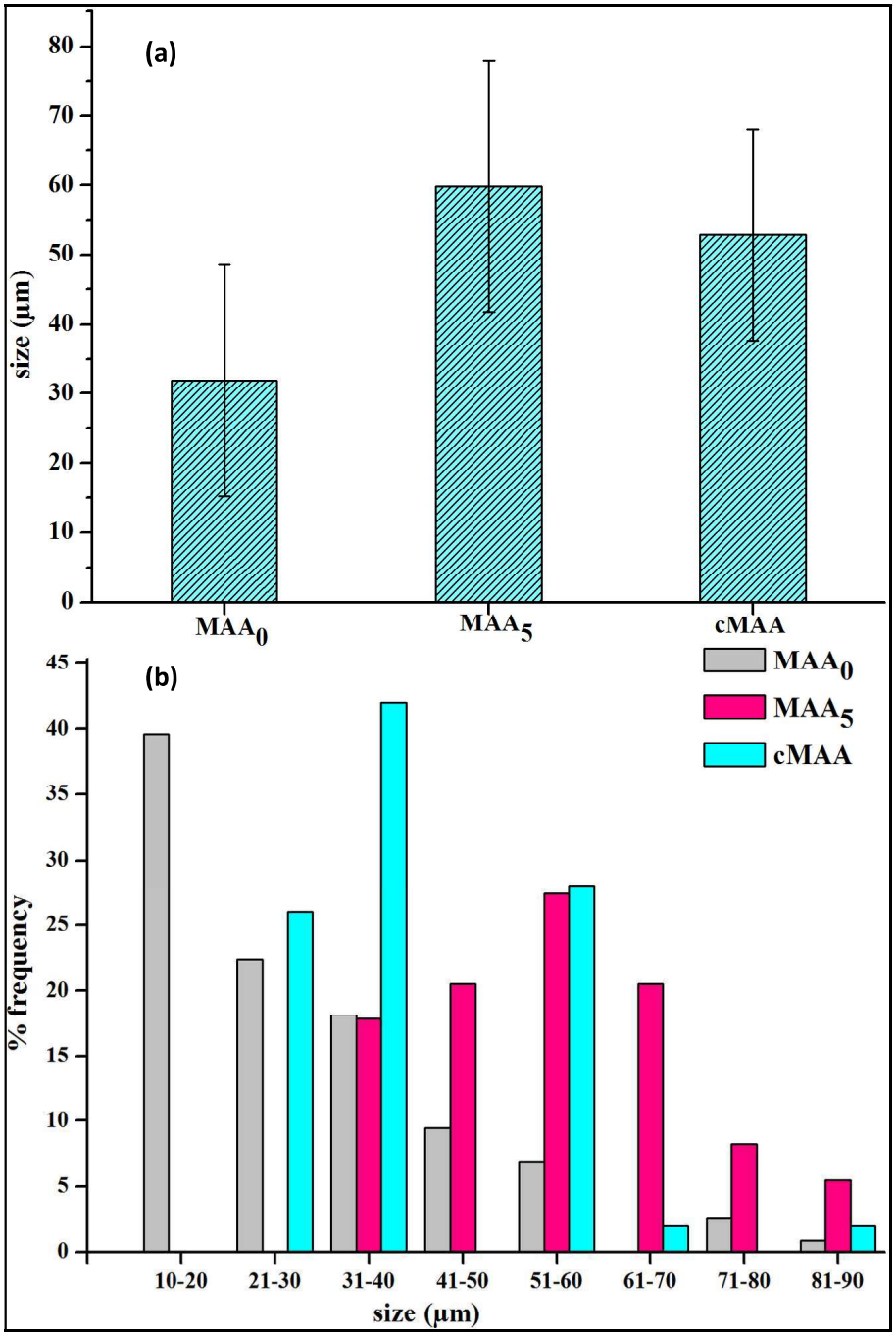

Figure 4b.1 (a) Mean particle size and (b) Particle size distribution of MAA_0, MAA_5, cMAA

Native HSA is a stable hydrated macromolecule consisting of a single folded polypeptide chain with about 50% of α-helix[181].The isoelectric point of HSA is 4.7. When HSA is heated at pH 5.1 (above it's isoelectric point), aggregates in the range of 10-50 µm are formed. When the temperature rises above 68°C, unfolding of the α-helix form occurs.

Increase in temperature increases the unfolding of the pocket containing the free sulfhydryl groups of cysteine-34, which is then available for intermolecular disulphide bridges. Albumin aggregation is initiated with the formation of intermolecular disulfide bridge exchanges and strengthened with the subsequent hydrogen bonding between independent molecules. On cooling at 20°C, the albumin aggregates get stabilized in β-pleated form. Stannous chloride being reducing in nature, might be assisting in the unfolding of the helical structure of MAA. It may be also possible that stannous might be interacting with the sulfhydryl group of cysteine-34 of albumin leading to the formation of larger aggregates. Hence, in order to understand the role of stannous chloride in the formation of MAA, in-house synthesis of MAA in the absence of stannous chloride (MAA_0) and in presence of stannous chloride (MAA_5) was carried out. During the heating procedure, it was observed that the formation of aggregates, indicated by appearance of a white precipitate, was significantly more rapid in the reaction mixture which had added stannous chloride in it (MAA_5). Moreover, the mean particle diameter of MAA_5 (59.9±18.1 μm) was larger than that of MAA_0 (31.9±16.7 μm) and closer to that of the commercial MAA sample (cMAA) (52.9±15.2 μm). This showed that stannous chloride has a strong influence on the particle formation in HSA.

Figure 4b.2 shows the morphology of the respective MAA preparations viewed at 100X final magnification under a light microscope. It was observed that the in-house synthesized MAA preparations had a tendency towards an elongated rod-like shape, while the particles of the commercial MAA kit under microscope showed a more compact morphology tending towards the spherical shape.

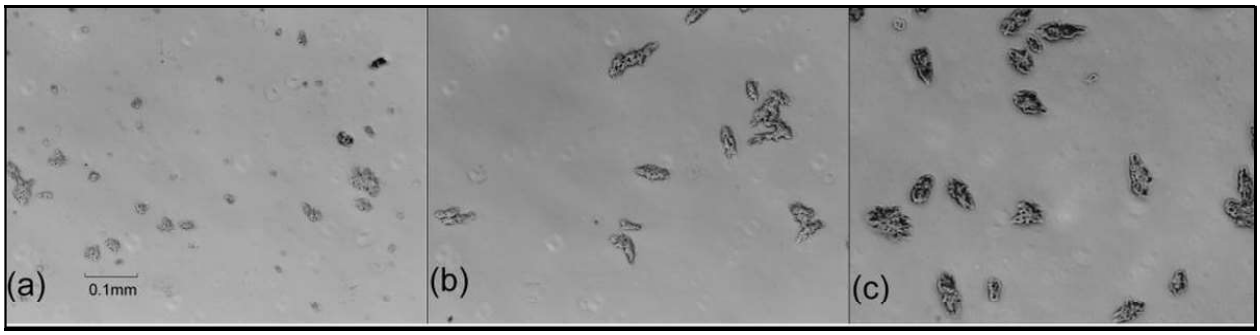

Figure 4b.2. Comparison of particle morphology of (a) MAA_0 (b) MAA_5 (c) cMAA under light microscope (100X magnification)

4b.4.2. Radiolabeling of the synthesized MAA with ^{68}Ga

Variation of radiolabeling yields of MAA_0 and MAA_5 with ^{68}Ga under different pH and temperature conditions is depicted in Figure 4b.3. It is well evident that both MAA_5 and MAA_0 gave poor radiolabeling yields with ^{68}Ga at room temperature and the radiolabeling yields increased with increase in temperature at both pH 4 and pH 6. MAA_5 exhibited superior radiolabeling yields with ^{68}Ga (in comparison to MAA_0) at all the temperatures and pH conditions studied. In case of MAA_5, the best radiolabeling yield (84.5±5.3 %, n=10) was obtained on incubation for 15 minutes at 75°C at pH 6. In addition, the radiochemical purity after centrifugation and re-suspension in saline was 98±0.8%. However, in the case of MAA_0, the radiolabeling yield was very less (49.9±1.3 %, n=10) even when the radiolabeling reaction was carried out for 15 minutes at 75°C at pH 6.

The exact chemistry of binding of ^{68}Ga to the microspheres is however not known. Mathias et al have earlier reported the ^{68}Ga labeling of commercial MAA at pH 6 and have postulated that probably ^{68}Ga gets adsorbed to the surface of the albumin microspheres as gallium hydroxide[173].

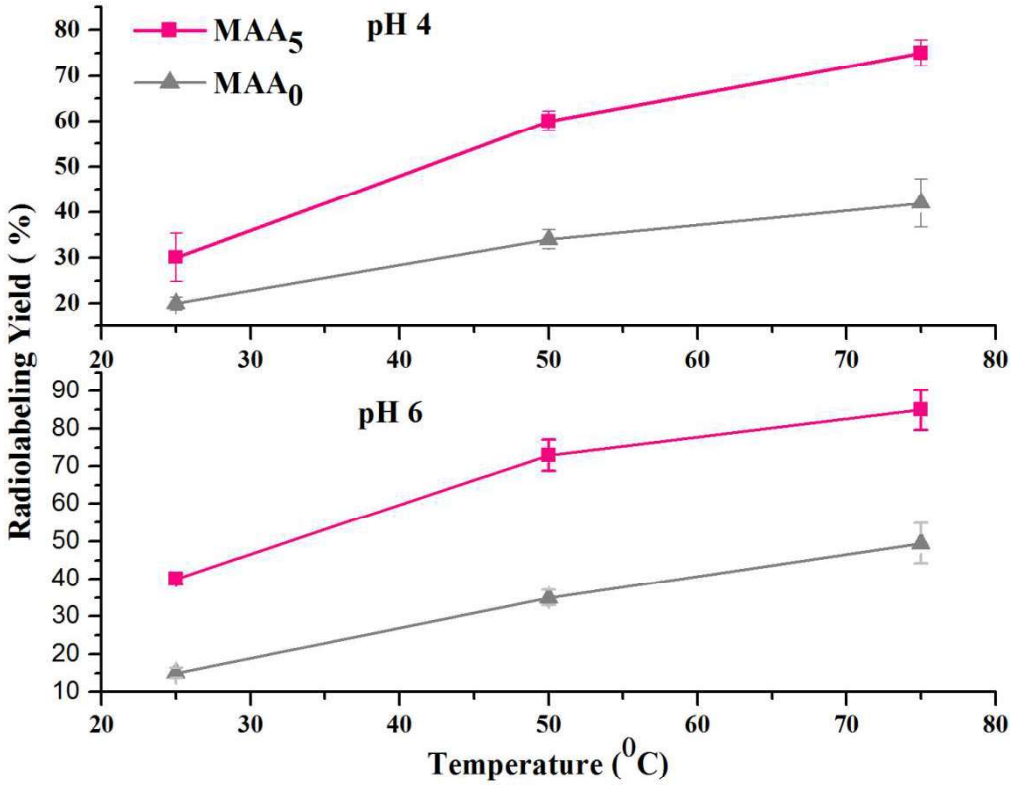

Figure 4b.3. ***Radiolabeling yield of ^{68}Ga-MAA$_0$ and ^{68}Ga-MAA$_5$ at different pH (pH 4 and 6) and temperature conditions (25 °C, 50 °C and 75 °C)***

The radiolabeling yield of ^{68}Ga labeled cMAA was 77.8±0.5 % (n=3, after incubation for 15 min at 75 °C at pH 6). The radiochemical purity after centrifugation and re-suspension in saline was 98±1.0 %.

4b.4.3. In vitro stability studies

The results of the *in vitro* stability studies of ^{68}Ga-MAA$_5$ and ^{68}Ga-MAA$_0$ carried out in serum at 37 °C are shown in Figure 4b.4. It is well evident from the figure that the serum stability of ^{68}Ga-MAA$_5$ (70.1±2.4 %) was significantly higher than that of ^{68}Ga-MAA$_0$ (26.5±2.5%) (45 minutes at 37°C). As ^{68}Ga-MAA$_0$ showed poor *in vitro* stability, further *in vivo* studies with ^{68}Ga-MAA$_0$ were not carried out.

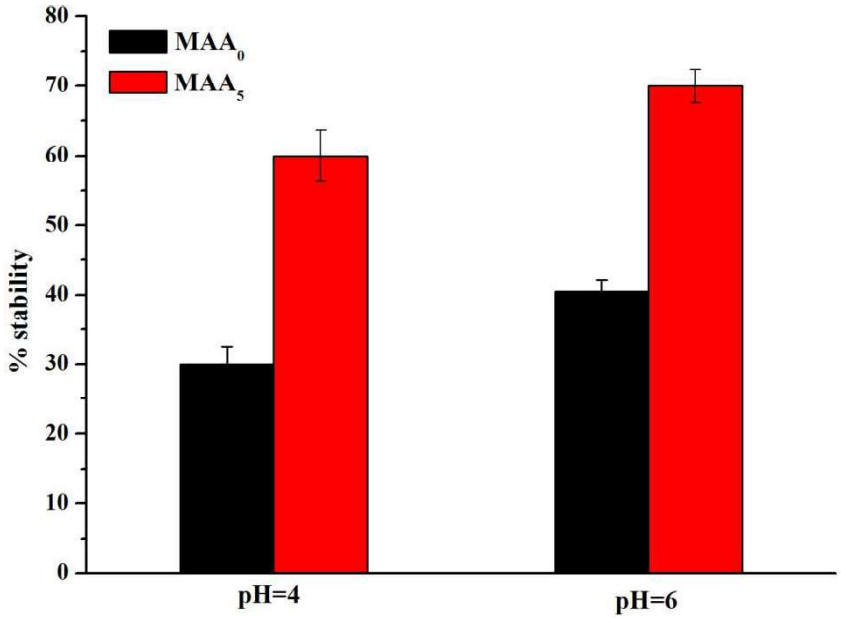

Figure 4b.4. Serum stability of ^{68}Ga-MAA$_0$ and ^{68}Ga-MAA$_5$ (45 min at 37 °C)

4b.4.4. In vivo studies of ^{68}Ga-MAA$_5$

(a) Biodistribution studies of ^{68}Ga-MAA$_5$ in comparison with that of ^{68}Ga-cMAA

The *in vivo* distribution patterns of ^{68}Ga-MAA$_5$ and ^{68}Ga-cMAA, at 15 minutes post-intravenous injection in Swiss mice are depicted in Figure 4b.5. The biodistribution profile of the in-house developed ^{68}Ga-MAA$_5$ was comparable to that of ^{68}Ga-cMAA. The uptake of ^{68}Ga-MAA$_5$ in the lungs at 15 min time point was 71.6±2.1 %ID while that of ^{68}Ga-cMAA was 83.5±2.3 %ID at the same time point. Negligible uptake of injected ^{68}Ga-MAA$_5$ activity was seen in other organs, especially the liver. Both the preparations showed small amount of blood activity, which was comparable.

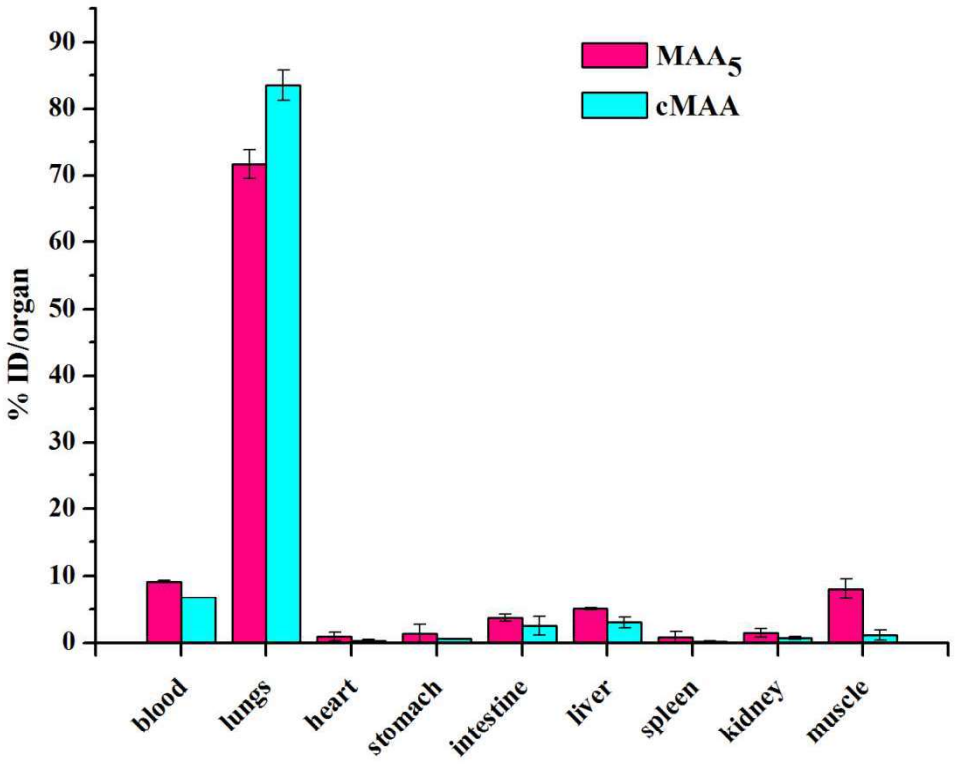

Figure 4b.5. Comparison of biodistribution profile of ^{68}Ga-MAA$_5$ and ^{68}Ga-cMAA at 15 min p.i.

(b) Cerenkov imaging

Localization of ^{68}Ga-MAA$_5$ in the target organ of the mouse was demonstrated by Cerenkov Luminescence Imaging (CLI). Representative pictures of CLI of an experimental animal captured at 10, 30 and 60 min post-administration (Figure 4b.6 a, b, c) of ^{68}Ga-MAA$_5$ showed preferential accumulation of ^{68}Ga-MAA$_5$ in the lungs at all the time points studied. Most of the ^{68}Ga activity was localized in the lungs with negligible activity in the liver. Thus, excellent images of the mouse could be obtained wherein the ^{68}Ga activity was seen to be localized only in the lungs even at 1 h post administration confirming the suitability of the in-house synthesized MAA for preparation of ^{68}Ga-MAA towards PET imaging of lung perfusion.

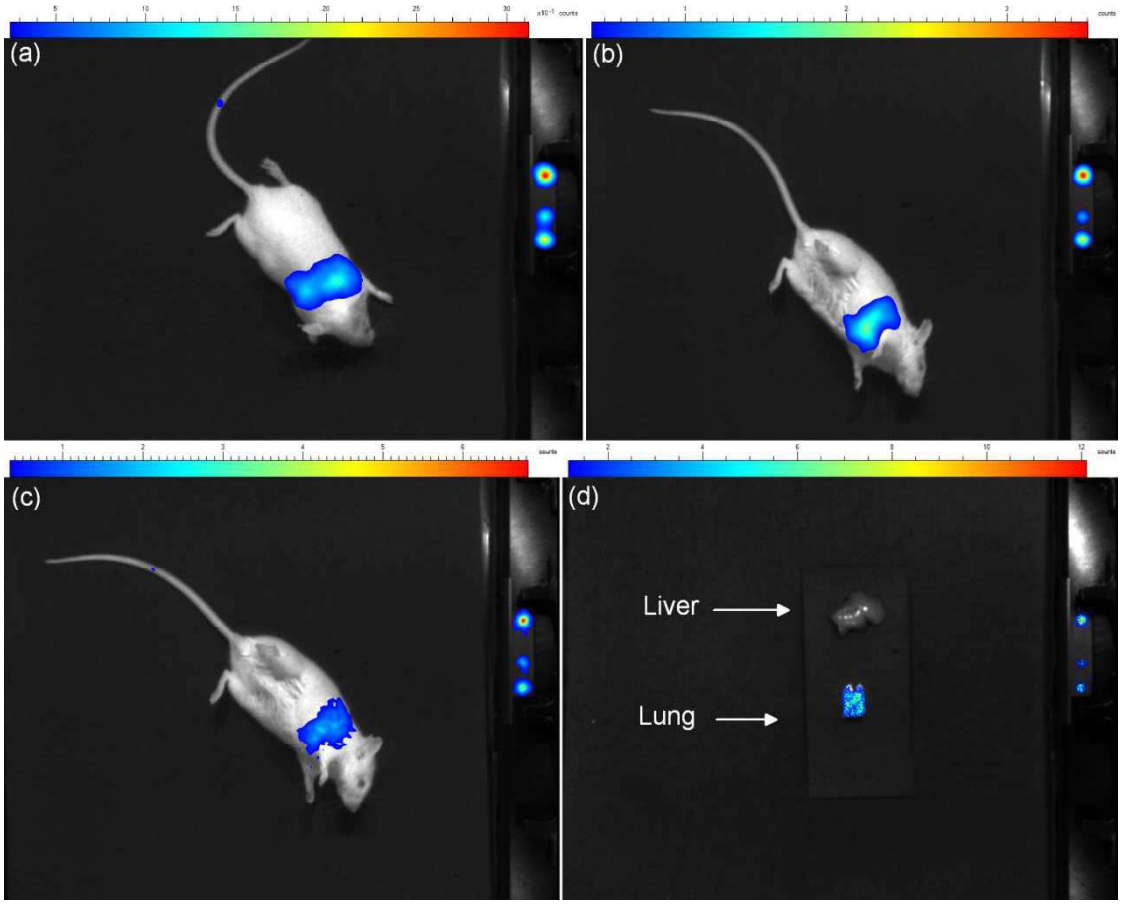

Figure 4b.6. Cerenkov images of ^{68}Ga-MAA$_5$ in Swiss mice at (a) 15 min (b) 30 min and (c) 60 min post administration (d) liver and lungs extracted at 60 min post administration

(c) Biodistribution studies of six month old MAA$_5$ kit radiolabeled with ^{68}Ga

The results of the biodistribution studies of six month old MAA kit are given in Figure 4b.7. These results show ≥ 80% uptake of ^{68}Ga-MAA$_5$ in the lungs in Swiss mice which was stable up to 1 h. These results suggest that the indigenously synthesized MAA$_5$ kit was stable up to the period of study (six months) when stored at 2-4 °C.

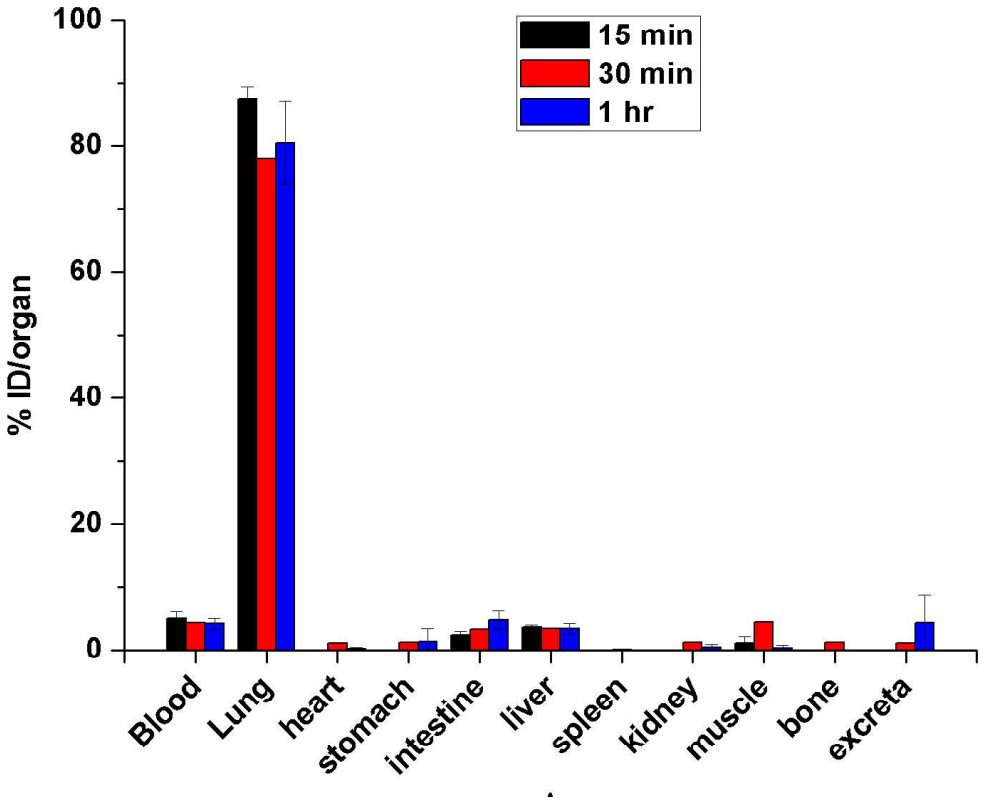

Figure 4b.7. Biodistribution profile of ^{68}Ga-labeled MAA$_5$ (Six months old lyophilized kit)

4b.5. CONCLUSIONS

An in-house optimized formulation of MAA for use as a ^{68}Ga-labeled lung perfusion radiopharmaceutical was successfully prepared as an alternative to the imported product. The particle size of MAA$_5$ was comparable to that of cMAA. Further, the MAA$_5$ particles exhibited good ^{68}Ga labeling yield and *in vitro* stability in comparison to the ^{68}Ga product prepared using commercial MAA kits. In addition, the *in vivo* distribution in Swiss mice of ^{68}Ga labeled in-house MAA preparation was comparable to that of ^{68}Ga-labeled commercial MAA formulation, both of which showed similar accumulation in the lungs. The in-house preparation thus shows considerable potential to be a logistically and economically advantageous option for the national nuclear medicine community. The biodistribution of ^{68}Ga-MAA could be successfully imaged using Cerenkov Luminescent Imaging showing stable accumulation of MAA in the lungs. This study opens the gateway for indigenous

development of MAA cold kits for fast and efficient radiolabeling with ^{68}Ga towards lung perfusion imaging.

REFERENCES

1. Weissleder R, Pittet MJ. Imaging in the era of molecular oncology. *Nature.* 2008;452: 580-590.
2. Liu S. The role of coordination chemistry in the development of target-specific radiopharmaceuticals. *Chem Soc Review*. 2004; 33: 445-461.
3. Jurisson S, Berning D, Jin W, Ma D. Coordination compounds in nuclear medicine. *Chem Rev.* 1993; 93:1137-1156.
4. Rahmim A, Zaidi H. Pet versus SPECT: strengths, limitations and challenges. *Nucl Med Comm.* 2008; 29:193-207.
5. Velikyan I. Prospective of ^{68}Ga-radiopharmaceutical development. *Theranostics.* 2014;4:47-80.
6. Wadsak W, Mitterhauser M. Basics and principles of radiopharmaceuticals for PET/ CT. *Europ J Radiol.* 2010;73:461-469.
7. Velikyan I. ^{68}Ga-Based radiopharmaceuticals: Production and Application Relationship. *Molecules.* 2015;20:12913-12943.
8. Banerjee SR, Pomper MG. Climical application of Gallium-68. *Appl Radiat Isot*. 2013;2-13.
9. Bartholoma MD, Louie AS, Valliant JF, Zubieta J. Technitium and gallium derived radiopharmaceuticals: Comparing and contrasting the chemistry of two important radiometals for the molecular imaging era. *Chem Rev*. 2010;110:2903-2920.
10. Roesch F, Filosofov DV. Production, radiochemical processing and quality evaluation of Ge-68, In: IAEA-TEC-DOC Radioisotopes and radiopharmaceuticals, Series 2: Production of long lived parent radionuclides for generators: ^{68}Ge, ^{82}Sr, ^{90}Sr and ^{188}W,

International Atomic Energy Agency, Vienna, 2010. ISSN 2077-6462; no. 2, STI/PUB/1436, ISBN 978-92-0-101110-7.

11. Roesch F. Maturation of a Key resource-The germanium-68/ gallium-68 generator: Development and New Insights. *Curr Radiopharm*. 2012; 5:202-211.
12. Gleason GI. A positron cow. *Int J Appl Radiat Isot.* 1960; 8: 90-94.
13. Greene MW, Tucker WD. An improved gallium-68 cow. *Int J Appl Radiat Isot.* 1961;12: 62-63.
14. Yano Y, Ange HO. A gallium-68 positron cow for medical use. *J Nucl Med.* 1964;5:484-487.
15. Roesch F. Past, present and future of ^{68}Ge/^{68}Ga generators. *Appl Radiat Isot*. 2013;24-30.
16. Chakravarty R, Shukla R, Ram R, Venkatesh M, Tyagi AK, Dash A. Development of a nano-zirconia based ^{68}Ge/^{68}Ga generator for biomedical applications. *Nucl Med Biol*. 2011;38:575-583.
17. Neirinckx AD, Davis MA. Potential column chromatography generators for ionic Ga-68. I. Inorganic substrates. *J Nucl Med.* 1979;20: 1075–1079.
18. Everest DA, Salmon JE. Studies in the chemistry of quadrivalent germanium: ion-exchange studies of solutions of germinates. *J Chem Soc.* 1954;2438–43.
19. Zhernosekov KP, Filisofov DM, Baum RP et al. Processing of generator produced ^{68}Ga for medical application. *J Nucl Med*. 2007;48:1741-1748.
20. Chakravarty R, Shukla R, Ram R, Venkatesh M, Dash A, Tyagi AK. Nanoceria-PAN Composite-Based Advanced Sorbent Material: A Major Step Forward in the Field of Clinical-Grade ^{68}Ge/^{68}Ga Generator. *Appl Mater Interfaces.* 2010;2:2069-2075.
21. Chakraborty S, Chakravarty R, Dash A, Pillai MRA. The Practicality of Nanoceria-Pan-Based ^{68}Ge/^{68}Ga Generator Toward Preparation of ^{68}Ga-Labeled Cyclic RGD Dimer as a

Potential PET Radiotracer for Tumor Imaging. *Cancer Biother Radiopharm*. 2013;28:77-83.

22. Chakravarty R, Chakraborty S, Ram R, Dash A, Pillai MRA. Long-Term Evaluation of 'BARC $^{68}Ge/^{68}Ga$ Generator' Based on the Nanoceria-Polyacrylonitrile Composite Sorbent. *Cancer Biother Radiopharm.* 2013;28:631-637.
23. Correria JDG, Paulo A, Radposinho PD, Santos I. Radiometallated peptides for molecular imaging and targeted therapy. *Dalton Trans.* 2011;40:6144-6147.
24. Price EW, Orvig C. Matching chelators to radiometal for radiopharmaceuticals. *Chem Soc Rev*. 2014;43:260-290.
25. Morgat C, Hindie E, Mishra AK, Allard M, Fernandez P. Gallium-68: Chemistry and radiolabeled peptides exploring different oncogenic pathways. *Cancer Biother Radiopharm*. 2013;28:85-97.
26. Bandoli G, Dolmella A, Tisato F, Porchia M, Refosco F. Mononuclear six coordinated Ga(III) complexes: A comprehensive survey. *Coord Chem Rev*. 2009;253:56-77.
27. Liu S. Bifunctional Coupling agents for radiolabeling of biomolecules and target-specific delivery of metallic radionuclides. *Adv Drug Del Rev*. 60;2008:1347-1370.
28. Saha GB. Fundamentals of nuclear pharmacy. 5th edition, Springer-Verlag, New York, 2004;151-172.
29. Lopaschuk GD, Ussher JR, Folmes CDL, Jaswal JS, Stanley WC. Myocardial Fatty Acid Metabolism in Health and Disease. *Physiol Rev*. 2010;90:207–258.
30. Neely JR, Roveflo M, Oram J. Myocardial utilization of carbohydrate and lipids. *Prog Cardiovasc Dis.* 1972;15:289-329.
31. Corbett JR. Fatty acids for myocardial imaging. *Semin Nucl Med*. 1999:29;237–258.
32. Tamaki N, Morita K, Kuge Y, Tsukamoto E. The Role of Fatty Acids in Cardiac Imaging. *J Nucl Med*. 2000;41:1525-1534.

33. Liedke Al. Alterations of carbohydrate and lipid metabolism in the acutely ischemic heart. *Prog Cardiovasc Dis*. 1981;23:321-336.

34. Padma S, Sundaram PS. Tracing ischemic memory by metabolic pathways: BMIPP and beyond. *Iran J Nucl Med*. 2016;24:11-22.

35. Peterson LR, Gropler RJ. Radionuclide Imaging of myocardial metabolism. *Circ Cardiovasc Imaging.* 2010, 3, 211-222.

36. Biswas SK, Sarai M, Yamada A, Motoyama S, Harigaya H, Hara T, Sugimoto K, Toyama H, Hishida H, Ozaki Y. Fatty acid metabolism and myocardial perfusion imaging for the evaluation of global left ventricular dysfunction following acute myocardial infarction: Comparisons with echocardiography. *Int J Cardiol*. 2010;138:290–299.

37. Ziegler SI. Positron Emission Tomography: Principles, Technology, and Recent Developments. *Nucl Phys A*. 2005;752:679c-687c.

38. Schwaiger M, Hicks R. The clinical role of metabolic imaging of the heart by positron emission tomography. *J Nucl Med.* 1991;32:565-578.

39. Gould KL. PET perfusion imaging and nuclear cardiology. *J Nucl Med.* 1991;32:579-606.

40. Klein MS, Goldstein RA, Welch MJ, et.al. External assessment of myocardial metabolism with [^{11}C]palmitate in rabbit hearts. *Am J Physiol*. 1979;237: H51-H58.

41. Goldstein RA, Klein MS, Welch MJ, Sobel BE. External assessment of myocardial metabolism with C-11 palmitate *in vivo*. *J Nucl Med.* 1980;21:342-348.

42. Lerch RA, Ambos HD, Bergmann SR, Welch MJ, Ter-pogossian MM, Sobel BE. Localization of viable, ischemic myocardium by positron emission tomography with 11C-palmitate. *Circulation.* 1981;64:689-699.

43. Shoup TM, Elmaleh DR, Bonab AA, Fischman AJ. Evaluation of trans-9-^{18}F-fluoro-3,4-methylene-heptadecanoic acid as a PET tracer for myocardial fatty acid imaging. J Nucl Med. 2005;46:297–304.

44. DeGrado TR, Kitapci MT, Wang S, Ying J, Lopaschuk GD. Validation of ^{18}F-fluoro-4-thia-palmi-tate as a PET probe for myocardial fatty acid oxidation: effects of hypoxia and composition of exogenous fatty acids. *J Nucl Med*. 2006;47:173–181.

45. Gropler RJ. PET radiotracers of the cardiovascular system. PET Clinics. 2009;4:69–87.

46. Otto CA, Brown LE, Wieiand DM, Beierwaltes WH. Radioiodinated fatty acids for Myocardial Imaging: Effects of Chain Length. *J Nucl Med*. 1981;22:613-618.

47. Mirtschink P, Stehr SN, Pietzsch HJ, et al. Modified "4 + 1" Mixed Ligand Technetium-Labeled Fatty Acids for Myocardial Imaging: Evaluation of Myocardial Uptake and Biodistribution. *Bioconj Chem*. 2008;19:97–108.

48. Cazzola E, Benini E, Pasquali M, Mirtschink P, Walther M, Pietzsch HJ, Uccelli L, Boschi A, Bolzati C, Duatti A. Labeling of Fatty Acid Ligands with the Strong Electrophilic Metal Fragment [^{99m}Tc(N)(PNP)]$^{2+}$. *Bioconjug Chem*. 2008;19:450.

49. Walther M, Jung CM, Bergmann R, Pietzsch J, et al. Synthesis and biological evaluation of a new type of ^{99m}technetium-labeled Fatty Acid for myocardial metabolism imaging *Bioconjug Chem*. 2007;18: 216.

50. Heintz AC, Jung CM, Stehr SN, Mirtschink P, et al. Myocardial uptake and biodistribution of newly designed technetium-labelled fatty acid analogues *Nucl Med Commun.* 2007;28: 637.

51. Lee BC, Kim DH, Lee I, et al. 16-Cyclopentadienyl tricarbonyl ^{99m}Tc 16-oxo-hexadecanoic acid: Synthesis and evaluation of fatty acid metabolism in mouse myocardium. *J Med Chem*. 2008;51:3630-3634.

52. Zeng H, Zhang H. Synthesis and biological evaluation of fatty acids conjugates bearing cyclopentadienyl-donors incorporated [^{99m}Tc/Re(CO)3]$^{+}$ for myocardical imaging. *Eur J Med Chem*. 2014;72:10-17.

53. Magata Y, Kawaguchi T, Ukon M, et al. A ^{99m}Tc-labeled long chain fatty acid derivative or myocardial imaging. *Bioconjug Chem*. 2004;15:389-393.

54. Mathur A, Subramanian S, Mallia MB, et al. Synthesis and bio-evaluation of a new fatty acid derivative for myocardial imaging. *Bioorg Med Chem*. 2008;16:7927-7931.

55. Normanno N, Bianco C, De Luca A, Maiello MR, Salomon DS. Target-based agents against ErbB receptors and their ligands: a novel approach to cancer treatment. *Endocr. Relat. Cancer.* 2003;10:1–21.

56. Yang P, Allen MS, Aubry MC, Wampfler JA, et al. Clinical features of 5,628 primary lung cancer patients: experience at Mayo Clinic from 1997 to 2003. *Chest*. 2005;128: 452–462.

57. Arora A, Scholar EM. Role of tyrosine kinase inhibitors in cancer therapy. *J. Pharmacol. Exp. Ther*. 2005; 315:971–979.

58. Normano N, Luca AD, Bianco C et. al. Epidermal Growth Factor Receptor (EGFR) signalling in cancer. *Gene*. 2006;366:2-16.

59. Gridelli C, Bareschino MA, Schettino C, Rossi A, Maione P, Ciardiello F. Erlotinib in non-small cell lung cancer treatment: Current status and future development. *Oncologist*. 2007;12:840–849.

60. Thomas SM, Grandis JR. Pharmacokinetic and pharmacodynamic properties of EGFR inhibitors under clinical investigation. *Cancer Treat. Rev*. 2004;30:255–268.

61. Schiller JH. New directions for ZD1839 in the treatment of solid tumors. *Semin Oncol*. 2003; 30:49–55.

62. Cohen MH, Johnson JR, Chen YF, Sridhara R, Pazdur R. FDA drug approval summary: erlotinib (Tarceva) tablets. *Oncologist*. 2005;10:461–466.

63. Boch C, Kollmeier J, Roth A, Stephan-Falkenau S, Misch D, Grüning W, Bauer TT, Mairinger T. The frequency of EGFR and KRAS mutations in non-small cell lung cancer (NSCLC): routine screening data for central Europe from a cohort study. *BMJ Open*. 2013; 3:e002560. doi: 10.1136/bmjopen-2013-002560.

64. Marchetti A, Martella C, Felicioni L, Barassi F, Salvatore S, et al. EGFR mutations in non–small-cell lung cancer: analysis of a large series of cases and development of a rapid and sensitive method for diagnostic screening with potential implications on pharmacologic treatment. *J Clin Oncol*. 2005;23:857–865.

65. Pao W, Miller VA, Politi KA, Riely GJ, Somwar R, Zakowski MF, Kris MG, Varmus H. Acquired resistance of lung adenocarcinomas to gefitinib or erlotinib is associated with a second mutation in the EGFR kinase domain. *PLoS Med*. 2005;2:e73. doi: 10.1371/journal.pmed.0020073.

66. Slobbe P, Poot AJ, Windhorst AD, Dongen GA. PET imaging with small-molecule tyrosine kinase inhibitors: TKI-PET. *Drug Discov Today*. 2012;17:1175–1187.

67. Hicks JW, Van Brocklin HF, Wilson AA, Houle S, Vasdev N. Radiolabeled small molecule protein kinase inhibitors for imaging with PET or SPECT. *Molecules*. 2010;15: 8260–8278.

68. Mishani E, Abourbeh G, Eiblmaier M, Anderson CJ. Imaging of EGFR and EGFR tyrosine kinase over expression in tumors by nuclear medicine modalities. *Curr Pharm Des*. 2008;14:2983–2998.

69. van Dongen GA, Poot AJ, Vugts DJ. PET imaging with radiolabeled antibodies and tyrosine kinase inhibitors: immuno-PET and TKI-PET. *Tumour Biol*. 2012;33:607–615.

70. Bonasera TA, Ortua G, Rozen Y, Krais R, et al. Potential ^{18}F-labeled biomarkers for epidermal growth factor receptor tyrosine kinase. *Nucl Med Biol*. 2001;28:359 –374.

71. Abourbeh G, Dissoki S, Jacobson O, Litchi A, et al. Evaluation of radiolabeled ML04, a putative irreversible inhibitor of epidermal growth factor receptor, as a bioprobe for PET imaging of EGFR-overexpressing tumors. *Nucl Med Biol*. 2007;34:55–70.

72. Neto C, Fernandes C, Oliveira MC, Gano L, Mendes F, Kniess T, Santos I. Radiohalogenated 4-anilinoquinazoline-based EGFR-TK inhibitors as potential cancer imaging agents. *Nucl Med Biol*. 2012;39:247– 260.

73. Holt DP, Ravert HT, Dannals RF, Pomper MG. Synthesis of [^{11}C]gefitinib for imaging epidermal growth factor receptor tyrosine kinase with positron emission tomography. *J Label Compd Radiopharm*. 2006;49:883–888.

74. Bourkoula A, Paravatou-Petsotas M, Papadopoulos A, Santos I, et al. Synthesis and characterization of rhenium and technetium-99m tricarbonyl complexes bearing the 4-[3-bromophenyl]quinazoline moiety as a biomarker for EGFR-TK imaging. *Eur J Med Chem*. 2009;44:4021–4027.

75. Fernandes C, Santos IC, Santos I, Pietzsch HJ, Kunstler JU, et al. Rhenium and technetium complexes bearing quinazoline derivatives: progress towards a ^{99m}Tc biomarker for EGFR-TK imaging. *Dalton Trans*. 2008;3215–3225.

76. Pisaneschi F, Nguyen QD, Shamsaei E, Glaser M, et al. Development of a new epidermal growth factor receptor positron emission tomography imaging agent based on the 3-cyanoquinoline core: Synthesis and biological evaluation. *Bioorg Med Chem*. 2010;18: 6634–6645.

77. Wang M, Gao M, Zheng QH. The first radiosynthesis of [^{11}C]AZD8931 as a new potential PET agent for imaging of EGFR, HER2 and HER3 signaling. *Bioorg Med Chem Lett*. 2014;24:4455–4459.

78. Johnstrom P, Fredriksson A, Thorell JO, Stone-Elander S. Synthesis of [methoxy-^{11}C]PD153035, a selective EGF receptor tyrosine kinase inhibitor. *J Label Compd Radiopharm*. 1998;41:623–629.

79. Petrulli JR, Sullivan JM, Zheng MQ, Bennett DC, et al. Quantitative analysis of [^{11}C]-Erlotinib PET demonstrates specific binding for activating mutations of the EGFR kinase domain. *Neoplasia*. 2013;15:1347–1353.

80. Memon AA, Jakobsen S, Dagnaes-Hansen F, Sorensen BS, Keiding S, Nexo E. Positron Emission Tomography (PET) imaging with ^{11}C-labeled Erlotinib: A micropet study on mice with lung tumor xenografts. *Cancer Res*. 2009;69:873–878.

81. Bahce I, Smit EF, Lubberink M, van der Veldt AA, et al. Development of [^{11}C]erlotinib positron emission tomography for *in vivo* evaluation of EGF receptor mutational status. *Clin Cancer Res.* 2013;19:183–193.

82. Huang S, Han Y, Chen M, Hu K, Qi Y, et al. Radiosynthesis and biological evaluation of ^{18}F-labeled 4-anilinoquinazoline derivative (^{18}F-FEA-Erlotinib) as a potential EGFR PET agent. *Bioorg Med Chem Lett*. doi: http://dx.doi.org/10.1016/j.bmcl.2017.08.066.

83. Traxl A, Beikbaghban T, Wanek T, Kryeziu K, et al. ^{11}C-Erlotinib PET cannot detect acquired Erlotinib resistance in NSCLC tumor xenografts in mice. *Nucl. Med. Biol.* 2017; 52:7-15.

84. Kolb HC, Finn MG, Sharpless KB. "Click Chemistry: Diverse Chemical Function from a Few Good Reactions". *Angew. Chem. Int. Ed*. 2001;40:2004–2021.

85. Tiwari VK, Mishra BB, Mishra KB, Mishra N,. Singh AS, Chen X. Cu-Catalyzed Click Reaction in Carbohydrate Chemistry. *Chem Rev*. 2016;116:3086–3240.

86. Liang L, Astruc D. The copper(I)-catalyzed alkyne-azide cycloaddition (CuAAC) “click” reaction and its applications. An overview. *Coord Chem Rev*. 2011; 255: 2933–2945.

87. Zhang FL, Huang Q, Zheng K, Li J, Liu JY, Xue JP. A novel strategy for targeting photodynamic therapy. Molecular combo of photodynamic agent zinc(II) phthalocyanine and small molecule target-based anticancer drug erlotinib. *Chem Commun.* 2013; 49: 9570-9572.

88. Shen C, Yuan M, Wu Q, Zhang P. Erlotinib derivative and preparation method and application thereof. Patent CN10369427 (A), 2014.

89. Huang S, Wang Q, Zheng X et al. EGFR positron tracer, a preparation method and application thereof. Patent CN104817542 (A), 2015.

90. Ikeda R, Vermeulen LC, Lau E, Jiang Z, Kavanaugh SM, Yamada K, Kolesar JM. Isolation and characterization of Erlotinib-resistant human non-small cell lung cancer A549 cells. *Oncol Lett*. 2011;2: 91-94.

91. Yoshimoto M, Kurihara H, Fujii H. Theragnostic Imaging Using Radiolabeled Antibodies and Tyrosine Kinase Inhibitors. 2015, DOI: http://dx.doi.org/10.1155/2015/842101

92. Backer MV, Backer JM. Imaging key biomarkers of tumor angiogenesis. *Theranostics*. 2012;166:1-6.

93. Cai W, Chen X. Multimodality molecular imaging of tumor angiogenesis. *J Nucl Med.* 2008;49: 113S–28S.

94. Chakravarty R, Chakraborty S, Dash A. Molecular imaging of breast cancer: role of RGD peptides. *Mini Rev Med Chem*. 2015;15:1073-94.

95. Danhier F, Le Breton A, Preat V. RGD-based strategies to target alpha(v) beta(3) integrin in cancer therapy and diagnosis. *Mol Pharm*. 2012;9:2961–73.

96. Weis SM, Cheresh DA. New approaches to image angiogenesis. *Nat Med*. 2011;17: 1359–70.

97. Cai H, Conti PS. RGD-based PET tracers for imaging receptor integrin alphav beta3 expression. *J Label Comp Radiopharm*. 2013;56:264–79.

98. Haubner R, Maschauer S, Prante O. PET radiopharmaceuticals for imaging integrin expression: tracers in clinical studies and recent developments. *Bio Med Res Int*. 2014;87: 1609.

99. Liu S. Radiolabeled cyclic RGD peptides as integrin $\alpha_v\beta_3$-targeted radiotracers: maximizing binding affinity via bivalency. *Bioconjug Chem*. 2009;20:2199–213.

100. Liu S. Radiolabeled multimeric cyclic RGD peptides as integrin $\alpha_v\beta_3$ targeted radiotracers for tumor imaging. *Mol Pharm*. 2006; 3:472–87.

101. Niu G, Chen X. PET imaging of angiogenesis. *PET Clin*. 2009; 4:17–38.

102. Tateishi U, Oka T, Inoue T. Radiolabeled RGD peptides as integrin $\alpha_v\beta_3$-targeted PET tracers. *Curr Med Chem*. 2012;19:3301–3309.

103. Iagaru A, Mosci C, Shen B, Chin FT, Mittra E, Telli ML, et al. ^{18}F-FPPRGD2 PET/CT: pilot phase evaluation of breast cancer patients. *Radiology*. 2014;273:549–559.

104. Kenny LM, Coombes RC, Oulie I, Contractor KB, Miller M, Spinks TJ, et al. Phase I trial of the positron-emitting Arg-Gly-Asp (RGD) peptide radioligand ^{18}F-AH111585 in breast cancer patients. *J Nucl Med*. 2008;49:879–86.

105. Dijkgraaf I, Yim CB, Franssen GM, Schuit RC, Luurtsema G, Liu S, et al. PET imaging of $\alpha_v\beta_3$ integrin expression in tumours with ^{68}Ga-labelled mono-, di- and tetrameric RGD peptides. *Eur J Nucl Med Mol Imaging*. 2011;38:128–37.

106. Knetsch PA, Petrik M, Griessinger CM, Rangger C, Fani M, Kesenheimer C, et al. [^{68}Ga]NODAGA-RGD for imaging alphavbeta3 integrin expression. *Eur J Nucl Med Mol Imaging*. 2011;38:1303–12.

107. Li ZB, Chen K, Chen X. ^{68}Ga-labeled multimeric RGD peptides for microPET imaging of integrin alpha(v)beta (3) expression. *Eur J Nucl Med Mol Imaging*. 2008;35:1100–8

108. Lopez-Rodriguez V, Gaspar-Carcamo RE, Pedraza-Lopez M, Rojas-Calderon EL, Arteaga de Murphy C, Ferro-Flores G, et al. Preparation and preclinical evaluation of

^{66}Ga-DOTA-E(c(RGDfK))$_2$ as a potential theranostic radiopharmaceutical. *Nucl Med Biol*. 2015;42:109–114.

109. Notni J, Pohle K, Wester HJ. Comparative gallium-68 labeling of TRAP-, NOTA-, and DOTA-peptides: practical consequences for the future of gallium-68-PET. *EJNMMI Research*. 2012;2:28.

110. Oxboel J, Brandt-Larsen M, Schjoeth-Eskesen C, Myschetzky R, El-Ali HH, Madsen J, et al. Comparison of two new angiogenesis PET tracers ^{68}Ga-NODAGA-E[c(RGDyK)]2 and ^{64}Cu-NODAGA-E[c(RGDyK)]2; in vivo imaging studies in human xenograft tumors. *Nucl Med Biol*. 2014;41: 259–67.

111. Pohle K, Notni J, Bussemer J, Kessler H, Schwaiger M, Beer AJ. ^{68}Ga-NODAGA-RGD is a suitable substitute for ^{18}F-Galacto-RGD and can be produced with high specific activity in a cGMP/GRP compliant automated process. *Nucl Med Biol*. 2012;39:777–84.

112. Antony AC. The biological chemistry of folate receptors. *Blood*. 1992;79:2807-2820.

113. Campbell IG, Jones TA, Foulkes WD, Trowsdale J. Folate binding protein is a marker for ovarian cancer. *Cancer Res*. 1991;51:5329-5338.

114. Antony AC. Folate receptors. *Annu Rev Nutr*. 1996;16:501-521.

115. Altiparmak B, Lambrecht FY, Bayrak E, Durkan K. Design and synthesis of ^{99m}Tc-citro-folate for use as a tumor-targeted radiopharmaceutical. *Int J Pharm.* 2010;400:8-14.

116. Guo W, Hinkle GH, Lee RJ. ^{99m}Tc-HYNIC-folate: a novel receptor-based targeted radiopharmaceutical for tumor imaging. *J Nucl Med*. 1999;40:1563-1569.

117. Ke CY, Mathias CJ, Green MA. The folate receptor as a molecular target for tumor-selective radionuclide delivery. *Nucl Med Biol*. 2003;30:811-817.

118. Ke CY, Mathias CJ, Green MA. Folate-receptor-targeted radionuclide imaging agents. *Adv Drug Deliv Rev*. 2004;56:1143-1160.

119. Lu J, Pang Y, Xie F, Guo H, Li Y, Yang Z, Wang X. Synthesis and *in vitro*/*in vivo* evaluation of ^{99m}Tc-labeled folate conjugates for folate receptor imaging. *Nucl Med Biol*. 2011;38:557-565.

120. Mindt TL, Müller C, Melis M, de Jong M, Schibli R. Click-to-chelate: *In vitro* and *in vivo* comparison of a ^{99m}Tc(CO)$_3$-labeled N(τ)-histidine folate derivative with its isostructural, clicked 1,2,3-triazole analogue. *Bioconjug Chem.* 2008;19:1689-1695.

121. Müller C, Schibli R. Folic acid conjugates for nuclear imaging of folate receptor-positive cancer. *J Nucl Med*. 2011;52:1-4.

122. Müller C, Schibli R. Prospects in folate receptor-targeted radionuclide therapy. *Front Oncol*. 2013;3:249.

123. Mathias CJ, Hubers D, Low PS, Green MA. Synthesis of [^{99m}Tc]DTPA-Folate and its evaluation as a folate-receptor targeted radiopharmaceutical. *Bioconjug Chem*. 2000;11: 253-257.

124. Müller C, Hohn A, Schubiger PA, Schibli R. Preclinical evaluation of novel organometallic ^{99m}Tc-folate and ^{99m}Tc-pteroate radiotracers for folate receptor-positive tumour targeting. *Eur J Nucl Med Mol Imaging*. 2006;33:1007-1016.

125. Müller C, Struthers H, Winiger C, Zhernosekov K, Schibli R. DOTA Conjugate with an albumin-binding entity enables the first folic acid–targeted ^{177}Lu-radionuclide tumor therapy in mice. *J Nucl Med*. 2013;54:124-131.

126. Okarvi SM, Jammaz IA. Preparation and *in vitro* and *in vivo* evaluation of Technetium-99m-labeled folate and methotrexate conjugates as tumor imaging agents. *Cancer Biother. Radiopharm*, 2006;21:49-60.

127. Reddy JA, Low PS. Folate-mediated targeting of therapeutic and imaging agents to cancers. *Crit Rev Ther Drug Carrier Syst*. 1998;15:587-627.

128. Trump DP, Mathias CJ, Yang Z, Low PS, Marmion M, Green MA. **S**ynthesis and evaluation of $^{99m}Tc(CO)_3$-DTPA Folate as a folate-receptor-targeted radiopharmaceutical. *Nucl Med Biol*. 2002;29:569-573.

129. Wedeking, PW, Wager RE, Arunachalam T, Ramalingam K, Linder KE, Ranganathan RS, Nunn AD, Raju N, Tweedle M. Metal complexes derivatized with folate for use in diagnostic and therapeutic applications. 2000; U.S. Patent 6093382.

130. Mathias CJ, Green MA. A kit formulation for preparation of ^{111}In-DTPA-folate, a folate-receptor-targeted radiopharmaceutical. *Nucl Med Biol*. 1998;25:585-587.

131. Mathias CJ, Wang S, Waters DJ, Turek JJ, Low PS, Green MA. Indium-111-DTPA-Folate as a potential folate-receptor-targeted radiopharmaceutical. *J Nucl Med*. 1998;39: 1579-1585.

132. Siegel BA, Dehdashti F, Mutch DG, Podoloff DA, Wendt R, Sutton GP, Burt RW, Ellis PR, Mathias CJ, Green MA, Gershenson DM. Evaluation of ^{111}In-DTPA-Folate as a Receptor-Targeted Diagnostic Agent for Ovarian Cancer: Initial Clinical Results. *J Nucl Med*. 2003;44:700-707.

133. Wang S, Luo J, Lantrip DA, Waters DJ, Mathias CJ, Green MA, Fuchs PL, Low PS. Design and synthesis of [^{111}In]DTPA-folate for use as a tumor-targeted radiopharmaceutical. *Bioconjug Chem*. 1997;8:673-679.

134. Fisher RE, Siegel BA, Edell SL, Oyesiku NM, Morgenstern DE, Messmann RA, Amato RJ. Exploratory study of ^{99m}Tc-EC20 imaging for identifying patients with folate receptor–positive solid tumors. *J Nucl Med*. 2008;49:899-906.

135. Leamon CP, Parker MA, Vlahov IR, Xu LC, Reddy JA, Vetzel M, Douglas N.. Synthesis and biological evaluation of EC20: a new folate-derived, ^{99m}Tc-based radiopharmaceutical. *Bioconjug. Chem*. 2002;13:1200-1210.

136. Al-Jammaz I, Al-Otaibi B, Al-Rumayan F, Al-Yanbawi S, Amer S, Okarvi SM. Development and preclinical evaluation of new ^{124}I-folate conjugates for PET imaging of folate receptor-positive tumors. *Nucl Med Biol*. 2014;41:457-463.

137. Al-Jammaz I, Al-Otaibi B, Amer S, Okarvi SM. Rapid synthesis and in vitro and in vivo evaluation of folic acid derivatives labelled with fluorine-18 for PET imaging of folate receptor-positive tumors. *Nucl Med Biol*. 2011;38:1019-1028.

138. Bettio A, Honer M, Müller C, Bruhlmeier M, Müller U, Schibli R, Groehn V, Schubige, AP, Ametamey SM. Synthesis and preclinical evaluation of a folic acid derivative labeled with ^{18}F for PET imaging of folate receptor–positive tumors. *J Nucl Med*. 2006;47:1153-1160.

139. Mathias CJ, Wang S, Lee RJ, Water DJ, Low PS, Green MA. Tumor-selective radiopharmaceutical targeting via receptor-mediated endocytosis of gallium-67-deferoxamine-folate. *J Nucl Med*. 1996;37:1003-1008.

140. Mathias CJ, Wang S, Low PS, Waters DJ, Green MA. Receptor-mediated targeting of ^{67}Ga-deferoxamine-folate to folate-receptor-positive human KB tumor xenografts. *Nucl Med Biol*. 1999;26:23-25.

141. Mathias CJ, Lewis MR, Reichert DE, Laforest R, et al. Preparation of ^{66}Ga and ^{68}Ga-labelled Ga(III)-deferoxamine-folate as potential folate- receptor-targeted PET radiopharmaceuticals. *Nucl Med Biol*. 2003;30:725-731.

142. Fani M, Wang X, Nicolas G, Medina C, et al. Development of new folate based PET radiotracers: preclinical evaluation of ^{68}Ga-DOTA-folate conjugates. *Eur J Nucl Med Mol Imaging*. 2011;38:108-119.

143. Müller C, Vlahov IR, Krishna H, Santhapuram R, Leamon CP, Schibli R. Tumor targeting using ^{67}Ga-DOTA-Bz-folate- investigations of methods to improve the tissue distribution of radiofolates. *Nucl Med Biol*. 2011;38:715-723.

144. Fani M, Tamma ML, Nicolas GP, Lasri E, et al. *In vivo* imaging folate receptor positive tumor xenografts using novel ^{68}Ga-NODAGA-folate conjugates. *Mol Pharmaceutics*. 2012;9:1136-1145.

145. Al-Jammaz I, Al-Otaibi B, Al-Hokbany N, Amer S, Okarvi S. Development and pre-clinical evaluation of new ^{68}Ga-NOTA-folate conjugates for PET imaging of folate receptor-positive tumors. *Anticancer Res*. 2014;34:6547-6556.

146. Xie F, Zhang C, Yu Q, Pang Y, Chen Y, Yang W, Xue J, LiuY, Lu J. Novel ^{99m}Tc radiolabeled folate complexes with PEG linkers for FR-positive tumor imaging: synthesis and biological evaluation. *RSC Adv*. 2014; 4: 32197-32206.

147. Schneider R, Schmitt F, Frochot C, Fort Y, Lourette N, Guillemin F, Müller JF, Barberi-Heyob M.. Design, synthesis, and biological evaluation of folic acid targeted tetraphenylporphyrin as novel photosensitizers for selective photodynamic therapy. *Bioorg Med Chem.* 2005;13:2799-2808.

148. Sourbron S, Ingrisch M, Siefert A, Reiser M, Herrmann K. Quantification of cerebral blood flow, cerebral blood volume and blood–brain-barrier leakage with DCE-MRI. *Magn Reson Med*. 2009;62:205–217

149. Mohs AM, Lu ZR. Gadolinium(III)-based blood-pool contrast agents for magnetic resonance imaging: status and clinical potential. *Expert Opin Drug Deliv*. 2007;4:149–164

150. Inoue Y, Momose T, Machida K, Honda N, et al. Quantitation of cerebral blood volume by ^{99m}Tc-DTPA-HSA SPECT. *Radiat Med*. 1992;10:184–188.

151. Croteau E, Benard F, Cadorette J, Gauthier ME, Aliaga A, Bentourkia M, Lecomte R. Quantitative gated PET for the assessment of left ventricular function in small animals. *J Nucl Med.* 2003;44:1655–1661.

152. Alexei A, Bogdanov Jr, Weissleder R, Brady TJ. Long circulating blood pool imaging agents. *Adv Drug Delivery Rev*. 1995;16:335–348.

153. Atkins HL, Klopper JF, Ansari AN. A comparison of Tc-99m-labelled human serum albumin and in vitro labelled red blood cells for blood pool studies. *Clin Nucl Med*. 1980; 5:166–169.

154. Baron JC, Frackowisk RSJ, Herholz K, Jones T, Lammertsma AA, Mazoyer B, Wienhard K. Use of PET methods for measurement of cerebral energy metabolism and hemodynamics in cerebrovascular disease. *J Cereb Blood Flow Metab*. 1989;9:723–742.

155. Kratz F. Albumin as a drug carrier: Design of produgs, drug conjugates, and nanoparticles. *J Control Release*, 2008;132:171-183.

156. Hoffend J, Mier W, Schuhmacher J, Schmidt K, Dimitrakopoulou-Strauss A, Strauss LG, Eisenhut M, Kinscherf R, Haberkorn U. Gallium-68-DOTA-albumin as a PET blood-pool marker: experimental evaluation *in vivo*. *Nucl Med Biol*. 2005;32:287–292.

157. Mier W, Hoffend J, Kramer S, Schuhmacher J, Hull WE, Eisenhut M, Haberkorn U. Conjugation of DOTA using isolated phenolic active esters: The labeling and biodistribution of albumin as blood pool marker. *Bioconjug Chem*. 2005;16:237−240.

158. Chang YS, Jeong JM, Lee YS, Kim HW, Rai GB, Lee SJ, Lee DS, Chung JK, Lee MC Preparation of ^{18}F-human serum albumin: a simple and efficient protein labeling method with ^{18}F using a hydrazone-formation method. *Bioconjug Chem*. 2005;16:1329–1333.

159. Wangler B, Quandt G, Iovkova L, Schirrmacher E, Wangler C, Boening G, Hacker M, Schmoeckel M, Jurkschat K, Bartenstein P, Schirrmacher R. Kit-like F-18-labeling of proteins: synthesis of 4-(Di-tert-butyl[F-18]fluorosilyl)benzenethiol (Si[F-18]FA-SH) labeled rat serum albumin for blood pool imaging with PET. *Bioconjug Chem*. 2009; 20:317–321.

160. Anderson CJ, Rocque PA, Weinheimer CJ, Welch MJ. Evaluation of copper-labeled bifunctional chelate–albumin conjugates for blood pool imaging. *Nucl Med Biol*. 1993; 20:461–467.

161. Basuli F, Li C, Xu B, Williams M, Wong K, Coble VL, Vasalatiy O, Seidel J, Green MV, Griffiths GL, Choyke PL, Jagoda EM. Synthesis of fluorine-18 radio-labeled serum albumins for PET blood pool imaging. *Nucl Med Biol*. 2015;42:219–225.

162. Todican A, Brunner S, Böning G, Lehner S, et al. [^{68}Ga]-Albumin-PET in the monitoring of left ventricular function in murine models of ischemic and dilated cardiomyopathy: Comparison with cardiac MRI. *Mol Imaging Biol*. 2013;15:441–449.

163. Sorensen J, Velikyan I, Antoni G, Langstrom B. ^{68}Ga-labeled human serum albumin. 2011;Patent: WO2011033112 A3.

164. Brady ED, Chong H, Milenic DE, Brechbiel MW. Development of a spectroscopic assay for bifunctional ligand-protein conjugates based on copper. *Nucl Med Biol*. 2004; 31:795–802

165. Lowry OH, Rosebrough WJ, Farr AL,Randal RJ. Protein measurement with the Folin phenol reagent. *J Biol Chem*. 1951;193:265-275.

166. Stehle G, Sinn H, Wunder A, Schrenk HH, Schutt S, Maier-Borst W, Heene DL. The loading rate determines tumor targeting properties of methotrexate- albumin conjugates in rats. *Anticancer Drugs*. 1997;8:677-685.

167. Miniati M, Sostman HD, Gottschalk A, Monti S, Pistolesi M. Perfusion lung scintigraphy for the diagnosis of pulmonary embolism: A reappraisal and review of the prospective investigative study of acute pulmonary embolism diagnosis methods. *Semin Nucl Med.* 2008;38:450–461.

168. Worsley DF, Alavi A. Radionuclide imaging of acute pulmonary embolism. *Semin Nucl Med.* 2003;33:259–278.

169. Charidra R, Shamoun J, Braunstein P, DuHov OL. Clinical evaluation of an instant kit for preparation of ^{99m}Tc-MAA for lung scanning. *J Nucl Med*. 1974;14:702–705.

170. Rangarajan V, Purandare NC, Sharma AR, Shah S. PET/CT: Current status in India. *Indian J Radiol Imaging*. 2008;18:290–294

171. Even GA, Green MA. Gallium-68-labeled macroaggregated human serum albumin, ^{68}Ga-MAA. *Int J Rad Appl Instrum B*. 1989;16:319–321.

172. Hayes RL, Carlton JE, Kuniyasu Y. A new method for labeling microspheres with Ga-68. *Eur J Nucl Med*. 1981; 6:531–533.

173. Mathias CJ, Green MA. Convenient route to [^{68}Ga]Ga-MAA for use as a particulate PET perfusion tracer. *Appl Radiat Isot*. 2008;66:1910–1912.

174. Maus S, Buchholz HG, Ament S, Brochhausen C, Bausbacher N, Schreckenberger M. Labelling of commercially available human serum albumin kits with ^{68}Ga as surrogates for ^{99m}Tc-MAA microspheres. *Appl Radiat Isot*. 2011;69:171–175.

175. Hnatowich DJ. Labeling of tin-soaked albumin microspheres with Ga-68. *J Nucl Med*. 1976;17:57–60.

176. Maziere B, Steinling C, Comar M. Stable labeling of serum albumin microspheres with gallium-68. *Appl Radiat Isot*. 1986;37:360–361.

177. Das S, Thorek DLJ, Grimm J. Cerenkov Imaging. *Adv Cancer Res*. 2014;124:213-234.

178. Thorek DLJ, Robertson R, Bacchus WA et. al. Cerenkov imaging- a new modality for molecular imaging. *Am. J Nucl. Med Mol Imaging*. 2012;2:163-173.

179. Al-Janabi MA, Yousif ZM, Kadim AH, Al-Salem AM. A new technique for the preparation of ready-to-use macroaggregated albumin (MAA) kits to be labelled with ^{99m}Tc for lung scanning. *Int J Appl Radiat Isot*. 1983;34:1473–1478.

180. Hunta AP, Friera M, Johnson RA, Berezenkoc S, Perkinsa AC. Preparation of Tc-99m-macroaggregated albumin from recombinant human albumin for lung perfusion imaging. *Eur J Pharm Biopharm*. 2006;62:26–31.

181. Wetzel R, Becker M, Behke J, Billwitz H, Bohm S, Ebert B, Hamann H, Krumbiegel J, Lassmann G. Temperature behavior of human serum albumin. *Eur J Biochem*. 1980;104: 469–478.